AN INVESTIGATION INTO THE BEHAVIOUR OF HOLLOW RIBBED (WAFFLE) RECTANGULAR REINFORCED CONCRETE SLABS AT ULTIMATE LIMIT STATE

by

Sai Lung HO, B.Sc.(Hons)

A Thesis Presented For the award of the
Degree of Doctor of Philosophy
of the
Council for National Academic Awards

Department of Civil Engineering,
Surveying & Building
Dundee Institute of Technology

July, 1989.

ACKNOWLEDGEMENTS

The author would like to express his sincere gratitude to his Supervisor Dr. Susanta Sarkar, Head of Department of Civil Engineering, Surveying & Building for his encouragement, guidance and supervision given to the author throughout the course of this research which have been invaluable and have made this research possible.

The author is indebted to the valuable advice and help received from his second Supervisor Dr. J.G.L. Munday, Senior Lecturer in the Department of Civil Engineering, Surveying & Building at Dundee Institute of Technology. Thanks are also due to my external supervisor Mr. C.M.C. Marshall, Senior Lecturer at Hatfield Polytechnic for his helpful discussion and advice. Dr. Thorpe is acknowledged for his assistance in the Finite Element Analysis. Thanks are also due to the staff of Computer Centre particularly Dr. J. Clayton and Mr. S. Gardner, for their help and advice.

Grateful thanks are given to the entire technical staff of the Department of Civil Engineering, Surveying & Building for their practical assistance, preparing and testing the models and specially to Mr. J. Galloway, Mr. A. Thomson and Mr. J. Webster who were most closely associated with and coordinated much of the technical work.

The author would like to record his thanks to the Dundee Institute of Technology for providing the research studentship which enabled him to carry out the work.

Finally, the author would like to take this opportunity to express his greatest appreciation and gratitude to his wife, Susan, for her patience and support throughout this work, and especially for her exceptional job typing the manuscript.

AN INVESTIGATION INTO THE BEHAVIOUR OF HOLLOW RIBBED (WAFFLE) RECTANGULAR REINFORCED CONCRETE SLABS AT ULTIMATE LIMIT STATE

by

Sai Lung HO, B.Sc.(Hons)

ABSTRACT

The elastic to ultimate load behaviour of reinforced concrete waffle slabs subjected to uniformly distributed load and 4-point loads are reported in this thesis. A total of twenty 1/4- and one 1/2-scale reinforced concrete waffle model slabs, with different area of steel and rib depth to slab thickness ratio and various edge conditions were made and tested to destruction.

The theoretical analysis of the slabs essentially consists of three phases:

(i) elastic behaviour up to the appearance of first cracks;
(ii) nonlinear behaviour due to progressive concrete cracking and yielding of reinforcements; and
(iii) ultimate load behaviour.

Two 2-dimensional elastic models viz., thin plate bending element and grillage element models, and one 3-dimensional elastic-fracture model using finite element package LUSAS/AN have been employed to investigate the applicability of these methods for the analysis of the slabs. In addition to these, three ultimate load methods viz., modified yield line method, equivalent open grillage analysis and modified strip method were developed and used to predict the ultimate load carrying capacity of the slabs.

Based on the experimental and theoretical results, it is concluded that the behaviour of R.C. waffle slabs is very similar to that of R.C. solid slabs except that waffle slabs tend to attract more bending moments at the support. As a result, the span moments of the slab are reduced when compared to the span moments given by BS8110 for solid slabs. The combined bending and torsion interaction at the rib joints is also considered in this investiagtion. It is found that for slabs with restrained edges membrance action significantly increases the load carrying capacity. A method of predicting this enhancement has also been developed. The theoretical results obtained by the proposed methods of analysis for the three phases above show a good correlation with the experiemntal results.

LIST OF TABLES

LIST OF FIGURES

NOTATIONS

b	is the width of the ribs;
D_1 , D_2	is the coupling rigidities;
Dxy,yx	are the torsional rigidities;
E	is Young's modulus of elasticity;
Ei	is the internal work done by the slab;
Ex	is the external work done on the slab;
fcu	is the compressive strength of concrete cube;
fcy	is the compressive strength of concrete cylinder;
σx,y,z	are the direct stresses in x-, y- and z-axes respectively;
ϵx,y	are the direct strains in x- and y-axes respectively;
γxy	is the shear strain in x-y plane;
G	is the elastic shear modulus of the plate;
h	is the overall depth of the slab;
Ix,y	are the second moments of area of the T-sections about x and y directions respectively;
Jx,y	are the polar second moments of area of the grillage element about x and y directions respectively;
Ls or Ly	is the short span of the slab;
M	is the applied moment;
Mcr	is the cracking flexural moment of plain concrete members;
Mx,y	are the bending moments about x and y axes respectively;
Mxy,yx	is the twisting moment respect to x-y plane;
Mu	is the ultimate moment of the section;
Mup	is the ultimte flexural moment of plain concrete members;
p(x,y)	is the uniformly distributed load;
P	is the point load;
ν	is Poisson's Ratio;
r	is the rib depth;
Rx,y	are the polar second moments of area of the ribs about x and y directions respectively;
Sx,y	are the rib spacings in x and y directions respective;
t	is the thickness of the top slab;
T	is the applied torsion moment;
Tx,y	are the torsional rigidities of the grillage beam in x and y axes respectively;
Tcr	is the cracking torsional moment of plain concrete members;
Tu	is the ultimate torsional moment of the section;
Tup	is the ultimte torsional moment of plain concrete members;
Vx,y	are the shear forces in x and y axes respectively;
w(x,y)	is the displacement of the plane in z direction;
Wh	is the ultimate load capacity obtained by Modified Strip Method;
Wp	is the ultimate load capacity obtained by Equivalent Open Grillage Analysis;
Wj	is the ultimate load capacity obtained by Modified Yield Line Method;

CONTENTS

CHAPTER 1

INTRODUCTION

1.1 INTRODUCTION

Reinforced concrete waffle slab construction has been used to improve the efficiency of slab systems since the 1950's. With advances in the fabrication of formwork and concrete handling and placing, waffle slabs are commonplace now in industrial and public buildings, multi-storey car parks and highway bridges, owing to their economic and architectural benefits. A reinforced concrete waffle slab consists essentially of a relatively thin top slab, acting compositely with an orthogonal grid of beams. The relatively close spacing of the ribs in this structural system produces a response to loads which is closer to that of a solid slab, rather than to a series of inter-connecting beams. However, the actual behaviour of this type of structure is complex due to the interaction between the top slab and the grillage of monolithically cast beams.

The behaviour of R.C. solid slabs subjected to transverse loads is well understood; however the behaviour of R.C. waffle slabs has not been widely investigated. Current codes of practice (5,14), recommend ultimate load design of waffle slabs within the provisions for the design of solid/flat slabs, provided certain requirements in respect of structural dimensions, rib spacing and suitable reinforcement are satisfied.

Since the initial interest in waffle slabs in the 1950's there have been only a few research investigations into the elastic behaviour and ultimate strength of R.C. waffle slab structures. Work carried out by Helal (21), Testa and Levy (68), Resis and Sokal (64), and Tebbet and Horrop (70,71) on elastic analysis methods and Marshall (42) and Ajdukiewicz and Kliszczewicz (2) on ultimate load analysis methods are fragmented and insufficient to confirm the aptness of the methods by which waffle slabs are now designed in accordance with the current ultimate load design methods. The current situation is clearly unacceptable given the increasing popular use of the waffle slab form of construction. Elastic analytical results have shown (64,70,71)

that there exist significent differences in bending moments between the working load behaviour of solid and waffle flat slabs. With the reduction of concrete sections at appropriate locations in the tension zones of waffle slabs, cracking and secondary effects such as interaction between bending and torsion, and membrane enhancement due to built-in supports may then become more important than they would be in solid slab structures. For these reasons, it was considered necessary to carry out a programme of work including experimental investigation to establish the behaviour of reinforced concrete waffle slabs under various loading and boundary conditions.

It is generally accepted (3,11,12,16,73,74) that the behaviour of ribbed slabs/plates can be predicted adequately by the solution of the classical plate bending theory. In fact, the exact solution of plate bending problems often involves a prohibitive amount of computation work but its fundamental principle is of paramount importance for the current analytical techniques in structures. The extensive use of grillage analogy on bridge deck system is well established (3,11,19) and the application of this analogy to ribbed plates and stiffened slabs is widely used in practice. The versatile and powerful finite element technique was found by McBean (44) to be highly efficient and accurate for the analysis of stiffened plate structures. Both of these grillage and finite element approaches used with the help of computer packages were considered suitable for the as elastic analysis of reinforced concrete waffle slabs.

Recently, modified yield line methods (2,43) were used to determine the ultimate load capacity of reinforced concrete waffle slabs. These methods provided a very good agreement with the experimental results. However, the test programmes in these investigations were limited to a certain extent in terms of loading and boundary conditions. It was considered that more work was required to verify the general applicability of the yield line analysis to R.C. waffle slab. As is now well known yield line analysis is regarded as an upper-bound or unsafe theorem. It may then be justified to accept that many practising engineers would prefer an alternative method, if available, giving results on the safe side. The lower-bound theorem of Hillerborg Strip Method (29,82) is potentially suitable in this respect and this method has also been considered in the present investigation.

Cracking in this form of structure may significantly affect the overall behaviour of the slabs causing a possiblity to reduce the factor of safety at working load condition. Two-dimensional finite element analysis is not capable of handling the development of cracking in the tension zones of slab. In view of this, a three-dimensional finite element waffle slab model, using elastic-fracture modelling (6,67) was considered necessary to be developed to provide an insight into the development of cracking, and their effect in the overall deflection of the slab. At the same time, it was thought that this model may take into account the effect of membrane action on the load carrying capacity of a restrained waffle slab.

With all these backgrounds in mind, a single panel of slab was chosen because only then could the parameters of: (i) rib-depth to slab thickness ratio; (ii) area of steel; and (iii) various boundary and loading conditions, be established by theoretical analysis, supported by experimental investigation. It was also considered important to establish the extent of the secondary effects such as combined bending and torsion, and the membrane action on the restrained and reinforced concrete waffle slabs.

1.2 AIM OF THE PROJECT

The aims of this research project were as follows:

(1) to study the elastic to plastic behaviour of reinforced concrete waffle slab subjected to uniformly distributed loads with various boundary conditions, and a system of concentrated loads with corner supports;

(2) to investigate the extent of applicability to waffle slabs of the most appropriate currently available methods of analysis for solid slabs, and if necessary, to develop an alternative method for predicting the ultimate capacity of waffle slabs; and

(3) to formulate design criteria for the ultimate strength of waffle slabs.

Two aspects of the investigation were conducted in parallel, viz.:

(a) experimental investigation using 1/4 scale waffle slabs with three major parameters as variables:

(i) the effective rib-depth to slab thickness ratio;
(ii) the area of steel; and
(iii) the loading and boundary conditions.

It was also considered that a 1/2-scale waffle slab, which corresponded to one of the 1/4-scale models was made and tested to failure in order to obtain the significance of the scale effect between these two types of models. For the purpose of the investigation, it was decided that the effect of shear in these slabs would be neglected.

(b) analytical investigations into the serviceability and ultimate limit states using the following methods:

(i) the finite element method and grillage analysis for working load conditions;
(ii) nonlinear analysis into the behaviour due to the development and propogation of cracks on the waffle slabs; and
(iii) the yield line method, the plastic hinge method and the strip method for ultimate load conditions.

This investigation is an attempt to establish a basis from which work may proceed to provide quantitative data of the elastic to plastic behaviour of reinforced concrete waffle slabs. By conducting this programme of investigation, it was expected that it would be possible to postulate a set of design criteria for reinforced concrete waffle slabs by comparison with the experimental and analytical results.

CHAPTER 2

REVIEW OF AVAILABLE LITERATURE

2.1 CURRENT CODE RECOMMENDATIONS

The Code of Practice CP110 (14) and its revised standard BS8110 (5) give separate simplified design methods for slabs supported on beams and for slabs supported on columns. The clauses concerned with the slabs supported on columns are very different in BS8110 to those in CP110, whereas only small differences occur for slabs supported on beams. It is apparent that BS8110 has taken in account the additional consideration of the restrained slab with unequal conditions at adjacent panels which may give rise to support moments differing significantly from those provided by the CP110. Major changes for the slab supported on columns are that the empirical design method has been completely left out and BS8110 concentrates on the continuous frame method supplemented with very different clauses to those in CP110. In contrast, the American Building Code, ACI 318-71 (1) has a unified approach to the simplified design of slabs, whether or not they are supported on beams. In this Code, it provides two very similar methods corresponding to those in CP110: they are the direct design method and the equivalent frame method. A summary of the design methods provided by these Codes is given in Table 2.1.

The codes also recommend ultimate load design for reinforced concrete waffle slabs, within the provisions for the design of flat slabs, provided the waffle slabs satisfy certain dimensional requirements. The structural sizes and layout recommended by BS8110 are as follows (in order to make a comparison, The American Concrete Institute Code, ACI 318-71 are also given in parentheses):

(i) Flange thickness shall not be less than 50mm (50mm) or 1/10 (1/12) of the clear distance between ribs, whichever is the greater.

(ii) Ribs must not be less than 65mm(100mm) wide, their depth must not be more than four times (three and

one-half times) their width, and the rib centre must not be more than 1.5m apart (the clear distance between ribs should not exceed 0.75m).

Apparently, both of these codes make no distinction in the distribution of moments between solid and waffle slabs, and the moment coefficients provided for flat slabs are mainly based on the elastic analysis of a square solid slab.

Table 2.1 Summary of the Design Methods for Reinforced Concrete Slabs.

	Slab supported on columns	Slab supported on beams
CP110	1) Empirical method 2) Continuous frame method	1) Design table for simply supported slabs. 2) Design table for restrained slabs.
BS8110	1) Continuous frame method (Amended)	
ACI	1) Direct Design method 2) Equivalent frame method	

In accordance with the experimental programme of this investigation, all eight series of tests were performed on rigid and flexible edge-supports. In view of this fact, it is appropriate to emphasise on the design approach for the beam-supported slabs. Both CP110 and BS8110 approaches providing the ultimate moment per unit width in the short and long span directions respectively can be determined by:

$$Msx = ksx.w.Ls^2 \quad (2.1a)$$

$$Msy = ksy.w.Ls^2 \quad (2.1b)$$

where, w is the design uniformly distributed load at the ultimate limit state;

Ls is the short span of the slab.

Two sets of moment coefficients depending on the aspect ratios and the boundary conditions of the slab are given in the code:

(i) For simply supported slabs which do not have adequate provision to resist torsion at the corners, and to prevent the corners from lifting: BS8110 Table 14; and

(ii) For restrained slabs which do have adequate provision to resist torsion at the corners, and to prevent the corners from lifting: BS8110 Table 15.

The moment coefficients in BS8110 Table 14 were obtained by Grashof-Rankine's elastic plate formulae for simply supported slabs, whereas the moment coefficients ksx and ksy in Table 15 for restrained slabs were modified from Taylor et al's values incorporated with the yield line theory. Taylor's values were magnified by a factor of 4/3 because the codes concentrated on the design reinforcement in the middle strip which only occupied three quarters of the total width of the slab. The support to span moment ratio of 4/3 was used by the code. It is, therefore, a contradictory situation in that simply supported slabs are designed by a lower-bound solution and on the other hand restrained slabs are designed by an upper-bound solution.

2.2 PREVIOUS EXPERIMENTAL AND THEORETICAL INVESTIGATIONS

2.2.1 Elastic Analytical Investigations

In 1950, Helal (21) produced a set of design coefficients for ribbed slabs spanning in two directions. These coefficients were directly based on the Grashof and Rankine Method, and were determined by Professor Saligar who idealized the ribbed slab as a system of interlacing beams. The maximum bending moment on a rib was derived by using the ratio of the deflection of the rib to that with the greatest deflection of the slab, Fig.2.1. The deflection ratio, Kn, was given in terms of distance of the rib from the middle rib, and the effective span lengths,

$$Kn = \frac{Yn}{Ym} = \frac{16}{5}\cdot\frac{ln}{L}\cdot\left[1 - 2\left(\frac{ln}{L}\right)^2 + \left(\frac{ln}{L}\right)^3\right] \qquad (2.2)$$

where, n represents ribs A, B, C etc.,
m represents mid rib M.

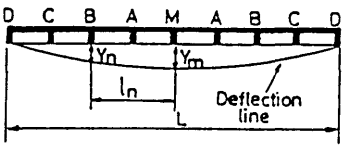

Fig.2.1 : Deflection Line of the Ribbed Slab

Thus, the average bending moment for the slab was defined by the following equation of

$$M(ave) = K(ave).M(max) \qquad (2.3)$$

where, $K(ave) = \frac{\sum Kn}{N}$ and N is total number of ribs.

Since the maximum moments obtained by Grashof and Rankine for solid slabs with simple supports are given as:

$$Mx = \frac{kx.w.Lx^2}{8} \qquad (2.4a)$$

$$My = \frac{ky.w.Ly^2}{8} \qquad (2.4b)$$

where kx and ky are coefficients which depend on the ratio of length to breadth of the solid slab in short and long spans respectively. Then, the average bending moments of a waffle slab were obtained as:

$$M(ave)x = \frac{K(ave)x.kx.w.Lx^2}{8} \qquad (2.5a)$$

$$M(ave)y = \frac{K(ave)y.ky.w.Ly^2}{8} \qquad (2.5b)$$

The coefficients K(ave)x and K(ave)y in imperial units were obtained for simply supported rectangular ribbed slabs. A design example was given for a ribbed slab with ten by eight panels, but serviceability limit states were not checked.

McBean (44), in 1968, demonstrated a highly efficient and accurate analysis of a stiffened plate system by finite element method. However, only a simply supported square plate, stiffened by one eccentric stiffener was analyzed. The results of this analysis was compared with another two sets of analytical results which were obtained using (i) the approximate solution with the Rayleigh-Ritz energy method, and (ii) the proposed exact solution by averaging the stiffener properties over the width of the plate. All the results obtained by these three methods gave a good agreement in the central deflections of the stiffened plate, and the comparison is reproduced in Table 2.2.

Table 2.2 Results of Analysis of Mid-span Deflection of Stiffened Plate Subjected to Uniformly Distributed Load Using Various Approaches

Solution method	No Stiffeners	Concentric Stiffener	Eccentric Stiffener
(a) Finite Element			
1x1 mesh	-	4.659	1.398
2x2 mesh	-	4.565	1.370
4x4 mesh	26.090	4.557	1.367
(b) Rayleigh-Ritz approach	25.389	4.475	1.261
(c) Exact Solution for 'averaged' stiffener	26.095	4.523	1.186

(Note: All deflections to be multiplied by 10^{-4})

To avoid inconsistencies inherent in the use of a substitute continuum for an orthotropic plate analysis on a ribbed plate, Dean and Omid'varan (15) developed a discrete continuous field approach for simply supported elastic rectangular plate with discrete one-way rib reinforcement. The solution obtained by this approach is very similar

to that of an orthotropic plate analysis. The solution is written as a double Fourier series containing an infinite number of terms with respect to the continuous variable and a finite number of terms with respect to the discrete variable. For boundary conditions other than the simple supports, corrective terms expressed in double series, are necessary to satisfy the compatibility at the supports. The solution obtained was about 10% higher compared to other work because it was reported that this analysis also included the membrane action between plate and ribs. However, only rib reinforcement in one direction was considered in the study. It appears that for plates with two-way reinforcement, the analysis involved may not be any easier than conventional orthotropic plate analysis.

In 1972, Resis and Sokal (64) produced an analysis of rectangular and square ribbed flat slabs using the orthotropic plate theory without considering any torsional rigidity i.e. Poisson's ratio and torsional effects were neglected. For this condition, the governing differential equation of orthotropic plate bending theory reduced to

$$Dx.\frac{\partial^4 w}{\partial x^4} + Dy.\frac{\partial^4 w}{\partial y^4} = -p(x,y) \qquad (2.6)$$

which was then solved by applying the principle of the minimum potential energy method. From this analysis, it can be shown that the moments in the column strips are relatively higher than those given in the codes - this can be seen from the results for an isotropic plain and ribbed square internal panel given in Table 2.3. It is probable that the increase in moments in the column strip and the reduction in moments in the middle strip can be attributed to the effect of ignoring the torsional stiffness of the ribbed panel.

In 1975, Testa and Levy (68) applied plate bending theory to two-way ribbed slabs with ribs at 45^0 to the sides and with zero torsional stiffness. The displacement function, ωp, of the particular solution for simply supported slabs with square hollow pots was simplified in the non-dimensional form of

$$\omega p = \frac{5}{12}.\cos\left(\frac{\pi}{2}\right)\left(\frac{x}{a}\right) \qquad (2.7)$$

The displacement function, ωh, of the homogenous solution for slabs with 45^0 ribs in non-dimensional form was also given as

$$\omega h = \frac{5}{12}.\cos\left(\frac{\pi}{2}\right)\left(\frac{x}{a}\right).f\left(\frac{y}{a}\right) \qquad (2.8)$$

The homogeneous differential equation was then obtained as

$$\left[\frac{2}{\pi}.f\left(\frac{y}{a}\right)\right]^4 + 6\left[\frac{2}{\pi}.f\left(\frac{y}{a}\right)\right]^2 + f\left(\frac{y}{a}\right) = 0 \qquad (2.9)$$

This equation was solved using Eqn.2.7 and Eqn.2.8 and yielded the general equation for the deflection of the ribbed slab as:

$$\omega = \frac{5}{12}.\cos\left(\frac{\pi}{2}\right)\left(\frac{x}{a}\right).\left[1+f\left(\frac{y}{a}\right)\right] \qquad (2.10)$$

Using this solution, the bending moments were then obtained with ICL 1900 computer subroutines. The deflection and bending moments of the 45^0 ribbed slab were comparatively smaller than those of the slab with ribs parallel to the edges. In this investigation, the bending moments in the longer direction is ignored because the side ratio of the slab is greater than 2.0. Negative bending moments are found, see Fig.2.2, distributed along the supports at two diagonal corners. Occurrence of these negative moments is probably due to the restraint provided by the skew rib in long-spanning direction. This may be the cause of the reduction in deflection and bending moments for skew ribbed slabs. In view of this, it is believed that torsion at these negative moment zones will certainly have an effect on the flexural strength of the slab.

In 1979, Tebbet and Harrop (71) conducted an analysis of a ribbed panel, based on a set of proposed three simultaneous partial differential equations. Solving this set of governing differential equations by the finite difference method, they found significant

differences between the theoretical distribution of moments in flat and ribbed panels. It is noticeable from the results shown in Table 2.3 that the reduced ratio of torsional to flexural stiffness in a ribbed panel causes an increase in the moments in the column strips.

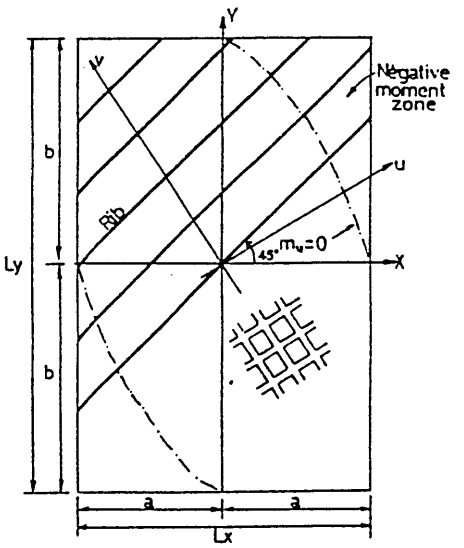

Fig.2.2 : Distribution of Moment for the 45° Ribbed Slab by Testa and Levy (115)

A comparison between the analytical results by Resis and Sokal (64), Tebbet and Harrop (71), and the design codes for a square internally flat slab is presented in Table 2.3. The coefficients for the individual strips are calculated by taking the design moment for the direction considered as a percentage of the total moment calculated for the whole slab. The distribution of the moments obtained from both analyses show a close agreement with CP110 and ACI 318-71 for a flat slab, but they significantly differ for a ribbed slab. For a ribbed slab the theoretical values of the column strip moments are substantially higher, and the middle strip moments are lower, than those obtained from the code's recommendations. The torsion effect of the slab causes an increase in moment in the middle strip by 4.5% of the slab moment, see Table 2.3, and this increase is balanced by the reduction in the moment in the column strip. Therefore, the total difference of 9% of the slab moment is caused by the presence of torsion in a ribbed slab.

Table 2.3: Distribution of Moments in Internal Square Plate Panel

	Plain/ribbed		Plain		Ribbed	
	CP110	ACI	Tebbet	Resis	Tebbet	Resis
Column +ve	22	21	20.8	20.5	25.5	25.6
strip -ve	46	49	50.4	50.0	56.9	61.3
Middle +ve	16	14	13.1	12.8	9.2	7.8
strip -ve	16	16	15.7	16.7	8.4	5.3

†Moments are expressed in percentages of the total slab moment.

The moment coefficients for rectangular plain and ribbed internal panels, suggested by Tebbet et al, are given in Tables 2.4 and 2.5 respectively. These results show that the variations in column strip and middle strip moments relate to the change of side ratio of the rectangular panel. It seems to indicate that the upper limit of span ratios of 1.33 and 2.0, used in BS8110 and ACI codes respectively, are inadequate in view of serviceability requirements. For the ribbed slab, Table 2.5, this can be explained by the fact that when the side ratio increases towards 1.6, the short span middle strip moments tend

Table 2.4: Moments in Rectangular Internal Flat Plate Panel

	Short Span				Long span			
Side ratio	Column strip		Middle strip		Column strip		Middle strip	
	+ve	-ve	+ve	-ve	+ve	-ve	+ve	-ve
1.0	20.8	50.4	13.1	15.7	20.8	50.4	13.1	15.7
1.2	22.9	53.4	11.0	12.7	19.0	47.6	14.7	18.7
1.4	25.1	55.8	9.1	10.0	18.1	45.4	15.6	20.9
1.6	27.0	57.8	7.3	7.9	17.5	43.7	16.1	22.7

†Moments are expressed in percentages of the total slab moment.

to zero. In such circumstances, a rectangular ribbed panel with side ratio equal to or greater than 1.25 will probably behave as a one-way spanning slab, as suggested in the report by Tebbet and Harrop.

Table 2.5: Moments in Rectangular Internal Ribbed Plate Panel

Side ratio	Short span				Long span			
	Column strip		Middle strip		Column strip		Middle strip	
	+ve	-ve	+ve	-ve	+ve	-ve	+ve	-ve
1.0	25.5	56.9	9.2	8.4	25.5	56.9	9.2	8.4
1.2	29.4	60.5	5.5	4.6	22.0	53.2	12.5	12.3
1.4	32.5	63.0	2.6	1.9	19.8	50.2	14.7	15.3
1.6	34.7	64.5	0.7	0.1	18.4	48.0	15.9	17.7

†Moments are expressed in percentages of the total slab moment.

From the above analytical investigations, it would be appropriate to note that:

(i) Elastic ribbed or waffle slabs can be analysed using orthtropic plate theory by conceptually replacing the system by an 'equivalent' homogenous orthotropic plate of uniform thickness. This idealized plate is assumed to obey the elastic theory for bending of thin plates.

(ii) The governing differential equations of the equivalent homogenous orthotropic plate can be solved by the following methods:

(a) Fourier series expansion;
(b) The finite element method;
(c) The minimum energy theorem; and
(d) The finite difference method.

(iii) The results obtained from methods (c) and (d) have shown that there exists significant differences in bending moments at working load for solid and waffle slabs. The torsion effect on the elastic behaviour of waffle slabs cannot be ignored.

It is felt that analyses using Fourier series expansion, minimum energy theorem and finite element method are extremely complex to use when torsion in a waffle slab is considered. The current highly popular and versatile finite element technique can handle the problem with desirable accuracy. With this technique, grillage analogy, which is always regarded as an alternative analysis for ribbed slabs, can also be used for comparison in the present investigation. This technique can probably be extended to nonlinear analysis which will provide insight into the effect of the development and propagation of cracking on the overall deflection of a reinforced concrete waffle slab. However, analytical solutions to the orthotropic plate problem are mainly based upon the assumptions of continuity and homogeneity. In fact, reinforced concrete material cannot entirely satisfy these requirements. Thus, a study and understanding of the actual behaviour of reinforced concrete structures is necessary.

2.2.2 Experimental Investigations at Ultimate Limit State

The first full-scale load test of this structural form was made by Magura and Corley (42) on the waffle slab roof of the Rathskeller Building in New York. Three tests were carried out at different locations in the building. Only the last test, which was intended to investigate the effect of in-plane forces on flexural strength of an internal slab, is relevant to the present work. The result showed that the behaviour of the structure was in accordance with their current design code i.e. ACI Code. Deflections computed using equivalent frame analysis were in good agreement with values obtained in the interior panel. However, the information provided for flexural bending of the slab was limited and the result of this investigation up to ultimate limit is somewhat questionable. These unreliabilities come from two sources:

(i) differential settlement which was reported before testing may have affected the actual behaviour of the slab during the test; and

(ii) the panel was not tested to failure and therefore the factor of safety could not be assessed.

Recently, Marshall (43) applied two methods of analysis, viz. equivalent slab method and open grillage analysis, to a series of reinforced concrete waffle model slabs. The former method involves replacing the waffle slab by an equivalent slab, which is then analysed by the yield line method (32,33), with the dimensions of the slab remaining unchanged. The latter analysis requires transformation of the actual slab into an equivalent slab before the system is analysed by the open grillage method with the yield pattern modified on the basis of the result obtained from the former method.

The experimental and theoretical results gave good estimates of the ultimate failure loads of reinfored concrete waffle slab models. The results are presented in Table 5.3. Marshall's model tests are invaluable with respect to the analysis of this structural system at the ultimate limit state but the test series was limited in scope in terms of boundary conditions and slab thickness to rib depth ratios.

Ajdukiewicz and Kliszczewicz (2) in 1986, reported an investigation on reinforced concrete waffle flat slabs, with three by two multi-panel, at ultimate limit state under selected strip loadings. The yield line method applied to this structural form was used in their analysis. The failure mechanism according to the test observations provided smaller collapse loads than the generally assumed mechanism given by yield line theory. Slab strength was underestimated by about 20% using this analysis on the actual failure mechanism. This reserve strength was reported as probably due to the membrane effects and the conservative evaluation of the ultimate strength of the slab panels.

From these investigations, the following conclusions can be drawn:

(i) Modified yield line method may be used to predict the ultimate strength of reinforced concrete waffle slabs;

(ii) Secondary effects of membrane action and interaction between bending and torsion moments at the ribs become more significant in this structural form; and

(iii) Equivalent open grillage analysis can be used to give a good estimate for predicting the ultimtae strength of reinforced concrete waffle slabs providing the appropriate failure mechanism can be found.

From these facts, modified yield line method and open grillage analysis will form the basis for analysis of waffle slabs at ultimate limit state. Yield line analysis is inevitably an upper bound theorem and the lower bound solution of Hillerborg's strip method will be included in the theoretical consideration. The effcts of combined bending and torsion moment and membrane action on restrained waffle slab are considered in the present investigation, and these will be discussed where it is appropriate.

CHAPTER 3

ELASTIC ANALYSES

3.1 INTRODUCTION

Application of orthotropic plate thoery to reinforced concrete slabs was pioneered by Huber in 1914. A significant amount of investigations was carried out by Westergaard in 1926. The importance of the elastic plate theory for the analysis of slabs was then being realised. It was Navier in 1820, who developed the first method of solution for the rectangular plates using double trigonometric series to transform the differential equations into a series of algebraic equations. Since then a number of methods based on this approach but with modified procedures have been developed and solutions for a range of isotropic plate problems have been produced. Excellent surveys covering the most commonly used methods of solution were presented by Timoshenko and Woinowsky-Krieger, and Bares and Massonnet.

Despite the fact that the classical methods of solution often involve an excessive amount of computational work and are sometimes prohibitive for certain problems, they provide the fundamental basis for assessment of more powerful and versatile numerical techniques such as grillage analogy and finite element methods. These numerical techniques obviate the shortcomings of classical theory and make it possible to extend the range of plate structures that can be analysed.

In 1948, Grinter initially proposed an equivalent grillage analogy for plane-stress problems which gradually became the most widely used computer aided method for analysing bridge deck structures. In 1950, Argyris, Turner and Clough et al developed the finite element technique for two-dimensional elastic structures. Since then this approach has become the most powerful analtytical technique at the present time. Its reputation is well deserved as it inherently possesses the versatility and accuracy desired by the engineer. The advent of modern computers extends its analytical ability enormously and it is widely available for computer aided analysis.

For the purpose of analysis in the present investigation, literature of the following approaches:

(i) Solution of orthotropic plate theory;
(ii) Approximate solution using an equivalent grillage system;
(iii) Approximate solution using the finite element method;

will be reviewed briefly in the following sections.

3.2 PLATE BENDING THEORY

A plate element with uniform thickness, t, is considered in Fig.3.1 with the origin in the mid-plane of the plate. The thickness of the plate is assumed small in comparison to the other dimensions of the element but the deflections are also assumed small when compared with that thickness. The Kirchhoff's hypothesis (16) for an elastic plate element can be applied as follows:

(i) normals to the mid-plane before bending remain normal to the mid-plane after bending;
(ii) the mid-plane remains unstrained during bending; and
(iii) the direct and shear stresses related to are z-axis negligible when compared with the other stresses, i.e. $\sigma z = \tau xz = \tau yz = 0$.

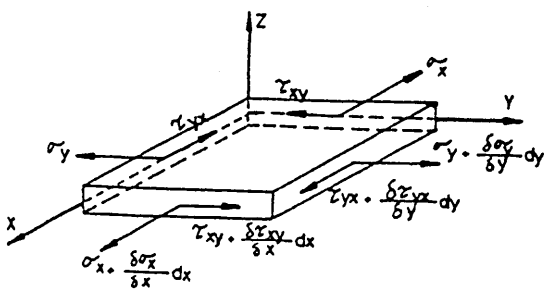

Fig.3.1 Stresses Acting on a Thin Plate Element

If a transvers load is applied on the plate element in z-direction, the displacements u and v in the direction of x and y axes, at any

point at a distance z from the middle plane in Fig.3.2 can be expressed in terms of the slope of the deflected plane by

$$u = -z.\frac{\partial w}{\partial x} \quad \text{and} \quad v = -z.\frac{\partial w}{\partial y} \tag{3.1}$$

where, w(x,y) is the deflection in the direction of the z axis.

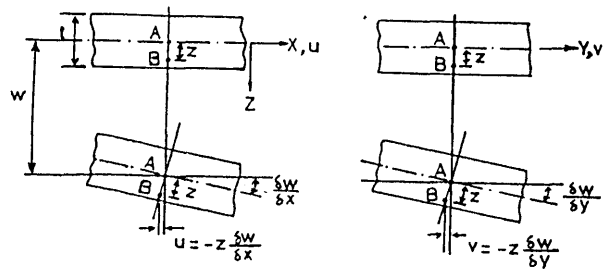

Fig.3.2 Deflection of a Thin Plate Element

The direct strains, εx and εy, at the same point are obtained by differentiating the first expression in Eqn.3.1 with respect to x, and the second with respect to y to give

$$\varepsilon x = \frac{\partial u}{\partial x} = -z.\frac{\partial^2 w}{\partial x^2}$$
$$\varepsilon y = \frac{\partial v}{\partial y} = -z.\frac{\partial^2 w}{\partial y^2} \tag{3.2}$$

The shear strain γxy, on the other hand, is obtained by differentiating the first expression in Eqn.3.1 with respect to y and the second expression with respect to x giving

$$\gamma xy = \frac{\partial u}{\partial y} + \frac{\partial v}{\partial x} = -2z.\frac{\partial^2 w}{\partial x \partial y} \tag{3.3}$$

Eqns.3.2 and 3.3 were derived by Cauchy (16). These strains can then be related to the direct and shear stresses according to Hooke's Law (16) in the matrix form:

$$\begin{Bmatrix} \varepsilon x \\ \varepsilon y \\ \gamma xy \end{Bmatrix} = \frac{1}{E} \begin{bmatrix} 1 & -\nu & 0 \\ -\nu & 1 & 0 \\ 0 & 0 & 2(1+\nu) \end{bmatrix} \begin{Bmatrix} \sigma x \\ \sigma y \\ \tau xy \end{Bmatrix} \qquad (3.4)$$

It is often necessary to express the stress/strain relationship in the inverse form in terms of the deformations as a set of homogeneous isotropic plate equations which are usually given in the form

$$\begin{Bmatrix} \sigma x \\ \sigma y \\ \tau xy \end{Bmatrix} = \frac{E.z}{(1-\nu^2)} \begin{bmatrix} 1 & \nu & 0 \\ \nu & 1 & 0 \\ 0 & 0 & (1-\nu) \end{bmatrix} \begin{Bmatrix} -\dfrac{\partial^2 w}{\partial x^2} \\ -\dfrac{\partial^2 w}{\partial y^2} \\ 2.-\dfrac{\partial^2 w}{\partial x \partial y} \end{Bmatrix} \qquad (3.5)$$

where E and ν are Young's modulus of elasticity and Poisson's ratio of the plate material respectively.

The stress distributions through the thickness of the plate can be seen in Fig.3.3 and these stress resultants are generally given in the following form:

$$Mx = \int_{-t/2}^{t/2} \sigma x.z.dz \quad ; \quad My = \int_{-t/2}^{t/2} \sigma y.z.dz$$

$$Mxy = -Myx = \int_{-t/2}^{t/2} \tau xy.z.dz \qquad (3.6)$$

$$Vx = \int_{-t/2}^{t/2} \tau xz.dz \quad ; \quad Vy = \int_{-t/2}^{t/2} \tau yz.dz$$

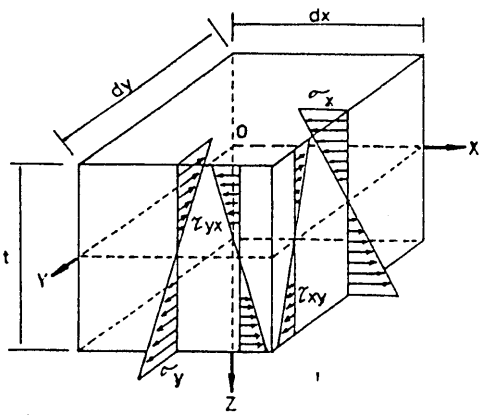

Fig.3.3 Distribution of Stresses on a Thin Plate Element

To solve for the stress resultants, the equilibrium and the compatibility of an element of the plate is considered as shown in Fig.3.4. For equilibrium, the sum of the moments about edges dx and dy, and the sum of the vertical forces are equal to zero. Thus

$$\begin{aligned} &\frac{\partial Vx}{\partial x} + \frac{\partial Vy}{\partial y} + p(x,y) = 0 \\ &\frac{\partial Mx}{\partial x} + \frac{\partial Myx}{\partial y} - Vx = 0 \\ &\frac{\partial Mxy}{\partial x} - \frac{\partial My}{\partial y} + Vy = 0 \end{aligned} \qquad (3.7)$$

These three equations can be combined to form a second order differential equation for a plate relating moments to load intensity in the form of

$$\frac{\partial^2 Mx}{\partial x^2} + 2.\frac{\partial^2 Mxy}{\partial x \partial y} + \frac{\partial^2 My}{\partial y^2} = -p(x,y) \qquad (3.8)$$

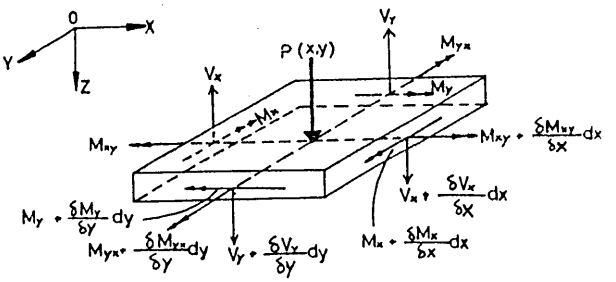

Fig.3.4 Free Body Diagram of a Thin Plate Element

Substituting the stresses from Eqn.3.5 into Eqn.3.6, the constitutive equations appropriate to classical plate bending thoery are given by

$$\begin{Bmatrix} Mx \\ My \\ Mxy \end{Bmatrix} = D \begin{bmatrix} 1 & \nu & 0 \\ \nu & 1 & 0 \\ 0 & 0 & (1-\nu)/2 \end{bmatrix} \begin{Bmatrix} -\dfrac{\partial^2 w}{\partial x^2} \\ -\dfrac{\partial^2 w}{\partial y^2} \\ 2.\dfrac{\partial^2 w}{\partial x \partial y} \end{Bmatrix} \qquad (3.9)$$

where, $$D = \frac{E.t^3}{12(1-\nu^2)}$$

There are no constitutive equations relating shear stresses to shearing displacements for classical plate theory because the shearing deformations are assumed to be negligible (16). As a result, the governing differential equation of classical isotropic plate bending can be obtained by combining the equilibrium and constitutive equations to give:

$$\frac{\partial^4 w}{\partial x^4} + 2.\frac{\partial^4 w}{\partial x^2 \partial y^2} + \frac{\partial^4 w}{\partial y^4} = \frac{-p(x,y)}{D} \qquad (3.10)$$

This formula is sometimes known as the 'Equation of Sophie Germain' (16) after the young French scientist who formulated the equation in 1815. It is conveniently written as,

$$(\nabla w)^4 = \frac{-p(x,y)}{D} \qquad (3.11)$$

where ∇ is the Laplacian operator. To obtain the solution (16) for a plate subjected to a given load intensity of p(x,y), a function w(x,y) must satisfy this governing fourth order equation and the boundary conditions of the plate.

3.2.1 Solutions for Plate Bending

The general approach to obtain a solution for a plate is based on the assumption that a suitable complementary function, which satisfies the governing equation but which is not necessary for the boundary conditions, is first found. A particular solution must then be determined which, in combination with the complementary function, would provide a complete solution to satisfy both the governing equation and boundary conditions. For a classical isotropic plate, the complementary displacement function, w_1, can be found (3,9,11,16,73,74) by reducing the governing Eqn.3.10 to

$$\frac{\partial^4 w_1}{\partial x^4} + 2\frac{\partial^4 w_1}{\partial x^2 . \partial y^2} + \frac{\partial^4 w_1}{\partial y^4} = 0 \qquad (3.12)$$

and its solution can be assumed in the series form

$$w_1(x,y) = \sum_m^\infty \sum_n^\infty Amn.Fmn(x,y) \qquad (3.13)$$

where, the function Amn is defined by an ordinary fourth-order differential equation, and the function Fmn is normally defined by a trigonometric series.

To satisfy the differential equation, the particular solution is established in a similar form to Eqn.3.11 as:

$$(\nabla)^4 w_2 = \frac{-p(x,y)}{D} \qquad (3.14)$$

where it is recommended that the load function p(x,y) is expressed in the form of a series similar to the complementary function. For the

particular solution, w_2 in Eqn.3.14 is also conveniently expressed in the form of a series similar to that of the load function. By combining the particular and the complementary solutions, the complete solution for the plate is given as $w(x,y) = w_1 + w_2$.

3.2.2 Navier's Solution

The solution for the plate bending problem was pioneered by Navier in 1820 and this solution is sometimes described as the solution of double trigonometric series (3). Consider a simply supported rectangular plate subjected to uniformly distributed load shown in Fig.3.5. The boundary conditions of the plate are:

(i) $w = 0$ at $x = 0$, a and $y = 0$, b
(ii) $Mx = 0$ at $x = 0$ and a
(iii) $My = 0$ at $y = 0$ and b

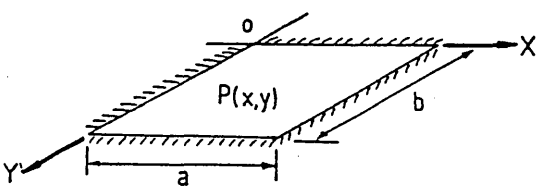

Fig.3.5 Simply Supported Rectangular Plate

Since the deflection and moment are zero at all edges, the complementary solution is not required i.e. $w_1 = 0$. Thus, the complete solution of the plate depends on the displacement function of the particular solution alone i.e. $w = w_2$. However, this displacement function, which must satisfy the above boundary conditions, is expressed in a form similar to the load function. The load function p(x,y) is expressed in the trigonometrical double series as

$$p(x,y) = \sum_{m}^{\infty} \sum_{n}^{\infty} Pmn.Fmn \qquad (3.15)$$

where, $$Fmn = \sin\left(\frac{m\pi x}{a}\right)\sin\left(\frac{n\pi y}{b}\right)$$

To satisfy Eqn.3.14 , the displacement function can then be written in a form similar to the load function

$$w2(x,y) = \sum_{m}^{\infty} \sum_{n}^{\infty} Bmn.Fmn \qquad (3.16)$$

Differentiating this equation with respect to x and y and then substituting the derivatives into the governing differential equation gives:

$$Pmn = D\pi^2.Bmn[(\frac{m}{a})^2 + (\frac{n}{b})^2]^2 \qquad (3.17)$$

Substituting the values from Eqns.3.15 to 3.17 into Eqn.3.11 and rearranging, the following integral form can be obtained:

$$Bmn = \frac{4}{D\pi^2N^2.a.b} \iint p(x,y).Fmn.dx.dy \qquad (3.18)$$

where, $$N = \left(\frac{m^2}{a^2} + \frac{n^2}{b^2} \right)$$

Then the double integral gives

$$\iint p(x,y).Fmn.dx.dy = \frac{4.p(x,y).a.b}{\pi^2 m.n} \qquad (3.19)$$

where, $m = 1,3,5.....$; $n = 1,3,5.....$

Substitution of this value in Eqn. 3.18 gives

$$Bmn = \frac{16.p(x,y)}{D\pi^6.m.n.N^2} \qquad (3.20)$$

Thus, the complete solution for the plate will be

$$w_2(x,y) = \frac{16.p(x,y)}{\pi^6 D} \sum_{m}^{\infty} \sum_{n}^{\infty} \frac{Fmn}{m.n.N^2} \qquad (3.21)$$

With the deflection of the plate expressed in Eqn.3.21, the moments at any point of the plate can then be determined as

$$Mx = \pi^2 D \sum_{m}^{\infty} \sum_{n}^{\infty} \left(\frac{m^2}{a^2} + \nu.\frac{n^2}{b^2}\right).Bmn.Fmn \qquad (3.22a)$$

$$My = \pi^2 D \sum_{m}^{\infty} \sum_{n}^{\infty} \left(\nu.\frac{m^2}{a^2} + \frac{n^2}{b^2}\right).Bmn.Fmn \qquad (3.22b)$$

$$Mxy = -\pi^2 D \sum_{m}^{\infty} \sum_{n}^{\infty} \frac{(1 - \nu).m.n}{a.b}.Bmn.Fmn' \qquad (3.22c)$$

where, $$Fmn' = \cos\left(\frac{m\pi x}{a}\right)\cos\left(\frac{m\pi y}{b}\right)$$

However, these equations were solved by Galerkin (16) for various dimensions of plates. The results of the mid-span displacement and moments are compiled in Table 3.1.

where,

$$w(x,y) = \alpha d.\frac{p(x,y).a^4}{E.t^3} \qquad (3.23)$$

$$Mx = \beta x.p(x,y).a^2$$

$$My = \beta y.p(x,y).a^2$$

The series of the complete solution is found to converge rapidly. Timoshenko (74) expanded only the first term of the series in Eqn.3.21 for the deflection of a square plate and gave

$$Wmax = 0.0454\frac{p(x,y).a^4}{E.t^3} \qquad (3.24)$$

This result is only about 2.5% differnt from the exact solution given in Table 3.1. However, the series in the bending and twisting moment equations have been found to converge much more slowly (9,16,74).

Table 3.1 Coefficients Obtained by Filoneuko-Borodich (16) for Simply Supported Rectangular Plates Subjected to Uniformly Distributed Load

b/a	αd	βx	βy
1.0	0.0443	0.0479	0.0479
1.1	0.0530	0.0553	0.0494
1.2	0.0610	0.0626	0.0501
1.3	0.0697	0.0693	0.0503
1.4	0.0770	0.0753	0.0506
1.5	0.0843	0.0812	0.0500
1.6	0.0906	0.0862	0.0493
1.7	0.0964	0.0908	0.0486
1.8	0.1017	0.0948	0.0476
1.9	0.1064	0.0985	0.0471
2.0	0.1106	0.1017	0.0464
3.0	0.1336	0.1189	0.0404
4.0	0.1400	0.1235	0.0384
5.0	0.1416	0.1246	0.0375
∞	0.1422	0.1250	0.0375

where, a is the shorter side of the plate;

3.2.3 Levy's Solution

The use of double series is inconvenient when derivatives of deflection are involved. An alternative method given by Levy is more general than Navier's solution. This method is valid for all cases with two opposite edges simply supported and the others may be supported in any manner. For the simply supported, infinitely wide slab, shown in Fig.3.6, which is commonly used as the basis of bridge deck analysis, the complementary function can be found in the same way as before by replacing the governing equation with the reduced form as in Eqn. 3.12. The deflection function in this case is assumed to be the trigonometric series

$$w_1 = \sum_{n}^{\infty} Yn(y).\sin(n\pi x/a) \qquad (3.25)$$

where, the functions Yn(y) are defined by differential equation of the fourth order (4,54,101,105) with respect to y,

$$(n')^4.Yn(y) - 2.(n')^2.Yn(y)^2 + Yn(y)^4 = 0 \qquad (3.26)$$

where, $n' = n\pi/a$

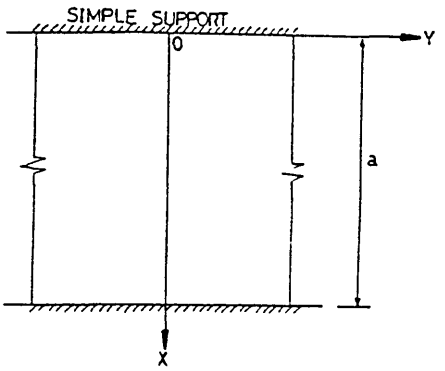

Fig.3.6 Simply Supported Plate with Infinite Width

The general solution for this homogeneous equation was developed by Filon (101) as

$$Y = A.\cosh(\lambda y) + B.\lambda y.\sinh(\lambda y) + C.\sinh(\lambda y) + D.\lambda y.\cosh(\lambda y) \qquad (3.27)$$

where, A,B,C and D are arbitrary constants.

Replacing the coefficients of function $\lambda = n'$, the solution of the deflection function becomes

$$Yn(y) = An.\cosh(n'y) + Bn.n'y.\sinh(n'y) + Cn.\sinh(n'y) + Dn.n'y.\cosh(n'y) \qquad (3.28)$$

Since the width of the plate is infinite in the y-direction, the load function is assumed to be a similar trigonometric series expressed in the x-direction as follows:

$$P(x) = \sum_{n}^{\infty} Pn.\sin(n\pi x/a) \qquad (3.29)$$

where,
$$Pn = \frac{4.p(x)}{\pi.n} \qquad (3.30)$$

The displacement funtion in the particular integral is taken conveniently in the form of

$$w_2 = \sum_{n}^{\infty} Wn.\sin(n\pi x/a) \tag{3.31}$$

Substituting these relations into Eqn. 3.14 yields

$$\left(\frac{n\pi}{a}\right)^4 Wn = \frac{4.p(x)}{D.\pi n}$$

Thus,
$$Wn = \frac{4.p(x).a^4}{n^5\pi^5 D} \tag{3.32}$$

Therefore, the displacement function can be determined in the following form

$$w_2 = \sum_{n}^{\infty} \frac{4.p(x).a^4}{n^5\pi^5 D}.\sin\left(\frac{n\pi x}{a}\right) \tag{3.33}$$

Hence, the complete solution will be

$$w = \sum_{n}^{\infty} \left[\frac{4.p(x).a^4}{n^5\pi^5 D} + Yn(y)\right].\sin\left(\frac{n\pi x}{a}\right) \tag{3.34}$$

Using symmetry about the y-axis, Cope and Clark (9) eliminated the coefficients Cn and Dn, and found the expressions for the coefficients An and Bn to be

$$An = -\left\{\frac{2p(x).a^4\left[\frac{n\pi b}{2.a}.\tanh\left(\frac{n\pi b}{2.a}\right) + 2\right]}{D.\pi^5.n^5\cosh\left(\frac{n\pi b}{2.a}\right)}\right\} \tag{3.35a}$$

$$Bn = \frac{2.p(x).a^4}{D.\pi^5.n^5.\cosh\left(\frac{n\pi b}{2.a}\right)}.\left(\frac{n\pi b}{2.a}\right) \qquad (3.35b)$$

Using these solutions, the mid-span deflection and moments can be obtained as follows:

$$w = \sum_{n}^{\infty}\left[\frac{4.p(x).a^4}{n^5\pi^5.D} - An.\cosh\left(\frac{n\pi y}{a}\right) + Bn.\frac{n\pi y}{a}.\sinh\left(\frac{n\pi y}{a}\right)\right.$$

where, $n = 1,3,5\ldots$ (3.36)

$$Mx = \frac{p(x)(a-x)}{2} + p(x).a^2.\pi^2(1-\nu).\sum_{n}^{\infty} n^2\{An.\cosh(n'y) + Bn[(n'y).\sinh(n'y) - \frac{2\nu}{(1-\nu)}.\cosh(n'y)]\}.\sin\left(\frac{n\pi x}{a}\right) \qquad (3.37a)$$

$$My = \frac{\nu.p(x)(a-x)}{2} - p(x).a^2.\pi^2(1-\nu).\sum_{n}^{\infty} n^2\{An.\cosh(n'y) + Bn[(n'y).\sinh(n'y) - \frac{2}{(1-\nu)}.\cosh(n'y)]\}.\sin\left(\frac{n\pi x}{a}\right) \qquad (3.37b)$$

$$Mxy = p(x).a^2.\pi^2(1-\nu).\sum_{n}^{\infty} n^2\{An.\sinh(n'y) + Bn[\sinh(n'y) + (n'y).\cosh(n'y)]\}.\cos(n'x) \qquad (3.37c)$$

This method of solution is more convenient than Navier's solution owing to the good convergence of the corresponding series. This was demonstrated by Timoshenko (74) who expanded the first two terms of the series of Eqn.3.34 for a square plate which gave

$$W_{max} = \left[\frac{5}{384} - \frac{4}{\pi^2}(0.68562 - 0.00025 + ...)\right]\frac{-p(x).a^4}{D}$$

$$= 0.00406\frac{-p(x).a^4}{D}$$

$$= 0.04433\frac{-p(x).a^4}{D.t^3} \qquad (3.38)$$

The second term of the series appears to be negligible, and considering only the first term of the series, the coefficient of deflection is correct to five decimal places compared to that obtained by Navier's solution in Table 3.1. Based on Levy's solution, Timoshenko obtained a set of results, tabulated in Table 3.2, which is more or less identical to Table 3.1, the only difference being that Timoshenko conveniently expressed the deflection coefficients αd, in terms of the flexural rigidity of the plate as

$$W_{max} = \alpha d.\frac{-p(x).a^4}{D} \qquad (3.39)$$

Table 3.2 Coefficients Obtained by Timoshenko for Simply Supported Rectangular Plates Subjected to Uniformly Distributed Load

b/a	αd	βx	βy
1.0	0.00406	0.0479	0.0479
1.1	0.00485	0.0554	0.0493
1.2	0.00564	0.0627	0.0501
1.3	0.00638	0.0694	0.0503
1.4	0.00705	0.0755	0.0502
1.5	0.00772	0.0812	0.0498
1.6	0.00830	0.0862	0.0492
1.7	0.00883	0.0908	0.0486
1.8	0.00931	0.0948	0.0479
1.9	0.00974	0.0985	0.0471
2.0	0.01013	0.1017	0.0464
3.0	0.01223	0.1189	0.0406
4.0	0.01282	0.1235	0.0384
5.0	0.01297	0.1246	0.0375
∞	0.01302	0.1250	0.0375

Table 3.3 Coefficients Obtained by Timoshenko For Built-in Supported Rectangular Subjected to Uniformly Distributed Load

b/a	αd	βx'	βy'	βx	βy
1.0	0.00126	-0.0513	-0.0513	0.0231	0.0231
1.1	0.00150	-0.0581	-0.0538	0.0164	0.0231
1.2	0.00172	-0.0639	-0.0554	0.0199	0.0228
1.3	0.00191	-0.0687	-0.0563	0.0327	0.0222
1.4	0.00207	-0.0726	-0.0568	0.0349	0.0212
1.5	0.00220	-0.0757	-0.0570	0.0368	0.0203
1.6	0.00230	-0.0780	-0.0571	0.0381	0.0193
1.7	0.00238	-0.0799	-0.0571	0.0392	0.0182
1.8	0.00245	-0.0812	-0.0571	0.0401	0.0174
1.9	0.00249	-0.0822	-0.0571	0.0407	0.0165
2.0	0.00254	-0.0829	-0.0571	0.0412	0.0158
∞	0.00260	-0.0833	-0.0571	0.0417	0.0125

where,

$$w = \alpha d.\frac{-p(x,y)a^4}{D}$$

$$Mx,y = \beta n.-p(x,y)a^2 \qquad (n = x', y', x \text{ and } y)$$

The close resemblance of these coefficients from both solutions suggests the validity of both methods applied to plate structures. Similarly, the results obtained by Timoshenko (74) for deflections and bending moments for uniformly loaded rectangular plates with all edges built-in are considered useful and therefore presented in Table 3.3. These results will be used as the basis for verifying the accuracy of the computer based simulations for the slab models.

3.3 ORTHOTROPIC PLATE THEORY

Reinforced slab decks are often regarded as orthotropic slabs due to their different stiffnesses in the orthogonal directions. It can be idealized by assuming the slab to be made of a homogeneous material with orthotropic elastic properties. The governing stress and strain relationship for the case of plane stress in x-y plane, with the x and

y axes positioned parallel to the material property axes, can be expressed in terms of three elastic constants, Ex, Ey and G, and Poisson's ratios, νx and νy, in the matrix form of

$$\begin{Bmatrix} \sigma x \\ \sigma y \\ \tau xy \end{Bmatrix} = \begin{bmatrix} Ex' & \nu y.Ex' & 0 \\ \nu x.Ey' & Ey' & 0 \\ 0 & 0 & G \end{bmatrix} \begin{Bmatrix} \varepsilon x \\ \varepsilon y \\ \gamma xy \end{Bmatrix} \qquad (3.40)$$

where, $Ex' = \dfrac{Ex}{1-\nu x.\nu y}$; $Ey' = \dfrac{Ey}{1-\nu x.\nu y}$

Ex and Ey are Young's moduli of elasticity, and νx and νy are Poisson's ratios in the direction of x and y axes respectively.

The Poisson's effect in the slab deck is mainly attributed to the material i.e. either steel or concrete. Therefore, this effect can be simplified (3) as:

$$\nu x.Ey' = \nu y.Ex' = E'' \qquad (3.41)$$

Substituting the stress from Eqn.3.40 into Eqn.3.9, the constitutive equations appropriate to classical plate thoery become

$$\begin{Bmatrix} Mx \\ My \\ Mxy \end{Bmatrix} = \begin{bmatrix} Dx & D_1 & 0 \\ D_1 & Dy & 0 \\ 0 & 0 & Dxy \end{bmatrix} \begin{Bmatrix} -\dfrac{\partial^2 w}{\partial x^2} \\ -\dfrac{\partial^2 w}{\partial y^2} \\ 2.-\dfrac{\partial^2 w}{\partial x \partial y} \end{Bmatrix} \qquad (3.42)$$

where, $Dx = \dfrac{Ex'.t^3}{12}$ or $\dfrac{Ex.t^3}{1-\nu x.\nu y}$

$Dy = \dfrac{Ey'.t^3}{12}$ or $\dfrac{Ey.t^3}{1-\nu x.\nu y}$

$$D_1 = \frac{Ex''.t^3}{12} \quad ; \quad Dxy = \frac{G.t^3}{12}$$

Therefore, the governing differential equation of classical orthotropic plate bending can be rearranged as

$$Dx.\frac{\partial^4 w}{\partial x^4} + 2(D_1 + 2Dxy).\frac{\partial^4 w}{\partial x^2 \partial y^2} + Dy\frac{\partial^4 w}{\partial y^4} = -p(x,y) \qquad (3.43)$$

With plate systems spanning in two directions, the effects of load are distributed among the longitudinal and transverse elements in direct proportion to their stiffnesses. Plates of orthotropic materials have important applications owing to their direction-dependent properties. The classical orthotropic plate equation given in Eqn.3.43 is often far too difficult to be applied and used for design purposes. This gives rise to various approximate solutions which may inevitably affect the accuracy of the results. For these reasons the application of both the classical and the approximate solutions is confined to a limited range of problems.

Owing to possible differences in the shape of the sections in x and y directions, the torsional rigidities Dxy and Dyx, and the coupling rigidities $D_1 x$ and $D_1 y$ are not necessarily equal but for simplicity they are normally considered to be so. For some practical analyses, the effects of the coupling rigidities are so small that they can conveniently be ignored.

3.3.1 Orthotropic Plate Theory as Applied to Flat Slab Deck

In 1923, Huber (3,9,11,44), pioneered the application of this orthotropic plate theory in the analysis of reinforced concrete slabs and bridges. By replacing the torsional and coupling rigidities of an orthotropic plate by a single torsional constant H, Huber reduced the differential equation to the simpler form

$$Dx.\frac{\partial^4 w}{\partial x^4} + 2H.\frac{\partial^4 w}{\partial x^2 \partial y^2} + Dy.\frac{\partial^4 w}{\partial y^4} = -p(x,y) \qquad (3.44)$$

where, $H = D_1 + 2Dxy$

Applying Navier's approach to a simply supported rectangular plate subjected to uniformly distributed load, Huber gave the solution for the displacement as

$$W = \frac{16.p(x,y)}{\pi^6} \sum\sum \frac{\sin(m\pi x/a).\sin(n\pi y/b)}{m.n.Fo} \qquad (3.45)$$

where, $Fo = \left(\frac{m}{a}\right)^4.Dx + 2\left(\frac{m.n}{a.b}\right)^2.H + \left(\frac{n}{b}\right)^4.Dy$

Based on the assumption of $H = \sqrt{(Dx.Dy)}$, Huber then evaluated a set of coefficients , and given in Table 3.4 for orthotropic plates with a range of side ratios from 1.0 to ∞. The deflections and bending moments of the plate can be conveniently determined from the following equations.

Table 3.4 Huber's Coefficients for Simply Supported Rectangular Orthotropic Plates, with $H = \sqrt{(Dx.Dy)}$, Subjected to Uniformly Distributed Load Extracted From Timoshenko and Woinowisky-Krieger

b/a	αd	βx	βy
1.0	0.00407	0.0368	0.0368
1.1	0.00488	0.0359	0.0447
1.2	0.00565	0.0344	0.0524
1.3	0.00639	0.0324	0.0597
1.4	0.00709	0.0303	0.0665
1.5	0.00772	0.0280	0.0728
1.6	0.00831	0.0257	0.0785
1.7	0.00884	0.0235	0.0837
1.8	0.00932	0.0214	0.0884
1.9	0.00974	0.0191	0.0929
2.0	0.01013	0.0174	0.0964
2.5	0.01150	0.0099	0.1100
3.0	0.01223	0.0055	0.1172
4.0	0.01282	0.0015	0.1230
5.0	0.01297	0.0004	0.1230
∞	0.01302	0.0000	0.1245

$$Wmax = \alpha d.\frac{p(x,y).b^4}{Dy}$$

$$Mx = [\beta x + \beta y.\frac{E''}{E'x}\sqrt{(\frac{Dx}{Dy})}].\frac{p(x,y).a^2}{\epsilon h} \qquad (3.46)$$

$$My = [\beta x + \beta y.\frac{E''}{E'y}\sqrt{(\frac{Dx}{Dy})}].p(x,y).b^2$$

where, $$\epsilon h = \frac{a.Dy}{b.Dx} \qquad (3.47)$$

After Huber, the concept of considering a bridge slab as an orthotropic plate for the purpose of stress analysis was accepted. This development was followed in 1946 by Guyon who applied the method to analyse a torsionless deck and provided a simplified solution for orthotropic plates of negligible torsional rigidity. Later in 1950, Massonnet derived generally valid relationships from the principles given by Guyon and extended the method to apply to the analysis of slab decks by taking account of the torsional rigidty of the deck only. The bases and the derivations using Guyon-Massonnet approach will be summarized as orthotropic plate theory in sections 3.3.2 as applied to a grillage system. But here, Levy's solution of an infinitely wide slab, subjected to uniformly distributed load in Fig.3.6, is useful which develops the relationship between the rigidities of the slab. The load function is

$$p(x) = \sum_{n}^{\infty} Pn.\sin(n\pi x/L) \qquad (3.48)$$

The displacement function to satisfy the boundary conditions is

$$w = \sum_{n}^{\infty} Yn(y).\sin(n\pi x/L) \qquad (3.49)$$

where, the function Yn(y), in this case, is expressed in exponential form

$$Yn(y) = A.\exp(\theta n.y) \qquad (3.50)$$

With zero load applied to the slab, the homogeneous differential equation becomes

$$Dn.\theta n^4 - 2.H.\left(\frac{n\pi}{L}\right)^2.\theta n^2 + Dx.\left(\frac{n\pi}{L}\right)^4 = 0 \qquad (3.51)$$

where, H is Huber's torsional constant.

This equation can be solved as a quadratic equation giving the root of:

$$\theta n = \pm\frac{n.\pi}{L}\sqrt{\left(\frac{H}{Dy} \pm \sqrt{\left[\frac{(H^2 - Dx.Dy)}{Dy}\right]}\right)} \qquad (3.52)$$

Based on this characteristic equation, Cusens and Pama (11) clarified three different cases for bridge decks to be dealt with by considering the relationship between flexural and torsional rigidities as follows:

(1) Torsionally stiff and/or flexurally weak bridge decks
i.e. $H^2 \geq Dx.Dy$

(2) Isotropic bridge decks
i.e. $H^2 = Dx = Dy$

(3) Torsionally weak and/or flexurally stiff bridge decks
i.e. $H^2 \leq Dx.Dy$

From these cases, it can be seen that the torsional rigidity of a slab is, in fact, a function of the flexural rigidities of the slab. Guidelines for the solutions of these three cases are described in details elsewhere (9,11).

It is appropriate here to summarize the theoretical development of flat slab analysis as follows:

(1) Reinforced concrete slab structures can be analysed as an orthotropic plate with homogeneous elastic properties. Based on this assumption, the slab can be solved by appropriate method of solution with an acceptable level of accuracy. Solutions for the orthotropic differential equations indicate that only a limited range of slabs can be analysed owing to the restrictions on the geometric shape, loading and boundary conditions.

(2) It is clear that the distributions of elastic stresses and deformations in a plate under various forms of transverse load are dependent upon the flexural and torsional rigidities of the slab. Accurate means of assessing the rigidities of the plate are of paramount importance, particularly for those using the approximate solutions.

(3) The exact solutions obtained by Navier and Levy can be used as a basis to verify the accuracy of the software packages such as GRIDS and LUSAS/AN which have been used extensively in the present work.

3.3.2 Orthotropic Plate Theory as applied to a Grillage System

A grillage is an assembly of beams with monolithic intersections which for the purposes of analysis may be idealised as an orthotropic plate and then analysed by equivalent plate thoery. Consider a section of a grillage as shown in Fig.3.7 where the spacings of the beams are Sx and Sy, and the widths are bx and by in the directions of x and y axes respectively. Since the beams are only connected at the intersections, the overall Possion's ratio effect on the stress-strain relationship should be modified accordingly by the ratios of bx/Sx and by/Sy (3,11). Therefore, the average strains in the direction of x and y axes may be written as

$$\varepsilon x = \frac{\sigma x}{Ex} - \nu y \cdot \frac{\sigma y}{Ey} \cdot \left(\frac{by}{Sy}\right)$$

$$\varepsilon y = \frac{\sigma y}{Ey} - \nu x \cdot \frac{\sigma x}{Ex} \cdot \left(\frac{bx}{Sx}\right) \qquad (3.53)$$

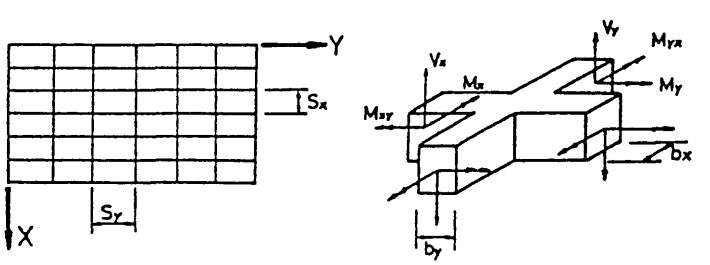

Fig.3.7 Free Body Diagram of a Grillage Element

These stress-strain equations can conveniently be expressed in the following matrix form

$$\begin{Bmatrix} \sigma x \\ \\ \sigma y \end{Bmatrix} = \frac{-z}{1-\nu x.\nu y.\frac{bx.by}{Sx.Sy}} \begin{bmatrix} Ex & Ex.\nu y.\frac{by}{Sy} \\ Ey.\nu x.\frac{bx}{Sx} & Ey \end{bmatrix} \begin{Bmatrix} \frac{\partial^2 w}{\partial x^2} \\ \\ \frac{\partial^2 w}{\partial y^2} \end{Bmatrix} \qquad (3.54)$$

The distribution of strains and stresses are shown in Fig.3.8. The moment resultants can then be obtained by integrating the stress over the depth of the beam section with respect to x and y axes.

$$\begin{Bmatrix} Mx \\ \\ My \end{Bmatrix} = \begin{bmatrix} Dx' & D_1' \\ \\ D_2' & Dy' \end{bmatrix} \begin{Bmatrix} \frac{\partial^2 w}{\partial x^2} \\ \\ \frac{\partial^2 w}{\partial y^2} \end{Bmatrix} \qquad (3.55)$$

where,

$$Dx' = \frac{Ex".t^3.bx}{12.Sx}$$

$$Dy' = \frac{Ey".t^3.by}{12.Sy}$$

$$D_1' = \frac{\nu y.Ex".t^3.bx.by}{12.Sx.Sy}$$

$$D_2' = \frac{\nu x.Ey".t^3.bx.by}{12.Sx.Sy}$$

$$Ex" = \frac{Ex'}{1-\nu x.\nu y.\frac{bx.by}{Sx.Sy}}$$

$$Ey" = \frac{Ey'}{1-\nu x.\nu y.\frac{bx.by}{Sx.Sy}}$$

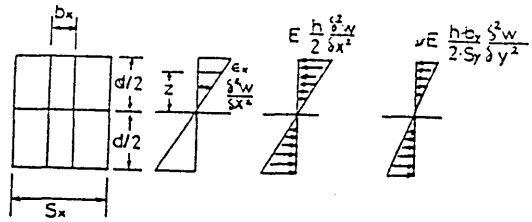

Fig.3.8 Distribution of Stresses and Strains of a Grillage Element

The twisting moments caused by the twist of the individual beams become

$$Mxy = Dxy' \cdot \frac{\partial^2 w}{\partial x \partial y} \quad ; \quad Myx = Dyx' \cdot \frac{\partial^2 w}{\partial x \partial y} \tag{3.56}$$

where

$$Dxy' = \frac{Tx}{Sx} \quad ; \quad Dyx' = \frac{Ty}{Sy}$$

and Tx and Ty are the torsional rigidites of the individual beams.

Subsituting Eqns.3.55 and 3.56 into the equilibrium equation 3.44, the total torsional rigidity, 2H, becomes

$$2H = Dxy' + Dyx' + \frac{(\nu x.Ey'' + \nu y.Ex'')t^3}{12} \cdot \left(\frac{bx.by}{Sx.Sy}\right) \tag{3.57}$$

For a concrete grillage, the values of Possion's ratio and the dimensional parameter ratios (bx.by/Sx.Sy) are normally small. Therefore, for some practical approximate analyses (16), the third terms of Eqn.3.57 can be ignored. The reduced governing equation for the equivalent beam grillage therefore becomes,

$$Dx' \frac{\partial^4 w}{\partial x^4} + (Dxy' + Dyx') \frac{\partial^4 w}{\partial x^2 \partial y^2} + Dy' \frac{\partial^4 w}{\partial y^4} = -p(x,y) \tag{3.58}$$

3.3.3 Orthogonal Plate Theory as applied to Ribbed Plate

A ribbed plate may be regarded as a grillage monolithic with a top slab. The behaviour of this system is closely comparable with the behaviour governed by the two structural systems mentioned in Sections 3.3.1 and 3.3.2. A solution of this system may be derived from these bases of plate bending theory and grillage analogy. For the purpose of analysis in the present investigation, the cross-sections of the ribbed plate are made to be identical in the x and y axes. The elastic modulus and Poisson's ratio of concrete are used for the top slab and the grillage. The stress-curvature equations for top slab element of the ribbed plate at a distance Z from the neutral axis as shown in Fig.3.9 can be reduced from Eqn.3.5 to

$$\begin{Bmatrix} \sigma x \\ \\ \sigma y \end{Bmatrix} = \frac{-E.z}{(1-\nu^2)} \begin{bmatrix} 1 & \nu \\ \\ \nu & 1 \end{bmatrix} \begin{Bmatrix} \dfrac{\partial^2 w}{\partial x^2} \\ \\ \dfrac{\partial^2 w}{\partial y^2} \end{Bmatrix} \qquad (3.59)$$

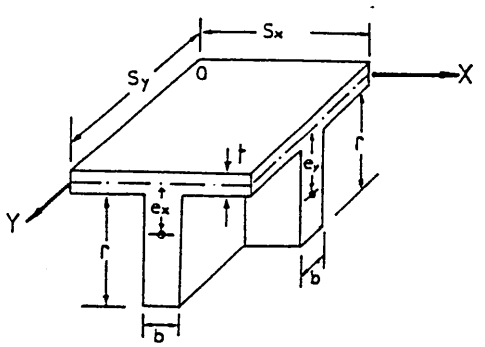

Fig.3.9 Notations for a Ribbed Plate Element

Similarly, as for the beam grillage, the stress-curvature equations can be reduced and modified from Eqn.3.54 to give:

$$\begin{Bmatrix} \sigma x \\ \\ \sigma y \end{Bmatrix} = \frac{-E.z}{\dfrac{bx.by}{Sx.Sy}(1-\nu^2)} \begin{bmatrix} 1 & \nu\dfrac{by}{Sy} \\ \\ \nu\dfrac{bx}{Sy} & 1 \end{bmatrix} \begin{Bmatrix} \dfrac{\partial^2 w}{\partial x^2} \\ \\ \dfrac{\partial^2 w}{\partial y^2} \end{Bmatrix} \qquad (3.60)$$

In this structural system, the top slab is assumed to be monolithic with the beam grillage, and the intersections of the beams are assumed to be rigidly connected. The distribution of the direct stress through the overall depth of an element can be represented by the combination of two stress blocks as shown in Fig.3.10. The moment resultant Mx per unit thickness, t, is obtained by taking moments of each individual force about the centre of the slab (11,12). Thus

$$Mx = -\frac{\partial^2 w}{\partial x^2}\left[\frac{E't^3}{12} + \frac{E''bx}{6Sx}\{[r - (ex - 0.5t)]^2 .(2r + ex + t) - (ex - 0.5t)^2 .(ex + t)\}\right]$$

$$- \frac{\partial^2 w}{\partial y^2}\left[\frac{\nu E't^3}{12} + \frac{\nu E''bx.by}{6Sx.Sy}\{[r - (ey - 0.5t)]^2 .(2r + ey + t) - (ey - 0.5t)^2 .(ey + t)\}\right] \qquad (3.61)$$

where,

$$Dx = \frac{E't^3}{12} + \frac{E''bx}{6Sx}\{[r - (ex - 0.5t)]^2 .(2r + ex + t) - (ex - 0.5t)^2 .(ex + t)\}$$

$$D_1 = \frac{\nu E't^3}{12} + \frac{\nu E''bx.by}{6Sx.Sy}\{[r - (ey - 0.5t)]^2 .(2r + ey + t) - (ey - 0.5t)^2 .(ey + t)\}$$

$$E' = \frac{E}{(1 - \nu^2)}$$

$$E'' = \frac{E}{(1 - \nu^2)\frac{bx.by}{Sx.Sy}}$$

Similarly the bending moment My is

$$My = -\frac{\partial^2 w}{\partial y^2}\left[\frac{E't^3}{12} + \frac{E''by}{6Sy}\{[r - (ey - 0.5t)]^2 .(2r + ey + t) - (ey - 0.5t)^2 .(ey + t)\}\right]$$

$$- \frac{\partial^2 w}{\partial x^2}\left[\frac{\nu E't^3}{12} + \frac{\nu E''bx.by}{6Sx.Sy}\{[r - (ex - 0.5t)]^2 .(2r + ex + t) - (ex - 0.5t)^2 .(ex + t)\}\right] \qquad (3.62)$$

where,

$$Dy = \frac{E't^3}{12} + \frac{E''by}{6Sy}\{[r - (ey - 0.5t)]^2 .(2r + ey + t) - (ey - 0.5t)^2 .(ey + t)\}$$

$$D_2 = \frac{\nu E't^3}{12} + \frac{\nu E''bx.by}{6Sx.Sy}\{[r - (ex - 0.5t)]^2 .(2r + ex + t) - (ex - 0.5t)^2 .(ex + t)\}$$

where, ex and ey are the distances measured from the centroid of the section to the mid-plane of the slab for both orthogonal directions.

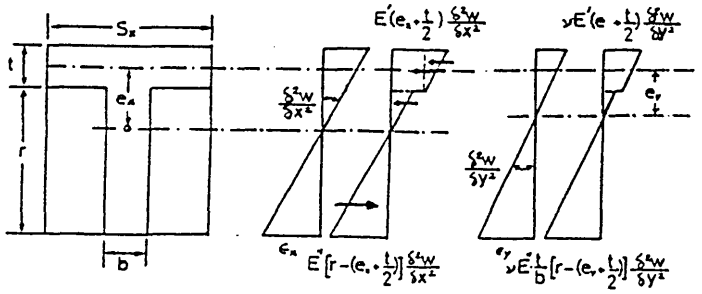

Fig.3.10 Distribution of Stresses and Strains of a Ribbed Plate Element

The twisting moments of the ribbed plate element may be determined in a way similar to that for the grillage system by considering separately the contributions from the top plate and the grillage of beams. Thus

$$Mxy = \left[\frac{Tx}{Sx} + \int_{slab} \tau xy.z.dA\right].\frac{\partial^2 w}{\partial x \partial y} \qquad (3.63)$$

$$= \left[Dxy' + \frac{G.t^3}{6}\right].\frac{\partial^2 w}{\partial x \partial y}$$

Similarly,

$$Myx = \left[Dyx' + \frac{G.t^3}{6}\right].\frac{\partial^2 w}{\partial x \partial y} \qquad (3.64)$$

Hence, the torsional rigidities of a ribbed plate are

$$Dxy = Dxy' + \frac{G.t^3}{6}$$

$$Dyx = Dyx' + \frac{G.t^3}{6} \qquad (3.65)$$

Therefore the total torsional rigidity 2H of a ribbed plate is given by

$$2H = Dxy' + Dyx' + \frac{Gt^3}{3} + \frac{\nu E'bx.by}{2Sx.Sy}.r\{h[h - (ex + ey)] + \frac{r}{3}\} \qquad (3.66)$$

From this equation it is seen that the total torsional rigidity of a ribbed plate is composed of the contributions of the beam grillage, the top plate and the effect of the interconnections of the top slab and grillage of beams. Giencke in 1955 (11) and Cusens, Zeidan and Pama in 1952 (12) derived the total torsional rigidity of a T-beam bridge deck in a form similar to Eqn.3.66. Since the eccentricities ex and ey of the section vary with the curvature, there are no definite values for ex and ey. However, Cusens and Pama expressed all

the horizontal forces acting in the x-direction, in relation to the stress distribution shown in Fig.3.10 as

$$\frac{\partial^2 w}{\partial x^2}\{E'ex.t.Sx + E''(ex - 0.5t) - E''[r - (ex - 0.5t)]^2 0.5bx\}$$

$$+ \frac{\partial^2 w}{\partial y^2}(\nu E'ey.t.Sx + \nu E''(ey - 0.5t)^2 . \frac{bx.by}{2Sy}$$

$$\nu E''[r^2 - (ex - 0.5t)]^2 . \frac{bx.by}{2Sy} = 0 \qquad (3.67)$$

Since the Poisson's ratio of concrete is small, the effect of the bending stress due to the curvature $\partial^2 w/\partial y^2$ was ignored by Cusens et al. Therefore, the equilibrium Eqn.3.67 reduces to

$$E'.ex.t.Sx + E''(ex - 0.5t)-[r - (ex - 0.5t)]^2 0.5bx = 0 \qquad (3.68)$$

And this equation can be rearranged as

$$ex = \frac{bx.r.(r + t)}{2(\frac{E'}{E''}.t.Sx + bx.r)} \qquad (3.69)$$

The term ex is interpreted by Cusens et al as the distance of the centre of the top slab from the centroidal axis of Tee-section in the x direction. The same assumptions and procedures are applied to the y direction which yield

$$ey = \frac{by.r.(r + t)}{2(\frac{E'}{E''}.t.Sy + by.r)} \qquad (3.70)$$

Using these values of ex and ey suggested by Cusens at el, the elastic flexural and torsional rigidities of the T-beam bridge deck can be determined from the above equations.

3.3.4 Flexural and Torsional Rigidities of Ribbed Slabs

Several other forms of elastic flexural and torsional rigidities in addition to those obtained by Cusens et al are presented here using the following notations:

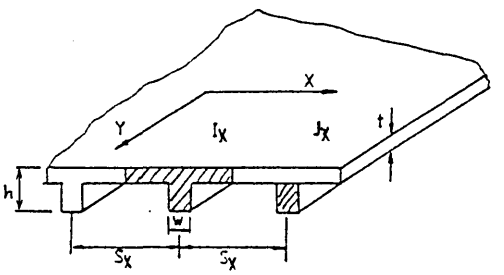

Fig.3.11 Notations for a One-way Ribbed Slab

G is the elastic shear modulus of the plate;
b is the width of the ribs;
t is the thickness of the slab;
h is the overall depth of the slab;
Ix and Iy are the second moments of area of the T-sections about x and y directions respectively;
Rx and Ry are the polar second moments of area of the ribs about x and y directions respectively;
Jx and Jy are the polar second moments of area of the grillage element about x and y directions respectively;
Sx and Sy are the rib spacings in x and y directions respectively.

Timoshenko (74) and Ugural (78) both recommend the very similar formulae for the rigidities of an orthotropic plate, reinforced by a set of equidistant ribs, spanning in one direction as shown in Fig.3.11 as

$$Dy = \frac{E.Sy.t^3}{12.[Sy - b + b.(t/h)]}$$

$$Dx = \frac{E.Ix}{Sx} \quad ; \quad D_1 = 0 \qquad (3.71)$$

$$Dxy = \frac{E.t^3}{12} + \frac{G.Rx}{Sx}$$

Powell and Ogden (58) conducted an analysis of orthotropic steel plate bridge decks in 1969 and they proposed a very similar procedure to obtain flexural and torsional rigidities as above except that,

(i) Dx is assumed to be the second moment of area of the deck slab per unit width, multiplied by $1/(1-\nu c^2)$; and
(ii) Gxy is determined by any empirical or semi-rational procedure for the T-section.

Clark (8) put forward a set of similar procedures for the beam- and slab-system spanning in two directions using the notations in Fig.3.12 applied in x and y directions,

$$Dx = \frac{E.Ix}{Sx} \quad ; \quad Dy = \frac{E.Iy}{Sy} \quad ; \quad D_1 = 0$$

$$Dxy = \frac{G.t^3}{12} + \frac{G}{4}.\left(\frac{Rx}{Sx} + \frac{Ry}{Sy}\right) \qquad (3.72)$$

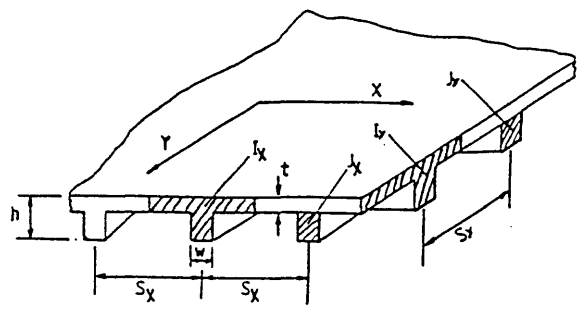

Fig.3.12 Notations for a Two-way Ribbed Slab

The values of the elastic rigidities for open grillage analysis can be obtained from these equations provided that a modification is made in

the polar second moments of area as follows:

$$J_{x,y} = R_{x,y} + \frac{S_{x,y}.t^3}{6} \qquad (3.73)$$

In the same manner, Timoshenko (74) also modified the torsional rigidities to facilitate the grillage analysis. The flexural rigidities are exactly the same as those in Eqn.3.72 but the torsional rigidity is modified in the form of

$$D_{xy} = \frac{J_x}{S_x} + \frac{J_y}{S_y} \qquad (3.74)$$

More recently, in 1983, Clark and Cope (9) proposed a unified idealization for a ribbed slab, spanning in two directions. The flexural rigidities are obtained as in Eqn.3.72, and torsional rigidities are given as below:

$$D_{xy} = \frac{E.t^3}{12.(1+\nu)} + \frac{E}{8.(1-\nu)}.\left(\frac{J_x}{S_x} + \frac{J_y}{S_y}\right)$$

$$D_1 = \frac{\nu.E.t^3}{12.(1-\nu^2)} \qquad (3.75)$$

The importance of the elastic rigidities has already been discussed. For flexural rigidity, conventional methods of obtaining second moments of area about the centroid of the Tee-section are likely to be predominantly adopted, and this was confirmed by Cusens et al (110). The analysis by Timoshenko (74) for a ribbed plate spanning in one direction appears to over-estimate (12) the flexural rigidity in the orthogonal direction. However, for a ribbed plate with equidistant ribs in two directions the flexural rigidities in both orthogonal directions can be determined adequately using conventional methods for second moments of area (8,9,12).

For Torsional rigidity, a general method of estimation based on the summation of the separate values applying to the components of the

T-section was proposed by Timoshenko and Goodier (73); it was then proved experimentally (40) to under-estimate the torsional rigidity by ignoring the effect of Poisson's ratio. Another proposal by Timoshenko (74), which is similar to that suggested by Clark (8), is found to be inadequate since it neglects the effect of Poisson's ratio in the ribs system. However, Cusens et al showed that the coupling effect due to Poisson's ratio at the intersections of the ribs increased the magnitude of the total torsional rigidity. This was observed by them from the experiments conducted using asbestos cement sheeting. These results were compared with the analytical results obtained from the formula suggested by Timoshenko and Woinowsky-Krieger, Giencke and Jackson. According to them a very good agreement was obtained and the significance of the coupling effect had been verified.

It may therefore be concluded that

(1) the conventional method of second moments of area may be adopted to determine the flexural rigidities of ribbed/waffle structures with equidistant ribs in both orthogonal directions (8,9,12); and

(2) the effects of Poisson's ratio and coupling on the torsional rigidity of a grillage cannot be ignored. Cusens and Pama's approach (11,12) may be used to determine the torsional rigidity taking account of these effects.

It is noted from the previous studies that the classical methods of solution are often far too difficult to be considered in general design practice and the application of classical solutions is confined to limited cases. This gives rise to various approximate solutions and numerical technique which can be used to solve far more general problems.

3.4 GRILLAGE ANALYSIS

3.4.1 Introduction

Mathematical solutions to the governing differential equations are generally tedious, and in some circumstances may not be possible. In 1948, Grinter originated the grillage analysis for plane-stress problems with various boundary conditions. In this method the actual two-dimensional plate structure is essentially replaced by a grillage with beam elements. The analytical process for such a substitute structural system is generally known as 'equivalent grillage analysis'. It is assumed that the x-y plane for each member coincides with the plane of the plate structure, and the z-axis is one of the principal axes for the cross-section, shown in Fig.3.13. The external loads are restricted to apply only on the beam members and at the joints in the z-direction or moments about the x- and y-axes. In this manner, the translations of the joints in the x-y plane and rotations about the z-axis can be ignored. Only three degrees of freedom occur at each end of each member i.e. rotations in x and y directions and displacement in z direction, see Fig.3.14.

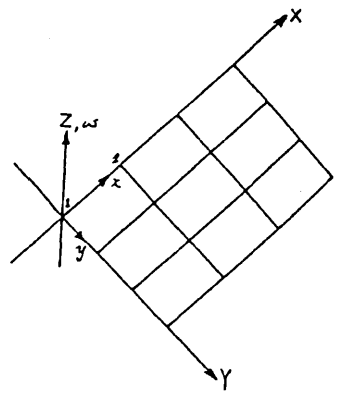

Fig.3.13 Layout of a Grillage System

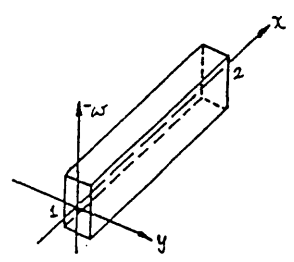

Fig.3.14 Displacements of a Grillage Element

Analysis of an actual beam grillage is often a highly redundant problem and, therefore, a displacement method such as the matrix stiffness method is useful. Restraining forces of a grillage member are introduced to prevent joint displacements regardless of the choice of the unknown displacements. Generalization of the overall stiffness matrix of a grillage is derived from the force-displacement relation, and the displacements of a member are defined only at the connected-regions or joints. These two properties generally make the grillage system more suitable for solution by the stiffness method. The constituive equations for such systems can be obtained from Section 3.3.2.

3.4.2 Generalization of the Stiffness Matrix

The basic principles of the stiffness method most commonly used are well established and the theory has been described in general terms elsewhere (40,41). Only a brief explanation is given of the generalisation of the stiffness matrix especially devised for the grillage analysis programs.

The basic force-displacement relationship in matrix form is

$$\{F\} = [k]\{d\} \tag{3.76}$$

where, F is the force matrix;
k is the stiffness matrix;
d is the displacement matrix.

The stiffness matrix for a member 1-2 is normally partitioned as

$$\begin{Bmatrix} f_1 \\ f_2 \end{Bmatrix} = \begin{bmatrix} K_{11} & K_{12} \\ K_{21} & K_{22} \end{bmatrix} \begin{Bmatrix} d_1 \\ d_2 \end{Bmatrix} \tag{3.77}$$

and, the expansion for each matrix element can be found in elsewhere (106,107).

The elements of the plane grillage differ from that of the rigid-jointed plane frame only by replacing the axial force (EA/L) of

the frame to a torque (GJ/L) of the grillage. If the direction cosines referred to the member, structures axes shown in Fig.3.15, the displacement matrix of node 1 with respect to the global axis is

$$\{d_1\} = \begin{Bmatrix} \theta x_1 \\ \theta y_1 \\ \omega z_1 \end{Bmatrix} = \begin{bmatrix} \cos\alpha & \sin\alpha & 0 \\ -\sin\alpha & \cos\alpha & 0 \\ 0 & 0 & 1 \end{bmatrix} \begin{Bmatrix} \theta x_1' \\ \theta y_1' \\ \omega z_1' \end{Bmatrix} \tag{3.78}$$

or $\{d_1\} = [\lambda]\{d_1'\}$

Proceeding with the operation for the whole member it gives

$$\begin{Bmatrix} \theta x_1 \\ \theta y_1 \\ \omega z_1 \\ \theta x_2 \\ \theta y_2 \\ \omega z_2 \end{Bmatrix} = \begin{bmatrix} \cos\alpha & \sin\alpha & 0 & 0 & 0 & 0 \\ -\sin\alpha & \cos\alpha & 0 & 0 & 0 & 0 \\ 0 & 0 & 1 & 0 & 0 & 0 \\ 0 & 0 & 0 & \cos\alpha & \sin\alpha & 0 \\ 0 & 0 & 0 & -\sin\alpha & \cos\alpha & 0 \\ 0 & 0 & 0 & 0 & 0 & 1 \end{bmatrix} \begin{Bmatrix} \theta x_1' \\ \theta y_1' \\ \omega z_1' \\ \theta x_2' \\ \theta y_2' \\ \omega z_2' \end{Bmatrix} \tag{3.79}$$

or $\{d\} = [\lambda t]\{d'\}$

where, $[\lambda t]$ is a 6x6 transformation matrix.

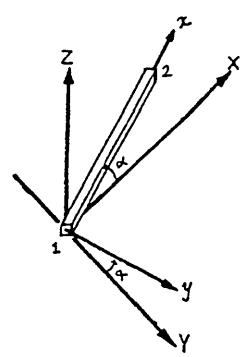

Fig.3.15 Coordinate Axes for a Grillage Element

Since this transformation matrix is orthogonal, its transpose matrix is identical to its inverse matrix i.e.

$$\{d'\} = [\lambda t]^T \{d\} \tag{3.80}$$

Similarly, this principle can be applied to the force matrix with respect to member axes

$$\{F\} = [\lambda t]\{F'\} \tag{3.81a}$$

and then to global axes

$$\{F'\} = [\lambda t]^T \{F\} \tag{3.81b}$$

From Eqn.3.76,

$$\{F'\} = [\lambda t]^T [k][\lambda t]\{d'\} \tag{3.81c}$$

Thus, the member stiffness matrix, [K], in terms of the global axes can be defined as

$$[K] = [\lambda t]^T [k][\lambda t] \tag{3.82}$$

Computers are used to advantage for the solution of such matrix equations for obtaining vertical displacements, bending and torsional moments for a given force matrix. The first computerized grillage program was introduced by Lightfoot and Sawko for the bridge deck problem. To facilitate the analysis, the deck was replaced by an equivalent grillage and the results were found to be highly acceptable. Since then, it has become the most widely used computer aided method for analysing bridge deck structures with the advantages of it being easy to comprehend and relatively inexpensive to use.

3.4.3 Conclusions

In the current investigation, an equivalent grillage analysis is considered as an alternative elastic analytical method for reinforced concrete waffle slabs. For the purpose of analysis, a waffle slab can be replaced by a grillage of beams intersecting at rigid joints called

nodes. The distribted bending and torsional stiffnesses of the slab are assumed to be concentrated in the nearest equivalent grillage beam. The beam members are assumed to be straight in plan with uniform cross-section and the external loads may be applied normal to the plane of the grillage.

To predict the behaviour of reinforced concrete waffle slabs by grillage analysis, it is first necessary to specify the elastic properties and the layout of the component beams. The accuracy of a solution is solely dependent on the aptness of the equivalent structural model. However, the approach described here is only acceptable in assessing the overall behaviour of the slab structure. In fact, the grillage system differs from the slab structure in two aspects:

1) the slab moments depend on the curvatures in both orthogonal directions but the grillage moments are solely proportional to the curvatures of the beam member;

2) the equilibrium of any slab element requires torques or twisting moments acting about the orthogonal directions to be equal. On the other hand, there is no physical principle to govern the torques or twisting moments in the grillage beams in orthogonal directions at any nodal joint.

It is clear that this method is principally applicable only for plate structures with negligible torsional stiffness and Poisson's effect. In this report, it is therefore to be accepted that although the grillage approach does not completely satisfy the required conditions of the exact behaviour of a waffle slab, it nevertheless serves as an efficient alternative method for comparison of the thoeretical and experimental results.

3.5 FINITE ELEMENT METHOD

3.5.1 Introduction

The reputation of the finite element method is well deserved as it is the most versatile and powerful analytical tool for a wide variety of problems. The advent of the high-speed computer has made this approach even more comprehensive. It was decided that this method would be used as one of the elastic analyses for the purposes of comparison in the current investigation.

As is well known the development of the finite element method was initiated in the 1950's as a result of two separate contributions: the first was the application of matrix analysis of structures; the second was the development of the digital computer. This technique was pioneered for two dimensional structures by Argyris, Turner and Clough et al. Since then, a vast number of publications have appeared dealing with a variety of structural problems using this approach. Basically, the finite element approach is an extension of the displacement method in two- and three-dimensional members in a continuum problem. In this method, the continuum is an assemblage of idealized discrete bodies, generally referred to as finite elements. These finite elements are connected only at the nodal points which possess an appropriate number of degrees of freedom. With assumed displacement fields, the stiffness matrix of the assemblage for the structure as a whole is derived from the equilibrium approach by applying virtual work theorem to the continuum. Manipulation of mass matrices by high-speed computer provides the solution of the nodal displacements, from which the internal stresses and strains can then be evaluated using the stress-strain relationship.

3.5.2 Bending Plate Element

In the current investigation, a rectangular finite element has been used to model the waffle slab. Therefore, only rectangular elements will be discussed here relating to thin plate structures with uniform thickness and negligable shear deformation.

3.4.2.1 Displacement Function

The definition of the 'displacement function', which governs the variation of the unknown quantities in a finite element is of paramount importance. The significance of this function is to satisfy the convergence criterion relevant to a particular problem. Two major features restrain the selection of the displacement field: the first concerns the economical generalization of the possible function; the second is associated with the modelling of realistic boundary conditions to an acceptable level. In general, a displacement function is selected so that it has unit value of the appropriate parameter at the node it refers to and has such an order of variation on the inter-element surfaces that the parameters specified on such interfaces uniquely define the function there. The rectangular element shown in Fig.3.16 has three degrees of freedom, one deflection and two rotations, at each node and therefore, there are 12 degrees of freedom for each element. A complete quadratic polynomial, which consists of 15 terms, is generally used rather than a trigonometric and Fourier series (65,76,84). Thus, it has three terms more than it requires. Therefore, the terms having x^4, x^2y^2 and y^4 are generally eliminated. The 12-term polynomial displacement function will be

$$\omega i = a_1 + a_2.x + a_3.y + a_4.x^2 + a_5.x.y + a_6.y^2 + a_7.x^3$$
$$+ a_8.x^2.y + a_9.x.y^2 + a_{10}.y^3 + a_{11}.x^3.y + a_{12}.x.y^3 \qquad (3.82)$$

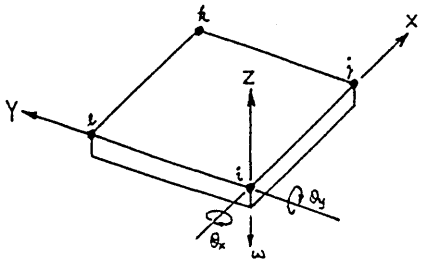

Fig.3.16 Rectangular Plate Element

The slopes $\partial w/\partial x$ and $\partial w/\partial y$ of any node can be obtained by differentiation as

$$\frac{\partial w}{\partial x} = a_2 + 2.a_4.x + a_5.y + 3.a_7.x^2 + 2.a_8.x.y + a_9.y^2 + 3.a_{11}.x^2y + a_{12}.y^3$$

$$\frac{\partial w}{\partial y} = a_3 + a_5.x + 2.a_6.y + a_8.x^2 + 2.a_9.x.y + 3.a_{10}.y^2 + a_{11}.x^3 + 3.a_{12}.x.y^2 \qquad (3.83)$$

Rearranging the x and y coordinates of nodal point i, the nodal displacement can be expressed as functions of the constants a in the following matrix equation

$$\begin{Bmatrix} \omega \\ \frac{\partial \omega}{\partial x} \\ \frac{\partial \omega}{\partial y} \end{Bmatrix} = \begin{bmatrix} 1 & x & y & x^2 & xy & y^2 & x^3 & x^2y & xy^2 & y^3 & x^3y & x.y^3 \\ 0 & 1 & 0 & 2x & y & 0 & 3x^2 & 2xy & y^2 & 0 & 3x^2y & y^3 \\ 0 & 0 & 1 & 0 & x & 2y & 0 & x^2 & 2xy & 3y^2 & x^3 & 3xy^3 \end{bmatrix} \begin{Bmatrix} a_1 \\ a_2 \\ . \\ . \\ . \\ a_{12} \end{Bmatrix} \qquad (3.84)$$

or simply $\{\delta i\} = [Ai]\{a\}$

where [Ai] is the element displacement function matrix.

To define the element as a whole, the nodal displacement equation becomes

$$\begin{Bmatrix} \delta i \\ \delta j \\ \delta k \\ \delta l \end{Bmatrix} = \begin{bmatrix} Ai \\ Aj \\ Ak \\ Al \end{bmatrix} \{a\} \qquad (3.85)$$

or simply expressed in the convenient form of

$$\{\delta\} = [A].\{a\}$$

$$\Rightarrow \quad \{a\} = [A^{-1}].\{\delta\}$$

where [A] is the element nodal displacement matrix.

The curvatures of the bending plate element at any point (x,y) are given as

$$-\left(\frac{\partial^2\omega}{\partial x^2}\right) = -2.a_4 - 6.a_7.x - 2.a_8.y - 6a_{11}.x.y$$

$$-\left(\frac{\partial^2\omega}{\partial y^2}\right) = -2.a_6 - 2.a_9.x - 6.a_{10}.y - 6.a_{12}.x.y$$

$$\frac{\partial^2 w}{\partial x \partial y} = 2.a_8.x + 2.a_9.y + 3.a_{11}.x^2 + 3.a_{12}.y^2 \qquad (3.86)$$

In a similar manner, the element strain matrix is obtained as

$$\{\varepsilon\} = [B]\{a\} \qquad (3.87a)$$

Thus, it can be written in the form of

$$\{\varepsilon\} = [B][A^{-1}]\{\delta\} \qquad (3.87b)$$

where [B] is element strain coefficient matrix.

Then, the appropriate stress-strain relationships of the orthotropic plate theory which were derived in Section 3.2 can be recalled here, which is given by

$$\{M\} = [D]\{\varepsilon\} \qquad (3.88)$$

3.5.2.2 Virtual Work Equation

The nodal forces acting at node i shown in Fig.3.14 can be defined as

$$\{Fi\} = \begin{Bmatrix} Vzi \\ mxi \\ myi \end{Bmatrix} \qquad (3.89)$$

where Vzi is transverse nodal force, mxi and myi are the bending moments.

Then, the total forces on the plate element are

$$\{F\} = \begin{Bmatrix} Fi \\ Fj \\ \\ Fk \\ Fl \end{Bmatrix} \tag{3.90}$$

Applying unit virtual displacement, $\{\bar{\delta}\}$ at each nodal point, where the unit virtual displacements are, in fact, equivalent to an identity matrix, i.e. $\{\bar{\delta}\} = [I]$, the external virtual work on the element is

$$\{Wex\} = \{\bar{\delta}\}.\{F\} = \{F\} \tag{3.91}$$

The internal virtual work on the element can be found by integrating the product of the internal stress resultants and strain due to the virtual displacements with respect to the x- and y-axes,

$$\{Win\} = \iint \{\bar{\varepsilon}\}^T .\{M\}.dxdy \tag{3.92}$$

From Eqns.3.87 to 3.88, it becomes

$$\{Win\} = \iint \{\bar{\delta}\}^T [A^{-1}]^T [B]^T [D][B][A^{-1}]\{\delta\}dxdy$$

Since $\{\delta\} = [I]$

$$\therefore \{Win\} = [A^1]^T .[k][A^{-1}]\{\delta\} \tag{3.93}$$

where [k] is the element stiffness matrix of

$$[k] = \iint [B]^T .[D][B].dxdy \tag{3.94}$$

Equating external virtual work to internal virtual work for the quadrilateral plate element,

$$\{F\} = [A^{-1}]^T .[k][A]\{\delta\} \tag{3.95}$$

Now the overall stiffness matrix, [K], for the whole structure is formed by systematic additions of individual element stiffness, and transformed appropriately from local to global coordinates.

$$[P] = [K]\{\delta\} \tag{3.96}$$

where, [K] is the overall structure stiffness matrix;
[P] is the external force matrix.

Thus, the unknown nodal displacement matrix $\{\delta\}$ is then found by solving Eqn.3.96, taking into account the appropriate boundary conditions. With the nodal displacements known, the stress resultants of the element are obtained from Eqns.3.87 to 3.88, giving

$$\{M\} = [D][B][A^{-1}]\{\delta\} \tag{3.97}$$

3.5.2.3 Isoparametric Plate Element

In order to provide flexibility in an analysis, elements which can be adapted to general shapes should be employed. The present best available such element is the isoparametric element which was introduced by Zienkiwicz (84). This is an element of general geometric form, whose shape interpolation functions are defined to be the same as the displacement interpolation functions, i.e. the number of shape coordinates must equal the number of displacement coordinates. These elements are based on strain or displacement assumptions. Finite element technique is adequately illustrated and described elsewhere (26,65,84). Therefore, only a brief treatment of isoparametric finite element leading to standard stiffness matrix generalization will be given here in view of the fact that this element was employed in the two-and three-dimensional analysis of the present work.

Consider a quadrilateral element, shown in Fig.3.17, with its nodal coordinates expressed in terms of its shape interpolation function,

$$x = \sum_{i}^{n} Ni(\xi,\eta)xi$$

$$y = \sum_{i}^{n} Ni(\xi,\eta)yi \tag{3.98}$$

where $Ni(\xi,\eta)$, i = 1 to n are interpolation functions in the curvilinear coordinates ξ and η.

xi and yi are the local x and y coordinates of node i.

n is the total number of nodes for the element.

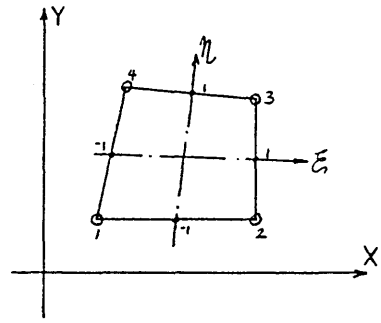

Fig.3.17 Linear Four-node Quadrilateral Element

Generally, these interpolation functions can be expressed in the form (104) of,

$$Ni = \frac{1}{4}(1 + \xi.\xi i)(1 + \eta.\eta i) \qquad (3.99)$$

where ξ and η are their curvilinear coordinates with the values of ± 1 or 0.

By definition, the displacement and shape interpolation functions are identical. Thus, the two stress functions Φx and Φy are assumed in the same form as the shape functions, that is,

$$\Phi x = \sum_{i}^{n} Ni(\xi,\eta).\Phi xi$$

$$\Phi y = \sum_{i}^{n} Ni(\xi,\eta).\Phi yi \qquad (3.100)$$

where Φxi and Φyi are the values of the stress functions of Φx and Φy at node i.

From Eqn.3.42, the moment functions can be expressed in the form of

$$\{M\} = [D]\begin{Bmatrix} \dfrac{\partial \Phi}{\partial x} \\ \\ \dfrac{\partial \Phi}{\partial y} \\ \\ \dfrac{\partial \Phi}{\partial y} + \dfrac{\partial \Phi}{\partial x} \end{Bmatrix} \tag{3.101}$$

or simply

$$\{M\} = [D]\{\Phi'\}$$

where, the displacement functions matrix at node i is

$$\{\Phi\}i = \begin{bmatrix} 0 & \dfrac{\partial Ni}{\partial x} & 0 \\ \\ 0 & 0 & \dfrac{\partial Ni}{\partial y} \\ \\ 0 & \dfrac{\partial Ni}{\partial y} & \dfrac{\partial Ni}{\partial x} \end{bmatrix} \begin{Bmatrix} \omega \\ \\ \Phi x \\ \\ \Phi y \end{Bmatrix} i \tag{3.102}$$

or simply

$$\{\Phi\}i = [N]\{a\}i$$

The relation of the curvilinear and Cartesian derivatives can be obtained by applying the partial defferentiation chain rule,

$$\begin{bmatrix} \dfrac{\partial}{\partial \xi} \\ \\ \dfrac{\partial}{\partial \eta} \end{bmatrix} = \begin{bmatrix} \dfrac{\partial x}{\partial \eta} & \dfrac{\partial y}{\partial \xi} \\ \\ \dfrac{\partial x}{\partial \eta} & \dfrac{\partial y}{\partial \xi} \end{bmatrix} \begin{bmatrix} \dfrac{\partial}{\partial x} \\ \\ \dfrac{\partial}{\partial y} \end{bmatrix} \tag{3.103}$$

The 2 x 2 partial derivative matrix is called the Jacobian matrix and is denoted by [J]. The relation of these equations provides

$$\begin{bmatrix} \frac{\partial Ni}{\partial x} \\ \\ \frac{\partial Ni}{\partial y} \end{bmatrix} = [J^{-1}] \begin{bmatrix} \frac{\partial Ni}{\partial \xi} \\ \\ \frac{\partial Ni}{\partial \eta} \end{bmatrix} \tag{3.104}$$

Standard procedure can now be followed. The stiffness matrix relating the nodal forces to the corresponding nodal displacement is

$$[K] = \iint [B]^T [D][B]|J| d\xi d\eta \tag{3.105}$$

Thus, the output stress resultants are given by Eqn.3.105, that is,

$$\{M\} = [D][B][A^{-1}]\{\Phi\} \tag{3.106}$$

Standard procedure for the overall stiffness matrix can be carried out as mentioned before in Section 3.5.2.2.

3.5.3 Summary

The derivation of displacement function in this process may suffer from two disadvantages (76): firstly, for a large number of degrees of freedom the matrix inversion will be expensive to manipulate; secondly, the inverse matrix of this displacement field sometimes may not exist. In order to obtain the same number of terms as that of the nodal parameters of a rectangular element, the most commonly used quadratic polynomials have to be reduced from fifteen to twelve terms, which will be discussed in the following section. As a result of missing out those terms, the curvatures at the end of a common boundary may not be sufficient enough to define it uniquely. Thus, full compatibility cannot be guaranteed. For this reason, the displacement function should be examined closely, in Fig.3.14 at $x = \pm k$

$$(\omega)x = [a_1 + a_2 x + x^2 + a_7 x^3] + [a_3 + a_5 x + a_8 x^2 + x^3]$$

$$+ [a_6 + a_9 x].y^2 + [a_{10} + a_{12} x].y^3 \qquad (3.107a)$$

$$\left(\frac{\partial \omega}{\partial y}\right)x = [a_3 + a_5 x + a_8 x^2 + x^3] + 2[a_6 + a_9 x].y$$

$$+ 3[a_{10} + a_{12} x].y^2 \qquad (3.107b)$$

It can be seen that the reduced quadratic polynomial still remains cubic and uniquely defines the end displacements and end slopes of the element, i.e. $\partial w/\partial y$. Hence, compatibility of displacements between adjacent elements at the nodes and along the boundaries are ensured. The curvatures normal to the boundary are also in a cubic form but this cubic expression is not sufficient to define the curvatures uniquely.

$$\left(\frac{\partial \omega}{\partial x}\right) = [a_2 + 2a_4 x + 3a_7 x^2] + [a_5 + 2a_8 x + 3a_{11} x^2]$$

$$+ [a_9].y^2 + [a_{11}].y^3 \qquad (3.108)$$

This deficiency also occurs in the curvatures normal to the y-direction. Because of this, compatibilty of the displacements between adjacent elements at the nodes and along the boundaries may not be maintained and satisfied. This displacement function is, therefore, regarded as a non-conforming function.

A program based on this quadratic polynomial displacement field was developed by Zienkiewicz (84) for rectangular elements which was used to illustrate the accuracy and the rate of convergence for square isotropic plates subjected to either central point or uniformly distributed load with either simply supported or fully fixed edges shown in Table 3.5. Although the convergence of this element is found to be reasonably fast, a variation in bending moments occurs inevitably due to the non-conforming shape function. Fig.3.18 shows the variation of bending moments of an isotropic rectangular simply supported plate subjected to a central point load. It was noted by Zienkiewicz that these nodal averages will underestimate the peak

bending moment and it was recommended that the approach values should be taken at the centroids of the elements. However, curve plotting using these values tends to be ragged, as shown in Fig.3.18, and a smoother curve was obtained (11) using the average values at the nodal points.

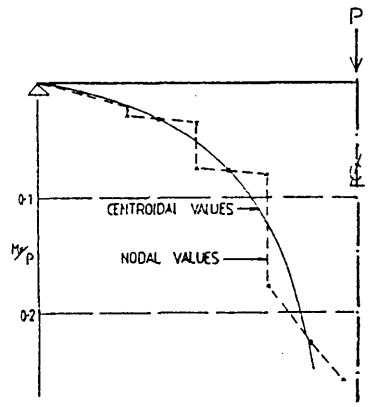

Fig.3.18 Centroidal and Nodal Bending Moments (11)

Source

Table 3.5 Central Deflection of an Isotropic Square Plate Using Different Meshes By Zienkiewicz (107)

Mesh	Simply Supported U.D.L. αu	Simply Supported C.C.L. αc	Fully Fixed U.D.L. αu	Fully Fixed C.C.L. αc
2x2	3.446	13.784	1.480	5.919
4x4	3.939	12.327	1.403	6.134
8x8	4.033	11.829	1.304	5.803
12x12	4.050	11.715	1.283	5.710
16x16	4.056	11.671	1.275	5.672
Exact (74)	4.062	11.600	1.260	5.600

† U.D.L. represents Uniformly Distributed Load
† C.C.L. represents Central Concentrated Load

where,

i) For U.D.L., the maximum displacement is

$$\omega(max) = [\alpha u.p(x,y).L^4/D].10^{-3}$$

ii) For C.C.L., the maximum displacement is

$$\omega(max) = [\alpha c.P.L^4/D].10^{-3}$$

It is the fact that the accuracy of these two methods of analysis is depended on the ability of the model to represent three very complex characteristics:

i) the behaviour of the material;
ii) the geometry of the structure; and
iii) the loading and boundary conditions.

Even when homogenous materials have properties differing widely from the elastic idealizations and when incorporated into a structure, they have innumerable variations of stiffness and strength due to composition of site- and life-history. The analysis almost invariably simplifies the geometry of the component of the structure to an assemblage of thin plates or beam grillage. The loading and boundary conditions are idealizations for the purpose of analysis and they are limited by the aptness of the assumptions. For these reasons errors are likely whatever method of analysis is used. It is therefore suggested that emphasis should be given mainly to consider the physical behaviour of the structure.

3.6 CONCLUSIONS

Based on the literature surveys, following conclusions can be drawn concerning techniques for analysing R.C. ribbed/waffle slab structures:

1) The structure can be analysed using orthotropic plate theory by conceptually replacing the system by an 'equivalent' homogenous orthotropic plate with uniform thickness, providing the resulting plate has the same elastic properties which obey the elastic theory for thin plate bending.

2) The methods of solution for a more general plate/slab structure are often too cumbersome to use or involve a prohibitive amount of computational work. Sound numerical solutions, incorporating the computer aided techniques, i.e. grillage analogy and finite element method are thought to be best suited for this purpose.

3) For use in these computerised techniques, the determination of the flexural and torsional rigidities are important and they can be obtained using:

i) the conventional method of obtaining the second moments of area to obtain the flexural rigidities of ribbed plate/slab structures with relatively close and equidistant ribs in both orthogonal directions; and

ii) Cusens et al's theory, taking into consideration the eccentricity of the section to determine the torsional rigidities of the slab the effects of Poisson's ratio of the ribs cannot be ignored.

CHAPTER 4

NONLINEAR ANALYSIS

4.1 INTRODUCTION

The use of reinforced concrete as a structural material is a standard feature of modern construction. Current design methods for R.C. structures are usually derived from elastic theories. Lately limit state design has been developed and applied to a wide range of reinforced concrete structures, and nonlinear analysis of R.C. structures has become increasingly important. R.C. structures have complex behaviour pattern primarily due to the following factors:

(i) the nonlinear response of the materials,
(ii) the influence of progressive cracking of concrete, and
(iii) the effects of bond slipage, aggregate interlock, dowel action, creep and shrinkage etc..

Development of finite element techniques permits an analysis of a highly indeterminate structural system which can be replaced by a system of finite element networks. The principle of this technique has been described in Section 3.5. This analytical procedure provides the unknown nodal displacements of the finite elements in two- and three-dimensional analyses. The essential features of this method for the nonlinear analysis of reinforced concrete structures and the influence of the above three factors are fully described elsewhere (6,67). Taking account of all of these factors in the analysis will be extremely complex. However, nonlinear analyses using the finite element approach with simplifying assumptions were satisfactorily used by Jofriet and McNiece (30), Cope and Vasudeva Rao (10), Lin and Scordelis (39), Hand and Pecknold and Schnobrich (20).

4.2 THE EFFECTIVE STIFFNESS APPROACH

Two basic approaches have been reported for the analytical investigation into the flexural behaviour of reinforced concrete slab structures. The first approach is an effective stiffness method which is based on standard plate bending elements with material nonlinearity

which is idealized from a simple bilinear moment curvature either obtained experimentally or evaluated from appropriate cracked section properties. This procedure is regarded as a direct and efficient method. Using this approach Jofriet and McNiece obtained the bilinear moment-curvature relationship from several empirical methods, which included the determination of effective moment for cracked section by Brandson and Beeby (30). Good agreement between the analytical and the experimental results for a corner supported, two-way slab are reported and shown in Fig.4.1. Apparantly, Beeby's method of rigidity calculation for cracked sections gives a better result than the other method.

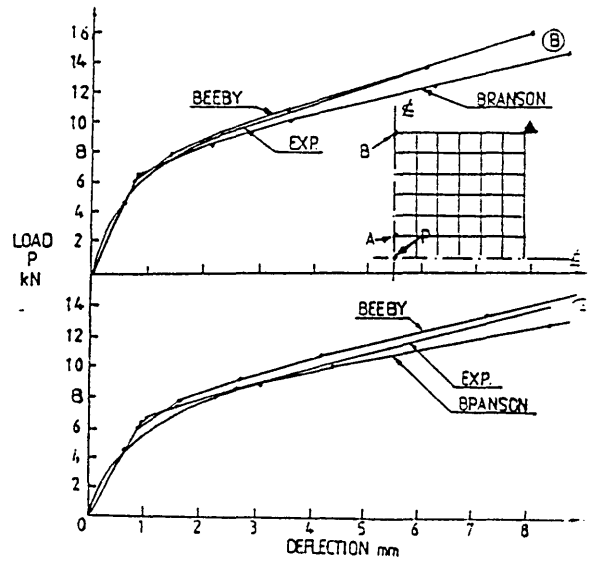

Fig.4.1 Deflections of Corner Supported Slab

Later in 1977, Cope and Vasudeva Rao (10) extended this approach with the assumptions that concrete was a nonhomogenous and anisotropic material, and had uniaxial stress-strain relationship in both tension and compression. Brittle failures in tension and compression were assumed to occur if the tensile and compressive strains reached the limiting values. Any residual forces in the cracked element were neglected and the reinforcement was assumed only to be stressed along its principal axis. The proposed analytical procedure was then applied to a corner supported slab subjected to a centrally concentrated load tested by McNiece. The comparison of the load deflection characteristic in Fig.4.2 shows a good agreement over a major portion of the graph. The distortion at the final stage was

reported as due to lack of ductile characteristic of the reinforcement.

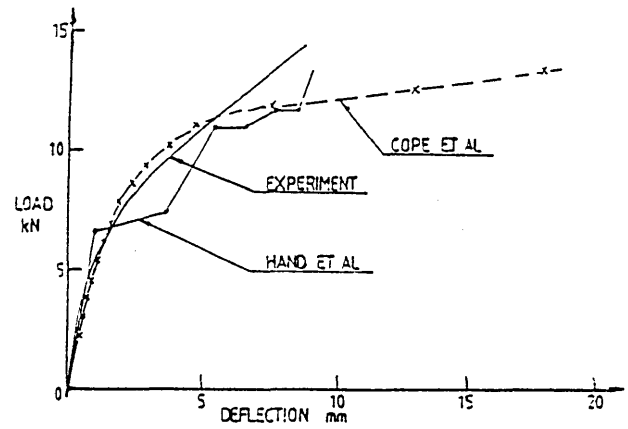

Fig.4.2 Comparison of Load-deflection Characteristic Between the Experimental and Theoretical Results for Corner Supported Slab Using Effective Stiffness Approach

4.3 THE LAYERED ELEMENT APPROACH

The second approach is the idealization of the structure into a number of finite layers as shown in Fig.4.3. Variations of properties through the depth of the layers can conveniently be introduced according to the material in each layer, for example steel can be represented as an equivalent smeared layer. If Kirchhoff's assumptions for a thin bending plate are used, a three-dimensional stress problem can be reduced to a two-dimensional problem. This technique was applied by Lin and Scordelis (39) and Hand, Pecknold and Scohnsbrich (20) using triangular and rectangular elements respectively.

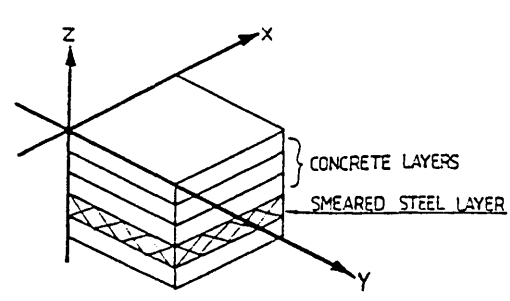

Fig.4.3 Layered Plate Bending Element

In this layered finite element approach, Hand et al assumed that the reinforcement behaved as perfect elastic-plastic material. The concrete was assumed to be tension limited at one end and Kupfer, Hilsdorf and Dusch yield criterion for biaxial compression on the other. In order to satisfly the boundary condition, a thin-shell layered finite element with 20-degrees of freedom was used in the analytical investigation. Lin and Scordelis extended Hand et al's approach by introducing a flat triangular element which could satisfy any arbitrary boundary geometry. In addition, the tension stiffening of the concrete between the cracked sections and the flow criterion of failure of concrete were taken into account in the investigation. The cracked element for both investigations can be characterized by the following stress-strain relationship as:

$$\begin{Bmatrix} \sigma x \\ \sigma y \\ \tau xy \end{Bmatrix} = \begin{bmatrix} 0 & 0 & 0 \\ 0 & E & 0 \\ 0 & 0 & \beta G \end{bmatrix} \begin{Bmatrix} \varepsilon x \\ \varepsilon y \\ \gamma xy \end{Bmatrix} \qquad (4.1)$$

where, β is a factor for aggregate interlock and any dowel action in the cracked section. Although these two investigations used similar stiffness/rigidity for the cracked elements, Hand's bilinear perfect elastic-plastic concrete material in compression gives a good approximation. On the other hand, Lin's stress-strain relationship taking account of the tension stiffening effect is more realistic. The comparison of the results using this approach, with and without tension stiffening, is shown in Fig.4.3. It is important to note that the analytical curves converge at the ultimate stage. It indicates that the ultimate respone is not affected by the magnitude of the tensile strength and the tension stiffening effect.

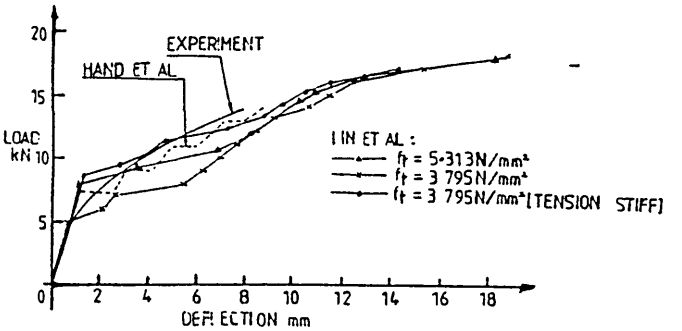

Fig.4.4 Results of Load-deflection Characteristic for Corner Supported Slab Using Layer Element Approach

The solution procedure for both methods is similar in that, the step by step procedure to take account of the effect of the cracked concrete elements is simulated by reducing the rigidity of the stiffness matrix of the elements. The accuracy of the anlysis is entirely dependent on the increment of load and the correctness of the modified stiffness matrices for cracked element. These analyses appear to be a valid and useful tool for the nonlinear analysis of R.C. structures.

From these studies, it is evident that concrete is the major contributor to the nonlinear behaviour of R.C. structures. The most important characteristic of concrete is its low tensile strength compared to its compressive strength; it is generally accepted that the ratio of the tensile to compressive strength is approximately 1 to 10 (50). It is this low tensile strength causing early concrete cracking which effectively reduces the stiffness of the structure. Therefore, an accurate modelling of cracking behaviour of concrete is inevitably the most significant factor for analysing an R.C. structure. Linear elastic-fracture models based on the concrete failure were developed and used as an analytical tool by many investigators (6,67) to study the nonlinear behaviour of R.C. structures.

It was decided that the cracking of concrete and the reinforcement nonlinearity would be considered here. The nonlinear effects attributed by bond slipage, aggregate interlock, dowel action, creep and shrinkage are still required to be well established, and therefore, it will not be considered in here.

4.4 FAILURE CRITERIA FOR CONCRETE

It has been shown that the strength of concrete under multi-dimensional states of stress is a function of that state of stress (6) and cannot be predicted by considerations of simple tensile, compressive and shear stresses independent of each other. Therefore, to find a proper representative formula for strength of concrete, the interaction of the stresses should be studied and before formulating concrete strength, a proper definition of failure must be reached i.e. criteria such as yielding, cracking and load-carrying capacity. No

unique model can be expected to represent completely the property of concrete under various stress conditions. For practical applications, which depend on those characteristics which are significant to the problem at hand, drastic idealizations of concrete strengh are essential in the mathematical modelling. The most commonly used failure criteria are described in the following sections.

4.4.1 Rankine Failure Criterion

Fractural failure is assumed to occur when maximum stress in any direction reaches the limiting strength. The equations generally describing the 'tension cut-off' surface defined by these criteria are

$$\sigma_1 = ft \quad ; \quad \sigma_2 = ft \quad ; \quad \sigma_3 = ft \tag{4.2}$$

where, ft is the tensile strength of concrete.

This assumption is constrary to that of Treaca and Von Mises criteria, according to which the failure occurs when the maximum shearing and octahedral shear stresses are reached respectively.

4.4.2 Mohr-Comlomb Failure Criterion

According to this criterion failure is assumed to occur when the shear stress on any plane at a point exceeds the value which depends linearly upon the normal stress, σn, in the same plane. This can be written as

$$|\tau| = C - \sigma n \tan\phi \tag{4.3}$$

where, C and ϕ are cohesion and angle of internal friction of the material respectively.

It is apparant that the Rankine failure criterion alone is inadequate for describing failure in the fracture-ductile state under the intermediate level of compressive stresses. Therefore, the combination of Mohr-Coulomb criterion with a maximum tensile cutoff appears to be a better approximate approach.

4.4.3 Bresler-Pister Failure Criterion

Failure is based on a limiting parabolic value of octahedral shear and normal stresses. The proposed stress relationship is expressed in the form of

$$\frac{\sigma oct}{fc} = A' - B'.\left(\frac{\sigma oct}{fc}\right) + C'.\left(\frac{\sigma oct}{fc}\right)^2 \qquad (4.4)$$

where, σoct is the octahedral stress of concrete;

fc is the compressive strength of concrete;

A', B' and C' are the material failure parameters which can be obtained experimentally.

Test results have shown a good agreement with this criterion. However, McHenry, Bellamy and Karni (67) indicated that discrepency arose for failure under general triaxial stress states. Despite this, the theory was reported to successfully model the failure of concrete under biaxial states of stress by Mikkola and Schnobrich (67).

The behaviour of concrete under biaxial stresses can be illustrated by the test results of Lin et al in 1972, Kupfer at al in 1969 and Tasuji et al (69) in 1978 which show that failure criteria based on the strength of concrete under compression-tension or tension-tension biaxial stress fields provide the most useful graphical representation, given in Fig.4.5.

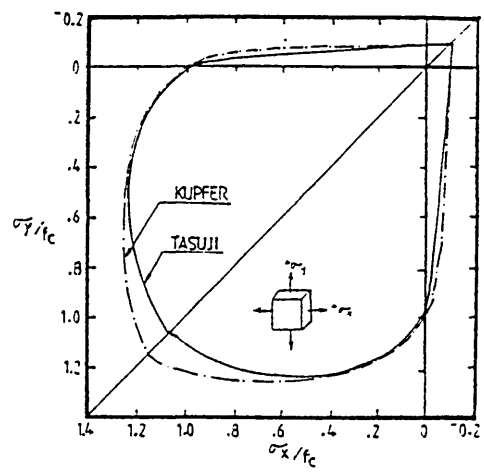

Fig.4.5 Result of Biaxial Strength Envelops

The state of stress in concrete in a reinforced solid/waffle slab subjected to transverse loading is generally agreed to be two-dimensional. Under different combinations of biaxial loading, concrete exhibits strength and stress-strain behaviour somewhat different from that under uniaxial conditions. There is general agreement that the strength of concrete in biaxial compression may be considerably higher than in uniaxial compression, and is fairly constant under biaxial and uniaxial tension. Under the combination of tension and compression concrete exhibits a noticeably reduced strength. Therefore a biaxial maximum stress envelope, similar to the Bresler-Pister criteria, combined with the tensile cut-off, can provide a useful guide for concrete strength modelling. The advantages of the combined criterion are that the deviations of the state of stress can be modelled as desired, and it provides a partial explanation regarding the modes of failure in concrete i.e. either tensile cut-off or compressive fracture, as follows:

4.4.4 Tensile Cut-Off

Cleavage fracture occurs when the maximum tensile stress is exceeded. A crack plane develops normal to the direction of the maximum principal stress and it weakens the material structure in that principal direction only. The cracked elements in the structure can be simulated by introducing a reduced isotropic material body on the continuum level.

4.4.5 Compressive Fracture

Shear slips occur when the maximum shear stress is reached. If the principal stresses are different in magnitude, failure will significantly weaken these two principal directions (6,67). Simpliflying this effect, Chen and Suzuki proposed perfectly brittle behaviour for concrete, such that after fracture the body is assumed to lose it's entire strength in any directions.

4.5 CRACKING MODELS

A number of different approaches for crack modelling have been developed to represent cracking during analytical studies of R.C.

structures using finite element techniques. Any particular cracking model to be chosen from the two alternatives previously mentioned depends upon the purpose of the analysis and the nature of the problem. Three different approaches are available for the nonlinear analysis of reinforced concrete which are:

(i) Smeared cracking modelling
(ii) Discrete cracking modelling
(iii) Fracture mechanics modelling

If information on overall load-deflection behaviour is important, the smeared cracking modelling will be a suitable choice for the structure. Otherwise, if information on the local behaviour is the prime objective of the studies, the discrete crack modelling is the best general choice, while for the special class of problems such as the notch sensitive fracture in metal, ceramics and rock mechanics, the fracture mechanics modelling may be useful. Most of the reported R.C. slab investigations have been modelled by the smeared cracking method because of the analytical nature. This model is also adopted in the current investigation. The study in this section therefore is mainly devoted to this model. Detailed descriptions of discrete cracking and fracture mechanics modelling may be found elsewhere (6,67).

4.5.1 Smeared Cracking Model

The uncracked concrete is assumed to be an isotropic elastic material; governing constitutive relations are given in Chapter 3. The cracks are assumed to be "smeared out" in a continuous fashion and represented by an infinite number of parallel fissures across the cracked concrete element as shown in Fig.4.6. These fissures are assumed to form in the planes perpendicular to the maximum principal stress axes. After cracking, the concrete element becomes orthotropic with modulus of elasticity in the direction of cracking reduced to zero. Therefore, the new incremental orthotropic constitutive stress-strain matrix can be written as

$$\begin{Bmatrix} \sigma x \\ \sigma y \\ \tau xy \end{Bmatrix} = \begin{bmatrix} 0 & 0 & 0 \\ 0 & E & 0 \\ 0 & 0 & 0 \end{bmatrix} \begin{Bmatrix} \varepsilon x \\ \varepsilon y \\ \gamma xy \end{Bmatrix} \qquad (4.5)$$

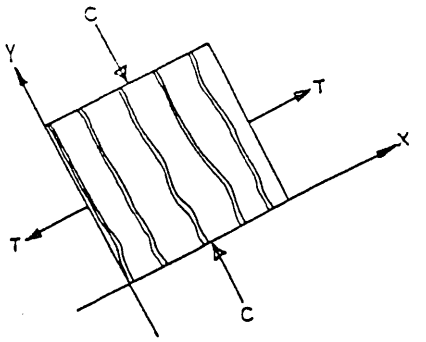

Fig.4.6 Idealization of Cracks in a Smeared Concrete Layer

In this version, the effect of aggregate interlocking, dowel action and the Poisson's ratio are neglected. The cracking model represented in Eqn.4.5 was employed adequately by Rashid (67) in 1968; the shear modulus factor, β, is reduced to zero in the rigidity matrix for the stated assumptions. This could eliminate the computation in the direction normal to the crack plane. In fact, it is reasonable to do so because the strain energy associatted with the crack plane would dissipate quickly after cracking.

4.6 CONCLUSIONS

For nonlinear analysis of an R.C. structure, concrete and reinforcement are considered to be the contributors to the overall stiffness or strength of the structure. To simplify the model it is normal to assume full kinematic continuity at nodal points between concrete and reinforcement elements; but in reality, these two materials have two different moduli of elasticity and this leads to a lack of compatibility between these elements, and bond failure and bar slippage are the consequent local effects.

The main objectives for the nonlinear analysis in the present investigation were an attempt to obtain the entire range of load-deflection behaviour up to the ultimate load carrying capacity, locations and development of cracks of the slab models, and then comparison with the experimental results. With these objectives in

mind, the layered element approach utilising 3-dimensional finite element analysis incorporated in 'LUSAS/AN' appears to be the appropriate choice.

It could be argued that the tensile cracking is the major factor causing the nonlinear behaviour of the slab models. It is also generally agreed that the stress state of concrete in a reinforced plate structure subjected to transverse loading can be approximated to a biaxial stress state. Therefore, the linear theory of elasticity combined with the criterion defining failure of concrete based upon the biaxial stress state is adopted.

The prime objective in here is the studies of overall load-deflection behaviour of R.C. waffle slabs. Therefore, the smeared cracking model approach was chosen to be employed for crack modelling. The cracks are assumed to be smeared out in a continuous fashion and the cracked elements are also assumed to remain in the continuum.

CHAPTER 5

ULTIMATE LOAD ANALYSIS

5.1 INTRODUCTION

Basically, there are three approaches for estimating the ultimate load capacity of reinforced concrete slab structures:

(1) The yield line method;
(2) The plastic hinge method; and
(3) The strip method.

The main advantages of these ultimate load methods can generally be described as follows:

(i) an improvement in the understanding of the behaviour of a structure under working load conditions;
(ii) a relatively better estimate of the degree of safety of a structure under applied loads; and
(iii) the ability to provide a safe design to be prepared for complex structures.

Because of these advantages, ultimate load methods of analysis and design have been gaining in popularity in the past two decades and are now widely accepted as suitable alternatives to the elastic approach. The general validity of the yield line and the strip methods for predicting the ultimate strength of reinforced concrete slabs is well established. The plastic hinge and yield line approaches have been extensively applied to rectangular and skew bridge deck structures. Literature surveys for the present work have shown that the modified yield line method and equivalent open grillage analysis utilising plastic hinge approach can satisfactorily be employed on reinforced concrete waffle slab analysis (2,43). Hillerborg's strip method is also included in this theoretical consideration of design for this type of structure.

5.2 YIELD LINE ANALYSIS

Reinforced concrete slab structures are normally designed to be under-reinforced so that under progressively increased loading, some of the reinforcement reaches yield stress well before the slab reaches its ultimate strength. When steel yields locally, moment redistribution takes place. Provided the slab is sufficiently ductile, local changes of curvature are dramatically increased, and progressive yielding eventually leads to the development of the collapse mechanism. It is evident that a failure mechanism consists of a set of relatively flat segments of the slab separated by narrow yielding zones. For the purpose of analysis, these zones are idealized as lines which are known as yield lines.

The significance of yield line formation was observed by Johansen (31), who, on the basis of this yield line formation together with the 'stepped yield criterion', postulated the hypothesis of yield line method of analysis. This hypothesis states that failure of a slab occurs when sufficient cracks have formed to give a valid yield line mechanism. With this valid collapse mechanism, the work equation can then be used to establish the failure load for that particular yield line pattern. To simplify the analysis, the slab is assumed to behave in a perfectly plastic manner and therefore the segments of the slab which are bounded by the yield lines are assumed to be flat and rigid. The total external work done to the applied load on these segments is equated to the total internal work dissipated by the slab in yielding. The work equation is then establised by applying a virtual displacement to a convenient point in the deformed slab; the corresponding displacements of the applied loads and the rotations of the yielded segments can be determined from the deformed shape of the slab. Thus the work equation can be expressed as follows:

$$\int p.\Delta.dA = \int Mn.\theta n.d(Ls) \qquad (5.1)$$

where p is the applied load intensity;

Δ is the displacement at the point of application of p;

A is the area of segment considered;

Ls is a short length of yield line at that point;

Mn is the yield strength of the section normal to the yieldline;

θn is the rotation of the segment normal to the yieldline.

The general problem when applying the yield line theory is to find the most critical yield pattern. It is possible to discover a lower failure load with a sligthly more complicated collapse mechanism. For example, for the square slab of side L shown in Fig.5.1, simply supported on all edges and subjected to a uniformly distributed load, the collapse load, p, for the failure mechanisms with increasing complexity can be shown to be:

(i) $p=24m/L^2$ for the mechanism of Fig.5.1a;
(ii) $p=22m/L^2$ for the mechanism of Fig.5.1b; and
(iii) $p=21.7/L^2$ for the mechanism of Fig.5.1c.

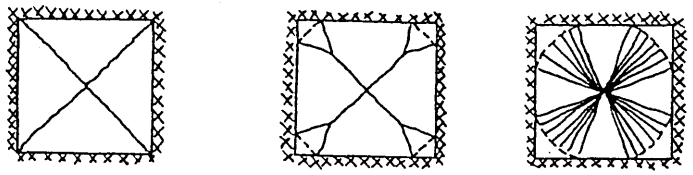

Fig.5.1 Collapse Mechanism for Simply Supported Square Slab Subjected to Uniformly Distributed Load

It is because of the iterative nature of this procedure, leading to an uncertain critical load, the collapse load given by the yield line method is either equal to or greater than the actual carrying capacity of the slab. It is therefore clear that the yield line method is either an upper bound solution or an unsafe theorem.

5.2.1 Equivalent Slab Methods

The general validity of yield line theory for predicting the ultimate strength of the slab is well established and this theory has been applied extensively to rectangular and skew slab bridges, with or without edge beams. A quasi-slab method was proposed by Reynolds (46) in which the edge beams of slab bridges were replaced by equivalent slabs on either side, having the same moment of resistance as that of the edge beams. The resulting equivalent slabs were then analysed as uniform slabs by yield line theory.

Later in 1967, Sawko and Saha (66) suggested a method to transform a beam and slab bridge to a quasi-orthotropic plate to facilitate yield line analysis. The effective width of a transformed bridge slab was considered as

$$We = N.S + \frac{2.Me.S}{Mt} \qquad (5.2)$$

where, N is number of main beams;
S is spacing of main beams;
Me and Mt are the ultimate moments of the L- and T-beams respectively.

The ultimate strengths in the orthogonal directions were obtained by dividing the total moment of resistance of the beams along a side by the length of that side. The yield line analysis was then applied to the resulting equivalent uniform slab. This procedure was applied to one of Reynold's grillage test with simple supports. The estimated load was found to be 7.6% lower than the experimental load. The reduction in the theoretical value was probably due to the effect of ignoring the torsional rigidities of the transverse edge beams over the supports. It is felt that this approach may be more justified when applied to a slab with smaller rib size, such as a waffle slab, rather than to the extreme case of the beam grillage.

In 1969, Reddy and Hendry (61) conducted an investigation into the ultimate load behaviour of composite steel-concrete bridge deck structures. The structure was analysed by two separate methods using the yield line approach. The first method is called an 'equivalent orthotropic' slab method, which is very similar to that of Sawko and Saha, but with a more detailed treatment for the transformation of the deck and the ultimate strength of the slab. The second method is known as the 'beam and slab' method which is discussed in section 5.2.2.

For an 'equivalent orthotropic' slab, the effective width of the transformed bridge deck with L-beams at either side was given by

$$We = (N-2).S + \frac{2.Me.S}{Mt} \qquad (5.3)$$

with notations as before except that the number of T-beams includes the L-beams in both directions.

The ultimate moment per unit width of the equivalent slab is given as

$$\mu e.m' = \frac{Mt + (S-Be).\mu m'}{S} \qquad (5.4)$$

where $\mu m'$ is the ultimate transverse sagging moment per unit width;
μe is the ratio of longitudinal to transverse moments.

Also, the effective width of the T-beams, Be, was obtained using

$$Be = \frac{S}{\sqrt{[1+12.(S/L)^2]}} \qquad (5.5)$$

where, L is the span of the bridge.

Two collapse modes were considered for each of the model tests. The modes of collapse for test models with three- and four-longitudinals are shown in Fig.5.2. Ultimate collapse loads for the three-longitudinal bridge are given as follows:

$$Pa = \frac{12.\mu e.\rho.m}{(1-\zeta)}$$

$$Pb = \frac{4.\sqrt{\mu i}.(3-4.\zeta).m}{\sqrt{[4(1-\zeta)^3 - 1]}} \qquad (5.6)$$

where, $\rho = h/L$

$\mu i = (\mu e + i.\mu')/(1+i)$

i is the ratio of the positive tranverse to negative transverse moment of the slab;

μ' is the ratio of negative longitudinal to negative transverse moment;

ζ is the ratio of distance between the loads to the span.

Eight bridge models with three- and four-longitudinal beams were tested to failure with loads applied to the interior and/or exterior beams. A good correlation between the theoretical and experimental values was obtained, as can be seen in Table 5.1. It was further concluded that the tendency of the tests to give higher values than that predicted by theory might be attributed to the membrane effect inherent in Tee-beam actions.

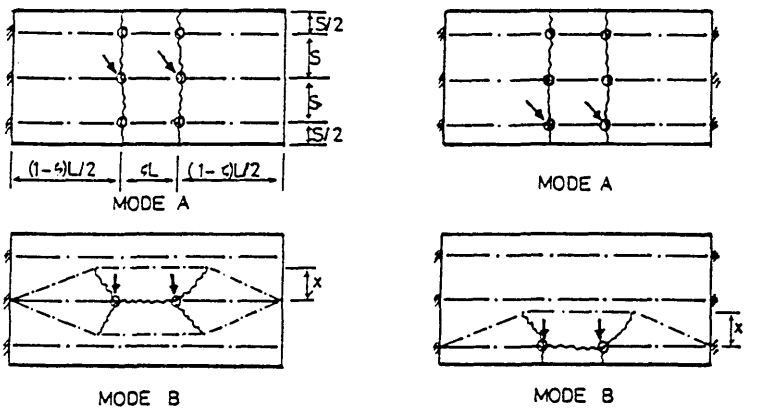

Three-longitudinal Bridge Model

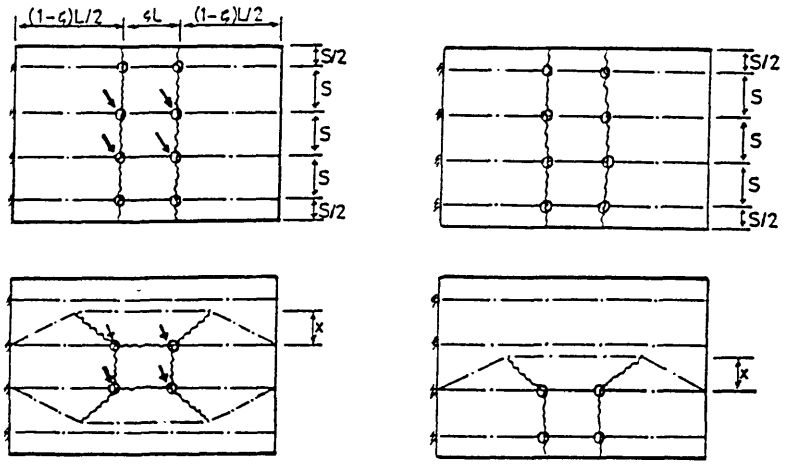

Four-longitudinal Bridge Model

Fig.5.2 Collapse Mechanisms of Three- and Four-longitudinal Bridge Models by Reddy and Henry

Recently, a series of six reinforced concrete waffle slab models were tested to failure by Marshall (43). The results and the observations of the tests indicated that the waffle slab models behave in a manner similar to that of R.C. solid slabs. To show the similarity of these two types of slabs, two collapse modes for slabs No.2 & 3 with simply supported edges subjected to uniformly distributed load is given in Fig.5.3. Two methods were used to estimate the ultimate load capacities of the slab models i.e. affine slab method and equivalent open grillage analysis. The latter method is discussed in section 5.3.

Table 5.1 Results of Bridge Model Tests By Reddy and Henry

	(1)	(2)	(3)	(4)	(5)
Model No.	Test load	Equivalent Slab Method Theoretical load	Ratio	Beam and Slab Theoretical Method load	Ratio
	[Tons]	[Tons]	(1)/(2)	[Tons]	(1)/(4)
A1	8.50	8.40	1.01	8.72	0.97
A2	9.15	7.95	1.16	8.96	1.05
A3	9.85	10.31	0.96	8.54	1.15
A4	8.50	7.63	1.12	7.78	1.10
B1	9.60	10.10	0.94	10.40	0.92
B2	9.70	9.14	1.06	9.23	1.05
B3	13.85	11.68	1.18	12.10	1.14
B4	8.60	8.65	0.99	9.13	0.94

In principle the affine slab method is more or less similar to normal yield line analysis for slabs. In contrast to the above mentioned methods for bridge deck structures, the overall dimensions of the waffle slab models remained unchanged. The ultimate moment capacity per unit length in one direction was obtained by dividing the total moment capacities of T- and/or L-sections in this direction by the full length of that side. The standard yield line analysis procedure was then applied to the slab model. The details of these six slab models are shown in Table 5.2 and a comparison of theoretical and experimental ultimate loads is tabulated in Table 5.3.

Table 5.2 Data of R.C. Waffle Slab Models by Marshall

Slab No.	Slab Thickness mm	Concrete Strength N/mm²	Support Conditions			
			West	North	South	East
1†	23	31	S	S	S	S
2	23	38	S	S	S	S
3	13	18	S	S	S	U
4††	13	32	F	S	F	F
5	23	25	S	S	S	U
6	13	25	S	S	S	S

§ † - Without Links; †† - With Top Steel at Built in Supports
§ S - Simply Supported; F - Fully Fixed; U - Unsupported

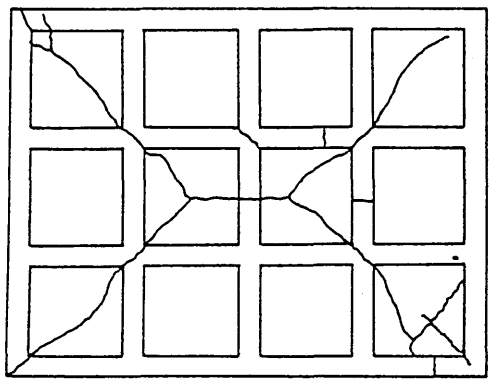

Slab Model No.2

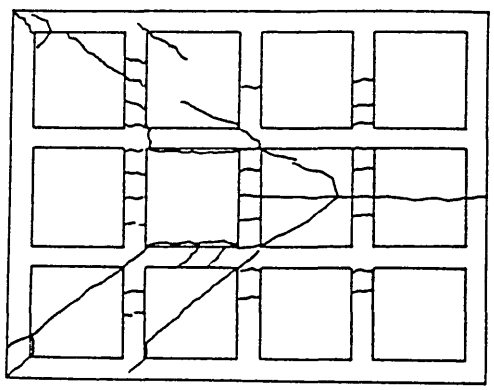

Slab Model No.3

Fig.5.3 Collapse Mechanisms of R.C. Waffle Slabs Tested by Marshall

Table 5.3 Theoretical and Test Results of R.C. Waffle Slab Models by Marshall

Slab No.	Theoretical Load		Test Failure Load	Load Factors	
	E.Y.L.A (1) (kN/m²)	E.O.G.A. (2) (kN/m²)	(3) (kN/m²)	(1)/(3)	(2)/(3)
1	54.7	53.0	55.7	0.982	0.952
2	54.7	53.9	62.1	0.881	0.868
3	35.8	34.2	36.0	0.994	0.950
4	69.4	76.9	109.5	0.634	0.702
5	35.8	34.7	32.9	1.088	1.055
6	54.7	50.3	50.8	1.077	0.990

§ E.Y.L.A. - Equivalent Yield Line Analysis;
§ E.O.G.A. - Equivalent Open Grillage Analysis.

5.2.2 Beam and Slab Method

This approach was also suggested by Reddy and Hendry (61) as an alternative to the equivalent orthotropic slab method. Conceptually, the beam and slab bridge system is divided into two individual structural elements i.e. longitudinal members and transverse slab. The longitudinal member consists of a main beam with an effective bridge deck on either side forming a composite T-beam. The remaining strip of slab adjoining the effective width of the composite sections is supported transversely by these composite T-beams. Thus, the ultimate strength of the bridge system is composed of the sum of the resistance moments along the yield lines in the deck together with the plastic moments of the hinges in the beams. The solutions using this approach for the collapse modes shown in Fig.5.2 were obtained to be

$$Pa = \frac{12.Mc}{(1-\zeta).L} + \frac{12.\mu m.(h-Be)}{(1-\zeta).L}$$

$$Pb = \frac{4.Mc}{(1-\zeta).L} + \frac{4\sqrt{\mu}.(3-4\zeta).m}{\sqrt{[4(1-\zeta)^3 - 1]}} \qquad (5.7)$$

A reasonably good agreement was found between the predicted and the test results, see Table 5.1.

This approach was extended by Nagaraja and Lash (48,49) in an attempt to predict the ultimate load capacity of R.C. highway bridge decks. The bending and torsional resistance of plastic hinges in beam elements were included in the analysis. The collapse mechanism for a two-beam bridge, without any interior transverse beams subjected to the line loads, is given in Fig.5.4. The work equation was developed as follows:

External work done by the applied line load Pl is

$$Eext = Pl.\frac{(L-a)}{L} \tag{5.8}$$

Internal work done by the structural elements of the slab deck in forming bending and torsional hinges, is

$$Eint = [2.Ms.(\frac{L}{S} + \frac{2.S}{L}) + 4.(\frac{Mb+Tp}{L})] \tag{5.9}$$

where Ms and Mb are the ultimate moments of the slab and beams respectively;

Tp is the torsional moment of restraint of the T-beam in pure torsion;

a is half of the length of the applied line load;

S is the spacing of the beams.

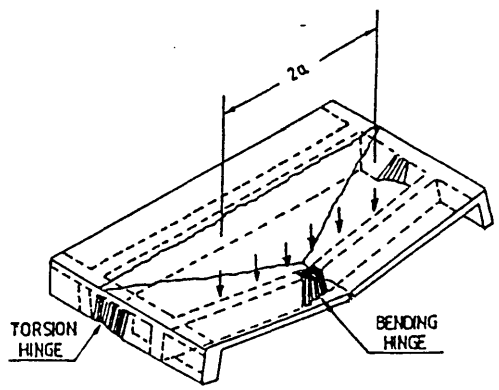

Fig.5.4 Collapse Mechanism of Two-Beam Bridge Models Subjected to the Line Loads by Nagaraja et al

Thus, the applied line load Pl can be given as

$$Pl = \left(\frac{L}{L-a}\right).Eint \qquad (5.10)$$

In these bridge model tests, it is important to note that interior diaphragms appear to make no significant contribution to the load capacity for single-lane loading, but they increase the possibility of shear-torsion failures. It was also found by Nagaraja and Lash that the bending moments of the longitudinal girders of a two-beam bridge were reduced by about 11% by the effect of the central diaphragm, and the torsion moments were increased by 18% in the same girders. The corresponding figures for the four-beam bridge were found to be 1% and 31% respectively. Considerable shear-torsion cracks were reported for these particular models with interior diaphragms. Despite these observations, the interaction between bending and torsion was assumed to be negligible, and the ultimate moment capacities in bending and torsion of the beams were determined independently. The torsion capacity was obtained by the sand heap analogy with an acceptable degree of accuracy, even when the contribution of reinforcements was ignored. The ultimate load capacities of these twelve bridge models are presented in Table 5.4 which show reasonable accuracy, with a discrepancy of about 10%. It appears that this discrepancy can be largely attributed to the effects of the bending/torsion interaction and the contribution of the reinforcement in torsion being ignored.

The close similarity of the predicted results obtained by Reddy and Hendry using these two approaches strongly suggested the validity of the yield line theory for bridge deck structures. The general applicability of the yield line concept to the bridge deck analyses with different procedures was substantiated by the works of Sawko and Saha and Nagaraja and Lash. In the light of these findings, it is considered that waffle slab structures would behave in a manner similar to that of solid slab structures and therefore, it is reasonable to use the equivalent slab method to analyse these structures. However, in highway bridges, where the beams are the main structural members, it seems reasonable to analyse them using the beam-and-slab method.

Table 5.4 Theoretical and Test Results of Bridge Models by Nagaraja and Lash

(1) Model No.	(2) Loading Type	(3) Theoretical Load (kN)	(4) Test Failure Load (kN)	(5) Load Factor (3)/(4)
1	2-Lane	29.814	28.924	1.038
2	2-Lane	28.479	28.034	1.016
3	1-Lane	37.823	41.828	0.904
4	1-Lane	41.828	44.053	0.950
5†	1-Lane	36.043	36.222	0.995
6	1-Lane	37.823	35.821	1.056
7	Mid-width	33.374	31.816	1.049
8	1-Lane	40.493	37.823	1.071
9	1-Lane	45.833	42.051	1.090
10	1-Lane	44.943	44.498	1.010
11	1-Lane	279.003	262.537	1.063
12	1-Lane	260.314	233.170	1.116

§All models were constructed with 2 longitudinal beams except the model marked † with four longitudinal beams.

5.3 PLASTIC HINGE METHOD - OPEN GRILLAGE METHODS

The plastic analysis of grillages was developed by Heyman (22,23) using the principle of kinematics. The method of solution is to find the minimum collapse load out of the several possible collapse modes using the virtual work equations. The work equation can be established by equating the total work done by the hinges in the collapse mechanism i.e. the rotation of the hinges, multiplied by the fully plastic moment, to the work done by the applied load. In further work on grillages, the effect of torsion in the formation of plastic hinges was considered and the general breakdown criterion of interaction between bending and torsion was introduced as

$$M^2 + (\alpha.T)^2 = Mo^2 \qquad (5.11)$$

where M and T are the applied bending and torsion respectively;
Mo is the fully plastic moment in pure bending;
α is the shape factor of the cross section.

The shape factor, α, was taken to be unity and the breakdown criterion combined with the associated Flow Law gave

$$\frac{M}{T} = \frac{\theta}{\phi} \tag{5.12}$$

where, θ and ϕ are the changes in bending and twisting angles respectively.

By solving the two Eqn.5.11 and Eqn.5.12 simultaneously, the following results are obtained:

$$M = \frac{\theta}{\sqrt{(\theta^2 + \phi^2)}}$$

$$T = \frac{\phi}{\sqrt{(\theta^2 + \phi^2)}} \tag{5.13}$$

The work done at the hinge is

$$Eint = M.\theta + T.\phi \tag{5.14}$$

Then, it becomes:

$$Eint = M.\sqrt{(\theta^2 + \phi^2)} \tag{5.15}$$

In fact, it is found that the load determined by this kinematic principle is always greater than the true collapse load. Thus, this principle provides the method for determining an upper bound solution for a grillage system.

In 1956, Reynolds (62,63) introduced the upper bound solution for prestressed concrete grillage bridges and proposed a procedure that plastic hinges could be inserted to make the structure statically determinate in which a maximum possible shear force and an unknown moment are assumed acting at these hinges. This enables a statically admissible system to be checked, and the collapse load, as an upper bound solution, to be obtained. For comparison with the experimental results, the theoretical ultimate loads for various grillages are

given in Table 5.5. In each case the statically admissible system was checked for the critical load as an upper bound solution. The analytical method gave a reasonable estimate of the ultimate load. It is noticeable that the underestimate of the ultimate strength is in the range of 8 to 18% and this may be attributed to underestimating the ultimate torque of the main beams, and ignoring the torsional effects on the transverse grillage beams.

Table 5.5 Results of Prestressed Concrete Grillage Models by Reynolds

(1)	(2)	(3)	(4)	(5)	(6)
Grillage No.	Crushing strength (lb/in)	Tensile strength (lb/in)	Test load (lb)	Theoretical load (lb)	Load factor (4)/(5)
1	6400	460	3250	3000	1.08
2	6500	430	3400	3000	1.13
3	6700	470	3540	3050	1.16
4	7100	510	3700	3250	1.14
5	7900	520	3600	3040	1.18
6	7600	410	3200	3130	1.02
7	7200	530	3600	3220	1.12
8	6600	490	7400	6500	1.14

Holmes (26) also applied the principle of kinematics to predict the upper bound collapse loads of five longitudinal steel grids with various numbers of transverse members, loaded by a single concentrated load applyed at the mid-span of either the edge or central longitudinal. Ninteen model grillages were tested with two-way simple supports. The comparison of the results are shown in Fig.5.5. The experimental results agree with the analytical values with about ±10% discrepancy. This may be due to the fact that the torsional stiffnesses of the longitudinal members over the supports were neglected.

In the light of these results, Holmes (27) conducted another investigation of the grillages in an attempt to quantify the torsion effect on grillages with torsional end restraint. The results showed that the provision of torsional stiffness on the continuous supports

at both ends significantly increases the collapse load of the grillages. This additional strength was attributed to the additional plastic hinges required to form a complete failure mechanism. This phenomenon is illustrated in Figs.5.6a and 5.6b. Seventeen grillage models were tested with torsionally stiff supports. Despite the ultimate loads being calculated as the upper bound, the actual loads from the tests tend to err on the safe side. All these tests provided sufficient evidence to indicate that the torsional stiffnesses of the longitudinal beams have a significant effect on the ultimate load of a grillage.

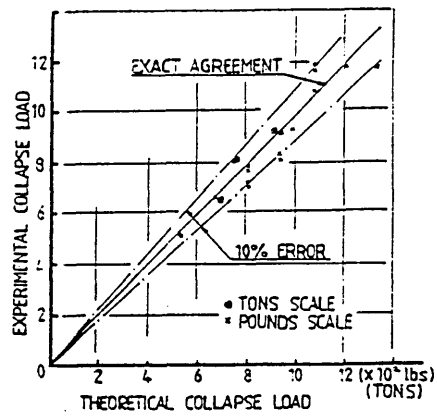

Fig.5.5 The Results of Nineteen Grillage Models by Holmes

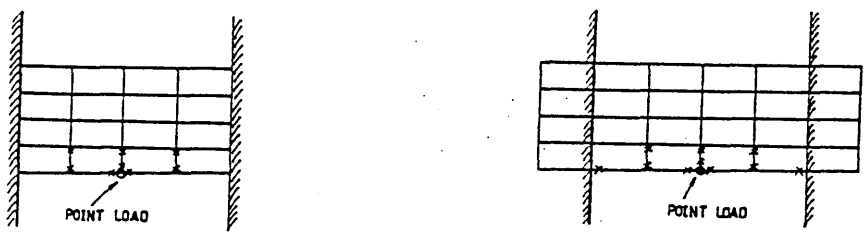

(a) Simply Supports (b) Torsionally Stiff Supports

Fig.5.6 Collapse Mechanism of Grillage Models with Simply and Torsionally Stiff Supports by Holmes

The analysis, based on a knowledge of the breakdown criterion for the formation of plastic hinges in a grillage system, under the action of combined bending and torsion, was extended by Holmes and Ray-Chaudhuri (28,60). Tresca's and Von Mises' yield conditions were adopted and

given in the general criterion equation

$$fb^2 + (\alpha.fs)^2 < fo^2 \qquad (5.16)$$

where fb and fs are the bending and shearing stresses;
fo is the resultant stress in simple bending;
α is a constant to which a value of 2 and $\sqrt{3}$ was assigned by Tresca's and Von Mises' yield conditions respectively.

In order to obtain the lower bound shearing stress distribution similar to that of a plastic section in pure torsion with reduced magnitude, Eqn.5.16 becomes

$$fs^2 < (fo/\alpha)^2 \qquad (5.17)$$

The ratio of this shearing stress to the corresponding resultant stress, based on the yield criterion, can be expressed in the form of the ratio, t, of applied torque, T, to the ultimate torsional capacity, Tu, of the section. It gives:

$$t = \frac{T}{Tu} = \frac{fs}{(fo/\alpha)} \qquad (5.18)$$

Similarly, for a normal stress distribution similar to that in pure plastic bending with reduced magnitude Eqn.5.16 gives,

$$fb^2 < fo^2 \qquad (5.19)$$

and, the corresponding non-dimensional bending parameter is

$$m = \frac{M}{Mu} = \frac{fb}{fo} \qquad (5.20)$$

Substitution of Eqn.5.18 and Eqn.5.19 into Eqn.5.16 then yields the significant approximate interaction curve:

$$m^2 + t^2 = 1$$

$$\text{or} \qquad \left[\frac{M}{Mu}\right]^2 + \left[\frac{T}{Tu}\right]^2 = 1 \qquad (5.21)$$

Since this yield criterion satisfies the equilibrium condition a statically admissible stress distribution with any set of stress resultants m and t lying in or on the circle defined by the equation can be traced.

Again, with the help of the associated flow law, the translations of a hinge correlates with the dimensionless stress resultants as:

$$\frac{m}{t} = \frac{\theta}{\beta.\phi} \qquad (5.22)$$

where, β is a parameter defined by Tu/Mu.

Hence, the total work done at a combination plastic hinge is given by,

$$Eint = \frac{Mu.\theta}{m} \qquad (5.23)$$

The comparison of the experimental and theoretical upper bound collapse loads for forty-six grillages can be seen in Fig.5.5. From this figure, it is seen that reasonable agreement is obtained in the range ±10% discrepancy.

In 1971, Heyman (24) indicated that a rectangular grillage of beams, loaded transversely would collapse with a mechanism involving both bending and twisting of the numbers. To obtain a lower bound collapse load, the formation of plastic hinges must satisfy the equilibrium condition and the circular yield criterion Eqn.5.21 with the help of its associated flow law. However, the construction of equilibrium equations is a tedious process and it becomes very cumbersome indeed for complex grillages. On the other hand, the derivation of upper bound solution remains simple, since hinge discontinuities are readily calculable from any assumed collapse mechanism, no matter how complex the structure is. This mothod of analysing grillages is analogous to the established procedures for calculating ultimate loads of

reinforced concrete slabs by yield line theory. The work equation in which the work dissipated in line hinges is equated to the work done by the applied loads, enables unsafe collapse loads to be established. The reliability and quality of such calculated loads depend on the 'reasonableness' of the assumed yield pattern or collapse mechanism.

Based on this upper bound approach, Marshall (43) applied the grillage analysis to reinforced concrete multi-panel, slab-beam systems. The actual slab system was transformed into an equivalent open grillage. The upper bound collapse load of each of the models tested was estimated for the collapse mode which was modified from the observed yield pattern. The modified failure mechanism for test slab No.4 is shown in Fig.5.7. The continuity of the top slab of the structure was assumed negligible and the interaction of bending and torsion was ignored. Therefore the bending and torsion capacities of the T- and L-beams could be determined independently. The ultimate torsional strength was obtained by the Sand Heap Analogy.

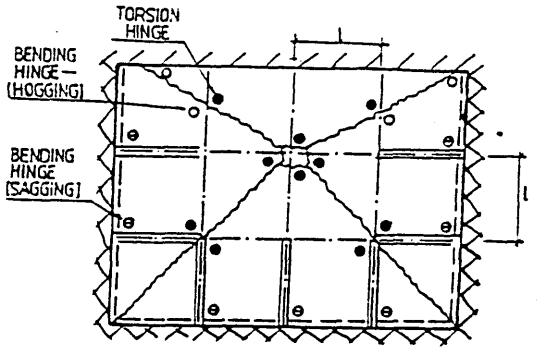

Fig.5.7 Modified Collapse Mechanism of Slab Model No.2 for Equivalent Open Grillage Analysis by Marshall

The external work done for the modified yield pattern in Fig.5.7 is

$$Eext = 4.w.l \qquad (5.24a)$$

and the internal work done by bending and tosional hinges is

$$Eint = 2(13Mi + 2Mt + 7Mt' + 4Te + 2Tc)/l \qquad (5.24b)$$

Equating these two equations gives

$$w = 76.9 \text{ kN/m}^2 \qquad (5.24c)$$

The results for the six model slab tests given in Table 5.3 have a very close agreement with the calculated ultimate loads using this equivalent open grillage approach.

Marshall's work gives strong indication that the reinforced concrete waffle slab may be analysed as an equivalent open grillage. His work on reinforced concrete waffle slabs was somewhat limited, however, in that only a few parameters were considered, and further work is necessary to confirm the general applicability of this method.

5.4 THE STRIP METHOD

Hillerborg's strip method is based on the lower bound concept and is normally used in the design of reinforced concrete slabs. This theorem states that a lower limit of carrying capacity in the slab can be determined if the distribution of moments for the applied load satisfies the equilibrium equation as well as boundary conditions, and if any moment throughout the slab does not violate the yield criterion. The equilibrium equation is given as before in Eqn.3.3.

$$\frac{\partial^2 Mx}{\partial x^2} - 2\frac{\partial^2 Mxy}{\partial x \partial y} + \frac{\partial^2 My}{\partial y^2} = -p(x,y) \qquad (5.25)$$

This criterion must be satisfied at any point in the slab. The moment field is deliberately made to coincide with the resistance moment field due to the reinforcement by considering that the twisting moments, Mxy and Myx, are assumed to be negligible. The reduced equilibrium equation can then be partitioned such that the proportions of load, κ and $(1-\kappa)$, shared by the x and y axes are respectively.

$$\frac{\partial^2 Mx}{\partial x^2} = -\kappa.p(x,y) \quad ; \quad \frac{\partial^2 My}{\partial y^2} = -(1-\kappa).p(x,y) \qquad (5.26)$$

A simply supported slab ABCD carrying a uniform distributed load, w, is shown in Fig.5.8. It is assumed that the load at any point on the slab is carried to the nearest support. The lines of load discontinuity are introduced to allocate the load distribution. With these lines of discontinuity, the bending moment diagrams for strips XX and YY can be directly determined as shown. Reinforcement can be provided accordingly so that the yield criterion is not violated in the slab. Hillerborg then suggested reasonable spacing of the reinforcement in uniform bands where the average maximum moment for strips within that band was taken as the design moment. This proposal was based on the moment redistribution within the slab. The average maximum moment for a chosen band within Fig.5.8 is given by:

$$M(ave) = \frac{w}{2}[(l_1 + l_2)/2]^2 . \kappa \qquad (5.27)$$

where, $\kappa = \frac{4}{3}\left[1 - \frac{1}{(l_1/l_2) + 2 + (l_2/l_1)}\right]$

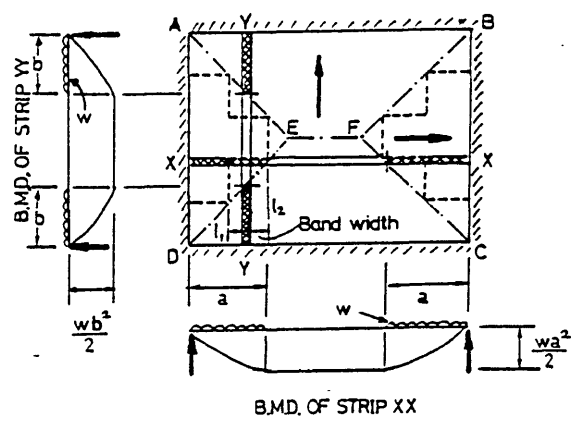

Fig.5.8 Idealized Load Dispersion and Bending Moment Diagrams by Hillerborg

The essential feature and attraction of the strip method are that it is a direct lower bound design approach for a slab with variable reinforcement, rather than a method of analysis for a slab with given uniform reinforcement. As it is regarded as an ultimate load design

method, it may be worth examining the working load behaviour of a waffle slab from the serviceability point of view. At the same time, alternative design methods recommended by the current codes are also considered here for comparison.

5.4.1 Comparison with Current Code of Practice

BS8110 (5) allows reinforced concrete waffle slabs to be designed by any of the methods listed as follows:

(i) Elastic analysis based on ultimate design load;
(ii) The yield line analysis; and
(iii) The strip method.

The ultimate strength of slabs designed using the Grashof-Rankine coefficients given in Table 13 of BS8110 is guaranteed to be on the safe side. However, it is evident that the working load behaviour of waffle slabs may not satisfy the acceptable level of the required limit states. In order to demonstrate this, the design of a simply supported square waffle slab with side-length, L, and subjected to uniform distributed load, w, is considered. The moments given by the Grashof-Rankine and the yield line methods are $M = 0.062wL^2$ and $M = 0.056wL^2$ respectively. For the purpose of comparison between solid and waffle slabs, the imposed load factor of 1.6 is applied and the self-weight of the slab is ignored. Therefore, the design ultimate moment, using high values on the safe side becomes $Mu = 0.0992wL^2$. The homogenous elastic moments for solid and waffle slabs, given by Tebbet (70) using the finite difference method, are $0.037wL^2$ and $0.069wL^2$ respectively. The moment ratio of working load to ultimate load conditions for the solid slab at mid-span is (0.037/0.0992=) 0.373 which is about one-third of its ultimate design strength. Thus, the slab is well within its elastic behaviour and remains mostly uncracked. In contrast, the ratio of (0.069/0.0992=) 0.696 which is obtained for the waffle slab, therefore is subjected to a much higher stress than that in the solid slab. As a result, the degrees of cracking and deflection are far more severe than the codes would anticipate in the design procedure.

Applying the strip method to the slab, the most suitable division of a waffle slab is suggested (70) to be the division into three strips

equal in width, as shown in Fig.5.9. The corresponding maximum strip moments for strips A-A and B-B are $0.028wL^2$ and $0.090wL^2$ respectively. Thus, the moment ratio of [0.069/(1.6x0.090)=] 0.479 is obtained which is much closer to the value anticipated by the British Standard.

To gauge the effect of the strip method, the steel volume (70) required by both design methods should be checked. The steel volume, Vh, in accordance with the code for the middle strip alone is:

$$Vh = 2x0.062wL^2x0.75L^2 = 0.093wL^4 \qquad (5.28)$$

The corresponding uncurtailed total steel volume, Vu, for the strip method, shown in Fig.5.9 is

$$Vu = 2x(2x0.0028 + 0.090)wL^2x(L^2/3) = 0.097wL^4 \qquad (5.29)$$

From these results, it can be seen that the working load behaviour of waffle slabs can be improved to a more acceptable level by the strip method without any increase in steel volume.

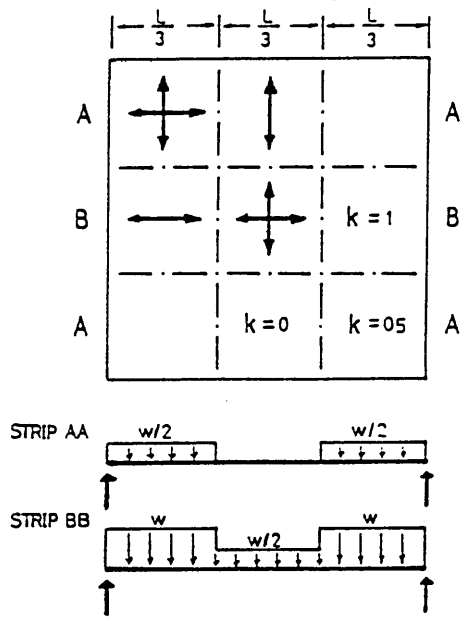

Fig.5.9 Idealized Load Dispersion Diagram by Tebbit

5.4.2 Reviews of Previous Works

A thorough investigation by Wood and Armer (82) concluded that if the reinforcement was chosen in accordance with the slab strip moments, then the method provided an exact solution for the collapse mechanism. For general design and construction purposes, it is more simple to keep the reinforcement uniform with different spacing in two directions. It is this uniform reinforcement which gives rise to reserve strength and moment redistribution before a complete collapse mechanism is formed. In fact, this reserve strength, contributing to the ultimate load capacity of the slab, can be readily checked by the conventional yield line analysis.

In the light of this fact, Thakkar and Sridhar (72) proposed a modified strip method using the weighted average moment to design a slab, Fig.5.10. In this method, the moment distribution curve along a supporting edge is averaged to that of an equivalent uniform moment at that edge. Therefore, the average moment distribution per unit width of the slab is derived for uniform orthotropic reinforcement along the whole length of the slab. This is illustrated in Fig.5.10. In particular, the weighted average moment for a built-in support about y-direction is given by

$$(Ms + Mm)y = \frac{1}{Lx}\cdot\frac{wLy^2}{24}\left[\left(\frac{Ly}{2} + \frac{3Ly}{4} + 3\left(Lx - \frac{5Ly}{4}\right)\right)\right] \qquad (5.30)$$

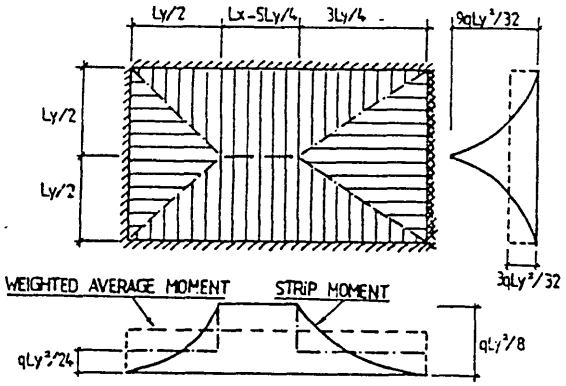

Fig.5.10 Idealized Load Dispersion and the Weighted Averages Moment Diagrams by Thakkar and Sridhar

For a simple support at this edge with Ly/Lx = α, the support moment, Ms, is equal to zero and the span moment, Mm, is therefore given as:

$$Mmy = \frac{wLy^2}{24}\left(3 - \frac{5\alpha}{2}\right) \qquad (5.31)$$

In the case of a fully restrained edge, the distribution between the span to support moment is suggested to be 2:1 in the light of the serviceability behaviour.
In this way, the slab design with uniform reinforcement based on the weighted average moment, can be checked by yield line analysis to assess the degree of safety. Hence the seviceability and the ultimate strength of the slab are both guaranteed by this design procedure.

It has been shown that the theoretical moments of waffle slabs can be reduced accordingly by design using the strip method. Economical design using this approach is proved to be valid. However, in accordance with BS8110, all regions of the slab should at least be reinforced with the minimum level of steel. Because of this, a uniform reinforcement layout may often be more economical in terms of total cost. It is the intention of the author to investigate whether or not this approach can be used in an attempt to analyse the waffle slab models albeit with adequate modification. In comparing the theoretical and experimental results, it is felt that the modified strip method (72) strongly indicates the possibility of developing this design approach into an analytical procedure for this type of slab structures.

5.5 INTERACTION BETWEEN BENDING AND TORSION

Generally all concrete members in a structure are subjected to axial, bending, shear and torsional loads. The behaviour of members subjected to axial and shear loads is well understood. However, the behaviour of concrete members subjected to torsion and bending is not yet fully defined. In the past, designers have considered torsion as a secondary effect which was usually ignored, or which could be adequately accounted for by the relatively large factor of safety inherent in design codes.

A literature search for the behaviour of reinforced concrete rectangular and Tee-beams, subjected to combined loading in the absence of shear, was carried out. The plastic analysis using the breakdown interaction criterion (22,23,24,28) was successfully applied to an open grillage. A number of experimental reports have been studied and the attempts to develop the relationship of the combined action are discussed in the following sections.

5.5.1 Reinforced Concrete Members Subjected to Bending and Torsion

5.5.1.1 Beams with Longitudinal and Transverse Reinforcement

Basically, there are three approaches for predicting the behaviour of fully reinforced concrete rectangular beams subjected to combined bending and torsion as follows:

i) Cowan's Theory (13);
ii) Lessig's Theory (38); and
iii) Walsh, Collins, Archer and Hall's Theory (81).

The Russian method by Lessig is the most widely used in this context and it has been extended by Walsh et al. All these theories are well described elsewhere. The objective of the present investigation into this aspect is to develop a simplifying relationship between bending and torsion for reinforced concrete Tee-beams based on available previous works. It is the author's intention that these theories, developed for the rectangular beams, would not be included in here. Instead of these, the reinforced Tee-members under combined loadings will be discussed hereafter.

Based on the proposed idealised concrete failure mode shown in Fig.5.11, Kirk (35) suggested two analytical methods for predicting the ultimate strength for T-beams subjected to combined loads. The first analytical approach is similar to the analysis of failure presented by Lessig (38) for a rectangular member. The second is similar to the analysis described by Walsh et al (81). Twenty-six Tee-beam specimens were tested by Kirk for this purpose and the results were in close agreement with the theoretical predictions. The ultimate torque is taken as the lower value computed by these two methods.

Kirk's Method [1] analysis is given as:

$$\text{Torque, } T = \left[\frac{h - a' - Xn/2}{(M/T) + \tan\theta n}\right].[Fl + 0.8.Vt.\tan\theta n] \qquad (5.32)$$

where,

$$\tan\theta n = \frac{-M}{T} + \sqrt{\left\{\left[\frac{M}{T}\right]^2 + \frac{Fl}{0.8Vt}\right\}}$$

$$Xn = \frac{Fl + 0.8Vt.\tan\theta n}{0.85fcy.b.(\tan\theta n + 1)}$$

$$Vt = \frac{Fs.b^2}{s.(b + 2h)}$$

where, n is the Mode number and M/T is taken in both cases as positive;

Fl and Fs are the forces developed in the bottom longitudinal steel and each stirrup leg respectively;

fcy is cylinder compressive strengh of concrete.

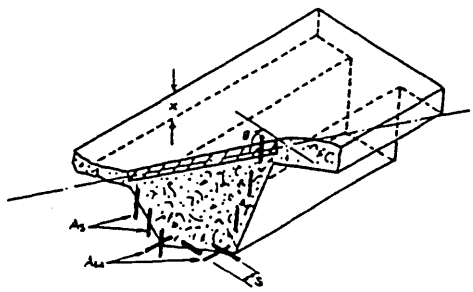

Fig.5.11 Failure Mode of the Idealized T-Beam Subjected to Bending and Torsion by Kirk

Kirk's Method [2] analysis gives:

$$\text{torque, } T = \frac{2.Mu.Vt}{Fl}\left\{\sqrt{\left[\left(\frac{M}{T}\right)^2 + \frac{Fl}{Vt}\right]} - \frac{M}{T}\right\} \qquad (5.33)$$

Two significant interaction relationships were obtained and they are:

(i) The interactive relationship of the torsional and flexural moments at first crack to the corresponding ultimate torsional and flexural capacities of plain members for the 24 beam tests given in Table 5.6 is approximated by a circular curve given by:

$$\left[\frac{Tcr}{Tup}\right]^2 + \left[\frac{Mcr}{Mup}\right]^2 = 1 \qquad (5.34)$$

The experimental results are shown in Fig.5.12.

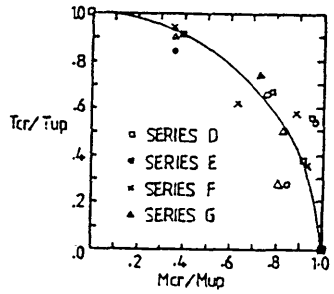

Fig.5.12 The Experimental Results of the Torsion-Bending Interaction of the Twenty-Four T-Beams at Cracking Load by Kirk

(ii) The interactive relationship between the applied torsion and flexural moments and their corresponding ultimate torsion and flexural moments for the 18 reinforced beams, in Table 5.7, can also be approximated by a circular curve yielding the following equation:

$$\left[\frac{T}{Tu}\right]^2 + \left[\frac{M}{Mu}\right]^2 = 1 \qquad (5.35)$$

where, T and M are the applied torsional and flexural moments respectively;

Tcr and Mcr are the cracking torsional and flexural moments of reinforced concrete members respectively;

Tu and Mu are the ultimate torsional and flexural moments of reinforced concrete members respectively;

Tup and Mup are the ultimate torsional and flexural moments of plain concrete members respectively.

The non-dimensional form of these experimental results is shown in Fig.5.13.

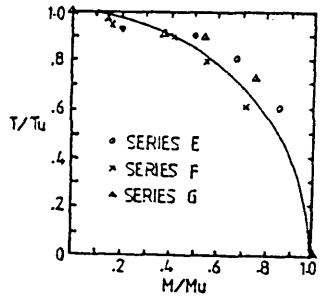

Fig.5.13 Results of the Torsion-Bending Interaction of the Eighteen Reinforced T-Beams at Ultimate Load by Kirk

Table 5.6 Results of the Twenty-Four T-Beams at Cracking Load by Kirk

Beam No.	Cracking Loads (in_kips)		Tcr / Tup	Mcr / Mup
	Tcr	Mcr		
D-1	16.20	0.00	1.00	0.00
D-2	14.70	3.72	0.88	0.39
D-3	10.90	7.45	0.67	0.78
D-4	9.00	9.22	0.56	0.96
D-5	6.07	8.77	0.38	0.91
D-6	0.00	9.60	0.00	1.00
E-1	16.80	0.00	1.04	0.00
E-2	14.10	3.59	0.87	0.37
E-3	11.11	7.58	0.69	0.79
E-4	9.12	9.37	0.56	0.98
E-5	4.67	8.24	0.29	0.86
E-6	0.00	9.70	0.00	1.01
F-1	14.00	0.00	0.86	0.00
F-2	13.10	3.34	0.81	0.35
F-3	8.62	5.92	0.53	0.62
F-4	8.12	8.37	0.50	0.87
F-5	5.02	8.84	0.31	0.92
F-6	0.00	9.40	0.00	0.98
G-1	15.10	0.00	0.93	0.00
G-2	13.60	3.46	0.84	0.36
G-3	11.10	6.91	0.69	0.72
G-4	7.60	7.86	0.47	0.82
G-5	4.32	7.64	0.27	0.80
G-6	0.00	9.50	0.00	0.99

Later, Kirk and Loveland (37) carried out two further analytical approaches by another failure mode, to predict the ultimate load capacity of unsymetrically reinforced Tee-beams, subjected to combined bending and torsion. These two methods yield the results as described in Eqn.5.32 and Eqn.5.33, where n is the mode number and M/T is positive for Mode 1 and negative for Mode 2.

Table 5.7 Results of the Eighteen T-Beams at Ultimate Load by Kirk

Beam No.	Ultimate Loads (in_kips)		Theoretical Loads (in_kips)		T/Tu	M/Mu
	T	M	Tu	Mu		
C-1	14.80	0.00	14.40	0.00	1.03	0.00
C-2	14.20	0.00	13.80	0.00	1.03	0.00
E-1	21.00	0.00	21.50	0.00	0.98	0.00
E-2	19.60	4.96	20.40	5.09	0.91	0.19
E-3	18.90	12.80	18.70	12.50	0.88	0.49
E-4	17.10	17.40	16.40	16.40	0.80	0.66
E-5	12.80	22.00	12.00	20.70	0.60	0.83
E-6	0.00	26.00	0.00	26.40	0.00	0.99
F-1	19.50	0.00	21.60	0.00	0.09	0.00
F-2	18.50	4.68	20.10	5.01	0.86	0.16
F-3	17.50	11.70	17.50	11.60	0.81	0.41
F-4	15.50	15.80	15.20	15.20	0.72	0.55
F-5	11.80	20.40	11.40	19.70	0.56	0.71
F-6	0.00	28.70	0.00	28.90	0.00	0.99
G-1	14.20	0.00	19.40	0.00	0.89	0.00
G-2	16.60	4.21	17.20	4.30	0.86	0.15
G-3	15.70	10.60	15.50	10.30	0.81	0.38
G-4	15.50	15.70	14.30	14.20	0.80	0.56
G-5	12.50	21.70	10.60	18.30	0.64	0.78
G-6	0.00	29.00	0.00	28.00	0.00	1.04

Eighteen unsymetrically reinforced concrete Tee-beams were tested under various combinations of bending and torsion. They found good correlation between the theoretical predictions and the experimental results. It is important to note that this programme of tests substantiated the previous findings and obtained better results of the interactive circular relationship in the non-dimensional form as described in Eqn.5.35.

Victor and Aravindan (80) conducted another thorough experimental and analytical study on the ultimate torsional strength of prestressed and reinforced concrete T-beams under combined loads. They proposed three modes of failure, obtained from the observations of the beams tested. The only difference in this investigation compared to Kirk's work is that the effect of overhanging flanges was taken into consideration in the analysis. The validity of the developed equations were verified by their own experimental results, as well as the results of a large number of beams reported by other investigators. It can be concluded that for a concrete T-beam under predominantly bending load, the provision of flanges provide some torsional resistance even without the provision of closed stirrups in the flangs. In contrast, a concrete T-beam under predominatly torsional moment could behave like a T-beam at ultimate stage, only if closed stirrups were provided in the flanges.

5.5.1.2 Beams with Longitudinal Reinforcement Only

Results of experimental investigations into the behaviour and strength of longitudinally reinforced rectangular and T-beams, subjected to combined bending and torsion have been published by Ramakrishnan and Vijayarangan (59), Victor and Ferguson (79), Kirk and Lash (36), and others.

Ramakrishnan and Vijayarangan (59) showed that the ultimate torsional strength of rectangular beams without stirrups depended only on the property of concrete i.e. the contribution from longitudinal reinforcement was insignificant. The results of these fourteen beam tests are shown in Table 5.8. It is important to note that the interaction equation given by Ramakrishnan et al showed a good approximation for the lower bound for any given member subjected to combined loadings. The equation is in the form of

$$\left[\frac{M}{Mu}\right]^2 + \left[\frac{T}{Tup}\right]^2 = 1 \qquad (5.36)$$

Further experimental work was carried out by Victor and Ferguson (79) on longitudinal reinforced T-beams subjected to combined loads. They

concluded from their tests that the increase in the ultimate torsional strength, due to the combined interaction was negligible. They also showed that the increase in the torsional capacity of concrete T-beams under pure torsional moment, due to the provision of longitudinal steel, was small and could be ignored; but the torsional resistance, from the flanges of the T-section, could not be neglected. The ultimate torsion capacity of any section under pure torque was obtained by the Sand Heap Analogy of the plastic theory.

From the test results, Kirk (35) indicated that the ultimate torsion capacity of a longitudinally reinforced concrete Tee-beam could be obtained as that for the corresponding plain Tee-beam. In fact, based on the test results, the torsion capacity of the plain concrete Tee-beam was satisfactorily predicted by the Sand Heap Analogy.

Table 5.8 Results of the Fourteen Rectangular Beams with All Stirrups Subjected to Bending and Torsion by Ramakrishnan and Vijayarangan

Beam No.	Concrete Strength Comp. fcu (N/mm^2)	Tension ft (N/mm^2)	Applied Bending Moment (kNm)	Applied Twisting Moment (kNm)	T / To	M / Mo
1	25.3	1.724	18.473	0.000	0.000	0.813
2	18.8	1.703	0.170	2.717	0.956	0.010
3	15.5	1.462	0.170	2.595	1.043	0.012
4	22.4	1.869	21.524	0.000	0.000	1.000
5	22.0	1.828	10.847	3.035	0.065	0.549
6	22.6	1.869	15.422	2.079	0.649	0.795
7	21.7	1.848	12.372	2.741	0.877	0.633
8	27.4	2.662	8.304	3.453	0.948	0.337
9	32.1	2.366	4.237	3.957	0.977	0.147
10	30.5	2.359	13.389	2.730	0.697	0.489
11	26.3	2.096	7.389	3.035	0.855	0.308
12	27.4	2.186	9.321	3.589	0.980	0.378
13	22.8	2.083	21.524	0.000	0.000	1.000
14	20.2	1.945	20.507	1.751	0.588	1.128

§ Mo = 21.524 kNm ; To = 3.331 kNm

5.5.2 Ultimate Torsional Capacity of Reinforced Tee-Beams

5.5.2.1 Sand Heap Analogy

Based on the membrane analogy, Nadai (47) developed the plastic theory of the "Sand Heap Analogy" for the torsional strength of the concrete section. The ultimate torque related to the shear stress is given as:

$$Tu = 2V.fsu \tag{5.37}$$

where, Tu is the ultimate torque determined plastically;
V is the volume of plastic membrane having a unit slope;
fsu is the ultimate shear stress.

For a concrete T-beam, having a cross-section given in Fig.5.14, its volume of the plastic membrane having a unit slope, can be expressed (35) as:

$$V = \frac{1}{4}.[b^2.(h - \frac{b}{3}) + t^2.(Sw - b)] \tag{5.38}$$

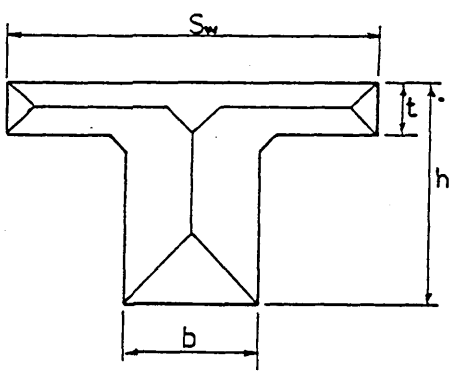

Fig.5.14 Cross-Section for T-Sections for Sand Heap Analogy

5.5.2.2 Ultimate Shear Stress for Concrete Members

It was found by Kirk (35) from his investigation of reinforced concrete Tee-beams that it was reasonable to assume that the ultimate shear stress of the member was taken as the tensile strength of the concrete obtained by direct tensile test. However, it is generally accepted that the tensile strength of concrete is proportional to the square root of the cylinder compressive strength of concrete, $\sqrt{fcy}$ in p.s.i. units. Because of this, it is more practical to express the

ultimate shear stress of a concrete member in terms of the compressive strength of concrete. The lower bound values of fsu were taken as $4\sqrt{fcy}$ and $3.5\sqrt{fcy}$ by Kemp (34) and Walsh et al (81) for applying the plastic theory to rectangular concrete members respectively. From the eleven tests on longitudinally reinforced T-beams, without stirrups, Victor and Ferguson (79) concluded that the ultimate shear stress of $5\sqrt{fcy}$ was a reasonable lower bound value for estimating the torsional strength of these members. The result of the tests are shown in Table 5.9.

Table 5.9 Results of the Eleven Tests on Longitudinally Reinforced T-Beams Without Stirrups by Victor and Ferguson

Beam No.	fcy (psi)	Cracking Load Trc (psi)	Plastic Theory Kp
T-1	3020	10.24	5.91
T-2	4650	10.65	5.06
T-3	4680	11.99	5.34
T-4	4650	12.00	5.40
T-5	4450	12.42	5.88
T-6	4920	8.73	3.88
T-7	4980	12.65	6.08
T-8	4820	11.99	5.70
T-9	4920	11.64	5.35
T-10	3770	14.04	6.80
T-11	3520	11.25	5.77
	Mean fcy		5.57

†fcy is the cylinder compressive strength of concrete.

Extensive experimental work on the combined bending and torsion of reinforced concrete T-beams was also conducted by Kirk (35). The plastic theory employed in the investigation gave satisfactory and consistent results for the cracking torque of Tee-beams subjected to pure torsion, given in Table 5.10. Kirk showed that the actual mean ultimate shear stress of plain concrete and longitudinally reinforced concrete T-beams was sligthly in excess of $5\sqrt{fcy}$.

It is clear that the nominal reinforcement provided in the rib sections and the top slabs of the models was intended to prevent any local shear failure. For the present investigation, the stirrups were

concentrated in the rib sections and did not extend to the top slab or flanges, and their spacings were relatively wide. Therefore, it is justified to consider that the idealized T-sections from the slab models can be treated as logitudinally reinforced concrete members. Based on all these results, it can be assumed that the provision of longitudinal reinforcement in an idealized T-section has a small effect on its ultimate torsion capacity under pure torsion, and this ultimate torsion capacity can be determined as the ultimate capacity of the plain T-sections using the Sand Heap Analogy.

In fact, Ramakrishnan et al's interaction relationship can be applied conveniently to the longitudinally reinforced T-beams tested by Kirk et al, and the results are verified in Fig.5.15. From this interaction diagram, it is concluded that this approximate interaction curve provides the lower bound moments for the sections subjected to torsion and bending.

Table 5.10 The Cracking Torque of Reinforced T-Beams Subjected to Pure Torsion by Kirk

Beam No.	fcy (psi)	Cracking Load Trc (psi)	Plastic Theory Kp
A-1	3440	14.00	5.04
A-2	3220	15.90	5.75
B-1	2540	13.00	5.30
B-2	3060	14.00	5.20
B-3	2740	13.00	5.09
C-1	3030	13.60	5.07
C-2	2980	14.40	5.40
C-3	3450	13.50	4.72
C-4	3080	13.40	4.95
C-5	4410	16.40	5.08
C-6	4370	16.40	5.09
C-7	3940	15.70	5.13
D-1	4750	16.20	4.83
E-1	4590	16.80	5.10
F-1	3980	14.00	4.55
G-1	4020	15.10	4.90
	Mean fcy		5.08

† Trc = 48.70•Kpx/fcy

5.5.3 Conclusions

From the above studies, the following conclusions can be drawn:

(1) The effect of the provision of longitudinal reinforcements in the idealized T-section is small and can be neglected.

(2) The ultimate torsion capacity of an idealized T-section can be determined as equal to the plain T-section using the Sand Heap Analogy.

(3) The lower bound value of $5\sqrt{fcy}$ in p.s.i. can reasonably be taken as the ultimate shear stress for plain and longitudinal reinforced concrete sections.

(4) A simplified interaction curve for combined bending and torsion based on the works from Ramakrishnan and Vijayarangan, and Kirk can be taken as

$$\left[\frac{T}{Tup}\right]^2 + \left[\frac{M}{Mu}\right]^2 = 1 \qquad (5.39)$$

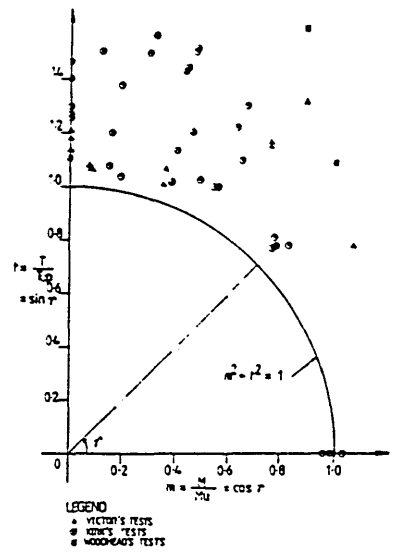

Fig.5.15 Simplified Bending-Torsion Interaction

5.6 THE MEMBRANE EFFECT

The phenomenon of 'arching' or 'membrane' action in concrete slabs has been widely reported. In the development of yield line theory, Johansen was aware of the presence of membrane action in some of his tests, but did not realize its full potential effect for the enhancement of the ultimate load capacity of slabs. Ockleston (33) obtained abnormally high failure loads on a series of full scale loading tests on slab panels, and his results sparked off an interest in this membrane phenomenon.

More recently, various series of tests have been carried out by Powell (57), Wood (9), Park (52), a team at Hatfield Polytechnic (18,45,56) and Ho (25), on the behaviour of under-reinforced concrete slabs with restrained edges subjected to uniformly distributed load. These studies have confirmed that the load carrying capacity of a slab can actually be several times greater than the theoretical load predicted by the yield line method. The results of these tests are given in Table 5.11 and Table 5.12, which show the results for reinforced and unreinforced slabs respectively, and Table 5.13 which shows the results obtained for reinforced concrete slabs with either one long side or one short side simply supported.

The earliest attempt to estimate the membrane enhancement was by Powell (57) who suggested a rigid-plastic solution for a beam based on the kinematic relations and equilibrium conditions. This approach was extended by Christiansen (7) who applied the compressive membrane action for beams to two-way spanning slabs. Christiansen reported a significant difference in the load-deflection relationship for simply supported and fully restrained R.C. beams subjected to a concentrated load at mid-span. Four simply supported beams, with identical cross-sections to that of the restrained beams, were tested and the results were compared with those of the restrained beams. A comparsion of the results for one of the beam tests can be seen in Fig.5.16. The difference in the two curves shows the load capacity enhanced by the membrane action. Christiansen then dervied the maximum membrane moment per unit width of a restrained beam as

$$Mm = fcu.h^2.x.(\kappa_1 - y - x) \qquad (5.40)$$

where, $x = (2.\kappa_2.y - y)/[4.(\kappa_2 - y)]$

$$0 = 3y^4 + (8\kappa_2 - 4\kappa_1)y^3 + (6\kappa_2^2 - 12\kappa_1\kappa_2)y^2 - 12\kappa_1\kappa_2^2 y + 4\kappa_1\kappa_2$$

$$\kappa_1 = 1 - (\Delta e/h) - (T_1 - T_2)/[fcu.h]$$

$$\kappa_2 = [fcu.L^2.(1 + \kappa)]/[8.Ec.h^2]$$

in which κ is the ratio of outward movement of supports to elastic frame, an approximate value of 1.2 was used (7);

Ec is the modulus of elasticity of the beam;

Δe is the elastic deformation of the beam;

T_1 and T_2 are the tensile strengths of the reinforcement at support and mid-span respectively.

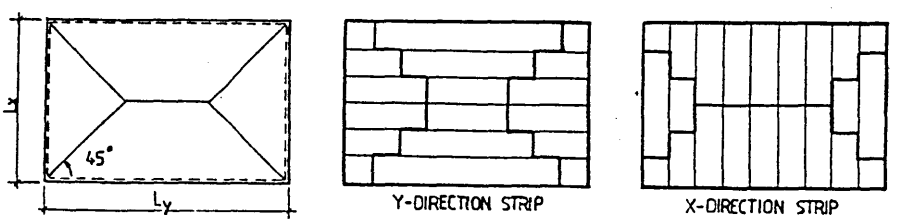

Fig.5.16 Idealized Yield Line Pattern and Strip System of R.C. Slab with Restrained Edges Subjected to Uniformly Distributed Load

This approach was further applied to two-way slabs and the ultimate strength was expressed in terms of the steel percentage and the span to effective depth ratio. Discrepancies were found in the prediction of the deflection at which maximum membrane action occurred. The excessive deflections obtained from the tests actually predicted a reduction of the theoretical enhancement of the slab. This reduction may possibly be due to an overestimate of the elastic shortening of the member subjected to the membrane stresses.

Table 5.11 Results of R.C. Slab Tests with All Edges Fully Fixed

Reference	Slab mark	Test load	Theoretical load by		Load factors	
			Park	Johansen		
		Wt	Wp	Wj	Wt / Wj	Wt / Wp
		(kN/m^2)				
Powell (57)	S46	311.0	247.4	38.0	8.18	1.26
	S47	266.8	271.6	38.0	7.02	0.95
	S50	332.4	257.8	67.7	4.91	1.29
	S54	365.5	297.9	106.4	3.44	1.23
	S55	330.1	283.3	106.4	3.57	1.34
	S56	342.8	345.6	172.8	1.99	0.99
	S59	351.1	341.4	172.1	2.04	1.02
	S62	427.1	418.2	365.4	1.61	1.02
	S63	465.2	401.6	263.3	1.77	1.16
Wood (82)	FS12	116.7	102.1	10.4	11.18	1.14
	FS13	84.8	98.2	20.7	4.09	0.56
Park (52)	A1	212.9	177.6	58.1	3.67	1.20
	A2	216.1	179.0	79.5	2.72	1.21
	A3	216.3	239.1	140.3	1.86	1.09
	A4	257.8	248.1	177.6	1.46	1.04
Parkman (56)	F1	59.0	46.5	10.2	5.70	1.27
	F2	70.0	56.5	12.4	5.65	1.24
	F3	86.0	68.0	20.7	4.15	1.26
Garnham (18)	M1	66.7	79.6	42.8	1.56	0.84
	M2	67.7	78.6	28.3	2.39	0.86
	M3	40.8	51.4	20.9	1.95	0.79
Ho (25)	H1	53.0	94.8	16.3	3.25	0.56
	H2	58.0	133.0	24.2	2.39	0.44
	H3	72.0	145.4	34.2	2.11	0.55
	H4	63.5	124.5	14.9	4.26	0.51
	H5	62.5	150.4	21.0	2.98	0.42
	H6	66.5	119.7	27.7	0.38	0.55

Table 5.12 Results of Unreinforced Concrete Slab Tests with All Edges Fully Fixed

Reference	Slab mark	Test load Wt	Park's load Wp	Load factor Wt/Wp
		(kN/m²)		
Powell (57)	S40	255.0	222.6	1.15
	S53	290.3	211.5	1.37
	S56	259.2	215.0	1.21
	S57	206.7	219.1	0.95
	S60	224.6	219.8	1.02
	S64	241.9	219.8	1.10
Wood (82)	FS14	64.3	87.2	0.74
Park (52)	D1	170.0	144.5	1.18
	D2	89.2	80.2	1.11
	D3	31.9	35.2	0.91
	D4	28.6	34.2	0.84
	D5	26.5	26.9	0.98
Garnham (18)	M4	34.4	51.0	0.67

Table 5.13 Results of R.C. Slab Tests with One Side Simply Supported and Three Sides Fully Fixed

Reference	Slab mark	Simple edge support	Test load Wt	Theoretical load: Park Wp	Theoretical load: Johansen Wj	Load factors Wt/Wj	Load factors Wt/Wp
			(kN/m²)				
Park (52)	B1	short	139.6	109.9	48.4	2.69	1.27
	B2	"	166.6	130.6	76.7	2.17	1.28
	B3	"	176.9	170.0	124.4	1.42	1.04
	B4	"	227.4	195.6	154.8	1.47	1.16
	C1	long	115.4	107.8	39.4	2.93	1.07
	C2	"	129.9	123.7	60.8	2.14	1.05
	C3	"	125.1	151.4	91.9	1.36	0.83
	C4	"	183.8	194.2	119.6	1.54	0.94
Makin (45)	MS2	short	37.3	83.4	35.1	1.06	0.65
	MS4	long	38.1	50.9	28.5	1.34	0.75

Brotchie and Holley (4) carried out a series of tests on forty-five slabs with laterally restrainted edges to investigate the compressive membrane action with various span to depth and reinforcement ratios. A formula for predicting the membrane enhancement for restrained slabs was developed based on the equilibrium, strain and displacement of a strip in the slab. The maximum membrane enhancement is given as follows:

$$Wm = 6.fcu.[(h/L)^2 - 0.00133.(1 - \rho/\rho')] \qquad (5.41)$$

The maximum membrane force per unit width is approximately,

$$Fm = fcu.t.[0.5 - 0.000165(L/h)^2] \qquad (5.42)$$

where, fcu is the compressive strength of concrete;
t is the thickness of the slab;
L is the length of span;
ρ is the reinforcement ratio;
ρ' is the reinforcement ratio required for a plastically balanced design.

From the test results, it was found that the stiffness of the slab is increased by the effect of external restraint on the edges. After the maximum load is reached, the strength of the slab deteriorates rapidly with excessive deformation. The effect of edge restraint on load carrying capacity was reported to be sensitive to deflection, particularly for thin slabs. However, the enhancement increased with the increase in the slab thickness i.e. reduced span to depth ratio, and larger deflections for thick slabs were also recorded. It is strongly suggested that large deflections are required to allow full plasticity of the slab for the development of the membrane action. In addition to this, the effect of compressive strength of the concrete and the reinforcement percentage are apparently the other two factors contributing to load capacity of the slabs. In these investigations reasonable agreement between the theoretical and experimental results were obtained.

Jacobson (29) in 1967 presented a fuller report based on his investigation into the membrane action using several fundamental

parameters viz, the effects of span to depth ratio, reinforcement ratio and the locations of restraint. From the report on the fifteen slabs tested, the following conclusions may be drawn:

(i) The deformation of slabs, with high span to depth ratio, is associated with a typical non-linear geometrical instability where the load capacity is governed by the geometrical changes at the plastic hinges;

(ii) The amount of the membrane enhancement increases as the reinforcement ratio decreases; and

(iii) The boundary conditions have a major effect on the behaviour of restrained slabs. The effect of geometrical changes associated with the locations of restraint at the boundary, is greater than all other effects;

On the basis of these experimental results, Park (52,55) presented a rigid-plastic strip theory for ultimate load, taking into account the membrane action. The assumptions made in this approach are similar to the Hillerborg strip method. The slab is considered to be composed of strips running in two directions with yield sections, at right angles to the direction of strips. The torsional stiffnesses and the shortening of the strips are ignored, and the additional assumptions are also compatible with those of Johansen's yield line theory. The idealised strips of the slab are shown in Fig.5.17.

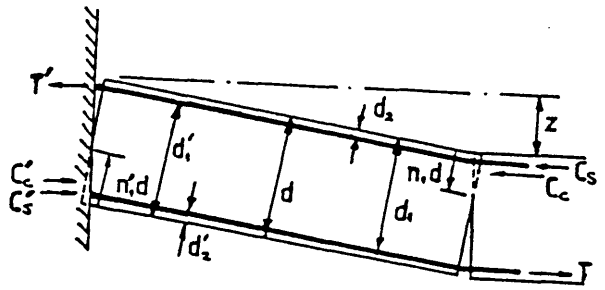

Fig.5.17 Internal Forces Acting in the Idealized Yield Section

At yielding, Park considered the stress resultants of the compressive forces in concrete, Cc, forces in compression steel, Cs, and forces in tension steel, T, at the strip to be statically equivalent to the membrane forces N, acting at mid-depth; similar conditions also

applied at the other end of the strip. Thus, the moments could be determined in terms of the unknown depth of concrete in compression in the strip. These unknown quantities could be obtained from the geometry of the deformed shape of the strip. From the virtual work equation, Park derived the load carrying capacity of the slab, with corner yield lines at 45^0 to the edges, with all edges fully restrained, in terms of the central deflection, z, in the form

$$W = \frac{24}{Ly^2(3\alpha - 1)}.\{\alpha Px_1 + Py_1 + z.[(\alpha - \frac{1}{2}).Px_2 + \frac{1}{2}.Py_2] + z^2(\alpha - \frac{1}{3}).P_3\} \qquad (5.43)$$

where Px_1, Px_2, Py_1, Py_2 and P_3 are Park's (34) constants with respect to x and y directions.

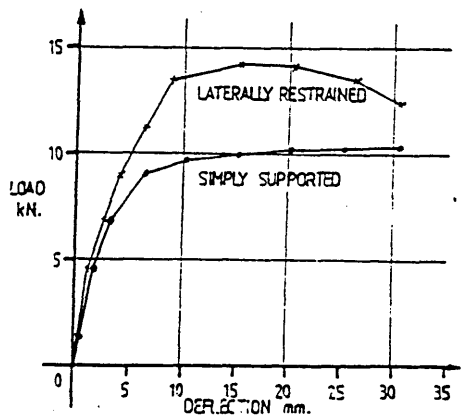

Fig.5.18 Load Deflection Characteristic of the Beam Tests by Christiansen

From his experimental work, Park found that for a rectangular slab, the maximum membrane enhancement, and hence the maximum ultimate load, occurred when the central deflection was approximately half the slab thickness. Substituting this derived deflection into Eqn.5.43, the ultimate load of the slab could be found.

It is clear that Johansen's yield line method will give results such that the term on the left in Eqn.5.43 is approximately equal to the second of the two terms on the right hand side. Thus, the effect of

membrane action is approximately represented by the first two terms on the right hand side of the equation.

Park (54) further applied this theory on twenty, nine-panel slab and beam floors models, with partial lateral restraint at all edges. A good correlation between experimental and theoretical results was obtained. However, it was concluded that to include compressive membrane action in the design more steel is required in the supporting beams. Extensive work (53) was also carried out to investigate the effects of partial restraint at all edges, and axial creep and shrinkage strains on compressive membrane actions. Another eight unreinforced concrete slabs were tested by Park under sustained loading. The essential findings from this investigation were that although the extended theory gave mostly conservative values compared with experimental results, the effects of axial strains and partial lateral restraint could reduce the enhancement of strength resulting from compressive membrane action.

Tong et al (75) took another view on the ultimate loads of slabs with restrained edges. They considered that the ultimate load capacity could be assumed to have two separate components: flexural strength provided by the reinforcement, Wf, and membrane enhancement due to the lateral restraint at the supports, Wm. These components could have a maximum value but they might not be mobilized simultaneously. Thus, a logical equation was suggested as

$$(Wf)max + (Wm)max > (Wu)max > (Wf)max \text{ or } (Wm)max \qquad (5.44)$$

The ultimate load of the slab, Wu, therefore should be less than the sum of the maximum values of the components but greater than either (Wf)max or (Wm)max whichever is larger. It was also indicated that the magnitude of the membrane moment was apparently a function of the vertical deflection and the compressive strength of the concrete in the slab. The critical deflection of a slab at failure was assumed to be half the effective depth of the slab. The membrane moments for both orthogonal directions are modified from the formula derived by Christiansen (7),

$$Mm = 0.2d^2.fcu \qquad (5.45)$$

where, d is the effective depth of the slab.

From the above studies, it is apparent that there is a good agreement between the experimental and theoretical results and it may be concluded that

(i) the locations of the edge restraint have a major effect on the load capacity;
(ii) the effect of membrane action increases with the thickness of the slab;
(iii) the load capacity increases as the steel percentage decreases;
(iv) the compressive strength of the concrete is a major contributory factor to the membrane enhancement; and
(v) the load carrying capacity is sensitive to the deflection of a slab.

Several theories have been advanced to predict the ultimate load capacity of restrained concrete slabs with different assumptions. However, all these theories can be summarized as the rigid-plastic strip approach. A review of the several test results (4,7,52,75) on under-reinforced concrete slabs indicates that a typical load-deflection characteristic can be obtained as shown in Fig.5.18 by Christiansen. Initially the slab behaves elastically, followed by elasto-plastic and then fully plastic behaviour. The ultimate load capacity is composed of two separate components due to flexural stength and membrane enhancement. For the development of membrane action, it is generally agreed that full plasticity of the slab must be reached (52) i.e. the steel should be at yield stress. At that instant, theoretically, the only forces to resist the applied load are the self-induced compressive membrane stresses of concrete acting along the yielded sections. The elastic/plastic deformations cannot be determined accurately due to the complexity of the stress conditions and, therefore, can be neglected for simplification, such as in Park's theory, by simply ignoring the shortening of the slab. Hence, based on the geometrical changes, the membrane moment can be estimated, as if an unreinforced concrete slab, in the form of the compressive strength of the concrete and the critical deflection of the slab.

CHAPTER 6

EXPERIMENTAL PROGRAMME AND RESULTS

6.1 EXPERIMENTAL PROGRAMME

To investigate the behaviour of rectangular reinforced concrete waffle slabs subjected to uniformly distributed and concentrated loads with various boundary conditions a total of twenty 1/4 scale and one 1/2 scale slabs were tested to failure. The programme of work was divided into nine series of tests with four different support conditions subjected to either uniformly distributed or 4-points load as given in Table 6.1.

Table 6.1 R.C Waffle Model Slabs Schedule

Slab No.	Loading condition	d/t ratio	No. of bars at mid-span	Support conditions
A1	U.D.L.	3	2	All four sides fully fixed
A2		3	3	
A3		3	4	
B1	U.D.L.	4	2	
B2		4	3	
B3		4	4	
C1	U.D.L.	5	2	
C2		5	3	
C3		5	4	
D1	U.D.L.	4	2	
E1	U.D.L.	3	4	One long side simply supported and the other sides fully fixed
E2		4	4	
E3		5	4	
F1	U.D.L.	3	4	One short side free and the other sides fully fixed
F2		4	4	
F3		5	4	
H1	U.D.L.	5	4	Supported at four corners
H2		5	4	
I1	4-Points loads	5	4	
I2		5	4	
J1*		4	4	

(Note: All reinforcing bars are 4.00mm diameter except the slab denoted with * has 6.00mm diameter.)

6.1.1 Description of Models

Three overall slab thicknesses of 55, 70 and 85mm were used for the 1/4 scale slab models with 50mm wide ribs in both orthogonal directions (170mm thick slab and 100mm wide in the 1/2 scale). A layout of six by five, 180mm square hollow pots was used for most of the model slabs. The exceptions were the 1/4-scale models with five by five, 226mmx180mm rectangular hollow pots used in series H & I; and the 1/2-scale model with 452mmx360mm rectangular hollow pots used in series J. A constant 15mm thick top slab was employed throughout the series of tests except for the 1/2-scale model which has a top slab thickness of 30mm. Four bars per rib were provided at the supports for fully restrained edges throughout these series of tests, and these edges were reinforced with two layers each of three 6mm diameter bars, top and bottom. Secondary reinforcement with two 3.19mm diameter bars per pot in both orthogonal directions were provided for every 1/4 scale models, Fig.6.1. All reinforcements had at least 4.5mm concrete cover. The schedule of the test slabs is given in Table 6.1.

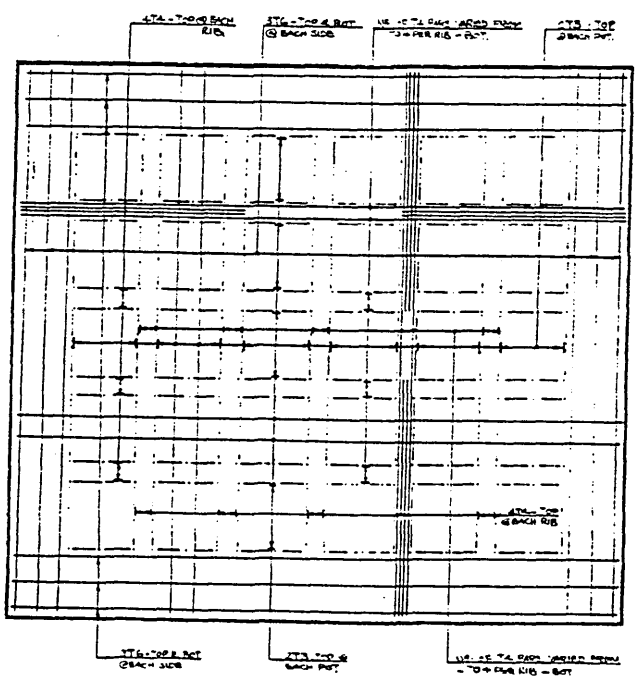

Fig.6.1 Reinforcement Details of 1/4 Scale Slab Model

6.1.2 Manufacture of Models

6.1.2.1 Model Scale

The selection of a model scale for this investigation was influenced by a number of factors such as space limitations and availability of equipment for testing and loading. The major aspect which required great care was to ensure that the model scale chosen would not produce misleading results due to scale or size effects. This is of great importance when the flexural and torsional behaviour of the slab up to ultimate load is being investigated. With the available test rig and loading system, a model with nominal quarter scale was selected for the majority of the test slabs.

6.1.2.2 Materials

Once the scale for the slabs was selected it was then necessary to produce a scaled concrete, or microconcrete. Apart from scaling the maximum aggregate size, it was necessary to ensure that the microconcrete mix would behave in a manner similar to that of full size concrete under the complex stress states which exist in the prototype (7). This could be achieved by suitably reducing the proportions of very fine sand, such that the ratio of tensile to compressive strength was similar to that of concrete use in full scale slabs.

A series of trial mixes was made in order to obtain a workable and representative mix to suit the model scale slab. The target tensile to compressive strength ratio was 0.08 at 28 days. From the results of the trial mixes, see Table 6.2 it was decided that a mix cóntaining Conplast 337 plasticiser at a dosage of 750ml per 50 Kg of cement, and a local zone 2 sand sieved to remove with particles of size larger than 3.35mm and smaller than 0.15mm, most closely satisfied the requirements. All sand was oven dried and sieved to the required size. A single batch of Ordinary Portland Cement sufficient for the whole programme of work was obtained and stored in sealed containers.

The 4.0mm diameter wire used in the model slabs was annealed by the manufacturers to give the required yield stress with a characteristic yield plateau before reaching the breaking strength. Due to the slenderness of the ribs and the relatively thin top slab, 3.19mm diameter mild steel wires were used for the transverse and secondary reinforcements.

Table 6.2a Results of Concrete Trial Mix

Trial Mix No.	W/C Ratio	Admixture Added	Sand Consitutient Percentage of Retained (mm)					
			3.25	2.36	1.18	0.60	0.30	0.15
4	0.686	Nil	0	5	13	14	23	45
5	0.686	2g †	0	0	20	20	40	20
6	0.742	17.4ml ‡	0	0	20	20	40	20
7	0.600	70.55ml♦	0	5	13	14	23	45
8	0.650	70.55ml♦	0	0	20	20	40	20
9	0.650	99.63ml♦	0	0	20	20	40	20
10	0.650	101.82ml♦	0	0	20	20	40	20

† Air-antraining Agent
‡ Cormix Plasticiser P2
♦ Conplast 337 Plasticiser

Table 6.2b Results of Trial Mix at Age 7-days

Trial Mix No.	Unit Weight ρ (Kg/m^3)	Slump Test (mm)	Tensile Strength ft (N/mm^2)	Compressive Strength fcu (N/mm^2)	Ten./Comp. Strength Ratio
4	2218	40	1.770	18.350	0.100
5	2102	60	1.910	16.530	0.116
6	2205	Coll.	2.250	21.570	0.104
7	2221	Coll.	2.338	27.130	0.086
8	2193	Coll.	2.674	25.530	0.105
9	2164	50	1.660	21.030	0.080
10	2234	Coll.	1.967	21.100	0.093

Table 6.2c Results of Trial Mix at Age 28-days

Trial Mix No.	Unit Weight ρ (Kg/m^3)	Slump Test (mm)	Tensile Strength ft (N/mm^2)	Compressive Strength fcu (N/mm^2)	Ten./Comp. Strength Ratio
4	2220	40	2.999	30.880	0.097
5	2112	60	2.405	25.300	0.095
6	2207	Coll.	2.430	30.330	0.080
7	2218	Coll.	3.250	37.590	0.087
8	2080	Coll.	3.310	36.070	0.092
9	2164	50	2.348	26.030	0.090
10	2243	Coll.	2.433	33.100	0.074

6.1.2.3 Reinforcement Cages

All stirrups were bent to size and the ends spot welded before being wired onto the main reinforcing bars. The required numbers of transverse reinforcement beam cages were first made. Then the longitudinal reinforcement was inserted and tied perpendicular to the transverse beam cages with the required numbers of stirrups in each pot. All main bars were bent up at both ends to provide anchorage. For the restrained edges, two layers of three 6mm diameter bars were added along the edges to increase the stiffnesses. Details of the reinforcement cages and typical cross-section of the ribs are given in Figs.6.2a to 6.2d.

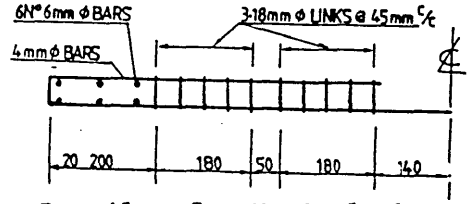

Fig.6.2a Reinforcement Details of a Typical Short Spanning Rib Cage

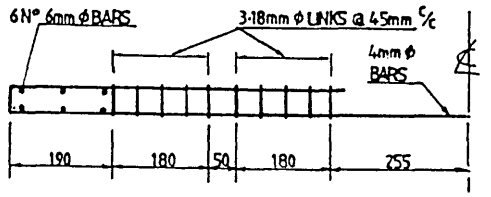

Fig.6.2b Reinforcement Details of a Typical Long Spanning Rib Cage

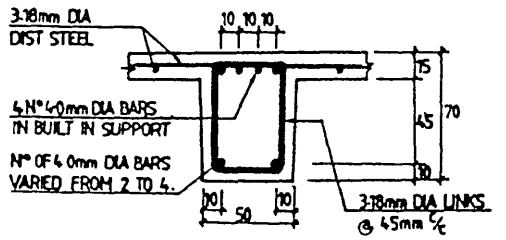

Fig.6.2c Typical Cross-Section of a Portion of Short Spanning Rib

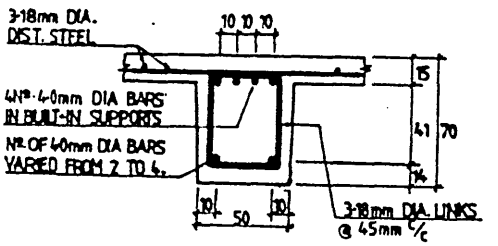

Fig.6.2d Typical Cross-Section of a Portion of Long Spanning Rib

6.1.2.4 Slab Form

The slabs were constructed using polystyrene blocks which proved to be an effective and easy to use method of forming the pots, Fig.6.3. The polystyrene blocks were trimmed to size within ±1mm tolerance, by an electrical hot wire cutting machine which produced a very good finished surface. These blocks were wrapped with very thin polythene film and then were fixed into position on the base plate of the mould by heavy duty 12mm wide double-sided tape. This type of fixing was chosen to prevent any cement paste seeping underneath the polystyrene blocks. Plastic parcel tape 50mm wide was used between the pot to provide a clean and smooth surface for concrete placing. Three different depths of polystyrene blocks, 45, 60 and 70mm, were used to suit the models with d/t ratios of 3, 4 & 5 respectively. Prior to casting, the steel pins to provide holes for the holding down bolts were placed in the formwork, as in Fig.6.4, and ligthly coated with a mixture of motor oil and grease for easy extraction.

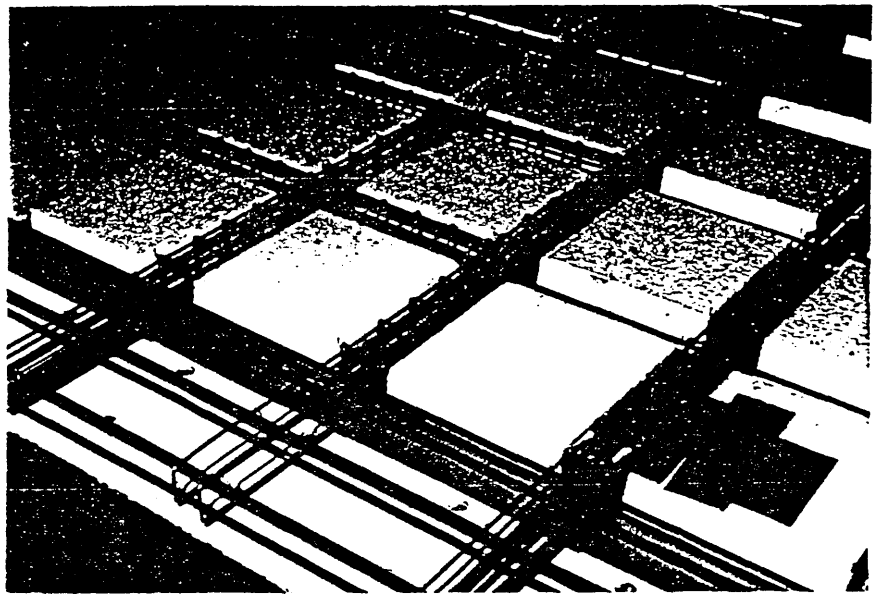

Fig.6.3 Polystyrene Blocks Fixed into the Reinforcement Cage

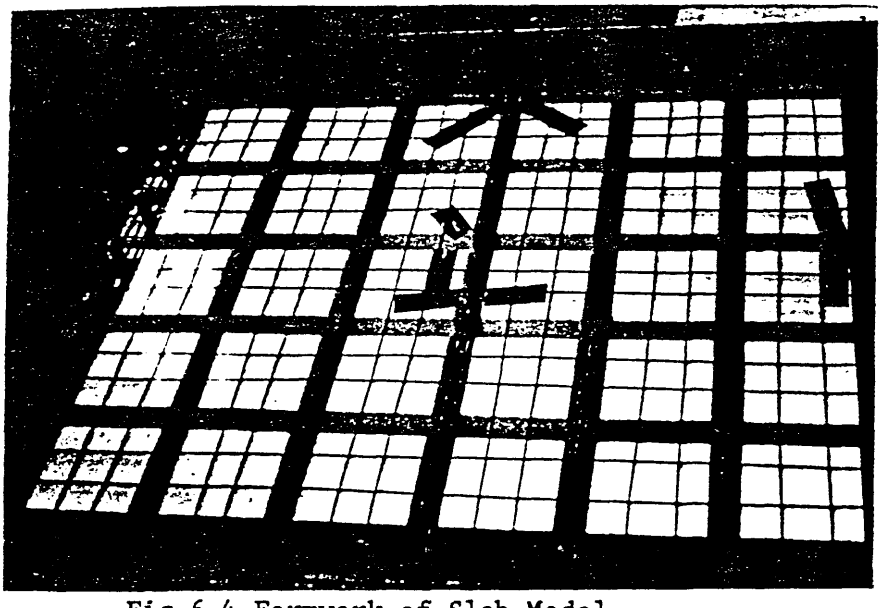

Fig.6.4 Formwork of Slab Model

6.1.2.5 Casting

The total volume of concrete for each slab was mixed in two equal batches. Control cubes and cylinders were prepared for each batch to determine the compressive and tensile strength of the concrete respectively. The fresh concrete was carefully placed first into the rib sections, then the edges and finally the top slab. The concrete was well compacted on a vibrating table which was specially installed for the work. The slabs were covered by wet sacks and plastic sheeting for 14 days after casting.

6.1.3 Loading System

The test rig consisted of upper and lower frames, both fabricated from Universal Channels and Beams respectively, and a specially made pneumatic rubber bag. The lower frame was made up of four Universal Beams, with 10mm thick web stiffeners at 90mm centers, which were welded together to form a rectangular frame. The top and bottom flanges of the frame were provided with 80 bolt holes each. The frame was then bolted onto a 25mm thick steel plate to provide the space for housing the pneumatic rubber bag. Removable wooden panels were placed against the interior stiffeners to provide an even surface for the rubber bag to bear upon. This complete frame system was supported by four short universal columns at each corner. The upper frame was made up of four Universal Channels fabricated with T-stiffeners to accommodate the 80 bolt holes which were in line with those on the top flanges of the lower frame. The details and the dimensions of the test rig are shown in Fig.6.5.

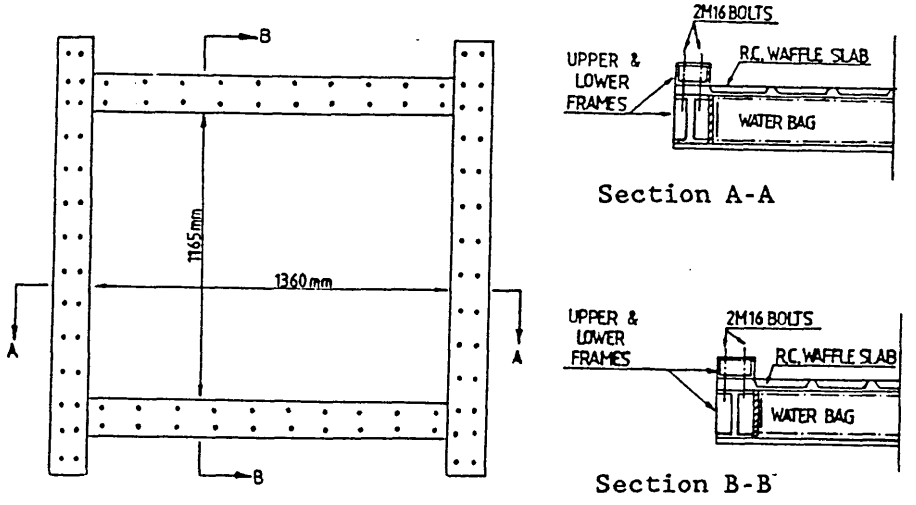

Fig.6.5 Plan of the Loading Rig - UDL

6.1.3.1 System with Uniformly Distributed Load

An air compressor unit was connected to the air-water pressure vessel from which the pressure was transmitted by water into the rubber test bag. The bag filled with water was restrained by the test rig on the sides and the base thus allowing a uniform upward loading to be applied over the whole area of the slab. An air supply bypass system was installed to control the range of pressure to be applied. The

accuracy of the applied loading was ensured by the two pressure guages which were arranged at the inlet and outlet of the rubber bag. Two main valves were used to regulate the pressure in the pressure vessel and the pneumatic rubber bag. A schematic view of the loading system is given in Fig.6.6.

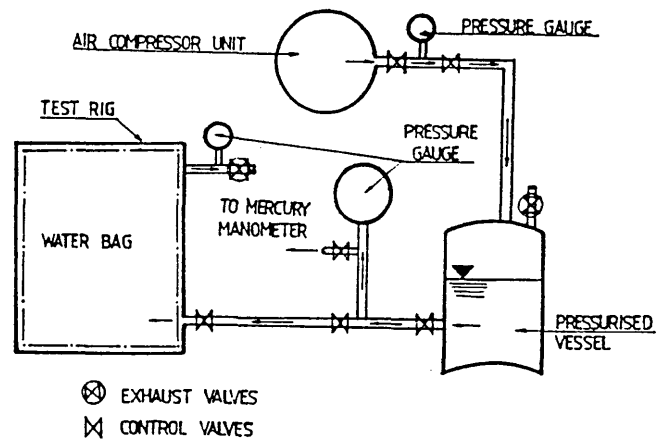

Fig.6.6 Schematic View of the Loading System

In order to strengthen the top frame to minimize edge rotations, all four upper frame channel sections were welded rigidly and four 16mm thick stiffening plates were mounted in each corner to increase the rigidity of the rig to provide the restrained edges for the test series A to D. The setting up of these slab models with all edges fully fixed is shown in Fig.6.7.

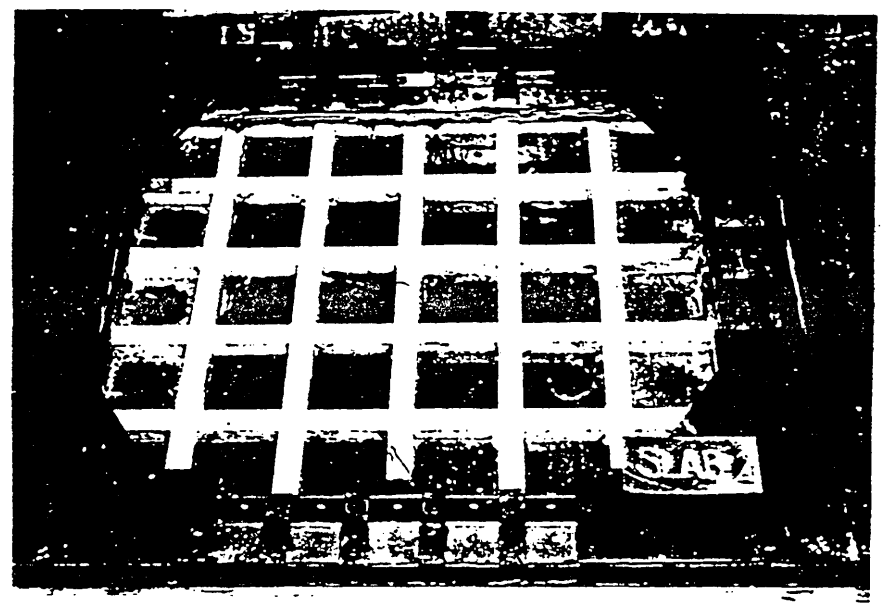

Fig.6.7 The Setting Up of Slab Model with All Edges Fully Fixed

For test series E, one of the longer edge of the test rig was modified to form a simple support edge for the slab models. A 6.00mm diameter bar was welded along each of the interior edges of the selected longer side of the upper and lower frames. These two 6.00mm bars, top and bottom, provided sufficient clearance for the rotation of the slab edge. The fully restrained condition for each of the other three edges were maintained by welding three 6.00mm diameter bars with equal spacing on each edge of the upper and lower frames in order to give the same level as that of the simply supported edge. Two layers of dental plaster were put above and below the fully fixed slab edges. The top frame was tightened up against the rig before the plaster finally set. The modified frame cross-section and the test set up for one of the models can be seen in Fig.6.8 and Fig.6.9 respectively.

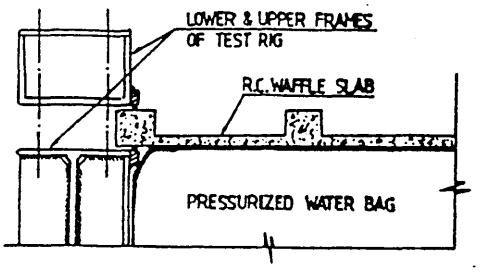

Fig.6.8 Details of Simply Supported Edge

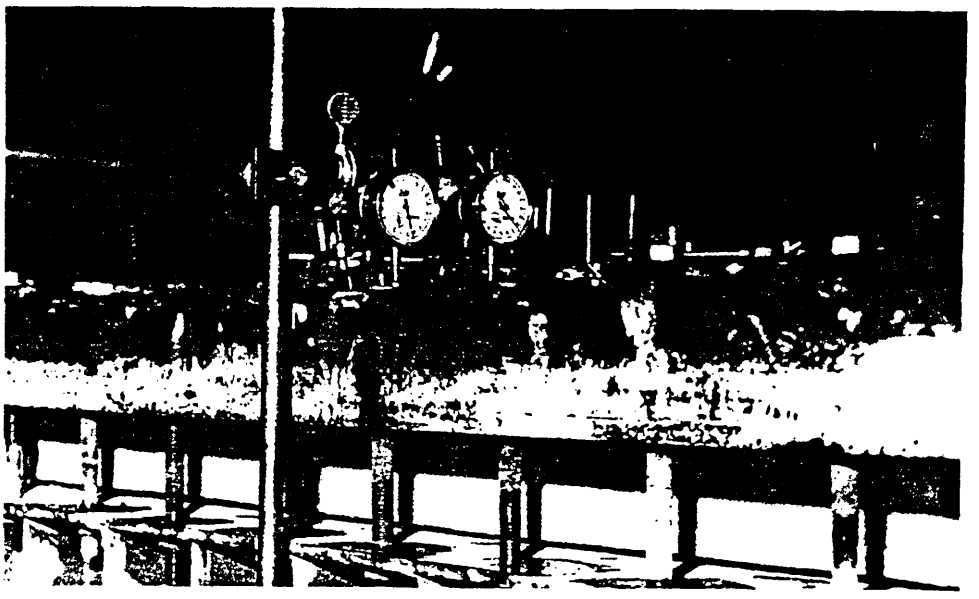

Fig.6.9 The Setting Up of Slab Models with Simply Supported Edge

For test series F, one of the shorter side frabricated channel was removed from the upper frame of the test rig in order to provide an unsupported edge. To prevent any damage of the pneumatic rubber bag during tests, a strip of flexible and heavy duty plastic nosing was mounted on the side panel along the edge. Details of the cross-section are shown in Fig.6.10.

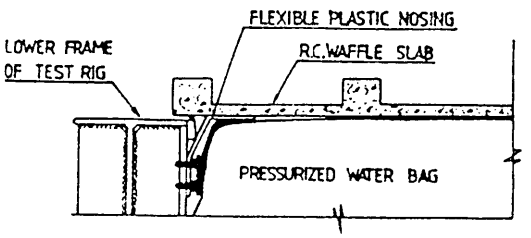

Fig.6.10 Details of Unsupported Edge

The test rig was then further modified to provide the corner supports for test series H. Three short Universal Channels, as shown in the Fig.6.11, were fabricated into box sections. Two of these box sections were bolted rigidly on the lower frame of the rig and the third was held across the corner bridging between those two sections. A ball bearing arrangement, which was used to simulate the corner support, was then put in position.

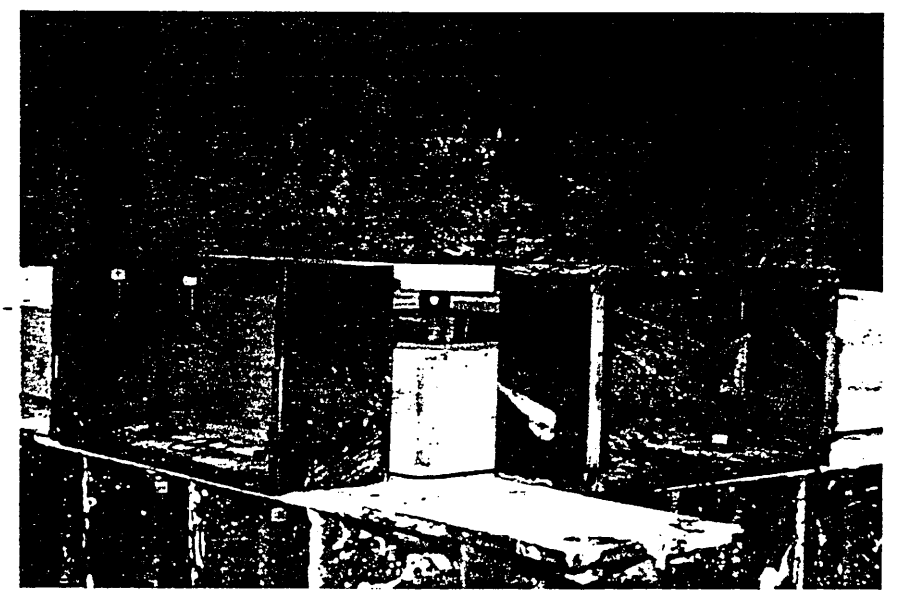

Fig.6.11 The Setting Up of the Column Support

6.1.3.2 System with 4-Points Load

Point loads were applied vertically downward by a computer controlled hydraulic jack rigidly fixed to a heavy structural steel frame which was bolted to the laboratory floor. The load from the jack was transmitted evenly to the four point loads by an arrangement of spreader beams, Fig.6.12. A load increment of 10N was obatinable from the controlled hydraulic system.

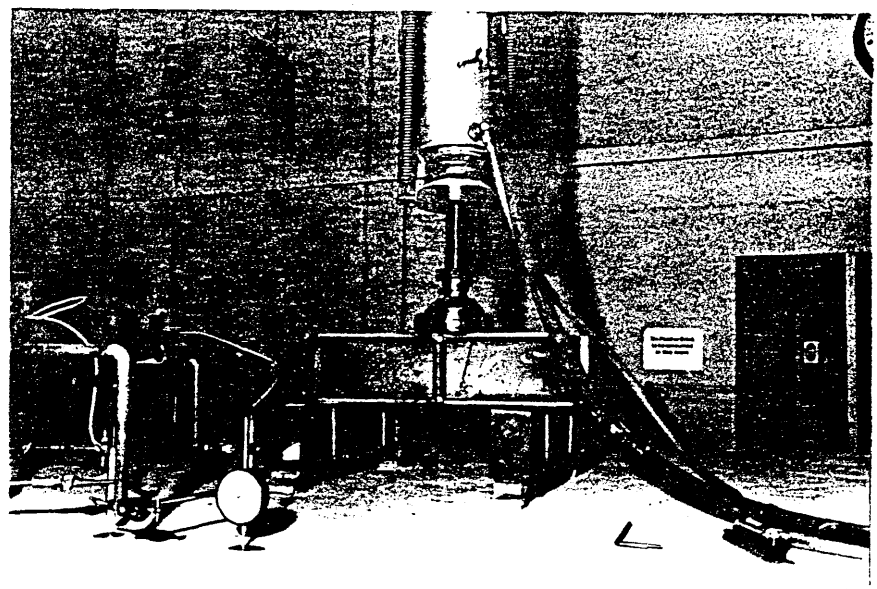

Fig.6.12 General View of Concentrated Loading System

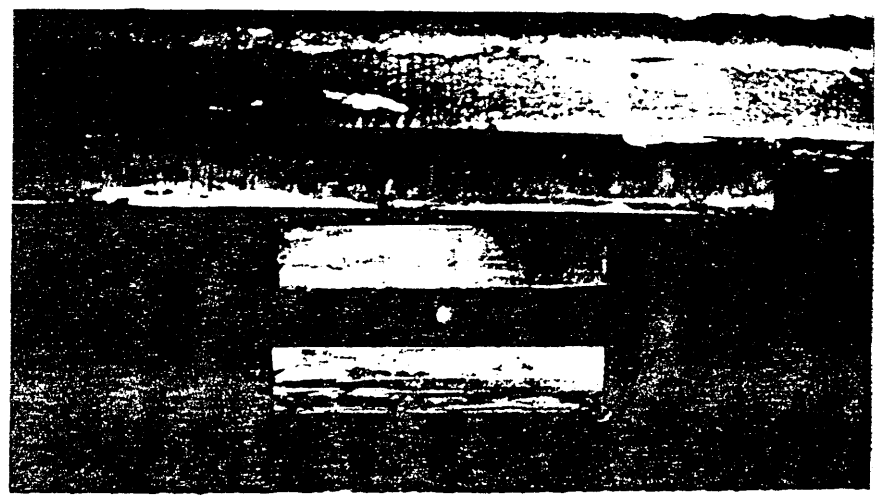

Fig.6.13 Ball Bearing Arrangement for Column Support

Four 152x152x30kg/m and four 254x254x107kg/m Universal Columns were used to simulate column supports for the slab models of test series I and J respectively. Each stanchion was held rigidly against its base plate by a 45mm diameter, 1.25m long steel rod through the 1m thick reinforced concrete floor slab in the laboratory. To provide enough clearance for the rotation of the slab corners, the same ball bearing arrangement was welded on a 20mm thick steel plate which was also secured by welding on the 30mm thick end plate of the stanchions as shown in Fig.6.13. The set up of the 1/2-scale model test is shown in Fig.6.14.

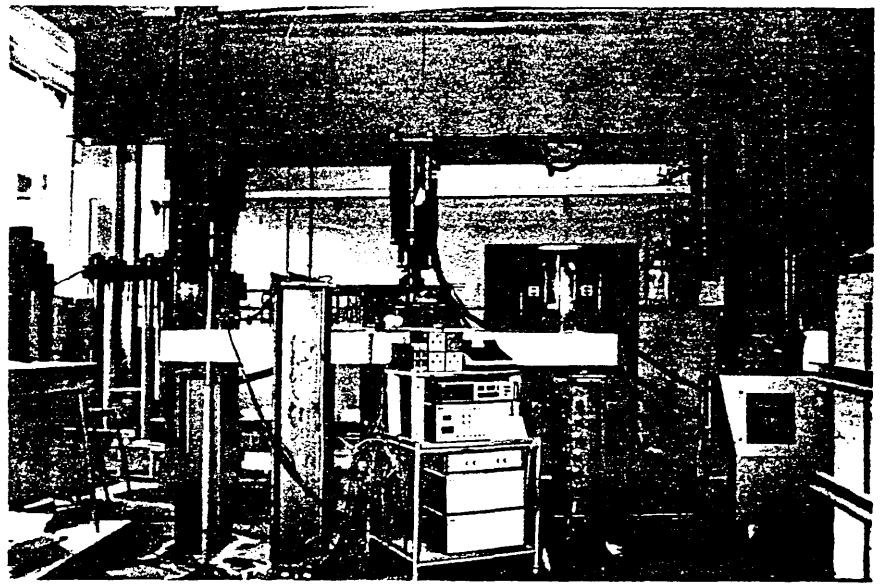

Fig.6.14 The Setting Up of the 1/2 Scale Model Test

6.1.4 Test Procedure

6.1.4.1 Preparation of Test

The moulds for manufacturing the reinforced concrete slabs were made using 20mm thick steel plates, which were stiffened by a fabricated Channel frame welded underneath. A 50mm diameter steel rod was rigidly welded to the middle of the resverse side of the moulds, parallel to their short span direction an extending about 200mm in length at both sides of the mould; this rod formed the pivot and

lifting arms for the purpose of turning and handling of the slab. The model waffle slabs were cured for 14 days before the turning and handling processes. The slab along with the mould was lifted at the lifting arms by a cross beam which was connected to the 5-ton overhead crane. The complete slab-mould system was then turned about the pivot arms and the model slab was put on the test rig with the loading face lying on the rubber bag.

With the exception of the slabs with column supports in Series I & J, all the slab models were tested upside down. To obtain an even surface between the model slab and the test rig a mixture of dental plaster was used as a bedding material. Two layers of this material were laid along the supporting edges of the slab model, between the slab and the upper and lower frames of the test rig. The supporting frames were bolted, gently by tightening the 80 M-16mm diameter bolts before the bedding mix set. The bolts were then tightened up using a torque wrench to a torque of 70 Nm. The exposed face of the slab was given a thin coating of whitewash to facilitate the tracing of propogation cracks during the tests.

Water was initially fed into the pneumatic rubber bag by applying a small amount of pressure in the loading system. The process was continued until the space was fully occupied by water, indicated by a small movement in the dial gauge which was mounted at the middle of the slab. The self-weight of the slab model was balanced by varying the level of the water supply which was connected to the end of the manometer. Although this adjustment was small, it was significant for those slabs with low ultimate strength.

6.1.4.2 Instrumentation

Each of the slabs was tested to destruction using a set incremental loading procedure. For each increment of load, deflections, the edge rotation and the concrete and steel strains at various locations of the slab were recorded. The loads corresponding to the first visible crack and the development of the cracks were also noted.

Transverse deflections of slabs at the selected locations were measured using eight transducers and several dial gauges mounted on a de-mountable frame, Fig.6.15. In order to obtain the steel strain, eight to ten strain gauges were attached to the reinforcements using Cyanoacrylate adhesive in several selected positions for each slab model. These strain gauges were protected with three waterproof coatings i.e. M-coat A, B & G, before casting. The transducers and strain gauges were monitored using a Solartron Data Logging system for each incremental load, and the results of the deflections and the steel strains were recorded in micro-strain by the line printer unit connected to the system. Concrete strains on the unloaded face of the slab were obtained by at twelve to sixteen locations using 'Demec' gauges. The rotation of the slab at the supporting edges was monitored using two precision dial gauges. For safety reasons, the concrete strains of the slabs in test series I & J were measured by PL-60 type 60mm long electrical resistance strain gauges using the Solartron Data Logging System. These strain gauges were fixed on the selected positions as shown in Fig.6.16 using P-2 adhesive and activator on the underside of the slab models.

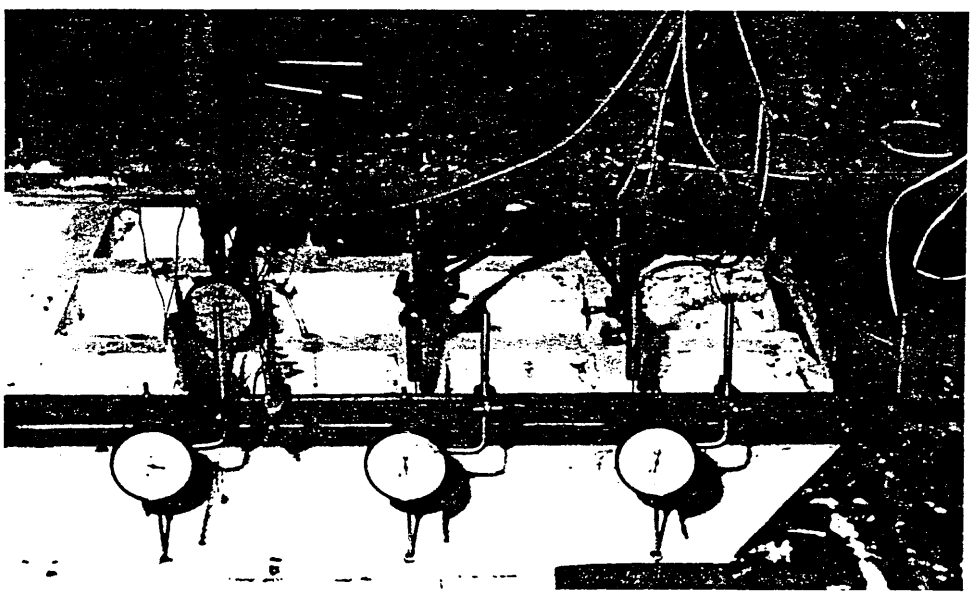

Fig.6.15 The Setting Up of the Transducers and Dial Guages

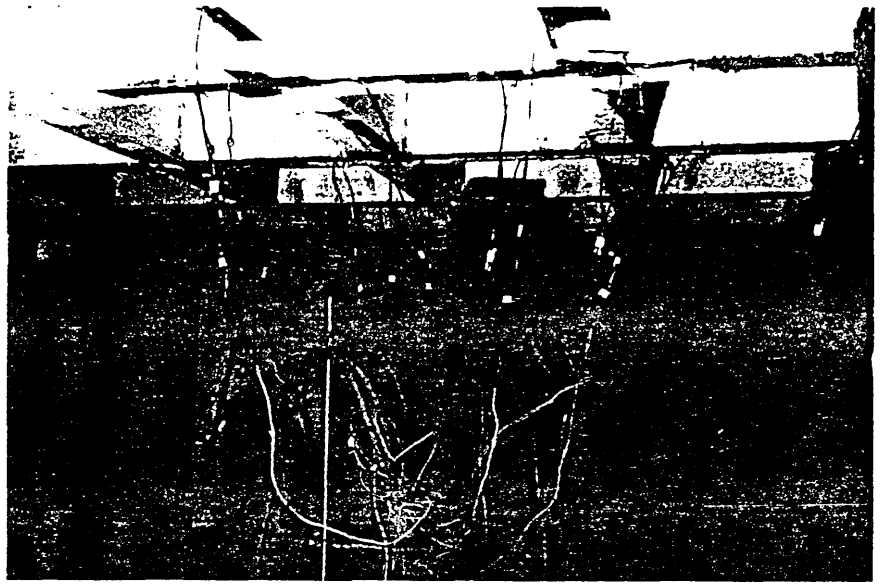

Fig.6.16 Arrangement of Strain Guages on the Unloaded Face of 1/2 Scale Model Slab

6.2 EXPERIMENTAL RESULTS

6.2.1 Properties of Materials

6.2.1.1 Concrete

The compressive and split cylinder strengths for the concrete of each test slab model are obtained. The statistical results for the relative density, compressive strength, tensile strength and compressive/tensile strength ratio of the whole programme of tests are summarized in Table 6.3.

It can be seen that the compressive strengths of the concrete are fairly consistent throughout with the mean compressive strength of 28.491N/mm^2 which is 95% of the design strength. The mean tensile strength obtained is relatively low at 2.380 N/mm^2. The mean tensile to compressive strength ratio of 0.079 is lower than the generally expected values of range from 0.1 to 0.091.

Table 6.3: Concrete Strength of Model Slabs

Slab No.	Relative density	Compressive strength (N/mm^2)	Tensile strength (N/mm^2)	Ten./Comp. ratio
A1	2.146	30.803	2.540	0.082
A2	2.054	23.970	2.067	0.086
A3	2.107	27.100	2.048	0.076
B1	2.103	25.717	2.317	0.090
B2	2.147	28.483	2.278	0.080
B3	2.142	28.700	2.143	0.075
C1	2.095	26.750	1.903	0.071
C2	2.071	29.700	2.684	0.090
C3	2.106	35.367	2.776	0.079
D1	2.086	32.417	2.348	0.073
E1	2.040	22.267	2.115	0.095
E2	2.011	29.067	2.472	0.085
E3	2.052	32.300	2.667	0.083
F1	2.084	32.867	2.794	0.085
F2	2.165	37.617	3.392	0.090
F3	2.120	27.967	2.232	0.080
H1	1.896	20.017	1.779	0.089
H2	2.007	23.017	2.002	0.087
I1	2.063	27.733	2.386	0.086
I2	2.012	27.950	2.660	0.095
J1	2.579	54.611	---	---
Mean	2.075	28.491	2.380	0.084

6.2.1.2 Reinforcements

The yield strength for all reinforcing steel used in this investigation is given in Fig.6.17 which was determined using the nominal cross-sectional area of the steel. The average strengths are given in Table 6.4.

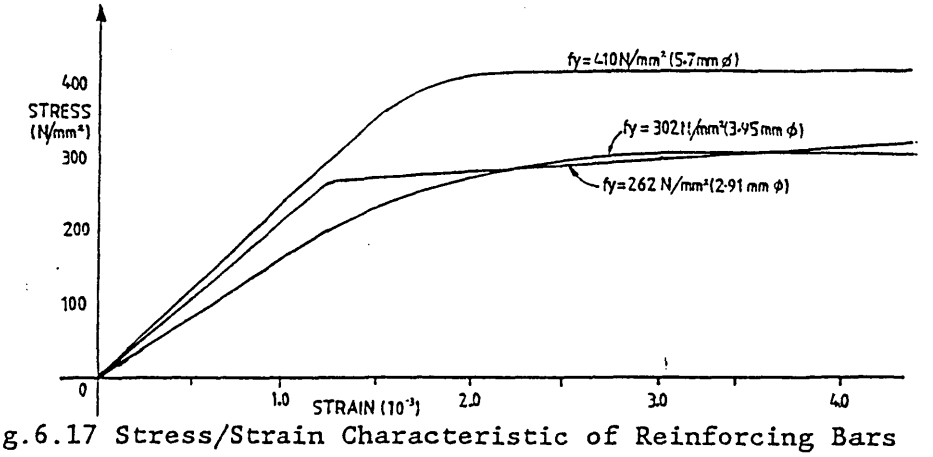

Fig.6.17 Stress/Strain Characteristic of Reinforcing Bars

Table 6.4: Yield Strengths of Reinforcing Bars

Dia. (mm)	Test load (kN)	Yield strength (N/mm^2)	Modulus of elasticity (kN/mm^2)
2.91	1.66	262.0	224
3.95	3.70	302.0	164
5.70	10.50	410.0	235

Table 6.5 Summary of Principal Test Results at Cracking Loads

(1) Slab No.	(2) Slab Thickness (mm)	(3) Cracking Load (kN/m^2)	(4) Mid-span Deflection (mm)
A1	55	34.475	1.73
A2	55	31.028	1.73
A3	55	41.369	1.81
B1	70	48.263	1.72
B2	70	62.055	1.78
B3	70	55.160	1.66
C1	85	51.713	1.17
C2	85	51.713	0.95
C3	85	48.265	0.80
D1	70	44.818	0.46
E1	55	20.685	2.20
E2	70	27.580	1.16
E3	85	30.028	0.82
F1	55	27.580	2.96
F2	70	27.580	1.20
F3	85	34.475	0.81
H1	85	7.000	2.00
H2	85	10.343	2.12
I1	85	5.832*	2.64
I2	85	5.832*	2.36
J1	170	25.000*	2.40

(Total of 4-points load denoted by *)

6.2.2 Results of R.C. Waffle Slab Tests

A large amount of data was obtained from the series of tests which included deflections and concrete and reinforcement strains for every incremental load. For each series of tests, a complete set of data for one of the slabs was selected and is given in Appendix A. The incremental load vs deflections, concrete and reinforcement strains for the complete set of results were plotted and are given in Appendix B. The failure modes of these slab models are also presented in

Table 6.6 Summary of Principal Test Results at Failure Loads

(1) Slab No.	(2) Slab Thickness (mm)	(3) Failure Load (kN/m^2)	(4) Mid-span Deflection (mm)	(5) Ratio (4)/(2)
A1	55	93.859	17.24	0.314
A2	55	95.992	19.50	0.355
A3	55	108.791	14.75	0.268
B1	70	141.348	20.60	0.294
B2	70	155.138	21.90	0.313
B3	70	165.480	23.10	0.330
C1	85	194.784	24.13	0.284
C2	85	210.298	26.30	0.309
C3	85	230.983	26.70	0.314
D1	70	268.905	29.00	0.414
E1	55	81.016	43.35	0.788
E2	70	115.491	33.50	0.479
E3	85	158.585	26.00	0.306
F1	55	64.469	35.00	0.636
F2	70	109.976	33.72	0.482
F3	85	136.521	38.38	0.452
H1	85	41.370	44.40	0.522
H2	85	43.094	50.30	0.592
I1	85	36.832	42.50	0.500
I2	85	30.832	60.00	0.706
J1	170	88.000	56.00*	0.636

(* - Dial gauges were end of travel)

Appendix C. Table 6.5 provides a summary of the principal information of the carrying load capacity of each slab model at the first visible cracks; Table 6.6 also provides a summary of the principal information of the ultimate load carrying capacity for the entire programme of test.

6.2.3 Characteristics of R.C. Waffle Slabs

6.2.3.1 Waffle Slabs with All Edges Fully Fixed

Initially, the deflections and concrete strains of the slabs behaved linearly to the applied load until the appearance of the cracks. The first cracks occurred almost simultaneously in the mid-span region of the interior ribs in both orthogonal directions. In most cases, the distinct diagonal cracks developed on the rib joints of the interior ribs in both directions with an angle orientated at about 45^0 to the axis of the ribs. As the deflections progressively increased, cracks normal to the rib axis eventaully occurred at fairly equal spacing along the ribs.

Concrete strains at the middle portion of the slab were comparatively higher than those near the supports. Until the ribs cracked, there was an increase in concrete strain particularly in the mid-span of the interior ribs. The reinforcing steel at the supports was subjected to higher stresses than that in the mid-rib even at low load intensity. After cracks fully developed, there was a large increase in strain at supports as shown in Fig.6.18 and Fig.6.19. The steel in supports and mid-ribs reached its yield point well in advance of the collapse of the slabs.

Prior to failure, a series of inclined cracks developed in the rib section of the ribs adjacent to the corners. These cracks spiralled along the exposed faces of the ribs with an angle varying from 40^0 to 50^0 to the rib axis, which can be seen in Fig.6.20. This indicates that these rib sections at the restrained corners are subjected to combined bending and torsion stresses in the slab before failure. More cracks appeared in the ribs as the deflections of the slabs increased nonlinearly. These cracks scattered in a pattern radiating from the centre to the four corners of the slab. The slabs failed immediately

after the crushing of the concrete at the supports of the ribs in the edges. A few cracks parallel to the long span direction on the centre of the slab also developed at failure. Extensive yielding of the slab caused large deflection at the middle of the slab. There was a phenomanal characteristic that a reduction of load capacity occurred during the yielding of the slabs. Finally, the slabs collapsed at a fairly constant residual strength as shown in Fig.6.21. The selected failure pattern of cracking for each test series is given in Fig.6.22.

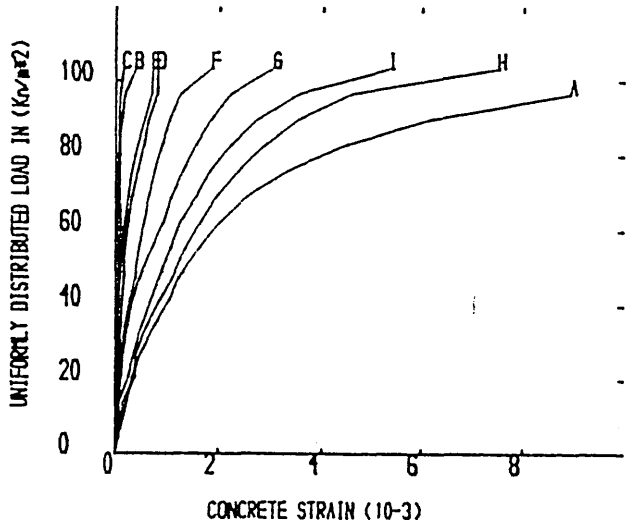

Fig.6.18 Load-Concrete Strain Curves for R.C.Waffle Model Slab A3

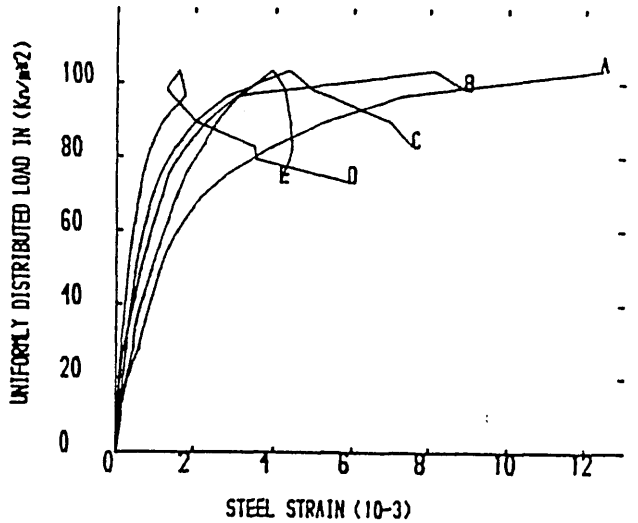

Fig.6.19 Load-Steel Strain Curves for R.C.Waffle Model Slab A3

Fig.6.20a Cracking View near the Restrained Support

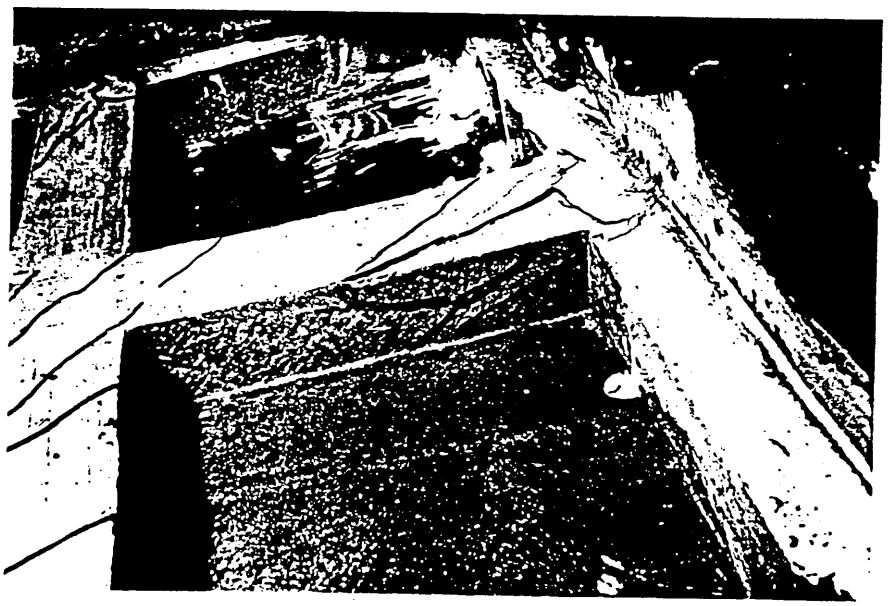

Fig.6.20b Close View of Spiral Cracks in Restrained Corner

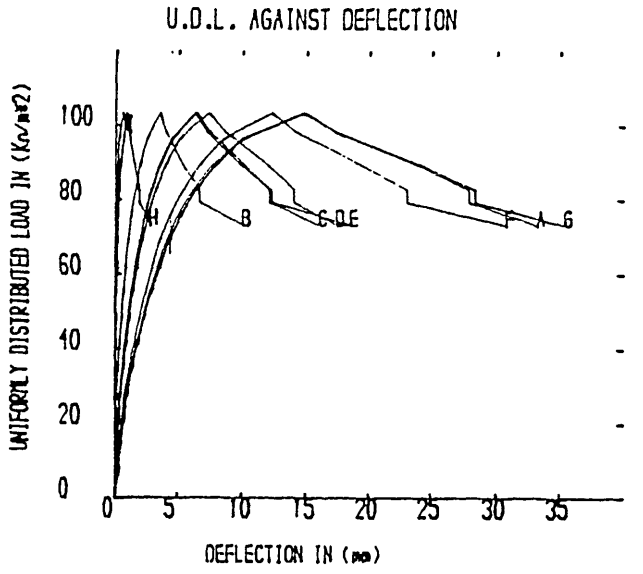

Fig.6.21a Load-Deflection Curves of R.C.Waffle Model Slab A3

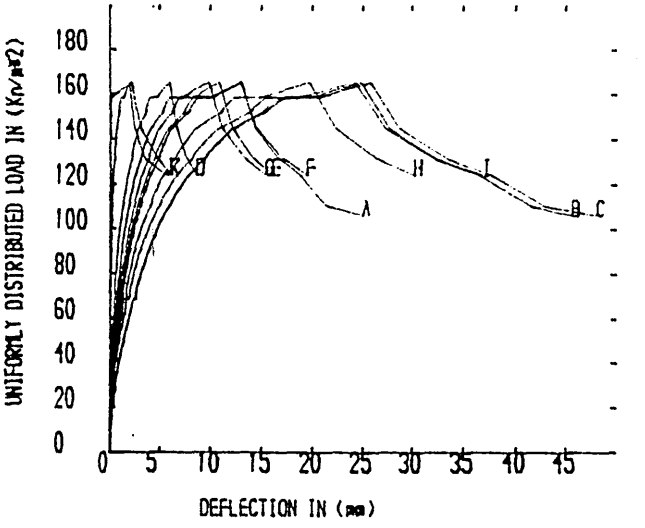

Fig.6.21b Load-Deflection Curves of R.C.Waffle Model Slab B3

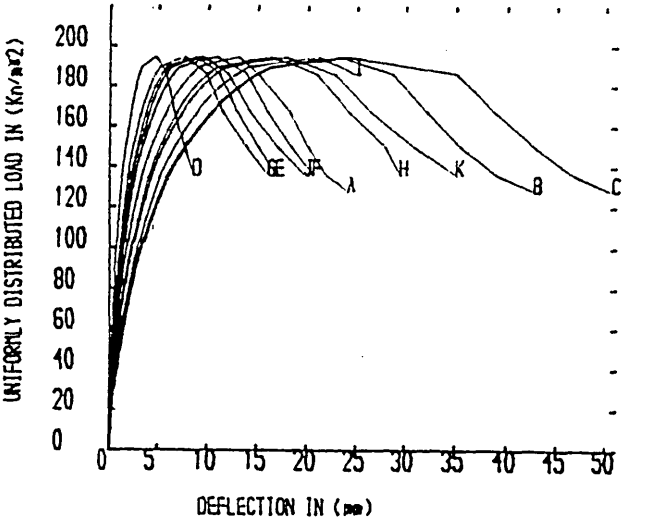

Fig.6.21c Load-Deflection Curves of R.C.Waffle Model Slab C3

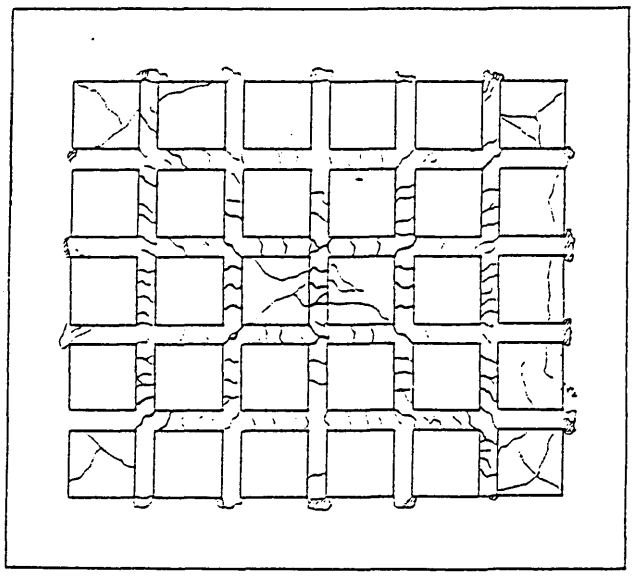

Fig.6.22a Failure Crack Pattern of R.C.Waffle Model Slab A3

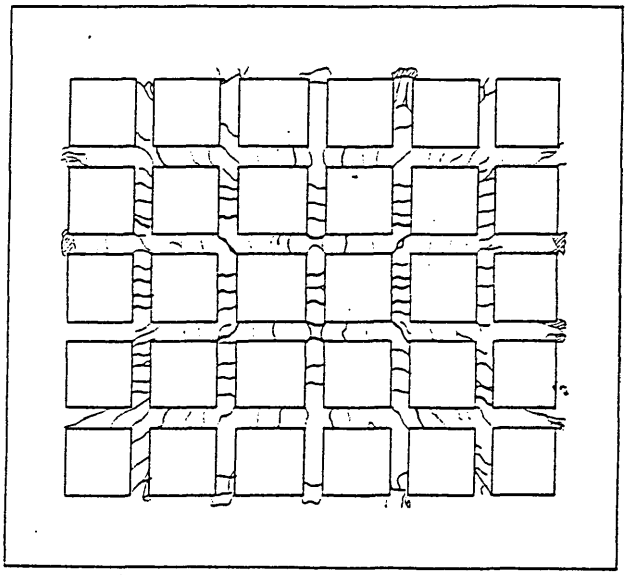

Fig.6.22b Failure Crack Pattern of R.C.Waffle Model Slab B3

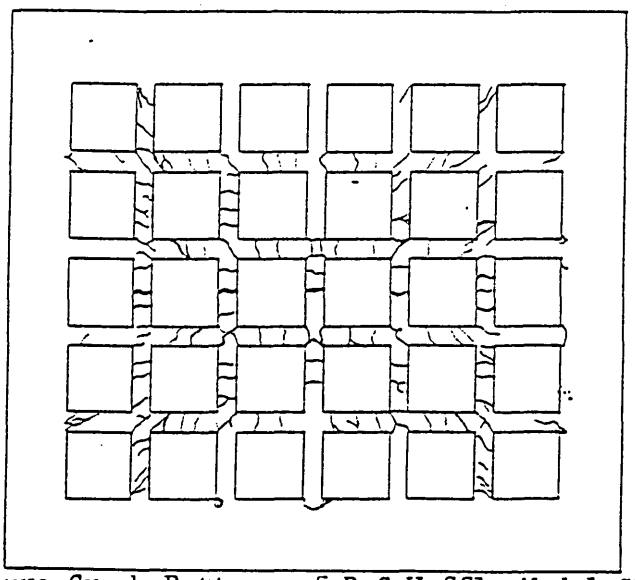

Fig.6.22c Failure Crack Pattern of R.C.Waffle Model Slab C3

Nine model slabs were tested with the same boundary condition and the failure crack patterns for these waffle slabs were similar. The control solid model slab D1 was tested with exactly the same boundary and loading conditions and its failure cracking pattern is shown in Fig.6.23. Cracks radiated from the centre of the slab to four restrained corners. In contrast to that of waffle model slabs, the failure pattern clearly exhibited the continuity of cracks and crushing of concrete along the supporting edges merely formed as crushing yield lines.

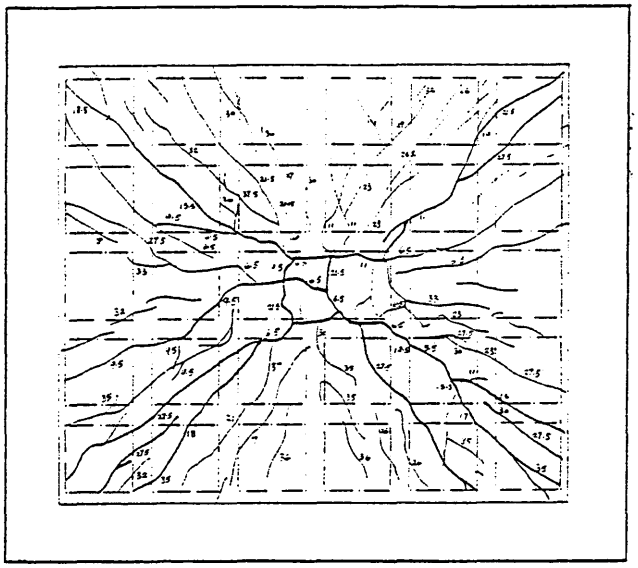

Fig.6.23 Failure Crack Pattern of R.C.Solid Model Slab D1

6.2.3.2 Waffle Slabs with One Long Edge Simply Supported and Others Edges Fully Fixed

The tests of R.C. waffle model slabs in series E produced a crack characteristics shown in Fig.6.24, and deflection characteristics shown in Fig.6.25 which are similar to that of series A to C, the only difference being that the centre to which the cracks radiated from each of the slab corners shifted slightly towards the simply supported edge. More spiral cracks than previous series of tests at an angle varying from 40^0 to 50^0 were observed in the rib-sections at the corners adjoining the simply supported edge. Diagonal cracks finally developed on the under-side of the top slab radiating from the two corners of the simply supported edge to the central portion of the slab. Concrete strains behaved linearly until cracks appeared in the

ribs. Strains at the middle of the slab were comparatively higher than those near the supports, see Fig.6.26. The steel at supports were subjected to higher strains than those in the mid-rib and yielding of steel occurred well before the collapse load of the slab was reached, see Fig.6.27. Prior to failure, the crushing of concrete was more severe at the supports of the ribs adjacent to the simply supported edge. The reduction of load carrying capacity also occurred during the extensive yielding of the slab.

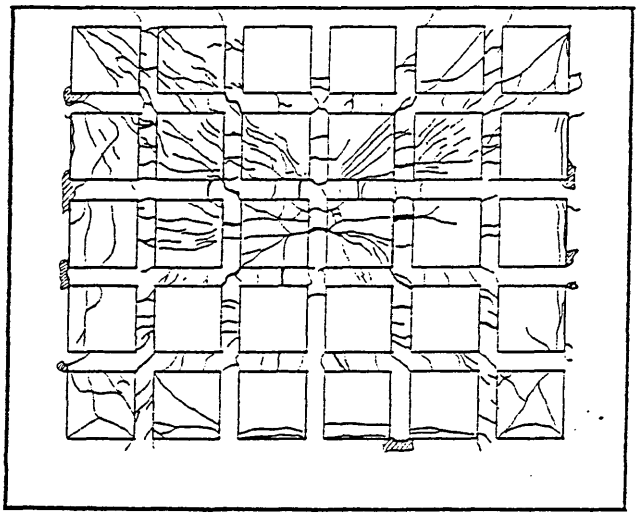

Fig.6.24 Failure Crack Pattern of R.C.Waffle Model Slab E3

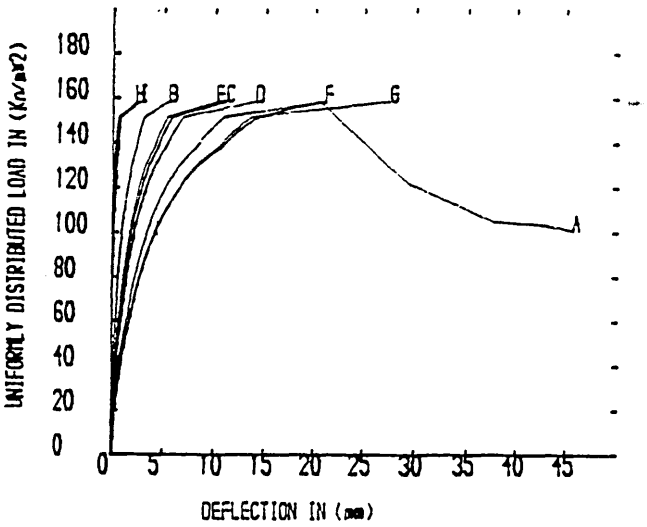

Fig.6.25 Load-Deflection Curves of R.C.Waffle Model Slab E3

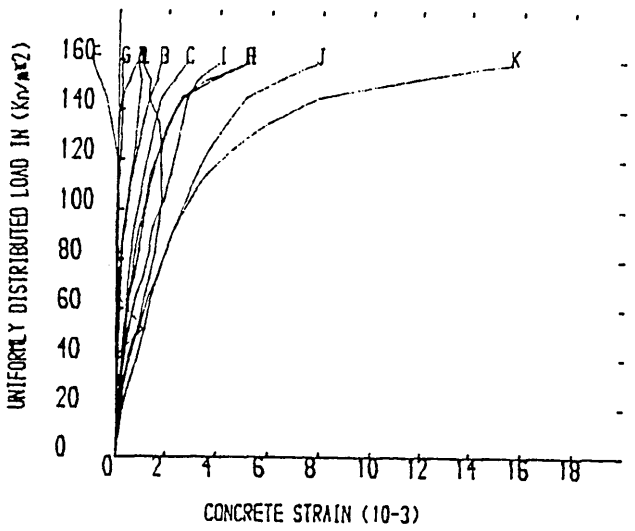

Fig.6.26a Load-Concrete Strain Curves of R.C.Waffle Model Slab E3

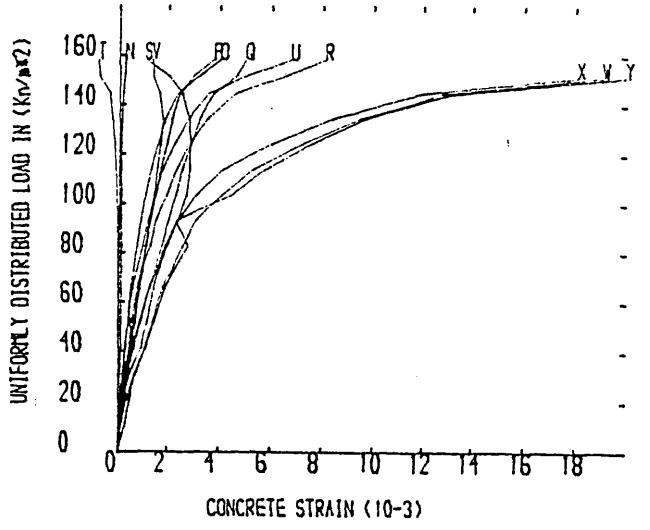

Fig.6.26b Load-Concrete Strain Curves of R.C.Waffle Model Slab E3

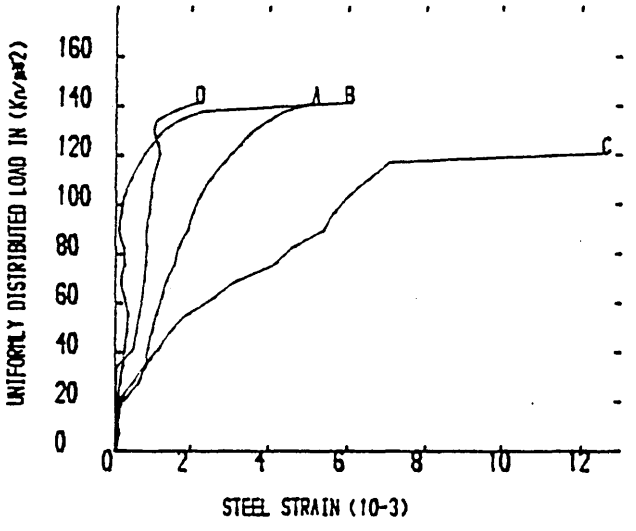

Fig.6.27 Load-Steel Strain Curves of R.C.Waffle Model Slab E3

6.2.3.3 Waffle Slabs with One Short Edge Free and Other Edges Fully Fixed

The tests of R.C. waffle model slabs in series F also gave similar deflection characteristic and development of cracks at the fully restrained portion of the slabs except that the other portion of the slabs associated with the free edges developed different cracking patterns. Cracks normal to the rib axis, in the short span, extended from the middle of the slab to the free edge as shown in Fig.6.28. These normal cracks at the free edge beam opened up extensively prior to the collapse of the slab. The crushing of concrete was also observed only at the restrained supports. Concrete and steel strains also behaved linearly before cracks occurred. Concrete strains in the middle of the slab and the free edge beam were comparatively higher than those near the restrained supports, see Fig.6.29. The steel at supports was subjected to higher stresses than that in the mid-rib even at the low load intensity, and yielding of steel occurred prior to the collapse of the slabs as shown in Fig.6.30. A small reduction in load carrying capacity also occurred in model slab A3, Fig.6.31.

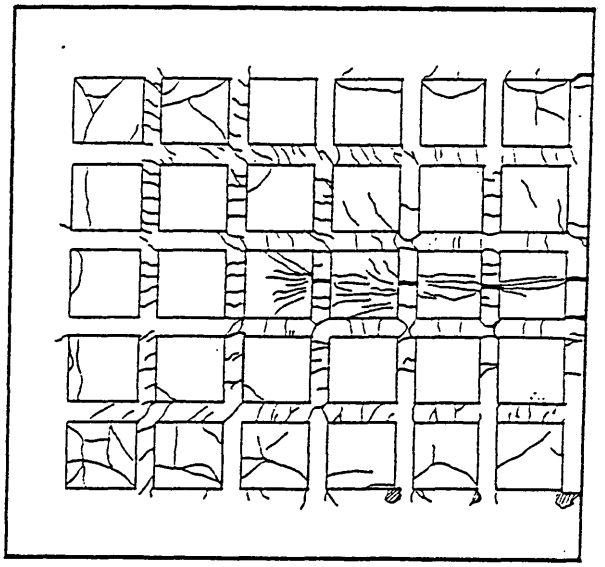

Fig.6.28 Failure Crack Pattern of R.C.Waffle Model Slab F3

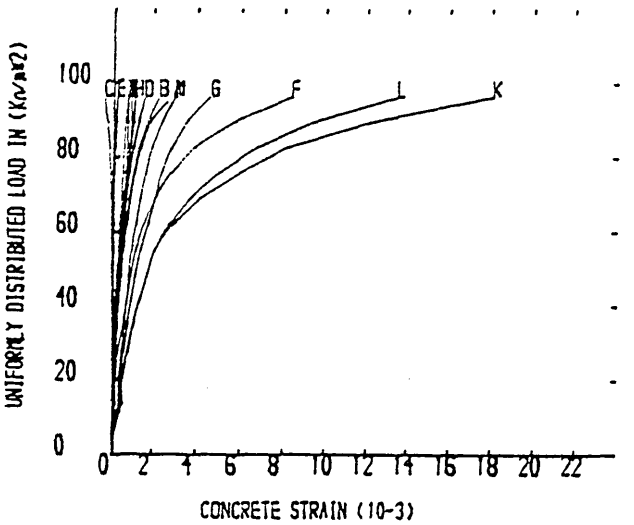

Fig.6.29a Load-Concrete Strain Curves of R.C.Waffle Model Slab F2

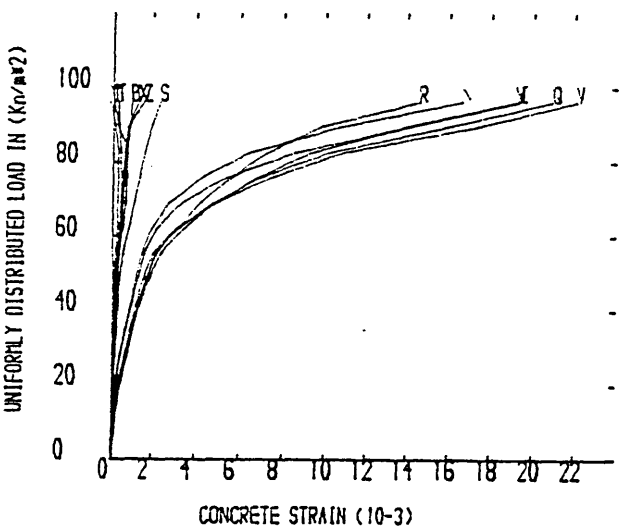

Fig.6.29b Load-Concrete Strain Curves of R.C.Waffle Model Slab F2

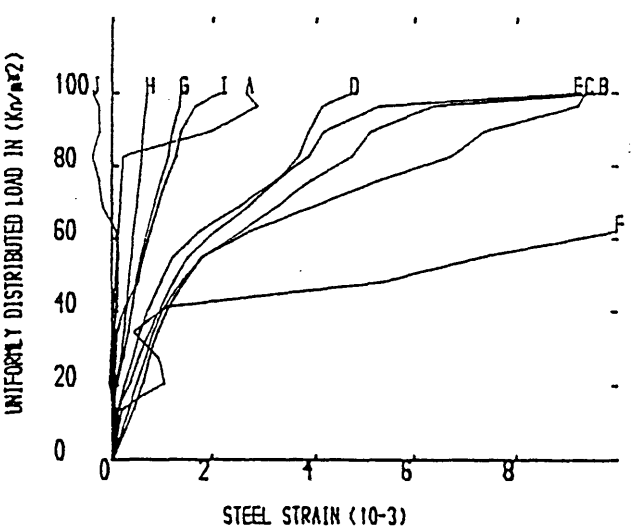

Fig.6.30 Load-Steel Strain Curves of R.C.Waffle Model Slab F2

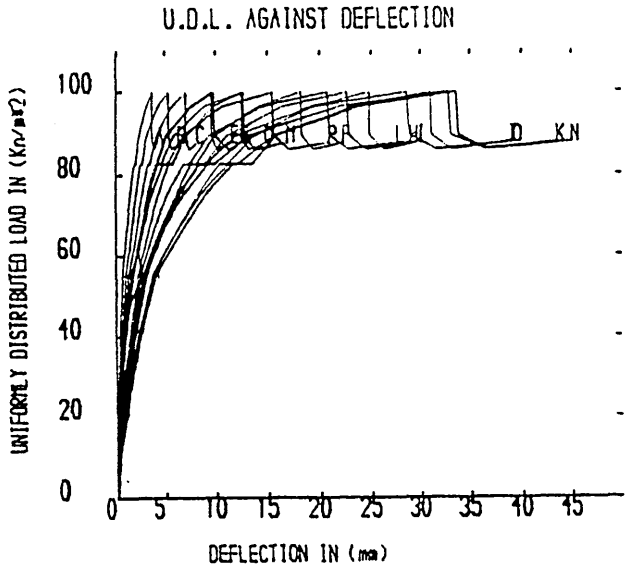

Fig.6.31 Load-Deflection Curves of R.C.Waffle Model Slab F2

6.2.3.4 Waffle Slabs with Four Corners Supported

The tests of R.C. waffle model slabs in series H, I, and J behaved linearly until the appearance of the cracks. The development of cracks was different to those of the R.C. waffle model slabs tested in series A to F but there was hardly any difference between the slabs subjected to the uniformly distributed load and 4-point loads. Cracks normal to the rib axis developed initially in the mid-ribs and soon followed in the middle of the edge beams in both directions as shown in Fig.6.32. As load increased, cracks in the middle of the ribs parallel to the long spanning direction widened up quicker than the cracks in the short spanning ribs as indicated by concrete strains and the increase in deflection responded nonlinearly. Prior to failure, the width of the cracks and the deflections in the middle of the long spanning edge beams increased rapidly. In contrast, the width of the cracks and the concrete strains in the middle of the short span edge beams reduced as shown in Fig.6.33 and the deflections decreased, see Fig.6.34. Eventually the slab collapsed with excessive yielding normal to the direction of the long span. No sign of spiral cracks was observed but diagonal cracks often occurred at the rib joints. The model slabs with an even number of ribs spanning in short direction gave a more distinct yield mechanism. On the other hand for the model slabs with an odd number of ribs, cracks appeared on either sides of the mid-rib, to form a complete mechanism.

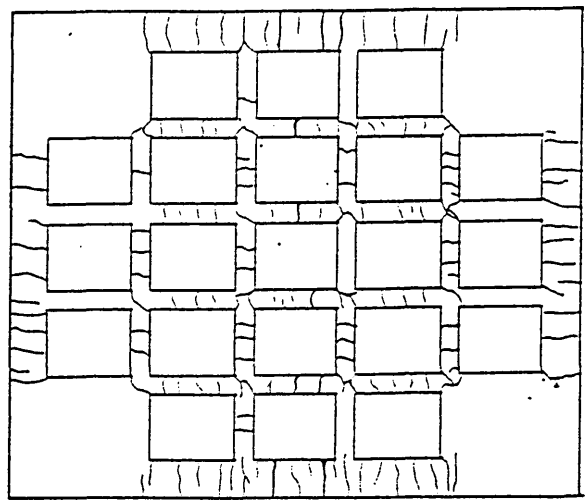

Fig.6.32a Failure Crack Pattern of R.C.Waffle Model Slab H2

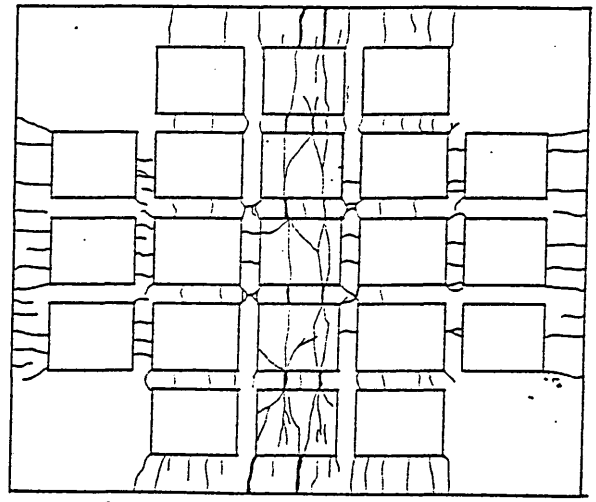

Fig.6.32b Failure Crack Pattern of R.C.Waffle Model Slab I2

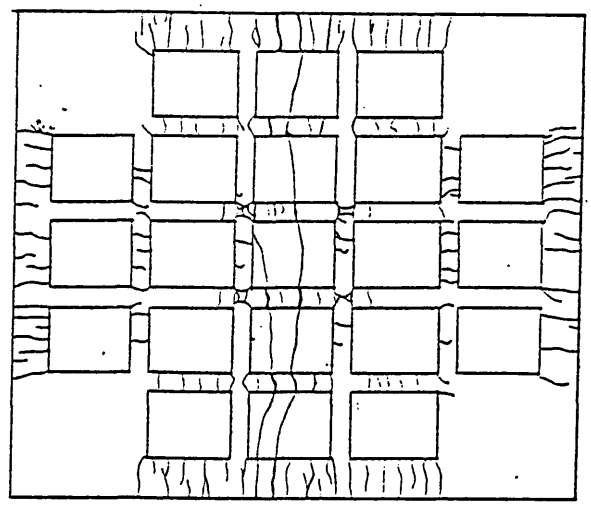

Fig.6.32c Failure Crack Pattern of R.C.Waffle Model Slab J1

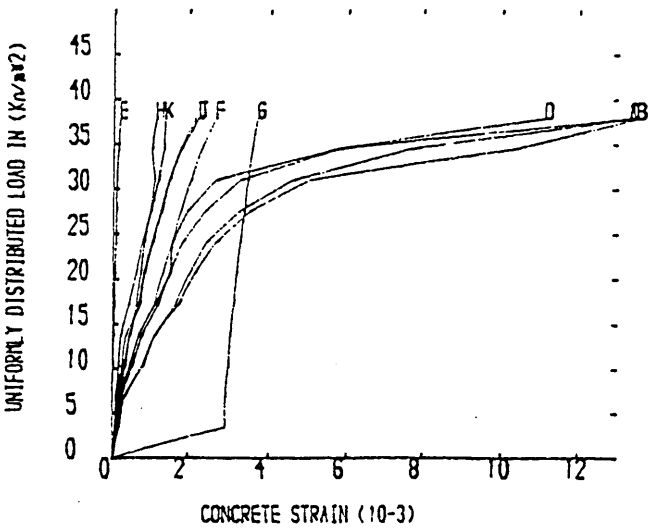

Fig.6.33a Load-Concrete Strain Curves of R.C.Waffle Model Slab H2

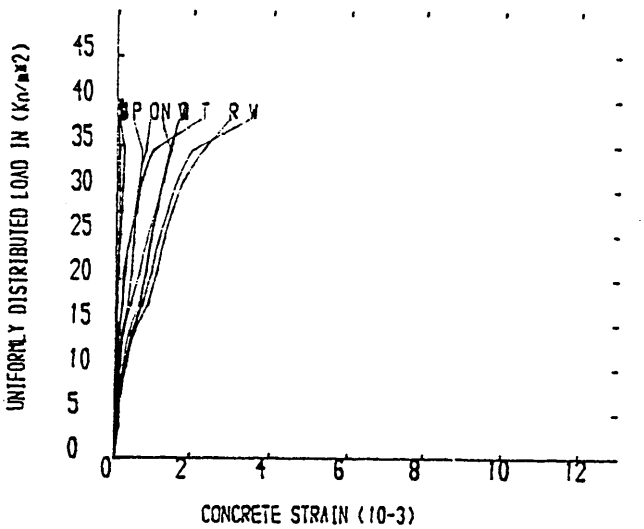

Fig.6.33b Load-Concrete Strain Curves of R.C.Waffle Model Slab H2

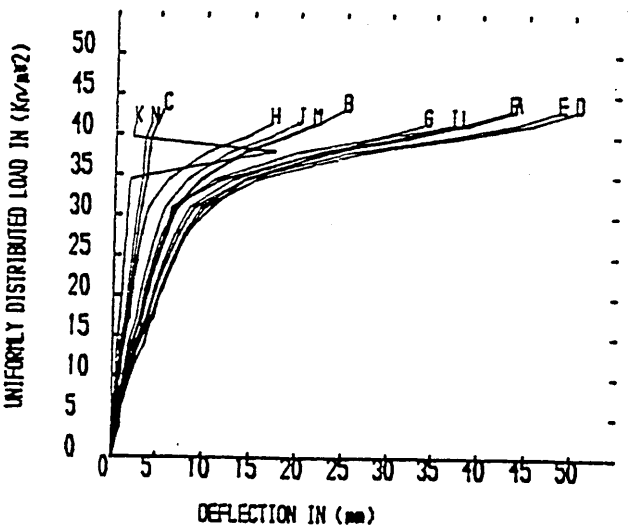

Fig.6.34 Load-Deflection Curves of R.C.Waffle Model Slab H2

CHAPTER 7

THEORETICAL ANALYSIS EMPLOYED AND RESULTS

7.1 GENERAL

The work carried out by Marshall (43) and the results of this investigation have indicated that the behaviour of reinforced concrete waffle slabs is similiar to that of reinforced concrete solid slabs subjected to the same loading and boundary conditions.

The load-deflection behaviour, prior to the development of cracking, is essentially linear and this tends itself readily to analysis by the elastic theory. When the ribs crack, there is a redistribution of stresses in the slab. The load-concrete strain characteristic becomes curved. At this stage, the steel strains increase and the deflections behave nonlinearly. This does not necessarily imply failure, it represents deflections which are not fully recoverable on unloading. Prior to failure, cracks continue to widen and collapse is characterized by the excessive yielding of the slab. It is because of this yielding characteristic of R.C. waffle slabs that the load carrying capacity of this type of slab can be analysed by the plastic approach.

Based on the results of the series of tests, reinforced concrete waffle slabs exhibit similar yield line patterns which were idealized by Johannsen (31) for reinforced concrete slabs at ultimate limit state. The yield line patterns for these R.C. model slabs are, therefore, idealized on the basis of the yield line approach. Inevitably, compressive membrane action has a significant effect on the load carrying capacity of an R.C. slab with restrained edges; therefore, this effect on the restrained rib supports of an R.C.waffle slab is also considered in here.

Up until now investigations have tended to disregard the effect of the bending and torsion interaction on the load carrying capacity of the slab on the assumption that twisting moment is small and can be ignored. However, the development of spiral cracking which occurred in the ribs at the restrained corners of the slabs in this

investigation has highlighted the fact that there is the need to consider the significance of this effect on the load carrying capacity of R.C.waffle slabs.

On the basis of these facts, the analytical investigation into the behaviour of R.C. waffle slabs are carried out in three parts dealing with:

(i) elastic behaviour up to the appearance of the cracks,
(ii) nonlinear behaviour due to progressive concrete cracking, and
(iii) ultimate load capacity of R.C. Waffle slabs.

7.2 ELASTIC ANALYSES USING FINITE ELEMENT METHOD

Two analytical models using finite element method are considered in the present investigation which are:

(1) Thin plate flexural element model based on the plate bending theory; and
(2) Grillage element model based on the grillage analysis.

The finite element package 'LUSAS/AN' which was used to analyse both of these methods allows flexible free format input, automatic data generation, flexible element and node numbering, solution order and comprehensive error diagnostics. It also provides the optional, clear, self-explanatory output, together with plotting modules facilities. The applications of the finite element method and grillage analysis require the input data which include title, control data, element topology, nodal co-ordinates, material properties, support conditions and load information. The output includes nodal deflections, reactions of the supports, stress resultants and strain at each node of an element.

7.2.1 Thin Plate Bending Element Model

A thin plate flexural element 'QF4' in two-dimension with higher order model capable of modelling most conditions was chosen to model the waffle slabs. The element formation is based on an isoparametric

approach with constraints to invoke the Kirchoff-hypothesis for thin plate. The variation of moments within the elements is regarded as linear, and the elements are numerically integrated with a 2x2 point rule. The element 'QF4' consists of 4 corner nodes as given in Fig.7.1. At each node, there are three degrees of freedom i.e. W, θx and θy, and two node co-ordinates in x- and y-axes. For the purpose of analysis, the R.C. waffle model slabs were idealized from a discreted T-section to the equivalent plates. Flexural and torsional rigidities with the consideration of Poisson effect were used instead of the material properties of the plate element. Therefore, the geometric property of the equivalent plate was assumed to be unity. The idealized T-section was modelled by these 'QF4' elements in both orthogonal directions. Using symmetry in both x- and y-axes, a mesh of 12x10 occupied a quarter of the reinforced concrete slab model as shown in Fig.7.2. Restraint on freedoms w, θx and θy was applied to the nodes at support except for those slab models with simply supported and free edges. The nodes on the line of symmetry were restrained in rotation about that line. The results using a quarter of the model for a plate with uniform thickness were compared to the full size model and the discrepancies of less than 0.01% were obtained with respect to the nodal displacements and stress resultants.

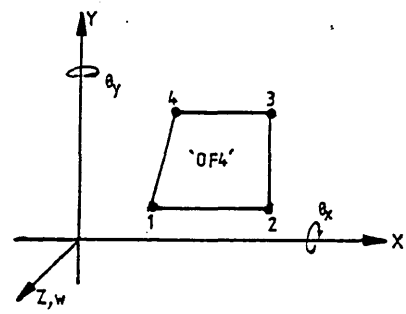

Fig.7.1 Thin Plate Bending Element 'QF4'

In addition, this model with various boundary conditions was checked with the exact solution. Results of the maximum deflections and moments for thin plate with all edges either simply supported or fully fixed compared to those results obtained by Timoshenko (74) are given in Tables 3.2 and 3.3. Two meshes of 6x5 and 12x10 were considered and the discrepancies are given in Table 7.1.

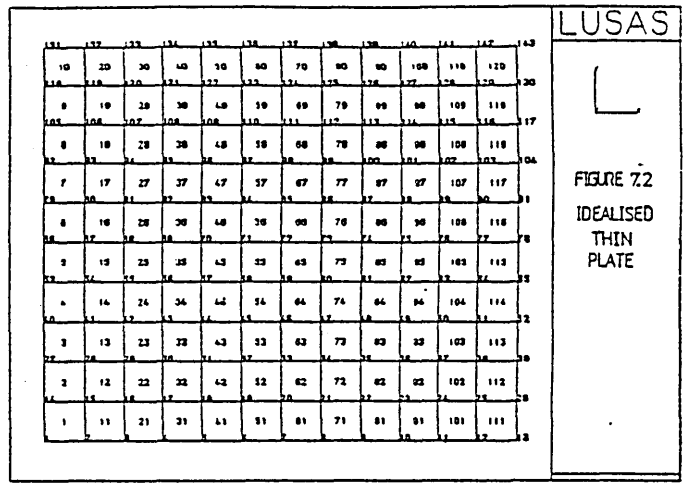

Fig.7.2 Finite Element Mesh of Thin Plate

Table 7.1: Plate with All Edges Either Fully Fixed or Simply Supported and Subjected to Uniformly Distributed Load

	OPBT	6x5 Mesh FEM (2)/(1)		12x10 Mesh FEM (4)/(1)		Edge and Loading Conditions
	(1)	(2)	(3)	(4)	(5)	
Defn. (mm)	13.226	13.264	1.003	13.269	1.003	Restrained Plate Subjected To U.D.L.
Mx	3648.7	3746.5	1.027	3681.2	1.009	
My	2752.2	2812.2	1.022	2771.7	1.007	
Mx'	7784.7	7741.1	0.994	7776.0	0.999	
My'	6713.3	6679.0	0.995	6706.0	0.999	
Defn. (mm)	43.459	43.543	1.002	43.594	1.003	Simply Supported Plate Subjected To U.D.L.
Mx	7660.4	7742.9	1.011	7687.9	1.003	
My	6064.3	6125.9	1.010	6083.8	1.003	

Notes:-

(i) Defn. = $0.0501w.Ly^2/D$
where, w is the aplied U.D.L. in kN/m^2;
Ly is the shorter length of the plate;
D is the flexural rigidity of the plate.

(ii) $Mx,y = \beta.w.Ly^2$
where, β is the coefficient of moment obtained from Tables 3.2 and 3.3 for x and y-axes.

(iii) OPBT is the orthotropic plate bending theory.

(iv) FEM is the finite element method.

7.2.1.1 Theoretical Considerations

The significance of the elastic rigidities in ribbed/waffle slab analysis was described in Section 3.3.3. The principle of this method of analysis for R.C. waffle slabs is based upon the studies carried out in Chapter 3. The following assumptions are made for the present analysis:

(1) A waffle slab can be idealized as an orthotropic plate by replacing the system by an equivalent homogeneous orthotropic plate of uniform thickness providing that the idealized plate has the same elastic properties as those of the original structure.

(2) The flexural rigidities, Dx and Dy, of the idealized section depend on the second moments of area which can be determined using conventional methods.

(3) The torsional and coupling effects on the idealized section are assumed to be contributed by the concrete material only. The torsional rigidity of the section and the coupling effect due to Poisson's ratio can be determined using Cusen et al's (11,12) approach taking into consideration the eccentricity of the idealized section.

7.2.1.2 Stiffness of R.C. Waffle Slabs

The constitutive equations for the elastic plate analysis formulated by the finite element program 'LUSAS/AN' are expressed essentially as follows:

$$\begin{Bmatrix} Mx \\ My \\ Mxy \end{Bmatrix} = \begin{bmatrix} Dx & D_1 & 0 \\ D_1 & Dy & 0 \\ 0 & 0 & Dxy \end{bmatrix} \begin{Bmatrix} \dfrac{\partial^2 w}{\partial x^2} \\ \dfrac{\partial^2 w}{\partial y^2} \\ 2.\dfrac{\partial^2 w}{\partial x \partial y} \end{Bmatrix} \qquad (7.1)$$

Thus, the determination of the flexural and torsional rigidites, and the Poisson effect should be obtained to suit the program.

(i) Determination of Flexural Rigidity

BS8110 recommends that relative stiffnesses be based on the consistent application of any one of three alternative assumptions for calculating second moment of area, I:

(i) the uncracked concrete section ignoring reinforcement;
(ii) the gross uncracked section including reinforcement on the basis of modular ratio; and
(iii) the transformed cracked section which is made up of the concrete area in compression, together with reinforcement on the basis of modular ratio.

For the purposes of analysis in the present investigation, it is considered that the I-value obtained using alternative (iii) is more appropriate to be used to prodict the deflections of the model slabs.

The flexural rigidities, Dx and Dy, of a finite element about an axis are assumed to be uniform along the width of the slab and equal to the product of the elastic modulus of concrete, Ec, and the second moment of area of the T-section, Ix,y, divided by the rib spacing, Sx,y.

$$Dx = \frac{Ec.Ix}{Sx} \quad ; \quad Dy = \frac{Ec.Iy}{Sy} \qquad \text{per unit width} \qquad (7.2)$$

The second moment of area of an idealized T-section can be obtained using the following assumptions:

(i) the second moment of area of a finite element can be determined by replacing the slab and rib to an equivalent T-section;
(ii) the effect of continuity in the top flanges between the idealized T-sections is assumed to be negligible;
(iii) the tensile strength of concrete is ignored;
(iv) all steel in tension is assumed to reach the yield point; and

(v) the effective width of the top flange is taken as the rib spacing and the second moments of area about x- and y-directions are equal, i.e. Dx = Dy, since the ribs are closely and equally spaced in both orthogonal directions.

The sagging moment of resistance was taken as a T-section and the compression depth of the concrete was calculated as for a T-beam while those subjected to hogging moments at the supports were treated as rectangular sections. Having determined the depth of concrete in compression, all the steel in the section was then transformed into the equivalent concrete. The neutral axis of the equivalent section was then found by taking moments about either the upper or the lower face of the section. The second moment of area of the section could then be given by:

$$Ix = \Sigma[Icc + A.(h')^2] \qquad (7.3)$$

where, Ix is the second moment of area of the idealized T-section about x-axis;

Icc is the second moment of area of the section about its centroid;

A is the area of the concrete section;

h' is the distance between the centroid of the concrete section and the neutral axis of the equivalent section.

(ii) Determination of Torsional Rigidity

Torsional rigidity using Cusen et al's approach requires to be modified to suit the computer program in this investigation. Generally, twisting moment is expressed in Eqn.3.64 as below:

$$Mxy = -\left[\frac{Dxy'}{2} + \frac{G.t^3}{12}\right].2.\frac{\partial^2 w}{\partial x \partial y} \qquad (7.4)$$

As a result, the rib depth, r, which is greater than the rib width, t, for this waffle model slab becomes

$$Dxy = \frac{Dxy'}{2} + \frac{G.t^3}{12} \qquad (7.5)$$

where Dxy' can be determined by St. Venants' classical theory on the torsion of prism.

$$\text{Thus,} \quad Dxy = \frac{G.k.t^3.r}{2.S} + \frac{G.t^3}{12} \qquad (7.6)$$

(iii) Determination of Poisson Effect

The Poisson effect or the coupling rigidity is dependent on the eccentricity of the section which is measured from the top surface of the slab to the centroid of the idealized T-section as shown in Fig.7.3. On the basis of the Cusen et al's approach, the coupling rigidity, D_1, can be determined as follows:

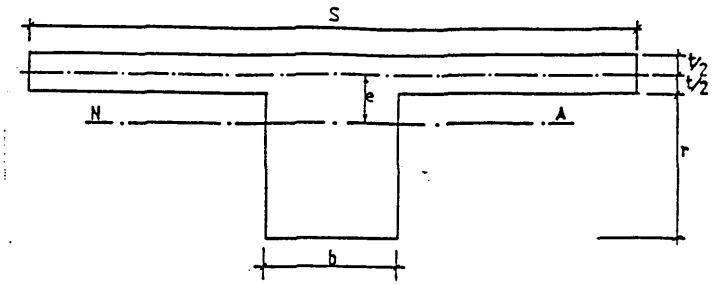

Fig.7.3 Idealized T-section

(a) if eccentricity, e < t/2

$$D_1 = \frac{\nu.E'(t/2 - e)^2.(t+e)}{6} + \frac{\nu.E''(t/2 + e)^2(t-e)}{6}$$

$$\frac{\nu E''b^2}{S^2}\left[\left(\frac{t}{2} + e\right).\frac{r(r+t)}{2} + \frac{r^2(4r+3t)}{12}\right] \qquad (7.7a)$$

(b) if $t/2 < e < t$

$$D_1 = \frac{\nu.E'(t/2+e)^2.(t-e)}{6} + \frac{\nu.E''(t/2-e)^2(t+e)}{6}$$

$$\frac{\nu E''b^2}{S^2}\left[\left(\frac{t}{2}-e\right).\frac{r(r+t-2e)}{2} + \frac{r^2(4r+3t-6e)}{12}\right] \qquad (7.7b)$$

(c) if $e > t$

$$D_1 = \frac{\nu.E'.t^3}{12} + \frac{\nu.E''.b^2}{6.S^2}\left\{\left[r - \left(e - \frac{t}{2}\right)\right]^2 .(2r + e + t) - \left(e - \frac{t}{2}\right)^2.(e + t)\right\} \qquad (7.7c)$$

7.2.1.3 Thin Plate Model Analysis

Flexural rigidities were computed from the equivalent concrete sections as described in Eqn.7.3. The torsional stiffnesses obtained were also based on the concrete sections only and the contribution of the presence of steel was ignored. An elastic modulus of concrete, Ec, of 28kN/mm^2 (14) was used throughout the elastic analyses. Neville (31) indicated that Poisson's ratio, ν, of concrete varies from 0.11 to 0.21. Therefore, a mean value of 0.15 was used in this analysis. The analytical procedure for R.C. waffle model slab B3 is presented in detail in this section. The flexural rigidity for the idealized T-section of model slab B3 shown in Fig.7.3 is determined as follows.

Flexural Rigidities for Model Slab B3:

Using elastic modulus of steel Es = 200.000 kN/mm^2
elastic modulus of concrete Ec = 28.000 kN/mm^2
the modular steel to concrete ratio, m = 7.143

For equilibrium of forces, compressive force in concrete is equal to tensile force in steel.

$$\text{Thus,} \qquad dn = \frac{fy.As + fyd.Asd}{k_1 . k_3 . fcu . Sx} \qquad (7.8)$$

The compressive concrete strength was obtained to be 28.67 N/mm^2. It yields the coefficients of the parabolic stress block as

$$k_1 . k_3 = 0.621 \quad ; \quad k_2 = 0.458$$

It is assumed that the main and the distribution steel yield. Thus, using the following data of

main steel yield stress,	fy = 300.0	N/mm^2
distribution steel yield stress,	fyd = 250.0	N/mm^2
area of main steel,	As = 50.266	mm^2
area of distribution steel,	Asd = 15.985	mm^2

Eqn.7.8 gives dn = 4.660 mm

Then transforming the steel into the equivalent concrete section as shown in Fig.7.4 and taking moment about the top surface of the section, the neutral axis NA is obtained as NA = 15.086 mm.

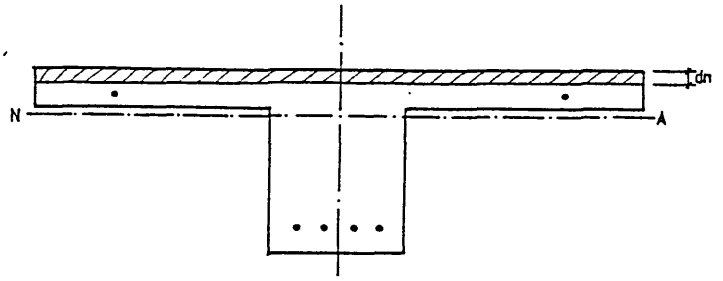

Fig.7.4 Idealized Section of Model Slab B3

The second moment of area of the equivalent concrete section is then found to be

$$Ix = Iy = 7.890 \times 10^5 \text{ mm}^4$$

Hence, at mid-span $D_x = D_y = (28\times10^3 \times 7.890\times10^5)/230$

$= 9.605\times10^7$ Nmm²/mm

Similarly, at support

$D_x = D_y = 9.553\times10^7$ Nmm²/mm

Torsional Rigidities of Model Slab B3:

The torsional rigidity for a composite T-section was computed using Cusen et al's approach.

Since $\frac{r}{b} = \frac{55}{50} = 1.1$

St.Venant's theory gives torsional coefficient k = 0.2126. From Eqn.7.6,

$$D_{xy} = D_{yx} = \frac{28\times10^3}{2(1+0.15)} \times \left[\frac{0.2126\times55\times50^3}{2\times230} + \frac{15^3}{12}\right]$$

$= 4.211\times10^7$ Nmm²/mm

This value is applicable to all elements at mid-spans and supports.

Poisson's Effect:

The Poisson's effect or coupling rigidity, D_1, was obtained as below. The eccentricity, e, for the model slab was found to be 15.086mm which is sligthly greater than the slab thickness of 15.0mm. Therefore, Eqn.7.7b is adopted in here and it yields

$D_1 = 1.445\times10^7$ Nmm²/mm (mid-span)

Similarly, the rigidity for the supports with eccentricity determined to be 24.754mm is given as

$D_1 = 1.075\times10$ Nmm²/mm

In addition to these values, the rigidities for the four corner elements with uniform thickness of 15.0mm are determined as

$$Dx = Dy = \frac{28\times10^3\times15^3}{12(1-0.15^2)} = 8.056\times10^6 \text{ Nmm}^2/\text{mm}$$

$$D_1 = \nu.Dx = 0.15\times8.056\times10^6 = 1.208\times10^6 \text{ Nmm}^2/\text{mm}$$

$$Dxy = \frac{28\times10^3\times15^3}{24(1+0.15)} = 3.424\times10^6 \text{ Nmm}^2/\text{mm}$$

The results of the flexural, torsional and coupling rigidities for all model slabs were determined and are given in Table 7.2.

Several trials were made to locate the points of contraflexure for model slabs with restrained edges in order to assign the elements with the appropriate flexural stiffness i.e. Tee- and rectangular-beams for mid-span and support respectively, to which they might be subjected to either hogging or sagging moment. The conclusion was reached that it is accurate enough to assume that the contraflexure line lies at the centre line of the exterior ribs running parallel to the edges in both orthogonal directions. This contention was substantiated by the fact that the concrete strains at these locations were recorded fluctuating at the zero value. The results for the slab model B3 are shown in Figs.7.5a, b, c & d. For comparison, Table 7.3 shows a summary of the principal information obtained from the analysis for the chosen six model slabs at experimental cracking load. To avoid repetitive, the analytical results for one slab from each of the series tests are shown in Fig.7.6 to Fig.7.11. The analytical results for the rest of the model slabs are also given in Appendix D.

It is noted in Fig.7.5a that the displacements of the idealized model slab is represented by a contour with evenly spaced intervals. This contour clearly indicates that the maximum deflections occur in the central region of the slab and conversely the displacements near the corner regions are extremely small. This displacement contour is, however, in close agreement with what had been observed during the tests.

Table 7.2: Sectional properties of 'QF4' elements.

Slab No.	Location	Mid-span Dx=Dy	Mid-span D_1	Support Dx=Dy	Support D_1	Mid. Dxy	Support
		10^7	10^7	10^7	10^7	10^8	10^8
A1	ALL	2.692	0.726	4.773	0.555		
A2	ALL	3.946	0.715	4.750	0.556	0.177	
A3	ALL	5.021	0.669	4.762	0.556		
B1	ALL	5.221	1.412	9.559	1.052		
B2	ALL	7.436	1.283	9.554	1.076	0.307	
B3	ALL	9.605	1.445	9.553	1.075		
C1	ALL	8.427	2.741	16.126	1.907		
C2	ALL	12.084	2.608	16.094	1.894	0.421	
C3	ALL	15.532	2.504	16.045	1.877		
D1	ALL	5.221	12.010	9.605	12.010	13.920	
E1	INTR	5.095	0.692	4.743	0.556	0.220	
	EDGE	9.490	2.230	9.485		0.406	
E2	INTR	9.591	1.442	9.552	10.740	0.307	
	EDGE	18.360	5.279	19.100		0.808	
E3	INTR	15.500	2.496	16.030	18.720	0.537	
	EDGE	30.020	9.452	32.060		1.040	
F1	INTR	4.927	0.643	4.777	0.554	0.220	
	EDGE	9.332	2.099	9.554		0.406	
F2	INTR	9.292	3.389	9.486	1.047	0.307	
	EDGE	17.930	5.091	18.970		0.808	
F3	INTR	15.770	2.557	16.130	1.909	0.537	
	EDGE	30.430	9.664	32.226		1.040	
H1	ALL	16.303	4.624	35.330	24.660	0.559	2.537
H2	X-AX	13.566	3.213	31.771	19.544	0.471	2.266
	Y-AX	16.100	4.549	35.056	24.340	0.559	2.536
I1	ALL	15.786	4.445	34.624	23.830	0.559	2.537
I2	X-AX	13.268	3.134	31.272	19.090	0.471	2.266
	Y-AX	15.771	4.440	34.602	23.800	0.559	2.536
JI	X-AX	26.800	23.210	65.420	141.700	3.770	
	Y-AX	32.100	32.970	73.150	177.800	4.468	

Notes:

(i) All units are in Nmm^2/mm.

(ii) For element at the corners,

$Dx = Dy = 8.056 \times 10^6$ Nmm^2/mm

$D_1 = 1.208 \times 10^6$ Nmm^2/mm

$Dxy = 3.424 \times 10^6$ Nmm^2/mm

Table 7.3: Comparison of the maximum deflection between the experimental and the analytical results at cracking load.

Slab No.	Cracking Load (kN/m^2)	Max. Deflection (mm)			Ratios	
		(1) EXP.	(2) F.E.M.	(3) G.A.	(2)/(1)	(3)/(1)
A2	31.028	1.73	1.806	1.873	1.044	1.083
B3	55.160	1.66	1.540	1.583	0.928	0.954
C1	51.713	0.95	1.072	1.125	1.128	1.184
E1	20.685	2.20	1.514	1.484	0.688	0.675
E2	27.580	1.16	1.110	1.074	0.957	0.926
E3	31.028	0.82	0.748	0.734	0.912	0.895

High concentration of hogging moments about x- and y-axes occur in the middle of the supports and these can be seen in Fig.7.5b & c. Sagging moments distribute reasonably uniform in the central region of the slab. This may explain why the appearance of the cracks of the slab developed almost simultaneously in the ribs in the central region. It is significant in Fig.7.5d to show that high twisting moments occour in the regions near the corners. The contour of these twisting moments appear in mirror image in both axes.

For model E series, the displacement contour in Fig.7.7a is slightly shifted toward the simply supported edge. Bending moment contours are similar to that of model slab B3 except there is no moment in the simply supported edge. Higher twisting moments are found in the corner regions closed to the simply supported edge as shown in Fig.7.7d. It is because the edge is allowed the slab to rotate in these regions. It is decided that the results for the rest of model slabs are more appropriate to be discussed in the following chapter.

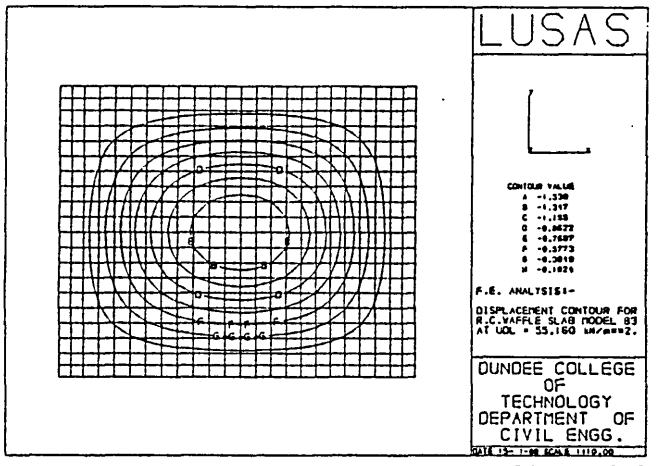

Fig.7.5a Displacement Contour For R.C. Waffle Slab B3

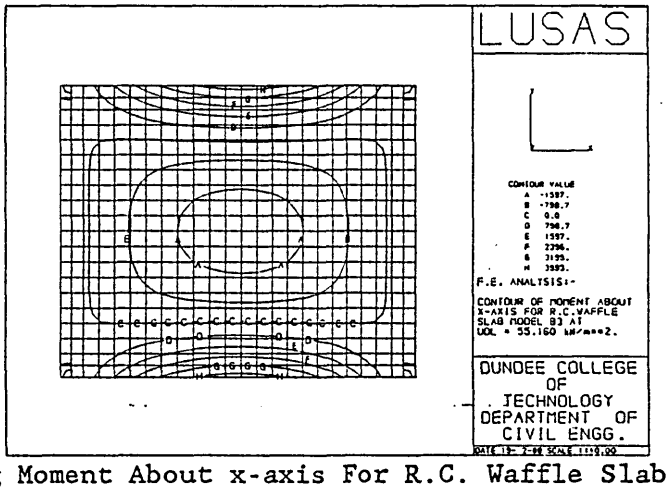

Fig.7.5b Bending Moment About x-axis For R.C. Waffle Slab B3

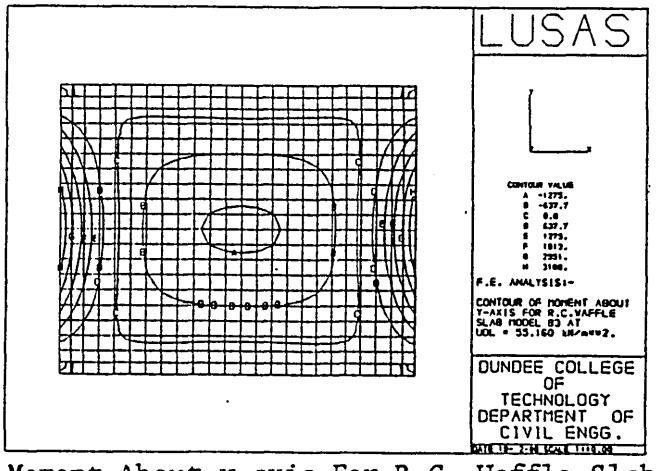

Fig.7.5c Bending Moment About y-axis For R.C. Waffle Slab B3

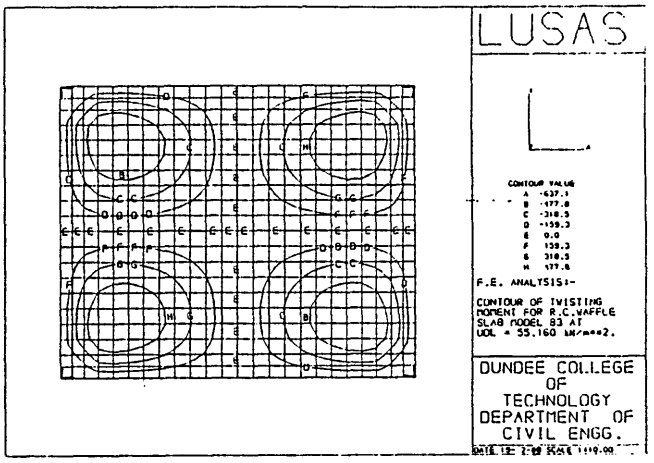

Fig.7.5d Twisting Moment For R.C. Waffle Slab B3

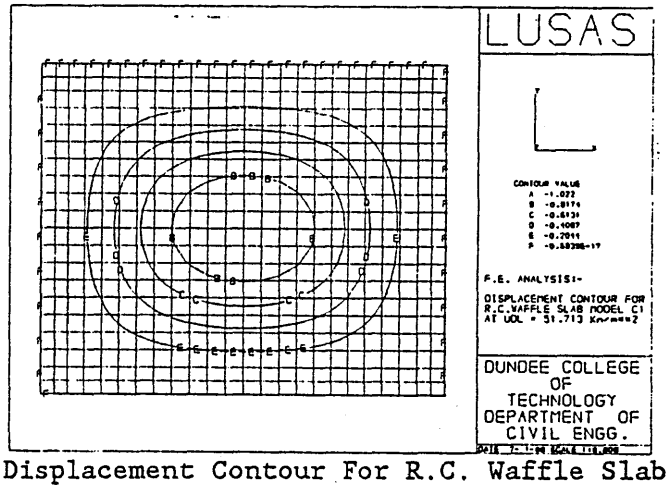

Fig.7.6a Displacement Contour For R.C. Waffle Slab C1

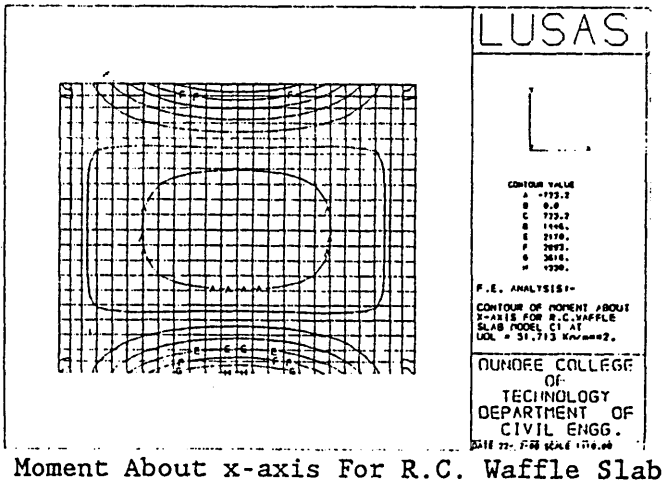

Fig.7.6b Bending Moment About x-axis For R.C. Waffle Slab C1

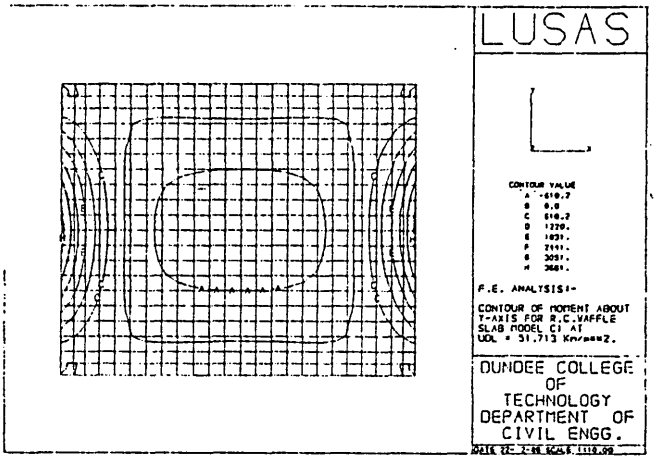

Fig.7.6c Bending Moment About y-axis For R.C. Waffle Slab C1

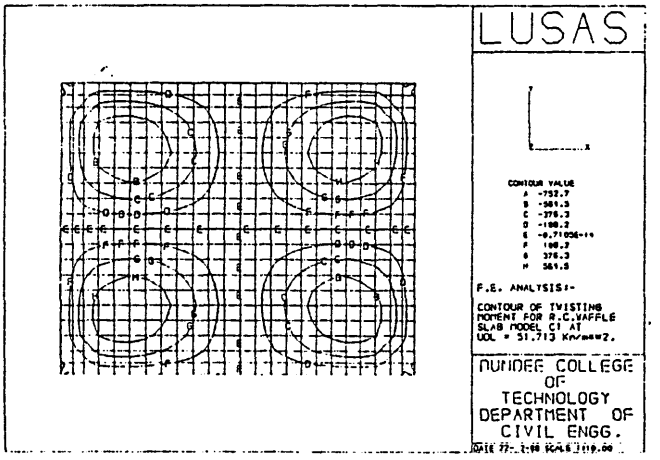

Fig.7.6d Twisting Moment For R.C. Waffle Slab C1

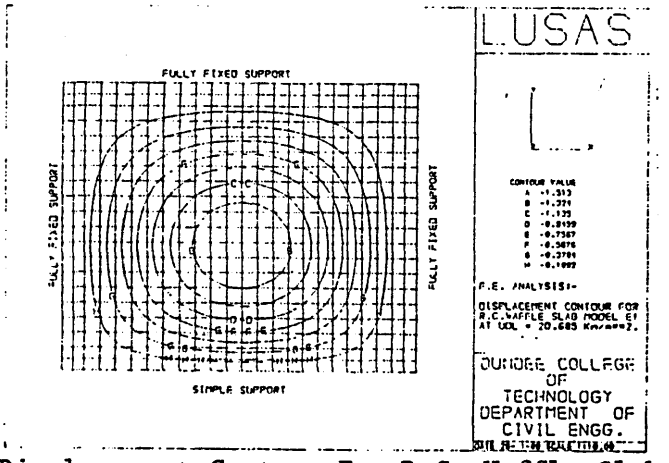

Fig.7.7a Displacement Contour For R.C. Waffle Slab E1

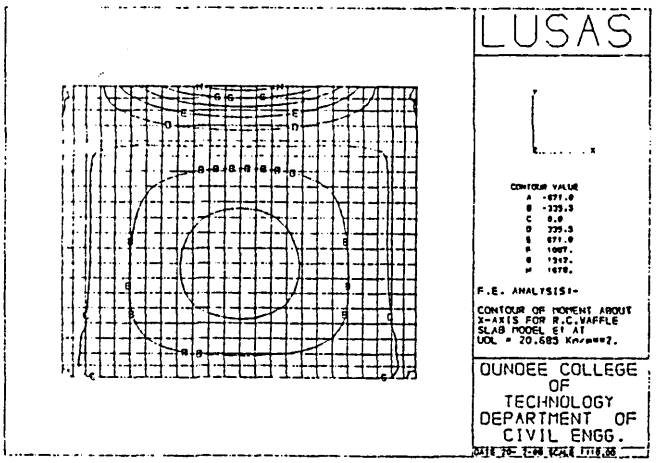

Fig.7.7b Bending Moment About x-axis For R.C. Waffle Slab E1

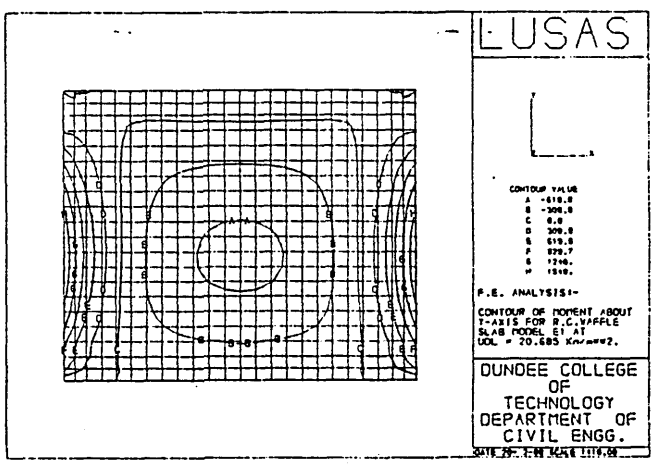

Fig.7.7c Bending Moment About y-axis For R.C. Waffle Slab E1

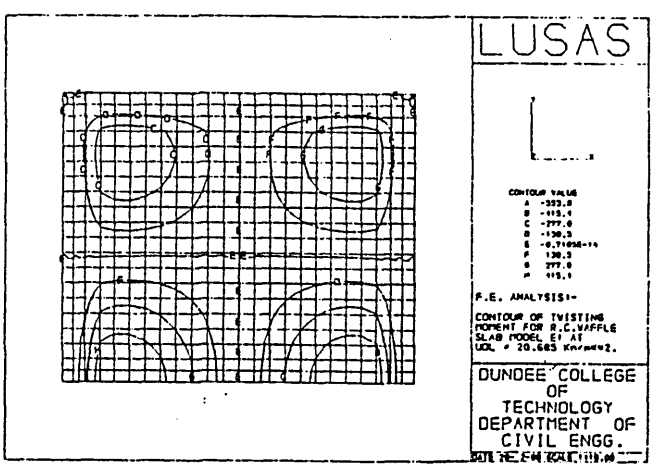

Fig.7.7d Twisting Moment For R.C. Waffle Slab E1

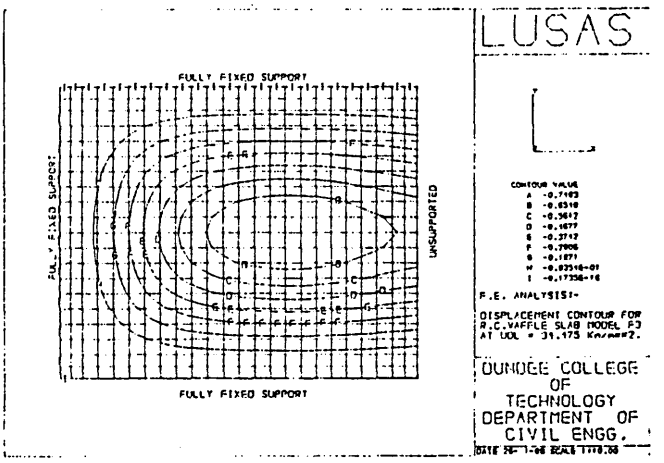

Fig.7.8a Displacement Contour For R.C. Waffle Slab F3

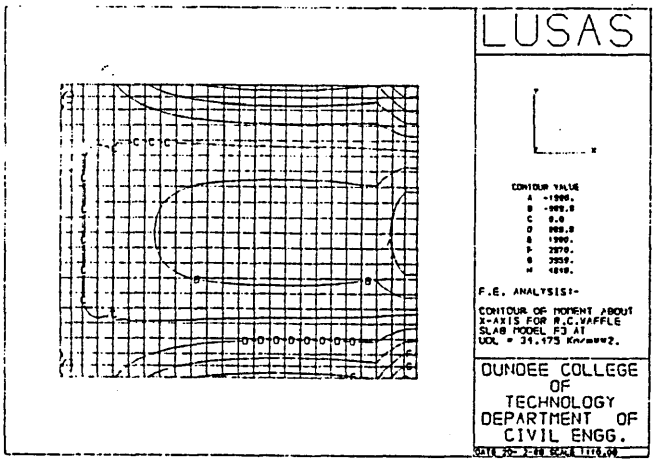

Fig.7.8b Bending Moment About x-axis For R.C. Waffle Slab F3

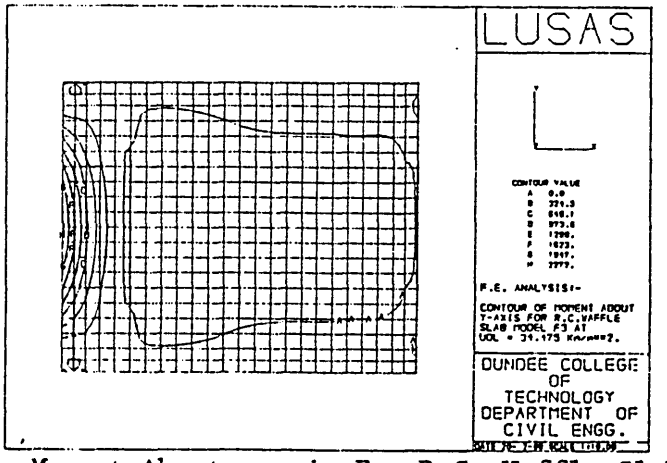

Fig.7.8c Bending Moment About y-axis For R.C. Waffle Slab F3

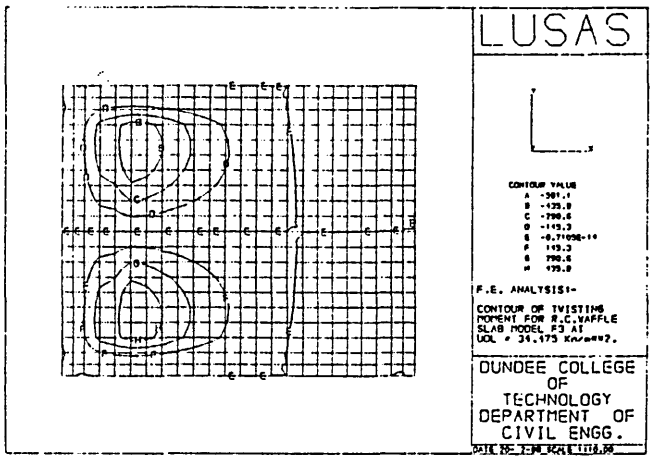

Fig.7.8d Twisting Moment For R.C. Waffle Slab F3

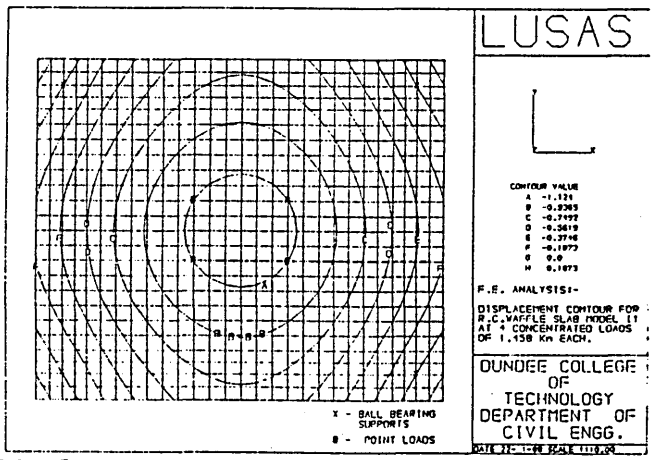

Fig.7.9a Displacement Contour For R.C. Waffle Slab I1

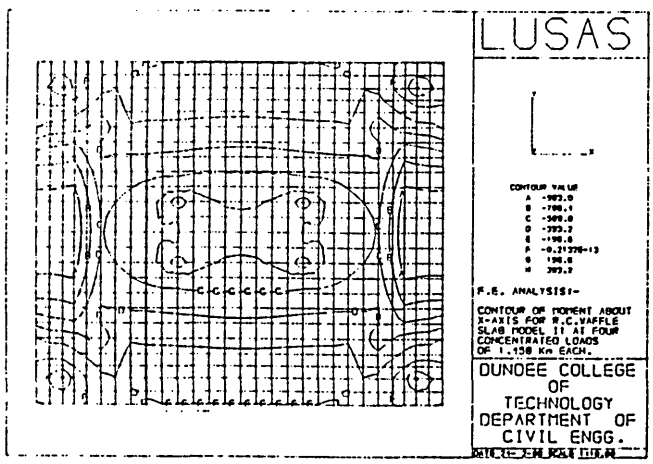

Fig.7.9b Bending Moment About x-axis For R.C. Waffle Slab I1

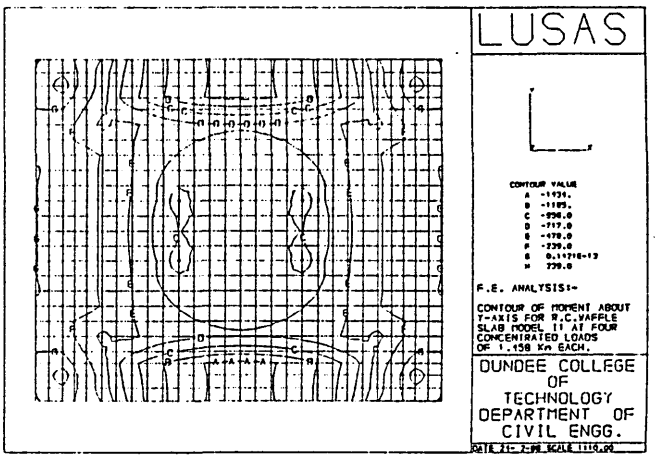

Fig.7.9c Bending Moment About y-axis For R.C. Waffle Slab I1

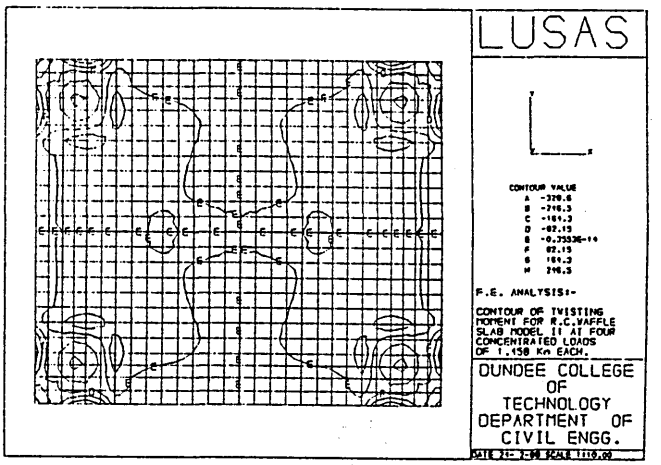

Fig.7.9d Twisting Moment For R.C. Waffle Slab I1

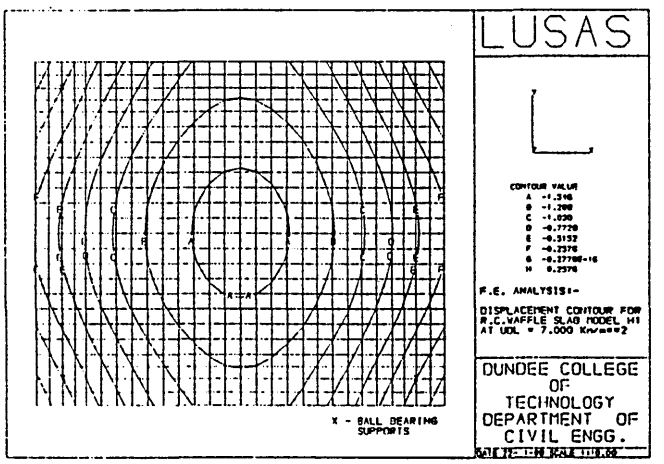

Fig.7.10a Displacement Contour For R.C. Waffle Slab H1

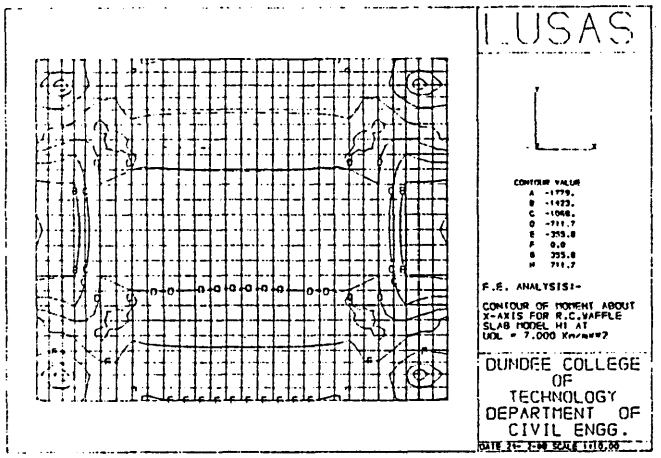

Fig.7.10b Bending Moment About x-axis For R.C. Waffle Slab H1

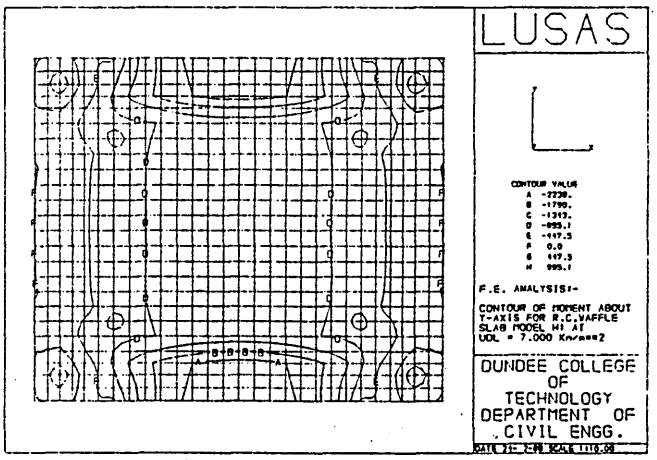

Fig.7.10c Bending Moment About y-axis For R.C. Waffle Slab H1

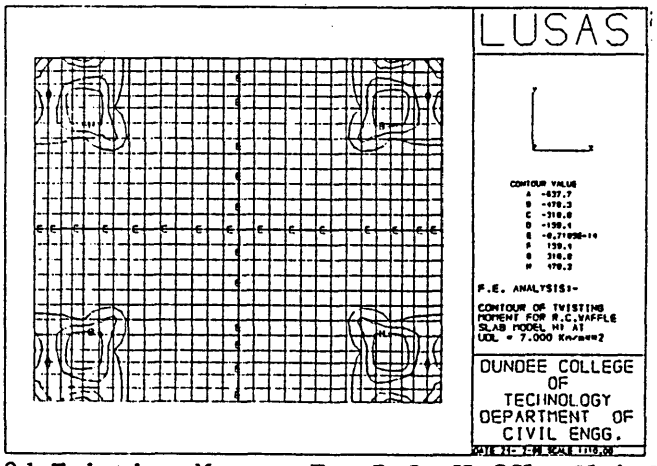

Fig.7.10d Twisting Moment For R.C. Waffle Slab H1

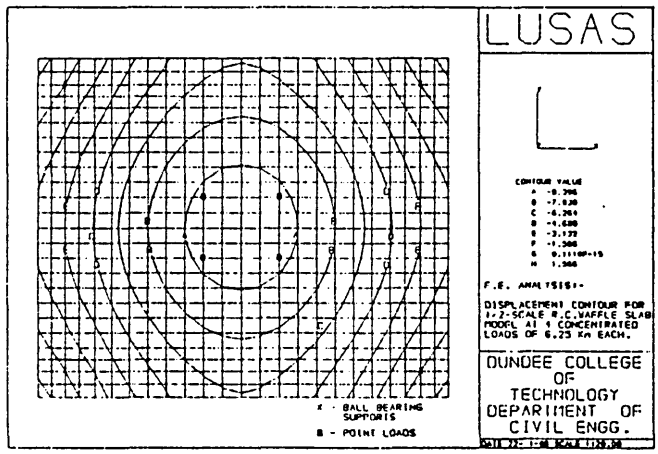

Fig.7.11a Displacement Contour For R.C. Waffle Slab J1

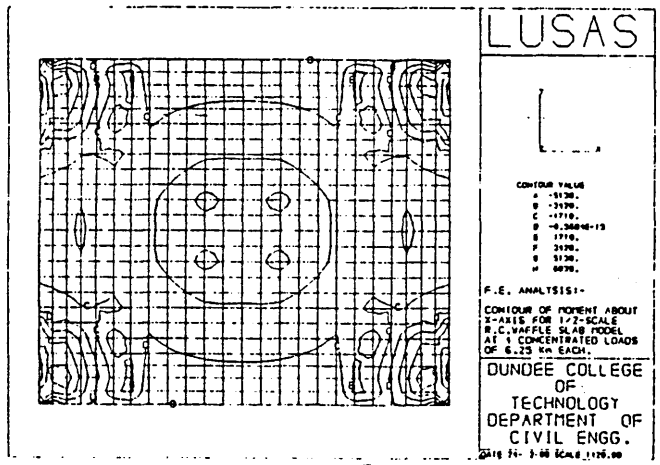

Fig.7.11b Bending Moment About x-axis For R.C. Waffle Slab J1

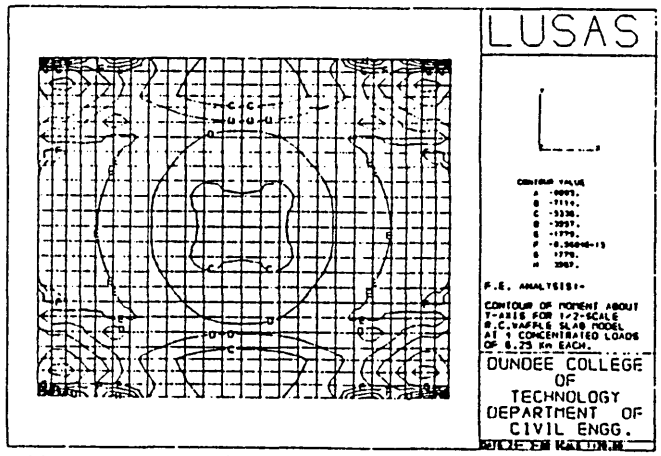

Fig.7.11c Bending Moment About y-axis For R.C. Waffle Slab J1

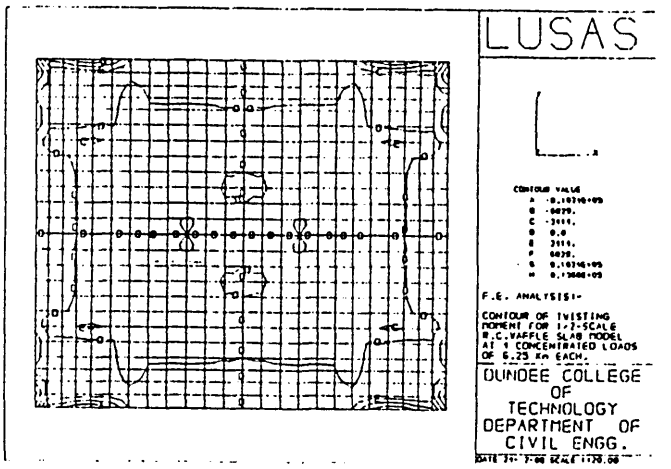

Fig.7.11d Twisting Moment for R.C. Waffle Slab J1

7.2.2 Grillage Element Model

Preliminary grillage analysis was carried out using the computer package 'GRIDS' throughout the early stage of the investigation. However, the more advanced and powerful computer package 'LUSAS/AN' was decided to be employed for the analysis of the grillage model rather than the 'GRIDS' package. A straight grillage element, 'GRIL', was chosen for this analysis. Each grillage element has two nodes and each node has three degrees of freedom i.e. W, θx and θy as shown in Fig.7.12.

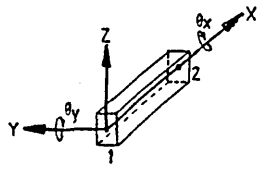

Fig.7.12 Grillage Element 'GRIL'

It was considered that the equivalent grillage should be arranged to coincide with the location of the ribs of the waffle slab models which reduces further complexity that may occur with other layout of the

grillage. Each grillage beam between any two intersection points was subdivided into four 'GRIL' elements giving a total of 196 'GRIL' element model, shown in Fig.7.13. This model was used for analysing the whole slab.

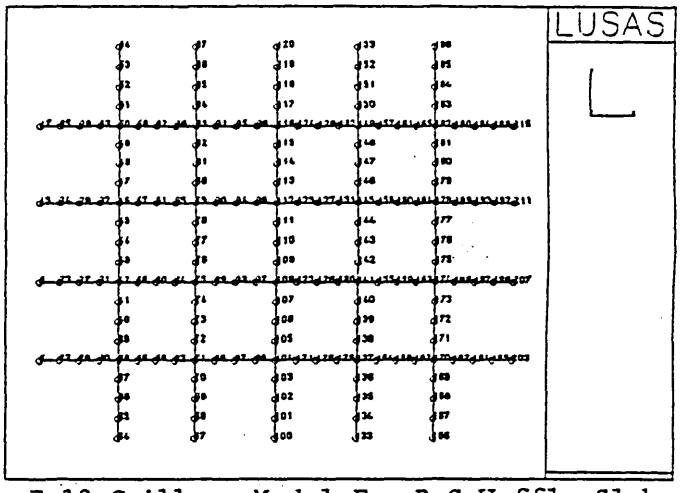

Fig.7.13 Grillage Model For R.C.Waffle Slabs

7.2.2.1 Theoretical Considerations

The following assumptions are made for the analysis:

(1)A waffle slab can be idealized as a grillage system using an equivalent grillage of beams intersecting at rigid nodes, providing the idealized grillage beam has the appropriate elastic properties of the original structure. This equivalent grillage is then analyzed by the standard elastic grillage analysis.

(2)Each of these grillage beams is obtained by replacing the monolithically cast slab and ribs by an equivalent T-section with the width of the flange equal to the spacing between the ribs.

7.2.2.2 Constitutive Equations for Grillage Element

The constitutive equations for the grillage analysis adopted by the presently used finite element program 'LUSAS/AN' are based on the stiffness matrix of a rigid-jointed space element shown in Fig.7.12 as follows:

$$\begin{Bmatrix} Px_1 \\ Py_1 \\ Pz_1 \\ Mx_1 \\ My_1 \\ Mz_1 \end{Bmatrix} = E \begin{bmatrix} \frac{A}{L} & 0 & 0 & 0 & 0 & 0 \\ 0 & \frac{12Iz}{L^3} & 0 & 0 & 0 & \frac{6Iz}{L2^2} \\ 0 & 0 & \frac{12Iy}{L^3} & 0 & \frac{-6Iy}{L^2} & 0 \\ 0 & 0 & 0 & \frac{J}{2L(1+\nu)} & 0 & 0 \\ 0 & 0 & \frac{-6Iz}{L^2} & 0 & \frac{4Iy}{L} & 0 \\ 0 & 0 & 0 & 0 & 0 & \frac{4Iz}{L} \end{bmatrix} \begin{Bmatrix} dx_1 \\ dy_1 \\ dz_1 \\ \theta x_1 \\ \theta y_1 \\ \theta z_1 \end{Bmatrix} \qquad (7.9)$$

As mentioned in Section 7.2.2, only three degree of freedom i.e. dz, θx and θy are important in this analogy. For each element, the geometric properties,

A - the cross-sectional area of the grillage element;
Iyy- the second moment of area about element y-axis;
Izz- the second moment of area about element z-axis;
J - the torsional contant of the grillage element;
As - the effective area for shear i.e. As = 1000A is recommended for the present investigtion.

are required to be determined. Since the equivalent concrete section was used to calculate the geometric properties, the elastic modulus and Poisson's ratio of concrete were used to determine the material properties for the grillage elements.

(i) Determination of Iyy

The second moment of area about y-axis of the idealized T-section shown in Fig.7.14 can be determined in the same way as described in Eqn.7.3 except that the value is considered to be for each individual grillage beam. In this analysis, the continuity between the adjacent flanges of the idealized T-sections is ignored.

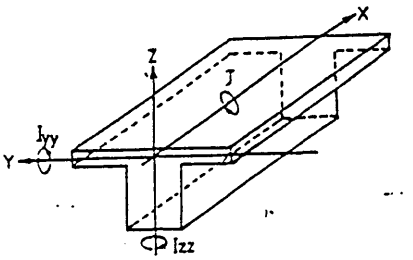

Fig.7.14 Idealized T-section

(ii) Determination of Izz

In order to suit the stiffness matrix shown in Eqn.7.15, the second moment of area about element z-axis is considered to be determined as plain concrete Tee-section as shown in Fig.7.14 on the basis that the load applies perpendicular to the grillage and the out of plane stresses and displacements are important.

(iii) Determination of Torsional Constant J

Two alternatives may be considered to obtain the torsional constant, J, for the idealized T-section. The assumptions (i), (ii) and (v) used for the evaluation of the flexural rigidity in Section 7.2.1.2 are applicable here, and the contribution of the torsional effects from the reinforcements are neglected.

Alternative (1): The torsional resistance for the equivalent grillage beam is considered to be equal to that described in Eqn.7.5 rather than that described in Eqn.3.66 to which the eccentricity, e, is measured from the mid-plane of the top slab to the centriod of the rib. In fact, it is important to take into account Poisson's effect on the T-section. The differential equation shown in Eqn.3.43, gives twisting moment, Mt, per unit length of the plate element as

$$\text{Mt/unit length} = 2H.\frac{\partial^4 w}{\partial x^2 \partial y^2} \qquad (7.10a)$$

From Eqn.3.44, the equation becomes

$$\text{Mt/unit length} = (2Dxy + D_1).2.\frac{\partial^4 w}{\partial x^2 \partial y^2} \qquad (7.10b)$$

St. Venant's classical theory expressed torque, T, as

$$T = G.J.\theta \qquad (7.11)$$

The torsional constant, J, for each idealized grillage element with rib spacing Sx can be obtained by equating Eqn.7.11 to Eqn.7.10b as

$$GJ = (2Dxy + D_1).Sx$$

Re-arranging,

$$J = \left(\frac{2Dxy + D_1}{G}\right).Sx \qquad (7.12)$$

Alternative (2): Due to the fact that an equivalent grillage beam element is transformed from the monolithically cast top slab and rib to the T-section, the torsional stiffness of this equivalent beam element may appropriately be assumed as a unique T-section rather than the section which is considered to be composed of integral components i.e. top slab and rib as described in alternative (1). The torsional constant can be computed using Prandtl's elastic membrane analogy for torsion (35). This analogy states that the volume under the deflected membrane, shown in Fig.7.15, is proportional to the torque, T. Thus, torque can be determined mathematically as

$$T = 2\iint \phi.dx.dy \qquad (7.13)$$

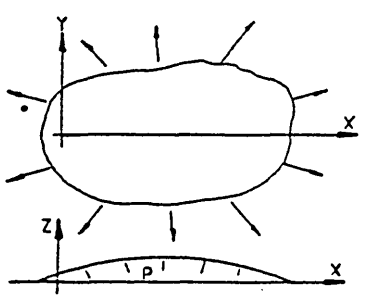

Fig.7.15 Deflected Membrane

where, the function ϕ must satisfy two conditions defined by the differential and boundary equations of

$$\nabla^2\phi = \frac{\partial^2\phi}{\partial x^2} + \frac{\partial^2\phi}{\partial y^2} = -2.G.\theta \qquad (7.14)$$

and $\phi = 0$

A finite mesh, shown in Fig.7.16, is applied to the cross section of the T-section to simulate the deflected membrane. The nodal displacements of this membrane are be determined using the finite difference method (74) which can satisfy both of those conditions given by the membrane analogy. The volume of this deflected membrane can then be obtained using a method of approximation. Thus, Simpson's Rule was employed to determine the volume of the deflected membrane based on the same finite mesh as shown in Fig.7.16.

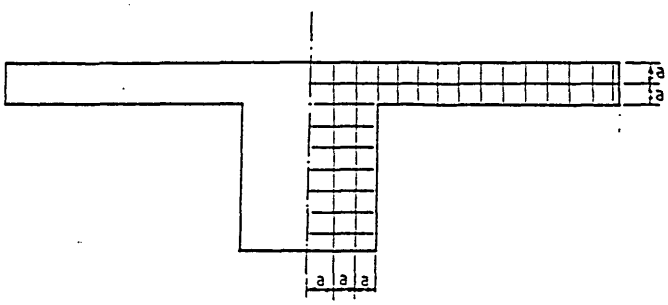

Fig.7.16 Finite Mesh Network

In accordance with St.Venant's theory (35,74) the torsional constant of an idealised Tee-section can then be obtained as

$$J = \frac{2 \iint \phi.dx.dy}{G.\theta} \qquad (7.15)$$

7.2.2.3 Grillage Model Analysis

In parallel with the previous model analysis, the analytical procedure for R.C.waffle model slab B3 is described here in detail. The second moment of area for the idealized T-section for the slab model was similar to that described in Section 7.2.1.2. From Table 7.2,

$$Dy = 9.605 \times 10^7 \text{ mm}^4/\text{mm} \quad \text{in mid-span}$$

Thus,
$$Iyy = \frac{9.605 \times 10^7 \times 230}{28 \times 10^3} = 7.890 \times 10^5 \text{ mm}^4$$

Similarly at supports,

$$Iyy = 7.847 \times 10^5 \text{ mm}^4$$

The second moment of area about element z-axis is

$$Izz = \frac{15 \times 230^3}{12} + \frac{55 \times 50^3}{12} = 1.578 \times 10^7 \text{ mm}^4$$

The torsional rigidity for a composite T-section was computed using both Cusen et al's approach in Eqn.7.12 and the 'Soap film analogy' in Eqn.7.15 using the finite difference program 'FDSOL'.

Rearranging Eqn.7.12, torsional constant can be determined as

$$J = \frac{(2Dxy + D1).Sx.2(1 + \nu)}{E} \qquad (7.16)$$

Thus,
$$J = \frac{(2 \times 0.307 \times 10^8 + 1.445 \times 10^7) \times 230 \times 2(1 + 0.15)}{28 \times 10^3}$$

$$= 1.434 \times 10^6 \text{ mm}^4 \quad \text{in mid-span}$$

Similarly at supports,

$$J = \frac{(2 \times 0.307 \times 10^8 + 1.075 \times 10^7) \times 230 \times 2(1 + 0.15)}{28 \times 10^3}$$

$$= 1.364 \times 10^6 \text{ mm}^4$$

Using Prandtl's membrane analogy with the help of the finite difference program 'FDSOL', the torsional constant for the model slab B3 is given as $1.812 \times 10^6 \text{mm}^4$ in Table 7.4. This constant was obtained and applied in the preliminary analysis during the early stages of the investigation. It was found that this constant was grossly over-estimated by Prandtl's membrane analogy, by about 26%, when compared to the value obtained using Cusen et al's approach. It was therefore decided not to consider the values in Table 7.4.

Table 7.4 Torsional Constants For R.C. Waffle Model Slabs

Slab Series	T-section (10^6 mm^4)	L-section (10^6 mm^4)
A	1.258	---
B	1.812	---
C	2.085	---
E1	1.258	1.132
E2	1.812	1.686
E3	2.085	1.968
F1	1.258	1.132
F2	1.812	1.686
F3	2.085	1.968

Table 7.5:- Sectional properties of 'GRIL' elements.

Slab No.	Location	A	Iyy		Izz	J		As	ELL
			Mid.	Supp.		Mid.	Supp.		
		10^3 mm^2	10^5 mm^4	10^5 mm^4	10^7 mm^4	10^6 mm^4	10^6 mm^4	10^6 mm^4	(kN/m^2)
A2	INTR	5.45	3.241	3.902	1.563	0.804	0.774	5.45	3.568
B3	INTR	6.20	7.890	7.847	1.578	1.434	1.364	6.20	6.343
C1	INTR	6.95	6.922	13.247	1.594	2.074	1.916	6.95	5.947
E1	INTR	5.45	4.185	3.896	1.563	0.962	0.937	5.45	2.379
	EDGE	4.10	3.898	3.896	0.810	1.190	0.998	4.10	1.189
E2	INTR	6.20	7.878	7.846	1.578	1.433	1.364	6.20	3.172
	EDGE	4.85	7.540	7.846	0.826	2.465	1.982	4.85	1.586
E3	INTR	6.95	12.729	13.167	1.594	2.501	2.384	6.95	3.568
	EDGE	5.60	12.331	13.167	0.841	3.479	2.608	5.60	1.784

Notes:

A - area of the element
Iyy - second moment of area about y-axis
Izz - second moment of area about z-axis
kt - torsional constant
As - effective shear area
ELL - equivalent line load
INTR - interior elements
Edge - simply supported elements in the edge
Mid - mid-span
Supp - Support

It is important to bear in mind that the continuity in the flanges of the model slab is ignored in this analysis. The results of the second moment of areas and torsional constants for the chosen six model slabs are given in Table 7.5. The analytical values of the bending and torsion moments for model slab B3 are shown in Fig.7.17. The principal analytical results of the chosen six model slabs at experimental cracking loads are also given in Table 7.3 for comparison.

The graphical representation of bending moment and torsion moments in Fig.7.17 to Fig.7.19 show that high hogging moments occur at the supports of the interior ribs. Sagging moments are reasonably distributed along the central portions of the interior ribs. These bear a close resemblance to that obtained using bending plate theory. Again, higher twisting moments are developed at the closest nodes nearest to the corners but not at the supports. Analytical results for model slab E1 are also given in Fig.7.20. Maximum twisting moments occur in the rib sections close to the corner along the simply supported edge. It gives a close agreement with the observations during the tests and also with the result obtained using bending plate theory. The maximum span moment is actually shifted toward the simply supported edge. It can also be seen that small amount of hogging moments are generated at the supports of the ribs connected to the simply supported edge.

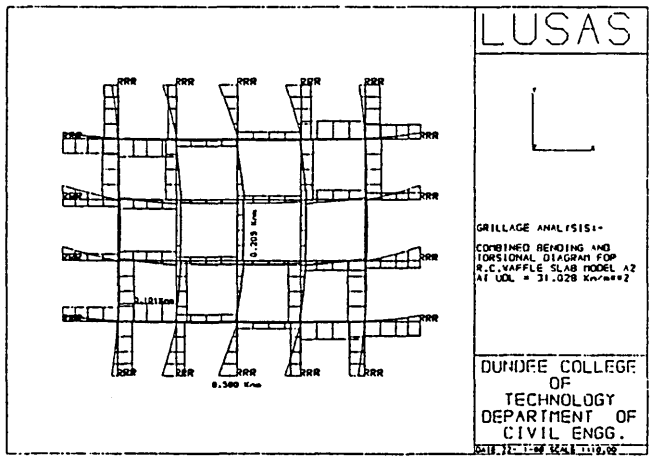

Fig.7.17 Bending and Twisting Moment Diagram
For R.C. Waffle Slab A2

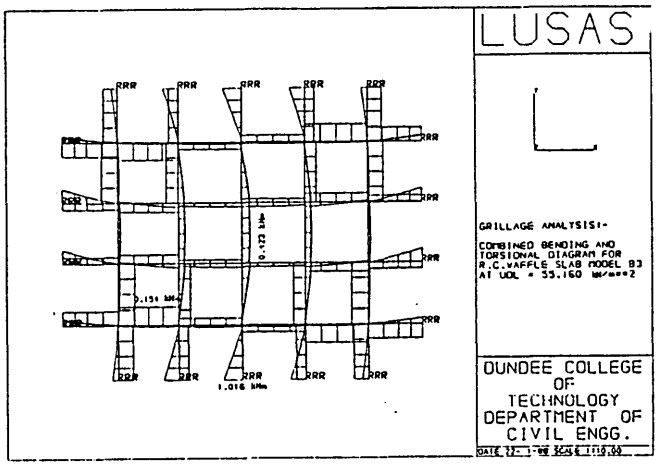

Fig.7.18 Bending and Twisting Moment Diagram For R.C. Waffle Slab B3

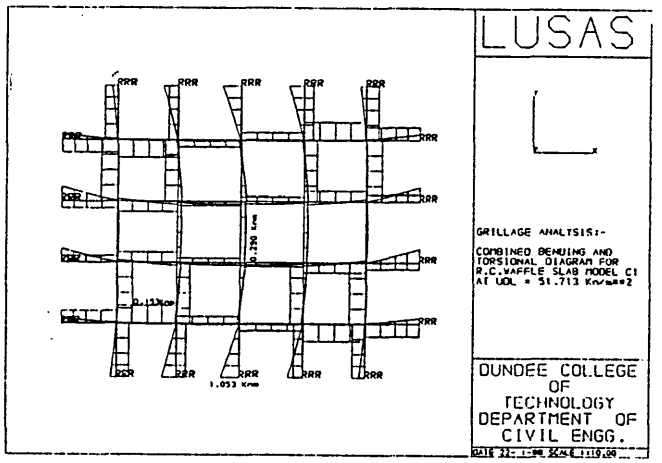

Fig.7.19 Bending and Twisting Moment Diagram For R.C. Waffle Slab C1

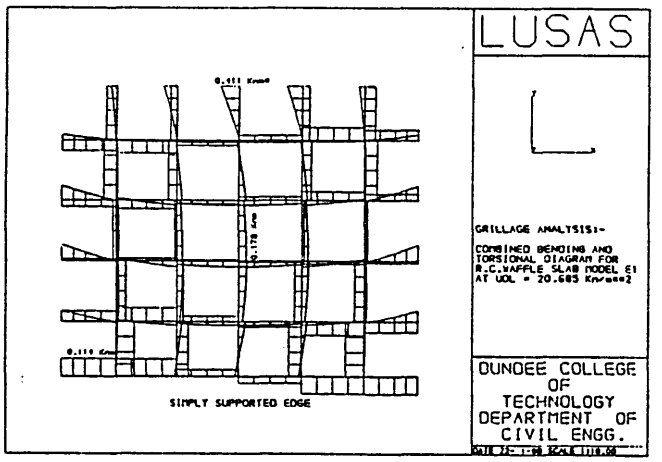

Fig.7.20 Bending and Twisting Moment Diagram For R.C. Waffle Slab E1

7.2.3 Moments Coefficients

Finite element mothod and grillage analysis are conveniently used to analyse the elastic behaviour of R.C. waffle slabs. The linear behaviour for the purpose of analysis in this investigation is considered only to apply up to the load which corresponded to the appearance of the first crack of the model slab. The aim is to establish which so that it may be used appropriately to compare with the ultimate moments for design given by the current code of practice.

In BS8110 (5), the width of middle strip is defined as three quarters of the width of the slab and it is stated that the edge strips of the slab in both orthogonal directions should be provided with nominal reinforcement. In order to provide a basis for comparison, only moments in the middle strips in both directions are considered in accordance with the code. These moments are then related to the coefficients of momentsin terms of wLy^2 for the results using FEM given in Table 7.6, where w is the design load and Ly is the short span of the slab. The coefficients provided by the Code for ribbed slabs with restrained edges are also given in Table 7.6. The moment coefficients obtained by analysis for these nine slab models are found to be quite consistent.

The same procedures were carried out to obtain the comparable moment coefficients from the results of the grillage analysis. The values are given in Table 7.7 for R.C. waffle slabs with all edges fully fixed, and for one long edge simply supported and the other three fully fixed. The sums of the support and span moments are found to be consistent throughout the analysis. The values of the moment coefficients in Tables 7.6 and 7.7 show a good agreement between these two elastic analyses. The comparison between these values indicates that the grillage analysis in this investigation tends to give less span moments than that by the finite element method. The differences in these two methods may possibly reflect the effect of ignoring the continuity in the top slab of the waffle slab in the grillage analysis.

Based on the rigidities of R.C. waffle model slabs A2, B3 and C1, three theoretical models of R.C. waffle square slabs were analyzed using bending plate theory and the moment coefficients are given in

Table 7.8. The results were compared to that obtained by Resis (64) and Tebbit (70,71) in Table 2.3. Comparison of these two sets of analytical values for R.C. waffle slabs shows that the theoretical values of span moments are substantially lower than the values given in BS8110. To be precise, the support moment coefficients by theoretical analyses are some 20% higher and the span moment coefficients 92% lower than those given in the BS8110.

Table 7.6 Moment coefficients for R.C. Waffle Slabs Using Finite Element Method

Slab No.	Support Moments		Mid-span Moments	
	βsx	βsy	βsx	βsy
A1	0.0498	0.0418	0.0143	0.0091
A2	0.0483	0.0405	0.0175	0.0110
A3	0.0472	0.0392	0.0198	0.0122
B1	0.0517	0.0429	0.0154	0.0099
B2	0.0504	0.0415	0.0183	0.0114
B3	0.0489	0.0402	0.0208	0.0121
C1	0.0516	0.0429	0.0151	0.0099
C2	0.0502	0.0415	0.0180	0.0115
C3	0.0489	0.0403	0.0203	0.0127
Mean	0.050	0.041	0.018	0.011
BS8110	0.042	0.032	0.032	0.024
E1	0.0526	0.0523	0.0224	0.0193
E2	0.0546	0.0556	0.0237	0.0208
E3	0.0547	0.0558	0.0232	0.0203
Mean	0.054	0.0546	0.0231	0.0201
BS8110	0.0557	0.037	0.0426	0.028

where, $Msx = \beta sx.w.Ly^2$
$Msy = \beta sy.w.Ly^2$
w is design load;
Ly is the short span of the slab.

Table 7.7 Moment Coefficients For R.C.Waffle Slabs Using Grillage Analysis

Slab No.	Support Moments		Mid-span Moments	
	βsx	βsy	βsx	βsy
A2	0.0473	0.0392	0.0165	0.0081
B3	0.0476	0.0390	0.0196	0.0100
C1	0.0507	0.0419	0.0136	0.0061
Mean	0.049	0.040	0.018	0.008
BS8110	0.042	0.032	0.032	0.024
E1	0.0508	0.0499	0.0202	0.0166
E2	0.0528	0.0517	0.0210	0.0172
E3	0.0531	0.0523	0.0205	0.0170
Mean	0.0552	0.0513	0.0206	0.0169
BS8110	0.0557	0.0370	0.0426	0.0280

Table 7.8 Moment Coefficients For Square R.C. Waffle Slabs Using Finite Element Method

Slab No.	Support Moments		Mid-span Moments	
	βsx	βsy	βsx	βsy
BS8110 (CP110)	0.032	0.032	0.024	0.024
A2	0.0382	0.0382	0.0129	0.0129
B3	0.0376	0.0376	0.0114	0.0114
C1	0.0396	0.0396	0.0133	0.0133
Mean	0.0385	0.0385	0.0125	0.0125

where $Msx = \beta sx.w.Ly^2$
$Msy = \beta sy.w.Ly^2$
w is design load;
Ly is the short span of the slab.

7.3 NONLINEAR ANALYSIS

In the present investigation, the nonlinear behaviour of R.C. waffle slabs was analysed using a three-dimensional finite element model. On the basis of the literature survey in Chapter 3, cracking of concrete was considered be the most significant contributing factor to the nonlinear behaviour of reinforced concrete waffle slabs. A linear elastic fracture model using step by step incremental loading was employed successfully in this investigation.

7.3.1 Elastic-fracture Model

The three-dimensional isoparametric element, 'HX16' shown in Fig.7.21, was used to model the concrete section of the waffle slab and the reinforcing bars were stimulated by linear bar element, 'BRS', with the same number of degrees of freedom as that of 'HX16' element. A 45^0 isometric view of a section from the model including the top slab and the rib is shown in Fig. 7.22. The bar element was rigidly connected to the solid element and a perfect bond between these two materials was assumed. The elastic modulus of concrete, Ec, of $28kN/mm^2$ and the elastic modulus of steel, Es, of $200kN/mm^2$ were used throughout the analysis. The Poisson ratios for concrete, νc, and steel, νs, were assumed to be 0.15 and 0.3 respectively.

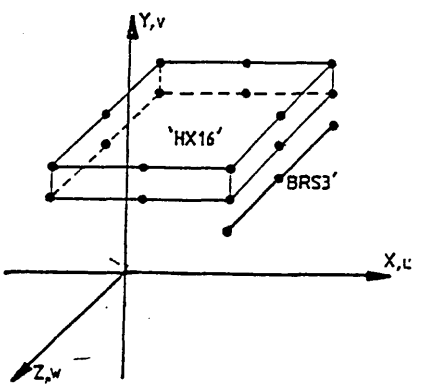

Fig.7.21 Three-dimensional Isoparametric Element 'HX16'

The major contributing factor to the nonlinear behaviour of a reinforced concrete waffle slab is the propagation of cracks in the

concrete sections at a low tensile stress. The effect of cracking was simulated by reducing the rigidities of cracked elements to the assumed level. The nonlinear characteristic of steel was simplified as perfect elastic-plastic material.

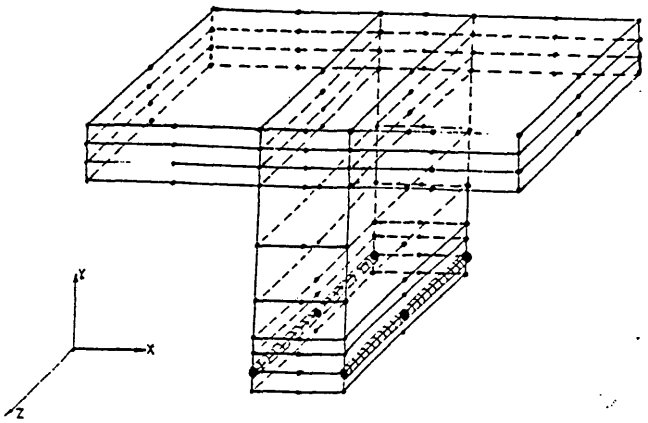

Fig.7.22 A Section of Three-dimensional R.C. Waffle Model Slab

7.3.2 Theoretical Considerations

The following assumptions have been made for this analysis:

(i) reinforced concrete waffle slabs can be modelled by the layered element approach which idealizes the slab into a number of finite layers;

(ii) reinforcement can be simulated by round bar elements perfectly bonded to the corner nodes of the concrete layered elements at the actual depths;

(iii) smeared cracking model for concrete is adopted so that if tensile stress in any principal axis exceeds the tensile stress limit of the element, the elastic modulus of concrete in that direction of cracking and the shear modulus of the element are reduced to zero: and the uncracked concrete elements are considered still to process their isotropic elastic material properties; and

(iv) failure criteria for concrete are adopted from the modified biaxial stress envelope combined with the tensile cut-off.

7.3.3. Modified Biaxial Stress Envelope

The significance of the octahedral shearing stress theory (74) is that it gives the octahedral shearing stress in three principal axes as

$$\tau g = \frac{1}{3}.\sqrt{[(\sigma_1 - \sigma_2)^2 + (\sigma_2 - \sigma_3)^2 + (\sigma_3 - \sigma_1)^2]} \qquad (7.17)$$

It is considered that the stress state of a reinforced concrete waffle slab can conveniently be expressed as a biaxial stress state. Therefore, the octahedral shearing is reduced to

$$\tau g = \frac{\sqrt{2}}{3}.\sqrt{(\sigma_1^2 + \sigma_2^2 - \sigma_1.\sigma_2)} \qquad (7.18)$$

On the basis of theory of failure, the octahedral shearing stress for a state of uniaxial tensile stress, as occurs in the standard tensile test, is generally given to be

$$\tau g = \frac{\sqrt{2}}{3}.ft \qquad (7.19)$$

For the purpose of analysis in this investigation, the uniaxial tensile stress, ft, can significantly be related to the biaxial stress state of the concrete as

$$ft^2 = \sigma_1^2 + \sigma_2^2 - \sigma_1.\sigma_2 \qquad (7.20)$$

Re-arranging the equation in general form as

$$1.0 = \left[\frac{\sigma_1}{ft}\right]^2 + \left[\frac{\sigma_2}{ft}\right]^2 - \left[\frac{\sigma_1}{ft}\right].\left[\frac{\sigma_2}{ft}\right] \qquad (7.21)$$

where, $\left[\frac{\sigma_1}{ft}\right]$ and $\left[\frac{\sigma_2}{ft}\right]$ are the non-dimensional parameters of the equation.

This non-dimensional equation is plotted with the parameters varying from +1.0 to -1.0 as shown in Fig.7.23. It is customary to describe the strength of concrete with respect to its compresssive strength. The tensile strength of concrete in is generally found to be within the range of 0.08 to 0.11 (31) of the compressive strength. Therefore, the compressive/tensile strength ratio of one-tenth was used throughout this analysis. Due to this property of concrete, the envelope in Fig.7.23a has to be modified into a stress envelope with respect to the compressive strength of concrete by multiplying all the non-dimensional parameters in tension, i.e. negative values, with one-tenth. The result provides a very important non-dimensional stress envelope as shown in Fig.7.23b. This modified biaxial stress envelope for concrete shows an excellent agreement with that recommended by Lin et al, Kupfer et al and Tasuji et al (69) in Fig.4.5.

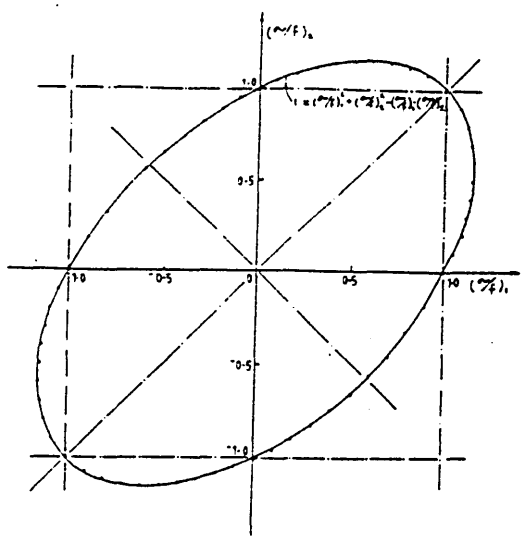

Fig.7.23a Non-dimensional Stress Parameter Diagram

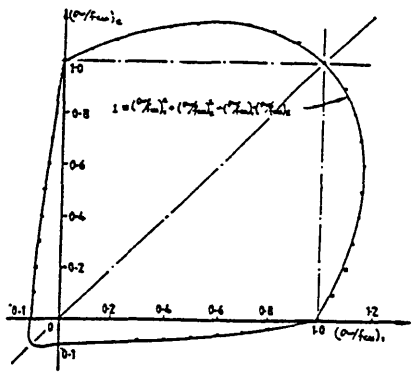

Fig.7.23b Modified Biaxial Stress Envelope

7.3.4 Tensile Cut-off

Cleavage fracture is assumed to occur when the maximum tensile stress is exceeded and cracks develop normal to the direction of the maximum principal stress. It is assumed that these cracks reduce the strength of the element to zero only in that principal direction. The resulting cracked element is then modified as an orthotropic plate element with reduced material property in that principal axis normal to the plane of crack.

7.3.5 Constitutive Equations for 3-D Isoparametric 'HX16' Element

The constitutive equations for this 3-dimensional isoparametric element in the finite element program 'LUSAS/AN' are based on the stiffness matrix as follows:

$$\begin{Bmatrix} \sigma x \\ \sigma y \\ \sigma z \\ \tau xy \\ \tau yz \\ \tau zx \end{Bmatrix} = \begin{bmatrix} d_{11} & d_{12} & d_{13} & 0 & 0 & 0 \\ d_{21} & d_{22} & d_{23} & 0 & 0 & 0 \\ d_{31} & d_{32} & d_{33} & 0 & 0 & 0 \\ 0 & 0 & 0 & d_{44} & 0 & 0 \\ 0 & 0 & 0 & 0 & d_{55} & 0 \\ 0 & 0 & 0 & 0 & 0 & d_{66} \end{bmatrix} \begin{Bmatrix} \varepsilon x \\ \varepsilon y \\ \varepsilon z \\ \varepsilon xy \\ \varepsilon yz \\ \varepsilon zx \end{Bmatrix} \qquad (7.22)$$

where, $d_{11} = \dfrac{1}{Ex}$; $d_{12} = \dfrac{-\nu yx}{Ey}$; $d_{13} = \dfrac{-\nu zx}{Ez}$

$d_{21} = \dfrac{-\nu xy}{Ex}$; $d_{22} = \dfrac{1}{Ey}$; $d_{23} = \dfrac{-\nu zy}{Ez}$

$$d_{31} = \frac{-\nu xz}{Ex} \quad ; \quad d_{32} = \frac{-\nu yz}{Ey} \quad ; \quad d_{33} = \frac{1}{Ez}$$

$$d_{44} = \frac{1}{Gxy} \quad ; \quad d_{55} = \frac{1}{Gyz} \quad ; \quad d_{66} = \frac{1}{Gzx}$$

The basis of this analysis is if that an average concrete stress of an element along a principal axis exceeds its governing stress criteria, the element is said to be either cracked or crushed. The average concrete stress in that principal axis is, therefore, assumed to be redistributed. In order to redistribute this stress to the other elements of the slab, the resultant stress in that particular axis alone will be reduced to be practically negligible. Based on the constitutive equations, the modulus of elasticity and the Poisson ratios with respect to that axis should be reduced to a significantly small value. Using this procedure, the development of cracking for R.C. waffle slabs can be traced progressively.

7.3.6 Analytical Procedure

Initially, the experimental failure load of the waffle model slab was divided into a number of increments. For each load increment, a three dimensional finite element analysis was carried out to determine the nodal stresses and deflections using the finite element package 'LUSAS/AN'. The result of each of these increments was checked against a certain allowable stress limit. The standard anlytical procedure consists of the following steps:

(1) The average stresses in the principal axes are determined on the basis of the result for each incremental load using the finite element analysis. Initially, each element is checked against the ultimate tensile and compressive stress criteria assumed in this analysis. If any average tensile stress of an element exceeds the assumed ultimate tensile stress in any principal direction, the modulus of elasticity of concrete of the element is then reduced to a minimal value close to zero only in that direction; however, if any element exceeds its assumed ultimate crushing strength, then the entire modulus of

elasticity of the element is reduced to the minimal values in any principal direction. Otherwise, the principal stresses are then compared with the stress criterion which is governed by the biaxial stress envelope described in Eqn.7.20.

(2) Steel stresses at any nodal point are also checked against the yield stress for every increment.

(3) If the average principal stresses in an element is within the failure criteria described above, the nodal stresses of this element are ready to be accumulated for the next increment in load.

(4) Having gone through these analytical procedures, a modified 3-dimensional model for the slab with reduced moduli of elasticity of concrete in the cracked and crushed elements is developed for the next increment in load.

Four individual programs were made, written in Fortran, for each of these steps in order to minimize the tedious work load and these programs are:

(i) CONSTRESS.FOR: to obtain the average concrete stresses acting in the principal axes;

(ii) CRACKING.FOR: to accumulate the average concrete stresses, to check against the governing stress criteria and to provide update data file for the next load increment;

(iii) BARSTRESS.FOR: to accumulate the steel stress in the bar elements and check against the assumed yield stress of steel;

(iv) DEFLECTION.FOR: to accumulate the displacements of all the nodes in every element.

This analysis was empolyed only to the R.C. waffle model slabs A1, A2, B3 and C1 with all edges fully fixed. The results are given in Fig.7.24 to Fig.7.27. It can be seen in Fig.7.24 that the analytical

load-deflection characteristic is too conservative by comparison with the experimental results. The disagreement between these results can be regarded as mainly due to the undesirable sudden pressure applied on this model slab during the early loading stage of the test. This undesirable loading had a significant effect on the overall load-deflection behaviour of the slab.

Based on the results of analysis, stresses at supports are found to exceed the ultimate tensile strength of the concrete even when the applied load is reached approximately 15% of the failure load of the slab. Cracks at these supports appeared comparatively earlier than those cracks which occurred in the mid-span. This indicates that stresses at the supports are considerably higher than those at mid-span. It is also noted that cracks appear almost simultaneously in the central region of the slab in both orthogonal directions. Since crack planes are defined normal to the principal axes only, cracks occured at right angles to each other as shown in Fig.7.28 in the rib joints in the central area. In theory, a body subjected to biaxial tensile stresses will fail in shear with the failure plane running diagonally to the element. These diagonal cracks can probably be deduced theoretically and be idealized as normal to a stress resultant. In fact, the locations of these diagonal cracks at the rib joints are comparable to those observed from the tests.

An excellent agreement between the experimental and analytical results for R.C. waffle slabs A2, B3 and C1 are shown in Fig.7.25, Fig.7.26 and Fig.7.27 respectively. On the basis of these results, it can be seen that this 3-dimensional model tends to underestimate the deflections slightly within the elastic range, and model overestimates the deflection in the nonlinear range by almost 10% when compared to the test results. The latter discrepancy probably reflects the effect of ignoring the aggregate interlock and dowel action in the concrete. It is also observed by comparing these results that the higher the rib to slab thickness ratio, the better the correlattion are between the analytical and experimental results.

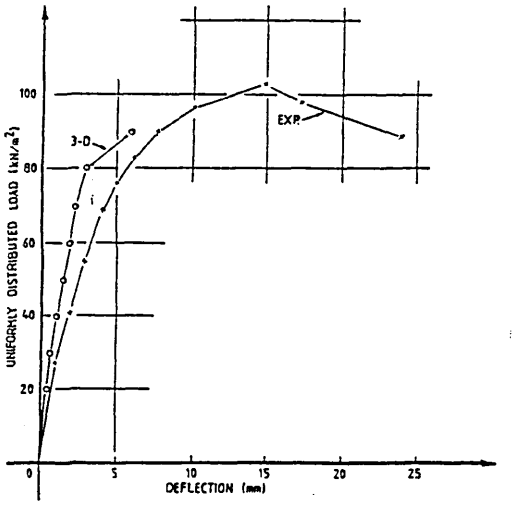

Fig.7.24 Load-deflection Curves For R.C. Waffle Slab A1

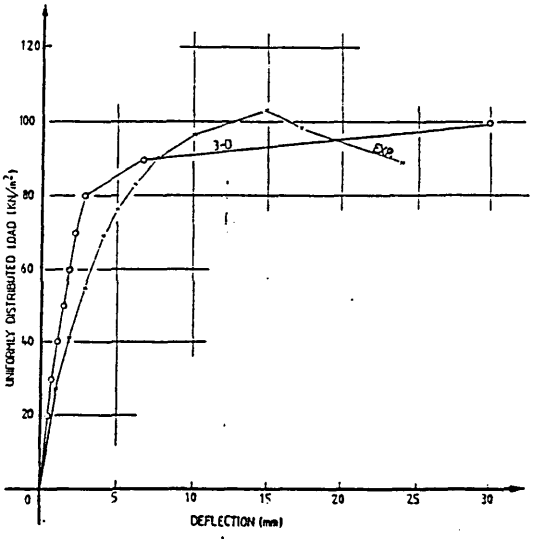

Fig.7.25 Load-deflection Curves For R.C. Waffle Slab A2

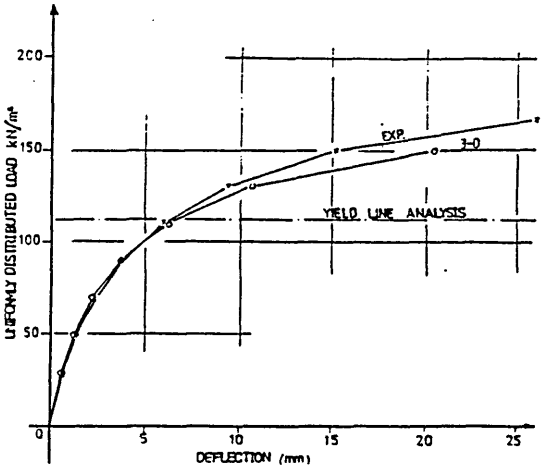

Fig.7.26 Load-deflection Curves For R.C. Waffle Slab B3

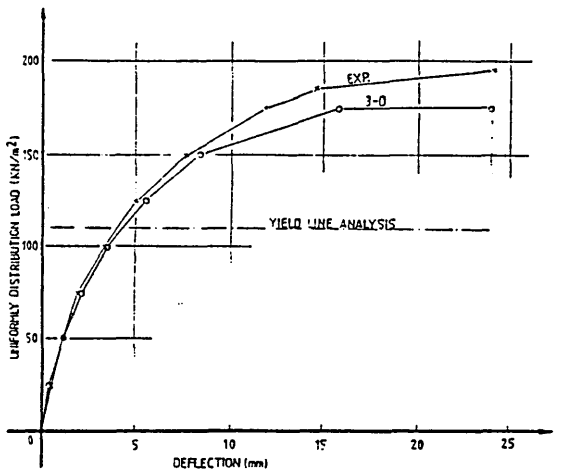

Fig.7.27 Load-deflection Curves For R.C. Waffle Slab C1

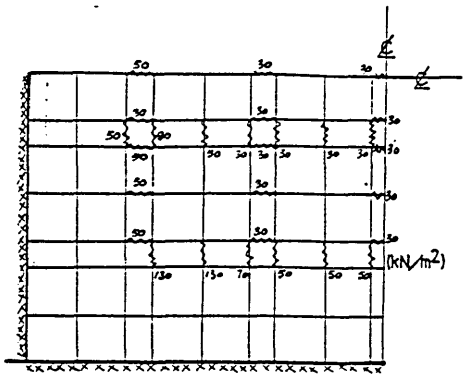

Fig.7.28 Analytical Crack Pattern of R.C. Waffle Slab B3

7.4 ULTIMATE LOAD ANALYSIS

Based on the literature survey, three analytical approaches are considered to have merit in predicting the ultimate load carrying capacity of an R.C. waffle slab. These are

Method [1]:- Modified Yield Line Method;
Method [2]:- Equivalent Open Grillage analysis utilizing the concept of the plastic hinge method; and
Method [3)]- Modified Strip Method.

7.4.1 Method [1] - Modified Yield Line Method

The results for the series of tests indicate that the failure patterns for R.C. waffle slabs are akin to those for R.C. solid slabs. In 1984, Marshall (43) showed that the ultimate load capacity of R.C. waffle slabs with simply supported edges can be predicted with reasonable accuracy by the yield line approach with appropriate modification. In the light of these facts, the principle of Johansen's yield line approach was adopted as one of the ultimate load analyses in the present work. 'Stepped' yield criterion and the principle of virtual work were applied and the upper bound solution was obtained by treating a reinforced concrete waffle slab as an equivalent orthotropic slab using the following assumptions:

i) Johansen's 'stepped yield criterion' is applicable to the R.C. waffle slab;
ii) The effective width of flanges of the T-section are equal to the rib spacing;
iii) Yield lines are generally straight and must end at slab boundaries;
iv) All reinforcement crossing the yield line is assumed to yield;
v) The effect of shear is ignored and no local failure of the slab is assumed; and
vi) The moment key line per unit width of a side is determinted by the total moments of the idealized T- and/or L-sections divided by the length of that side.

In the present work, the waffle slabs had equally spaced ribs, spanning in both directions, which in fact stiffened the effective flanges of the T-sections. The effective width of flanges were taken as being equal to the spacing of the ribs. This assumption was in accordance with that suggested by Reddy and Hendry (44). The overall dimensions of the waffle slab remained unchanged. The computation of the ultimate strength of an idealized T-section was determined as for R.C. T-beam. At fully fixed edges, the supports of the ribs were considered as rectangular sections. The equivalent moment of resistance per unit width was taken as the strength of the total number of T- or rectangular sections over the full length of a side divided by the length of that side.

The work equation is formed by equating the dissipation of internal energy to the expenditure of energy by the external load

$$[\int P(x,y)dx.dy] = [\theta n \int Mn.dl] \qquad (7.23)$$

where, P(x,y) is applied load per unit area;
Mn is the normal moment per unit length;
θn is the normal rotation of the yield line;
dl is the length of yield line.

7.4.1.1 Analysis For R.C. Waffle Model Slabs in Series A, B and C

On the basis of the test results, the yield line pattern for series A, B & C model slabs is sshown in Fig.7.29 for which the dissipation of internal energy is given by:

$$Ei = 4m.(1+i')/\alpha + 2m(iy+iy').\alpha/\beta \qquad (7.24a)$$

and the expenditure of external energy is

$$Ex = \alpha.Wj.L^2.(3-2\beta)/6 \qquad (7.24b)$$

Thus,
$$\frac{m}{Wj} = \frac{\alpha^2.L^2.(3\beta - 2\beta^2)}{24\beta.(1+i')+12\alpha^2(iy+iy')} \qquad (7.24c)$$

$$\text{Since} \qquad \frac{\partial f_1(\beta)}{\partial f_2(\beta)} = \frac{\partial f_1(\beta)/\partial\beta}{\partial f_2(\beta)/\partial\beta} \tag{7.25}$$

$$\text{Therefore,} \qquad \frac{\alpha^2 L^2.(3\beta - 2\beta^2)}{24\beta\,(1+i')+12\alpha^2\, iy+iy')} = \frac{\beta^2.L^2.(3-4\beta)}{24.(1+i')} \tag{7.26}$$

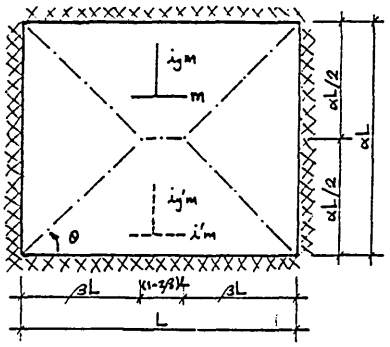

Fig.7.29 Assumed Yield Pattern For Series A, B and C Model Slabs

Analysis for R.C. Waffle Slab B3:

The slab data have already been reviewed in Section 7.2.1.3 and the idealized T-section for this model slab is shown in Fig.7.4. The depth of neutral axis for the concrete section, dn, is obtained as in Eqn.7.8 except that at ultimate state, the effective stress of the distribution steel, fyd, should be determined appropriately by the triangular strain block. It is assumed that the main steel yields at the strain of 0.0045 as shown in Fig.6.17 and the elastic strain limit of distribution steel is 0.00125. Thus, the effective stress of the distributed steel can be obtained theoretically as

$$fyd = \frac{250}{0.00125}.\left[0.0045\frac{9.5-dn}{56-dn}\right] \tag{7.27}$$

Solving Eqn.7.8 and Eqn.7.27 simultaneously, the depth of neutral axis was determined to be 4.018mm. Taking moment about the line of action of the concrete compressive force, it gives

$$Mtx = fy.As.(60-k_2.dn) + fyd.Asd.(9.5-k_2.dn) \quad (7.28)$$

$$= 0.89 \times 10^6 \text{ Nmm/rib}$$

Therefore, the span moment in short span is

$$mx = (5.Mtx)/1.33$$
$$= 3.346 \text{ kNm/m}$$

Similarly, the support and span moments in the other directions are obtained using the same procedures as

Support moment in short span	mx' = 3.706 kNm/m
Span moment in long span	my = 2.986 kNm/m
Support moment in long span	my' = 3.336 kNm/m

Hence, $i' = 3.706/3.346 = 1.108$
$iy = 2.986/3.346 = 0.892$
$iy' = 3.336/3.346 = 0.997$

Substituting these results in Eqn.7.26 for R.C. waffle slab B3, it gives

$$0 = 48(1+i').\beta^2 + 48.\alpha^2.(iy+iy').\beta + 36.\alpha^2(iy+iy')$$
$$\Rightarrow \quad 0 = \beta^2 + 0.6132\beta - 0.4599 \quad (7.29)$$

The root of the quadratic equation is found to be $\beta = 0.4377$

and $$\theta = \tan^{-1}\left(\frac{0.8271}{2x0.8271}\right) = 43^\circ 22' 30''$$

Hence, $Wj = 111.955 \text{ kN/m}^2$

Applying the same procedure for R.C. waffle slabs in series A, B and C, the analytical ultimate loads are obtained and are given in Table 7.9. In addition, the results of the control solid slab D1 is also given in the same table for comparison.

7.4.1.2 Analysis For R.C. Waffle Model Slabs in Series E

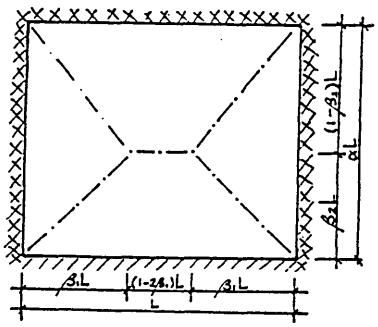

Fig.7.30 Assumed Yield Pattern For Series E Model Slabs

Based on the test results, the yield line pattern for series E model slabs is deduced in Fig.7.30. Thus, the dissipation of internal energy is

$$Ei = m\{\frac{(1+\beta_2 i')}{\alpha\beta_2(1-\beta_2)} + \frac{2\alpha(iy+iy')}{\beta_1}\} \qquad (7.30a)$$

and the expenditure of external energy is

$$Ex = \alpha.Wj.L^2.(3-2\beta_1)/6 \qquad (7.30b)$$

Thus,
$$\frac{m}{Wj} = \frac{\alpha L^2}{6}\{\frac{\beta_1\beta_2(1-\beta_2)(3-2\beta_1)}{\beta_1.(1+\beta_2 i')+2\alpha^2(iy+iy')\beta_2(1-\beta_2)}\} \qquad (7.30c)$$

Differentiating the equation with respect to β_1 and β_2 respectively gives

$$\beta_1 = \frac{\sqrt{(4+3A)} - 2}{A} \qquad (7.30d)$$

$$\beta_2 = \frac{\sqrt{(9-2i'+i'^2)} - (3-i')}{2i'} \qquad (7.30e)$$

$$\text{where,} \qquad A = \frac{1+\beta_2 i'}{\alpha^2(iy+iy')\beta_2(1-\beta_2)}$$

The analytical results for R.C. waffle slabs in series E are also given in Table 7.12.

7.4.1.3 Analysis For R.C. Waffle Model Slabs in Series F

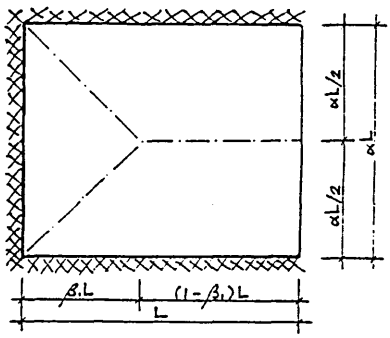

Fig.7.31 Assumed Yield Pattern For Series F Model Slabs

Based on the test results, the yield line pattern for series F model slabs is deduced in Fig.7.31. Thus, the dissipation of internal energy is

$$Ei = 4m.(1+i')/\alpha + m(iy+iy').\alpha/\beta \qquad (7.31a)$$

and the expenditure of external energy is

$$Ex = \alpha.Wj.L^2.(3-2\beta)/6 \qquad (7.31b)$$

$$\text{Thus,} \qquad \frac{m}{Wj} = \frac{\alpha^2.L^2.(3\beta-2\beta^2)}{24\beta.(1+i')+6\alpha^2(iy+iy')} \qquad (7.31c)$$

Differentiating the equation with respect to β, it gives

$$\beta = \frac{(9 - 2\alpha^2.\beta) + (81 - 120\alpha^2.Ci + 4\alpha^4.Ci^2)}{14} \qquad (7.31d)$$

where $$Ci = \frac{(iy+iy')}{(1+i')}$$

The analytical results for R.C. waffle slabs in series F are given in Table 7.12.

Table 7.9 :- Comparison Between Experimental Loads and Ultimate Loads Using Modified Yield Line Method for R.C. Waffle Slabs.

(1) SLAB No.	(2) Test Failure load (Wt)	(3) Modified Yield line Method (Wj)	(4) (Wt-Wj)	(5) Wj / Wt
		(kN/m^2)		
A-1	93.859	62.569	31.290	0.667
A-2	95.992	70.670	25.322	0.736
A-3	108.791	80.504	28.287	0.740
B-1	141.348	85.738	55.610	0.607
B-2	155.138	99.179	55.959	0.639
B-3	165.480	111.955	53.525	0.677
C-1	194.784	110.390	84.394	0.567
C-2	210.298	127.057	83.242	0.604
C-3	230.983	143.839	87.144	0.623
D-1	268.905	85.025	183.880	0.316

7.4.1.4 Analytical Results For R.C. Waffle Slabs in Series A to F

On the basis of Table 7.9, it can be seen that the employed modified yield line analysis clearly underestimates the load carrying capacities of R.C. waffle model slabs by as much as 43.3%. This is

considered , inevitably, due to the effect of membrane action induced in the restrained edges when the middle portion of the slab is deflected vertically. There is evidence to indicate that the increase in the effective depth of the ribs has more effect than the increase in the area of steel in the ribs. The most important factor of this enchancement is that the load capacity of the slab is significantly reduced by the changing of the restrained edge to a simply supported edge and then to an unsupported edge.

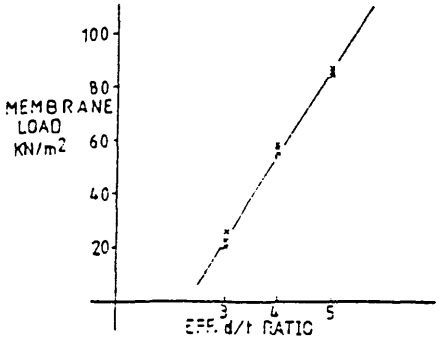

Fig.7.32 Membrane Load Capacity Via Effecive d/t Ratios

It is interesting to note that the enhanced load capacities due to membrane action for the slabs as shown in column 4 in Table 7.9 and these results are plotted against the effective depth to slab thickness ratios in Fig.7.32. The consistency of the results for each series A, B and C strongly suggests that the magnitude of this load capacity is probably dependent upon the depth of the ribs and significantly the area of the steel has little effect on the load enhancement. It is believed that the prediction of enhanced load capacity due to membrane action combined with the ultimate load analysis using yield line method constitutes the best approach for assessing the load carrying capacity of R.C. waffle slabs. For this to be of significance the enhanced load capacity can be predicted by assuming the membrane action is dependent upon the depth of the ribs and the increase in the area of steel in the sections has negligible effect on this enhancement. These findings primarily formed the basis for predicting the enhanced load capacity of an R.C. waffle slab with restrained edges. The derivation for this analysis is given in the following section.

7.4.1.5 Derivation of Membrane Enhancement

On the basis of the load-deflection characteristic curve of the beams tested by Christiansen (7) shown in Fig.5.18, the maximum load capacity, Wmax, of the slab is considered to be the sum of the flexural load capacity obtained by ultimate load method, Wu, such as yield line method and the enhanced load capacity due to the membrane action, Wm. Thus, the actual load carrying capacity of an R.C. waffle/solid slab can be given as

$$Wmax = Wu + Wm \tag{7.32}$$

This assumption is in accordance with Tong et al's (75) logical equation which was reviewed in section 5.6. This equation quantifies that the maximum load capacity of the slab is reached when the flexural strength of the slab is exceeded and the membrane forces along the yield lines are fully developed at the critical deflection of the slab. The magnitude of the load capacity due to membrane action increases as a function of the vertical deflection, δ, at the central point of the slab. Thus, the analysis can simplify the transition stage of the elasto-plastic zone of the load-deflection characteristic.

A rigid-plastic strip method is developed to estimate the additional strength due to the membrane forces. The assumptions made for the analysis are: (i) plane sections remain plane after bending; (ii) the membrane forces, N, are generated constantly along yield lines across the ribs and the effects on the overhanging flanges are ignored; (iii) the critical deflection, δc, of the slab at failure can be determined from the test results; and (iv) for rigid-plastic material, the shortening of the strip due to axial forces is negligible, and the intermediate strip between two yield sections remains straight.

A deflected strip shown in Fig.7.33 shows the compressive membrane forces, N, generated equal and opposite in each portion of strips. This force can be obtained as

$$N = k_1 k_3 \times fcu \times dn \tag{7.33}$$

Taking moment about the support, the membrane moment is

$$Mm = N \times la \tag{7.34}$$

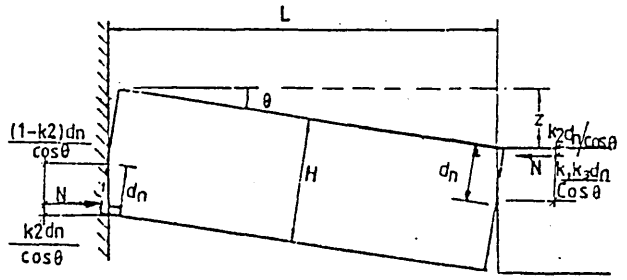

Fig.7.33 Idealization of a Deflected Strip

The lever arm, la, of the strip is a function of δ, H and dn, and it can be determined as

$$la = [(H-dn) + \frac{(1-k_2).dn}{\cos\theta}] - [\delta + \frac{k_2.dn}{\cos\theta}] \tag{7.35}$$

Thus,
$$la = (H-dn)+(1-2.k_2).dn.\sec\theta - \delta \tag{7.36}$$

In order to obtain the maximum membrane moment, Eqn.7.33 and Eqn.7.35 are substituted into Eqn.7.34 The resulting equation is then differentiated with respect to dn, giving

$$\frac{\partial(Mm)}{\partial(dn)} = k_1 k_3 .fcu.[(H-dn) + 2.(1-2.k_2).dn.\sec\theta - \delta] \tag{7.37}$$

When θ is small, $\tan\theta = \sin\theta = \delta/L$

and
$$\cos\theta = 1 - 2.\sin^2(\theta/2)$$

$$= \frac{2.L^2 - \delta^2}{2.L^2}$$

For maximum compression concrete depth, i.e. $\partial(Mm)/\partial(dn) = 0$, the equation can be arranged as

$$[2.L^2 - \delta^2 + (H-2.dn)].\delta = 2.L^2.(H-4.k_2.dn) \qquad (7.38)$$

This gives

$$dn = \frac{(H-\delta).(2.L^2-\delta^2)}{2.(4.k_2.L^2-\delta^2)} \qquad (7.39)$$

From the above equations, the membrane moment is found to depend on the length of half of the strip, overall thickness and central deflection of the strip. In fact, the length of half the strip is comparatively much greater than the central deflection, therefore the effective compression concrete depth for membrane actions, dn, can be obtained approximately as

$$dn = \frac{(H - \delta)}{4.k_2} \qquad (7.40)$$

With the depth of neutral axis, the lever arm can be obtained from Eqn.7.36. Substituting this lever arm into Eqn.7.33 and Eqn.7.34, the moment induced by the membrane action can be determined as

$$Mm = \frac{k_1 k_3}{8.k_2}.fcu.(H-\delta)^2 \qquad (7.41)$$

It is assumed that the diagonal yield line pattern of 45^0 gives sufficient accuracy (52) for the analysis. For the purposes of analysis, it is assumed that the membrane forces are generated within the rectangular sections only. The critical deflection of the slab was given on the basis of experimental results of approximately 1/3 the overall slab thickness. This is comparatively small when compared to Park's value of half the effective depth for a restrained solid slab. Therefore, the deflections for every rib section along the yield lines can be determined. Thus, the work done by the membrane force in each of the yielded rib sections can be accumulated. The external work done is assumed to be the same as that used to determine the ultimate load capacity due to flexure, i.e.

$$\text{External work} = \frac{1}{6}.Wj.Lx.(3.Ly-Lx) \qquad (7.42)$$

where Wj is the applied load per unit area, and
Lx and Ly are lengths of the long and short spans of the slabs respectively.

In order to verify this analysis, Eqn.7.41 and Eqn.7.42 were applied to two sets of previous slab tests (51,57) for R.C. slabs with restrained edges. The analytical results are given in Tables 7.10 and 7.11. Both of these tables show an excellent correlation between the experimental and theoretical results. Hence, this analysis was used to estimate the load capacity enhanced by the membrane action for both R.C. waffle and solid slabs with restrained edges.

Taking into account the predicted membrane capacity, the analytical load capacities using Eqn.7.32 show an excellent agreement with the failure load obtained from the tests, and these can be seen in Table 7.12. From these results, it can be concluded that the ultimate load of an R.C. waffle slab with restrained edges should take into acount the contribution of the membrane effect as well as the flexural strength of the slab.

The equation of the membrane moment was applied to the mixed boundary conditions of Series E and F model slabs based on the assumption that edges without any physical restraint, such as simply supported and unsupported edges cannot induce any membrane forces at these edges. The analytical and experimental results for these series of slab tests are also given in Table 7.12. A close agreement is reached and this provides a good clarification for the assumption made for the simply supported and unsupported edges of R.C. waffle and solid slabs.

Table 7.10:- Results Of The Load Capacity Due To Membrane Action For Unreinforced Concrete Slabs With Restrained Edges

(1) Reference	(2) Slab No.	(3) Concrete strength fcu (N/mm^2)	(4) Failure load (kN/m^2)	(5) Predicted membrane load (kN/m^2)	(6) Load factor (5)/(4)
Powell (57)	S40	51.4	255.0	240.9	0.945
	S53	47.1	290.3	223.4	0.770
	S56	47.9	259.2	226.6	0.874
	S57	49.6	206.7	233.5	1.129
	S60	49.7	224.6	234.0	1.042
	S64	49.8	241.9	234.4	0.969
Wood (51)	FS14	35.8	64.3	88.7	1.379
Park (51)	D1	43.4	170.0	152.4	0.897
	D2	42.8	89.2	83.6	0.937
	D3	44.4	31.9	37.3	1.169
	D4	38.4	28.6	33.1	1.157
	D5	30.7	26.5	27.5	1.037
					1.025

Table 7.11:- Results Of The Load Capacity Taking Account Of Membrane Action For R.C. Slabs With Restrained Edges

(1) Reference	(2) Slab No.	(3) Concrete strength fcu (N/mm^2)	(4) Failure load (kN/m^2)	(5) Park's ultimate load (kN/m^2)	(6) Predicted membrane load (kN/m^2)	(7) Load factor (5)+(6) / (4)
Powell (57)	S46	50.2	311.0	38.0	236.0	0.881
	S47	56.2	266.8	38.0	260.7	1.119
	S50	46.7	332.4	67.7	221.7	0.871
	S54	51.4	365.6	106.4	240.9	0.950
	S55	46.2	330.1	106.4	219.7	0.988
	S58	50.1	342.8	172.8	235.6	1.191
	S59	49.2	351.1	172.1	231.9	1.151
	S62	51.4	421.1	265.4	240.9	1.202
	S63	45.5	465.2	263.3	216.9	1.032
						1.043

Table 7.12:- Comparison Between The Analytical And Experimental Results For R.C. Waffle Slabs In Series A To F

SLAB No.	Wj	Wm	Wu	Wt	Wu / Wt
	(kN/m^2)				
A1	62.569	31.234	93.803	93.859	1.000
A2	70.670	23.954	94.624	95.992	1.009
A3	80.504	30.132	110.636	108.791	0.983
B1	85.738	45.033	130.771	141.348	1.081
B2	99.179	47.544	146.723	155.138	1.057
B3	111.955	46.595	158.550	165.480	1.044
C1	110.390	69.565	179.955	194.784	1.082
C2	127.056	71.968	199.024	210.298	1.056
C3	143.839	83.512	227.351	230.983	1.016
				Mean	1.036
D1	85.025	216.801	301.826	268.905	1.122
E1	65.960	5.262	71.222	81.016	0.879
E2	92.804	17.505	110.309	115.491	0.955
E3	119.026	36.044	155.070	158.585	0.978
				Mean	0.937
F1	61.867	6.429	68.296	64.469	1.059
F2	85.517	18.227	103.744	109.976	0.943
F3	107.257	22.849	130.106	136.521	0.953
				Mean	0.985

where Wt is the test failure load;
Wj is the ultimate load obtained by yield line analysis;
Wu = Wj + Wm ;
Wm is the load capacity due to membrane action.

7.4.1.6 Analysis For R.C. Waffle Slabs Supported at Four Corners

The composite action of a slab and beam system is one of the complicated aspects of the general theory of structures. The absence of the rigid supports along the edges of the slab requires more thorough analysis to elucidate the critical collapse mechanism of the slab not only from the pitch-roof type but also the modes associated with unsupported edges. The yield line patterns deduced for the model slab tests in Series A to F are no longer applicable, on their own merit, for R.C. waffle slabs supported by four corners. It is inevitable that yield line analysis is one of the most commonly used upper-bound solutions which inherits the advantage of requiring no valid stress field in the slab. For analysis, however, it is necessary to ensure that the assumed yield pattern for the critical load of a slab supported at four corners should be relevant to the actual failure cracking pattern.

For the slab models of Series H and I subjected to uniformly distributed and 4 point loads respectively, several possible slab and beam mechanisms were considered as shown Fig. 7.34a, b, c, d, e, f, g, h, i & j.

(i) Analysis For R.C. Waffle Slabs In Series H

Four possible collapse mechanisms for R.C. waffle slabs with different pot sizes subjected to uniformly distributed load are given in Fig.7.34a to Fig.7.34d. For each of these mechanisms, the work equation is developed from the first principle.

Mode A as shown in Fig.7.34a gives

Internal work, $$Ei = 4m(1+\mu\alpha)/\alpha \qquad (7.43a)$$

External work, $$Ex = Wj.\alpha L^2(3-\alpha)/6 \qquad (7.43b)$$

Thus, $$Wj = \frac{24m(1+\mu\alpha)}{\alpha^2 L^2(3-\alpha)} \qquad (7.43c)$$

Mode B as shown in Fig.7.34b gives

$$Ei = 2.\left\{\frac{\Sigma Mx}{\alpha L} + \frac{\Sigma My}{L}\right\} \qquad (7.44a)$$

$$Ex = \frac{Wj.\alpha L^2}{2} \qquad (7.44b)$$

Thus,

$$Wj = \frac{4}{\alpha L^2}\left\{\frac{\Sigma Mx}{\alpha L} + \frac{\Sigma My}{L}\right\} \qquad (7.44c)$$

Mode C as shown in Fig.7.34c gives

$$Ei = 4\Sigma My/L \qquad (7.45a)$$

and

$$Ex = Wj.\alpha L^2/2 \qquad (7.45b)$$

Thus,

$$Wj = \frac{8\Sigma My}{\alpha L^3} \qquad (7.45c)$$

Mode D as shown in Fig.7.34d gives

$$Ei = 4\Sigma Mx/\alpha L \qquad (7.46a)$$

and

$$Ex = Wj.\alpha L^2/2 \qquad (7.46b)$$

Thus,

$$Wj = \frac{8\Sigma Mx}{\alpha^2 L^3} \qquad (7.46c)$$

Based on these equations, the analytical results for each of these collapse mechanisms for every model slab in Series H are given in Table 7.13. The results of the tests indicated that the failure mode of the slabs showed a good resemblance to mode C. The discrepancies of the results based on this mode are less than 2.0% and 4.7% for model slabs H1 and H2 respectively. It is surprising that the pitch roof collapse mode yields a load capacity which overestimates the experimental results by 96%.

Table 7.13: The Analytical Results For R.C. Waffle Slabs In Series H

Collapse mode	Model Slab H1		Model Slab H2	
	Theoretical load (kN/m^2)	Load factor	Theoretical load (kN/m^2)	Load factor
(A)	80.665	1.950	72.150	1.674
(B)	40.555	0.980	41.055	0.953
(C)	58.684	1.419	52.707	1.225
(D)	49.619	1.199	46.881	1.088

where the experimental loads for model slabs H1 and H2 are obtained to be 41.370 and 43.094 kN/m^2 respectively.

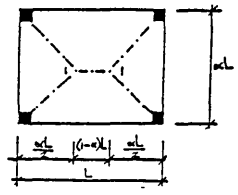

Mode A

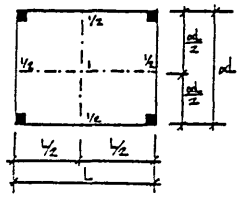

Mode B

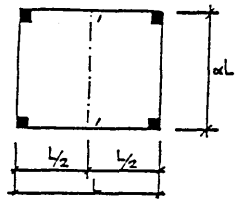

Mode C

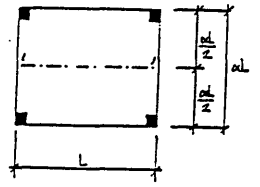

Mode D

Fig.7.34a-d Assumed Yield Patterns For R.C.Waffle Slabs In Series H

(ii) Analysis For R.C. Waffle Slabs In Series I

Another six possible collapse mechanisms for R.C. waffle slabs with different pot sizes subjected to four concentrated loads are also given in Fig.7.34e to Fig.7.34j. For each of these mechanisms, the work equation again is developed from the first principle.

Mode E as shown in Fig.7.34e gives

$$Ei = 4m(1+\mu\alpha)/\alpha \tag{7.47a}$$

$$Ex = 4Pj\sqrt{[2(\beta_1^2+\beta_2^2)]} \tag{7.47b}$$

Thus,

$$Pj = \frac{m(1+\mu\alpha)}{\sqrt{[2(\beta_1^2+\beta_2^2)]}} \tag{7.47c}$$

Model F as shown in Fig.7.34f gives

$$Ei = 2m(1/\beta_2 + \mu\alpha/\beta_2) \tag{7.48a}$$

$$Ex = 4Pj \tag{7.48b}$$

Thus,

$$Pj = \frac{m(\mu\alpha\beta_1+\beta_2)}{2\beta_1\beta_2} \tag{7.48c}$$

Mode G as shown in Fig.7.34g gives

$$Ei = 4\Sigma Mx/\alpha L \tag{7.49a}$$

$$Ex = 8\beta_1 Pj/\alpha \tag{7.49b}$$

Thus,

$$Pj = \Sigma Mx/(2\beta_1 L) \tag{7.49c}$$

Mode H as shown in Fig.7.34h gives

$$Ei = 4\Sigma My/L \tag{7.50a}$$

$$Ex = 8\beta_2 Pj \tag{7.50b}$$

Thus,

$$Pj = \Sigma My/(2\beta_2 L) \tag{7.50c}$$

Mode I as shown in Fig.7.34i gives

$$Ei = \frac{2\Sigma Mx}{\alpha L} + \frac{2\Sigma My}{L} \qquad (7.51a)$$

$$Ex = \frac{8Pj\sqrt{(\beta_1^2+\beta_2^2)}}{\sqrt{(1+\alpha^2)}} \qquad (7.51b)$$

Thus,

$$Pj = \frac{2\sqrt{(1+\alpha^2)}\{\Sigma Mx+\alpha\Sigma My\}}{8\alpha L\sqrt{(\beta_1^2+\beta_2^2)}} \qquad (7.51c)$$

Mode J as shown in Fig.7.34j gives

$$Ei = \frac{\Sigma Mx}{\beta_1 L} + \frac{\Sigma My}{\beta_2 L} \qquad (7.52a)$$

$$Ex = 4Pj \qquad (7.52b)$$

Thus,

$$Pj = \frac{1}{4L}\left\{\frac{\Sigma Mx}{\beta_1} + \frac{\Sigma My}{\beta_2}\right\} \qquad (7.52c)$$

Table 7.14: The Analytical Results For R.C. Waffle Slabs In Series I

Collapse mode	Model Slab I1		Model Slab I2	
	Theoretical load (kN/m^2)	Load factor	Theoretical load (kN/m^2)	Load factor
(E)	44.837	1.217	35.779	1.160
(F)	44.837	1.217	36.548	1.185
(G)	45.236	1.228	40.359	1.309
(H)	37.775	1.026	31.362	1.017
(I)	42.428	1.152	35.691	1.158
(J)	41.510	1.127	35.874	1.164

where the experimental loads for model slabs I1 and I2 are obtained to be 36.832 and 30.832 kN/m^2 respectively.

Based on these equations, the analytical results for each of these collapse mechanisms for every model slab in Series I are given in Table 7.14. The results of the tests indicates that the failure mode of the slabs showed a good resemblance to mode H. The discrepancy of the results based on this mode is +2.6 and +1.7% for model slabs I1 and I2 respectively. The pitch roof collapse mode yields a load capacity which overestimates the experimental result for model slab I1 by only 21.9%.

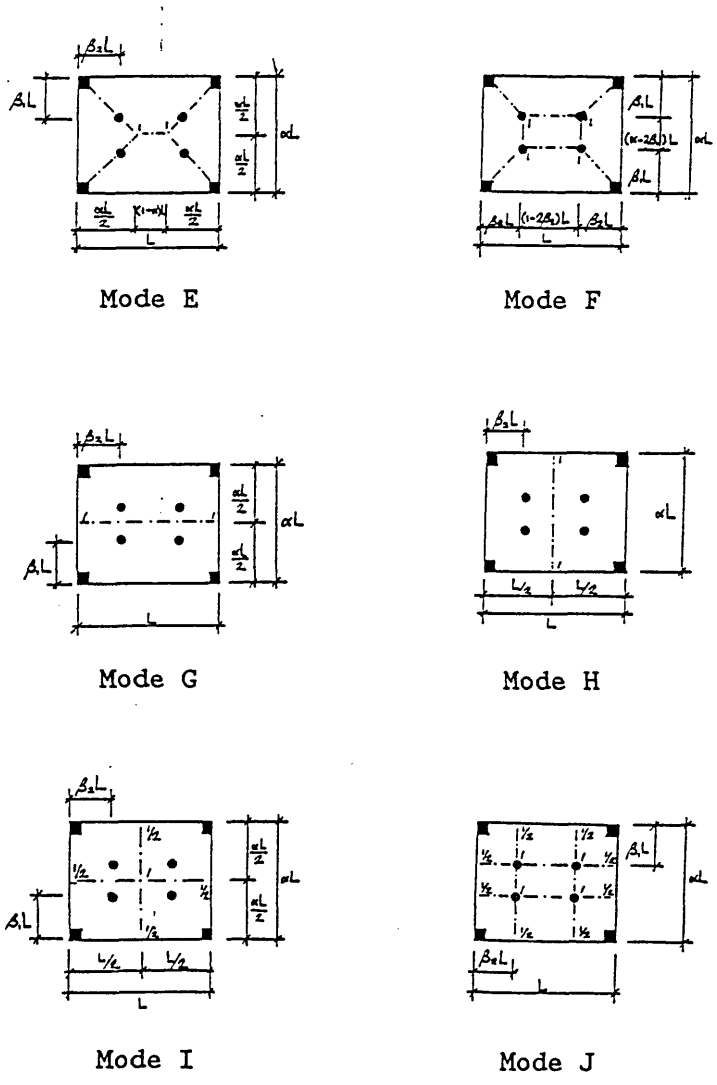

Fig.7.34e-j. Assumed Yield Patterns For R.C.Waffle Slabs In Series I And J

(iii) Analysis Of 1/2-scale R.C. Waffle Slab J1

The overall dimensions of the model slab are 2.60m wide by 3.06m long and the effective spans are 2.2m and 2.66m respectively. The overall depth of the section consists of a 30mm thick top slab and 140mm deep ribs. The idealized T-sections have 552mm flange and 150mm effective depth in short span; and 460mm flange and 144mm effective depth in long span. Other relevant data are:

Concrete strength	fcu = 54.611 N/mm^2
Yield stress of steel	fy = 410.000 N/mm^2
Area of steel in ribs	As(rib) = 102.070 mm^2
Area of steel in edge beams	As(beam) = 204.140 mm^2

$\therefore$ $k_1 k_3 = 0.5$; $k_2 = 0.42$

Based on this data, the moments of resistance are determined as follows,

Mty about short span	= 5.968 kNm
Mtx about long span	= 6.350 kNm
Mby about short span	= 11.769 kNm
Mbx about long span	= 12.540 kNm

Hence, $\Sigma Mx = 4x6.350 + 2x12.540 = 50.480$ kNm

$\Sigma My = 4x5.968 + 2x11.769 = 47.410$ kNm

$mx = 4x6.350/2.66 = 9.549$ kNm/m

$my = 4x5.968/2.20 = 10.851$ kNm/m

$\alpha = 2.200/2.66 = 0.827$; $\mu = 10.851/9.549 = 1.136$

$\beta_1 = 0.870/2.66 = 0.327$; $\beta_2 = 1.054/2.66 = 0.396$

Using these values, the theoretical load capacity for each of the collapse modes in Fig.7.34e to Fig.7.34j were obtained. The results are given in Table 7.15. From the test result, the yield pattern of the slab can be deduced as mode H in Fig.7.34h. Thus, Eqn.7.50c gives

$$Pj = \frac{47.410}{2x0.396x2.66} = 22.491 \text{ kN}$$

$$\therefore \quad \Sigma Pj = 4x22.491 = 89.962 \text{ kN}$$

Hence, the factor of analytical to experimental load is 1.013.

Table 7.15: The Analytical Results For R.C. Waffle Slabs In Series J

	Model Slab J1	
Collapse mode	Theoretical load (kN/m^2)	Load factor
(E)	101.999	1.148
(F)	103.712	1.167
(G)	116.070	1.307
(H)	90.017	1.013
(I)	103.011	1.160
(J)	103.043	1.160

where the experimental load for model slab J1 is obtained to be 88.840 kN/m^2.

(iv) Analytical Results For R.C. Waffle Slabs In Series H To J

The analytical results from Table 7.13 to Table 7.15 show that the experimental loads are close to those loads obtained for modes C and H for model slabs subjected to uniformly distributed and four concentrated loads respectively. It is evident that the collapse patterns from the model slab tests in the present investigation yield a good agreement to the assumed combined beam and slab mechanism which has a mininum load capacity. It is therefore of prime importance to obtain the correct collapse mechanism when the yield line approach is used to predict the load capacity of this type of slab. What is less obvious from the analysis point of view is the mode for slabs with rigid supported edges. In order to allow the conventional pitch-roof collapse mode to occur, the load carrying capacity in Eqn.7.43c must theoretically be less than those load capacities obtained from Eqn.7.45c and Eqn.746c. Thus, this provides two criteria for the

analysis as

$$\frac{Mbx}{m.L} > \frac{3(1+\mu\alpha)}{2(3-\alpha)} - \frac{1}{2} \qquad (7.53a)$$

and

$$\frac{Mby}{\mu m.\alpha L} > \frac{1}{\mu\alpha^2}\cdot\frac{3(1+\mu\alpha)}{2(3-\alpha)} - \frac{1}{2} \qquad (7.53b)$$

(ii) Similarly, for R.C. waffle slabs subjected to four concentrated loads, the load capacity from Eqn.7.47c should be less than those load capacities given by Eqn.7.49c and Eqn.7.50c and can be shown as

$$\frac{Mbx}{m.L} > \beta_1 \cdot \frac{(1+\mu\alpha)}{\sqrt{[2(\beta_1^2+\beta_2^2]}} - \frac{1}{2} \qquad (7.53c)$$

and

$$\frac{Mby}{\mu m.\alpha L} > \frac{\beta_2}{\mu\alpha}\cdot\frac{(1+\mu\alpha)}{\sqrt{[2(\beta_1^2+\beta_2^2]}} - \frac{1}{2} \qquad (7.53d)$$

where Mbx and Mby are the ultimate moments of the edge beams in x and y axes respectively;

m and μm are the ultimate moments/unit length in x and y axes respectively;

μ is the ratio of moments of my/mx; and

α is the side ratio of short to long span.

These criteria for slabs supported by columns should be satisfied only if the slab mechanism is desired. Otherwise, the failure mode may probably be one of the combined slab and beam mechanisms which has the least load carrying capacity which is in accordance with the results of the present investigation. The slab data from these two series of tests were checked against these criteria and the results are given in Table 7.16 and Table 7.17. These results clearly suggest that the pitch roof collapse mode is unlikely to occur for model slabs in these Series.

The load carrying capacity of a slab basically depends upon the moments of resistance in both axes and the actual dimensions of its

spans. Therefore, the ratio of the moments of resistance and the side ratio of a slab of short to long span provide a basis to establish the critical load of a waffle slab supported by columns. To determine the probable critical collapse mode, an additional criterion can be produced from the relationship between the ratio of moments of resistance in both axes and the side ratio of the slab by equating the load capacity of mode D to mode C for slabs subjected to uniformly distributed load. It gives

$$Rm = \frac{\Sigma My}{\Sigma Mx} = \frac{1}{\alpha} \qquad (7.54a)$$

Similarly, equating the load capacity of mode G to mode H for slabs subjected to four concentrated loads, it yields

$$Rm = \frac{\Sigma My}{\Sigma Mx} = \frac{\beta_2}{\beta_1} \qquad (7.54b)$$

where, Rm is moment resistance ratio of $\Sigma My/\Sigma Mx$.

Thus, if the ratio of moments of resistance, Rm, is less than the reciprocal of the side ratio of a slab, α, the load capacity for mode H will be less than that of mode G (mode D for U.D.L.). Then, mode H (mode C) becomes the collapse mechanism of the slab. On the other hand, if the ratio of moments of resistance is greater than the reciprocal of the side ratio, the collapse load for mode G (mode D) will become critical. Based on Eqns.7.54a & 7.54b, the results for model slabs in Series H and I given in Table 7.18 indicate a good correlation to the collapse mechanism with the least load carrying capacity. From these results, a conclusion can be drawn that R.C. waffle slabs supported by columns give a completely different failure mechanism to slabs with rigid supports. However, the collapse mechanism of an R.C. waffle slab can be predicted by taking into consideration the ratio of moments of resistance and the side ratio of the slab to satisfy the criteria described in Eqn.7.53a to Eqn.7.54d. The critical load of the slab should then be the least load from any possible collapse modes of the slabs.

Table 7.16 : Edge Beam To Span Moment Ratio For R.C. Waffle Slabs In Series H To I

Slab No.	mx (kNm/m)	my (kNm/m)	Mbx (kNm)	Mby (kNm)	Mbx / m.L	Mby / μm.αL
H1	4.148	3.772	2.095	1.981	0.380	0.477
H2	3.351	3.808	2.131	2.011	0.478	0.480
I1	4.185	3.804	2.136	2.016	0.380	0.482
I2	3.365	3.823	2.151	2.029	0.481	0.483
J1	9.549	10.85	12.54	11.77	0.429	0.417

Table 7.17 Theoretical Results For R.C. Waffle Slabs In Series H To J

Slab No.	μ	$\frac{3(1+\mu\alpha)}{2(3-\alpha)} - \frac{1}{2}$	$\frac{1}{\mu\alpha^2}\cdot\frac{3(1+\mu\alpha)}{2(3-\alpha)} - \frac{1}{2}$
H1	0.909	0.709	1.445
H2	1.136	0.836	1.227

Slab No.	μ	$\frac{\beta_1.(1+\mu\alpha)}{\sqrt{[2(\beta_1^2+\beta_2^2)]}} - \frac{1}{2}$	$\frac{\beta_2}{\mu\alpha}\cdot\frac{(1+\mu\alpha)}{\sqrt{[2(\beta_1^2+\beta_2^2)]}} - \frac{1}{2}$
I1	0.909	0.375	0.665
I2	1.136	0.375	0.626
J1	1.136	0.373	0.626

Table 7.18 Theoretical Values Obtained From Eqns.7.54a & 7.54b For R.C. Waffle Slabs In Series H To J

Slab No.	ΣMy	ΣMx	Rm	β_2 / β_1	$\frac{1}{\alpha}$
H1	8.111	9.707	0.834	---	1.209
H2	8.216	8.718	0.942	---	1.209
I1	8.238	9.864	0.835	1.000	---
I2	8.264	8.778	0.941	1.211	---
J1	47.410	50.480	0.939	1.211	---

7.4.2 Method [2] - Equivalent Open Grillage Analysis

Based on the observation of the development of cracking and the results of the failure patterns for the series of tests, spiral cracks fully developed prior to the failure of the model slabs. This suggests that bending and torsion interaction may have significant effect on the load capacity of the R.C. waffle slabs. In this analysis, the model slabs are idealized by an equivalent open grillage. Again, each grillage beam was idealized as a T-section as described in Section 7.3.1.1. The equivalent grillage is then analyzed by applying the Plastic Hinge Method taking into consideration combined torsion and bending interaction at the hinge.

On the basis of the literature survey, if the effect of the stirrups in the ribs on the torsional strength is ignored, the procedure involved in the evaluation of the equivalent moment of resistance for the combined loading can be simplified. Keeping this in mind, Ramakrishnan's simplified interaction relationship (59) is adopted in the present investigation as follows:

$$\left[\frac{T}{Tup}\right]^2 + \left[\frac{M}{Mu}\right]^2 = 1 \qquad (7.55)$$

This equation was applied to the test data of the previous investigations (35,36,37,79,80,83) and the results are given in Fig.7.35. More than 98% of these results are lying outwith the area bounded by the interaction curve and the x- and y-axes. It is evident that this equation gives a safe interaction relationship of the combined bending and torsion moments.

7.4.2.1 Analytical Consideration

As reviewed in Section 5.3, the total work done on a plastic hinge is

$$Ep = M.\theta + T.\phi \qquad (7.56)$$

From Eqn.5.18 and Eqn.5.20, the work equation becomes

$$Ep = Mu[\theta\cos\gamma + \beta.\phi\sin\gamma] \qquad (7.57)$$

where, β = Tup/Mu

γ = $\tan^{-1}$(T.Mu/Tup.M) or $\tan^{-1}$(T/βM)

It can be seen that the work done on a plastic hinge depends not only on the rotation and twisting angle but also on dimensionless parameters β. From the simplified circular interaction curve shown in Fig.7.35, the dimensionless stress resultants for bending and torsion can be written in the trigonometric forms of

$$m = \cos\gamma \; ; \quad t = \sin\gamma \; ; \quad t/m = \tan\gamma \tag{7.58}$$

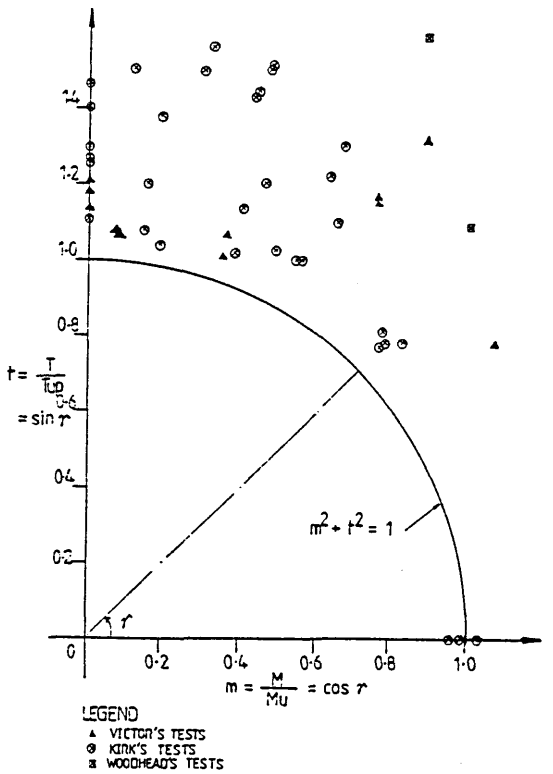

Fig.7.35 Results Of Beam Tests subjected To Combined Bending And Torsion

To maximize the work done on a plastic hinge, Eqn.7.57 is differentiated with respect to the angle of the interaction γ,

$$\frac{\partial Ep}{\partial \gamma} = Mu[-\theta.\sin\gamma + \beta.\phi.\cos\gamma] \tag{7.59}$$

For $\partial Ep/\partial\gamma = 0$, it gives

$$\gamma = \tan^{-1}\left[\frac{\beta.\phi}{\theta}\right] \qquad (7.60)$$

From the results of the modified yield line analysis, the angles of the diagonal yield lines were found to be in the range of 42.5^0 to 44.5^0. Therefore, it could be assumed that the angle of crack is approximately 45^0. Thus, the angle of twist is equal to the angle of rotation in a plastic hinge. With this assumption, the number of plastic hinges required to form a complete mechanism is reduced to a minimum and Eqn.7.60 is simplified to

$$\tan\gamma = \beta$$

Hence, $$Ep = Mu.\theta.\sec\gamma \qquad (7.61)$$

The upper bound collapse load for this equivalent open grillage can then be determined from the yield pattern obtained from the tests. The assumed yield pattern employed in this analysis is consistent with that used in Method [1] in Section 7.4.1. Since the ribs are equally spaced in both orthogonal directions, the angle of rotation at a plastic hinge is equal to the angle of twist at any point along the yield line i.e. $\theta = \phi$. The moment of resistance of grillage beam elements whether a T- or a rectangular section, can be determined as described in Section 7.4.1.1; the moment capacity should then be modified to the equivalent moment in simple bending as described in Eqn.7.61. Hence, the internal work done by a grillage is the summation of work done by all plastic hinges which form the collapse mechanism.

It was found that the waffle slab subjected to the applied load behaved in a way similar to that of the solid slab. Therefore, the actual external work done by the equivalent grillage system is assumed to be equal to the work done by the same load applied to a R.C. waffle slab. Method [1] and Method [2] are based on the upper bound yield line approach, the difference between these methods being the different basis for the dissipation of internal energy by the waffle slab.

7.4.2.2 Analysis of R.C. Waffle Slabs Using Open Grillage Analysis

(i) Analysis For R.C. Waffle Slab B3

From the assumed collapse mechanism shown in Fig.7.36, it gives

$$\beta = \alpha/2 \quad ; \quad \theta = \phi$$

From Section 7.4.1.1, the average moment of resistance of the grillage beam for both orthogonal directions is found to be

$$Mu = (0.890+0.821)/2 = 0.856 \text{ kNm/rib in mid-span}$$
$$Mu' = (0.986+0.917)/2 = 0.952 \text{ kNm/rib at supports}$$

By ignoring the contribution from the steel, the torsional capacity for the concrete T-section in both mid-span and support was obtained using Sand Heap Analogy described in Eqn.5.38. It is assumed that the ultimate shear strength of concrete is $0.3714\sqrt{fcu}$ in N/mm^2 ($5\sqrt{fcy}$ in p.s.i. units). Thus, the torsion capacity, Tup, is obtained to be

$$Tup = 0.183 \text{ kNm/rib}$$

Then, $\gamma = \tan^{-1}(0.183/0.856) = 12.067^0$

and $\gamma' = \tan^{-1}(0.183/0.952) = 10.887^0$

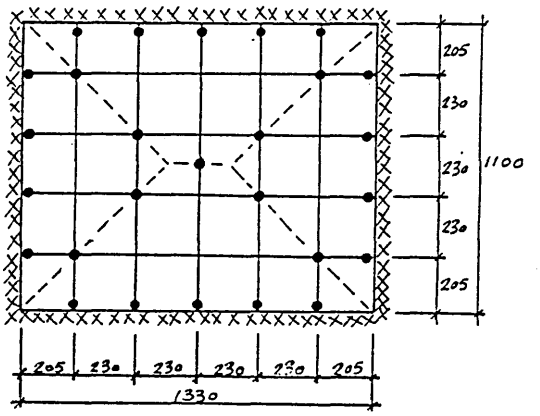

Fig.7.36 Assumed Collapse Mechanism For R.C. Waffle Slabs In Series A To D

The total internal work done by four plastic hinges due to pure bending and sixteen plastic hinges i.e. eight in the suppports and

eight in the mid-span, due to combined bending and torsion is given as

$$Ei = 2.[Mu+Mu'+2.(4.\frac{Mu}{\cos\gamma} + 4.\frac{Mu'}{\cos\gamma'})].\frac{2}{\alpha.L} \qquad (7.62)$$

$$= 60.241 \text{ kNm}$$

The total external work done by the slab is given as

$$Ex = Wp.\alpha.L^2.(3-2\beta)/6 \qquad (7.63)$$

$$= 0.53Wp$$

Hence, $Wp = 113.663 \text{ kN/m}^2$

(ii) Analysis For R.C. Waffle Slab E2

Based on the test results, the modified collapse mechanism is shown in Fig.7.37. The average moments of resistance Mu and Mu' for this model slab are determined as

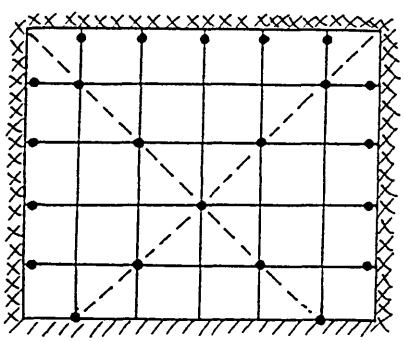

Fig.7.37 Assumed Collapse Mechanism For R.C. Waffle Slabs In Series E

$Mu = (0.890+0.821)/2 = 0.856$ kNm/rib

$Mu' = (0.987+0.919)/2 = 0.953$ kNm/rib

$Tup = 0.183$ kNm/rib

Thus, $\gamma = \tan^{-1}(0.183/0.856) = 12.067^0$

$\gamma' = \tan^{-1}(0.183/0.953) = 10.870^0$

The total internal work done,

$$Ei = \frac{5}{1.1}\left(\frac{4Mu'}{\cos\gamma'} + \frac{Mu'}{3} + \frac{13Mu}{3\cos\gamma} + \frac{6Mu}{5} + \frac{5Tup}{3}\right) \quad (7.64)$$

$$= 40.958 \text{ kNm}$$

Total external work done,

$$Ex = 0.488Wp$$

Hence, $Wp = 83.931 \text{ kN/m}^2$

(iii) Analysis For R.C. Waffle Slab F3

Based on the test results, the modified collapse mechanism is shown in Fig.7.38. The average moments of resistance for this model slab are

$$Mu = (1.113+1.046)/2 = 1.080 \text{ kNm/rib}$$
$$Mu' = (1.265+1.198)/2 = 1.232 \text{ kNm/rib}$$

Moments of resistance for the L-beam in the unsupported edge,

$$Mb + Mb' = 2.312 \text{ kNm}$$
$$Tup = 0.221 \text{ kNm/rib}$$

Thus,
$$\gamma = \tan^{-1}(0.221/1.080) = 11.566^\circ$$
$$\gamma' = \tan^{-1}(0.221/1.232) = 10.170^\circ$$

Total internal work done,

$$Ei = \frac{4}{1.1}\left[4\left(\frac{Mu'}{\cos\gamma'} + \frac{Mu}{\cos\gamma}\right) + 3(Mu'+Mu) + (Mb+Mb')\right] \quad (7.65)$$

$$= 67.870 \text{ kNm}$$

Total external work done,

$$Ex = 0.631Wp \text{ kNm}$$

Hence, $Wp = 107.559 \text{ kN/m}^2$

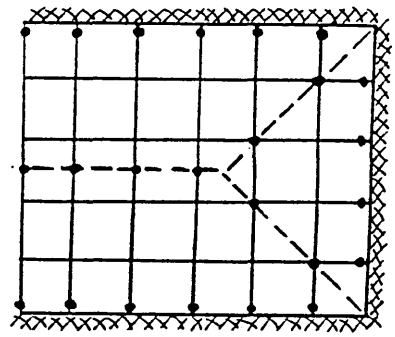

Fig.7.38 Assumed Collapse Mechanism For R.C. Waffle Slabs In Series F

7.4.2.3 Analytical Results For R.C. Waffle Slabs

The theoretical results using this analysis for R.C. waffle slabs in Series A to F are given in Table 7.19. This table also provides the results obtained by modified yield line method i.e. Method [1]. It can be seen that the load obtained using this analysis have an excellent correlation to those load capacities obtained by Method [1]. However, on the basis of Eqn.7.61, the bending and torsion interaction increases the moment capacity by the value of $\sec\gamma$ which is directly related to the ultimate strength ratio of torsion to bending of the section. The analysis shows that the ultimate torsional to flexural strength ratios of the model slabs are small. The largest angles of interaction, γ and γ' are found to be 24.042^{o} and 12.67^{o} for model slab A1. As a result, the increase in moment capacity for a combined hinge is small. In theory, the moment resistance should increase significantly with the increase in torsional resistance of the section. It can be seen that the predicted load capacity, using this method, of the control solid slab D1 is 35% higher than that obtained by Method [1]. However, more tests are required to substantiate this finding for R.C. solid slabs. It is appropriate in here to draw a conclusion that in practice the effect of bending and torsion interaction on the ultimate load capacity of R.C. waffle slabs is small and negligible. The amount of increase due to this effect can be estimated by $\sec\gamma$ where γ is the angle of interaction of the ultimate strength of the section.

Table 7.19:- Comparison Of The Experimental And Theoretical Results Using Equivalent Open Grillage Analysis

Slab No.	Test Failure Load	Modified Yield Line Analysis Method [1]	Equivalent Open Grillage Analysis Method [2]		
			Angle	Angle	Load Capacity
	Wt	Wj	γ	γ'	Wp
	(kN/m^2)		(Deg.)	(Deg.)	(kN/m^2)
A1	93.859	62.569	24.042	12.430	64.999
A2	95.992	70.670	16.665	12.101	72.209
A3	108.791	80.504	12.470	11.860	81.912
B1	141.348	85.738	21.510	10.450	88.274
B2	155.138	99.179	15.680	10.890	101.356
B3	165.480	111.955	12.067	10.887	113.663
C1	194.784	110.390	18.889	9.150	113.335
C2	210.298	127.057	13.770	9.240	129.117
C3	230.983	143.839	12.230	10.710	146.281
D1*	268.905	85.025	52.850	30.710	114.689
E1	81.016	65.960	12.650	12.080	60.228
E2	115.491	92.804	12.067	10.870	83.931
E3	158.585	119.026	11.530	10.080	108.126
F1	64.469	61.867	12.430	11.630	61.353
F2	109.976	85.517	11.990	10.640	85.483
F3	136.521	107.257	11.566	10.170	105.746

* Denoted R.C. Solid Slab

7.4.3 Method [3] - Modified Strip Method

So far, the modified yield line method and equivalent open grillage analysis have been employed in the present investigation. These two approaches share the same principle that the relation between the moment capacity of the slab and the applied load is determined by assuming that at failure there is no overall loss of energy as the slab undergoes a small vertical displacement. Having postulated a valid mechanism, the external work done by the applied loads is equated to the internal work done by the slab in the yield lines in taking up compatible rotations. This provides the useful relationship between the moment capacity of the slab and the applied loads for the valid mechanism. However, a more direct approach to obtain this relationship is developed based on the lower bound solution of Hillerborg strip method (29). The development of this approach is derived from the equilibrium equation in Eqn.5.15.

7.4.3.1 Theoretical Considerations

The equilibrium equation of the lower bound theorem of plasticity is given as

$$\frac{\partial^2 Mx}{\partial x^2} + \frac{\partial^2 My}{\partial y^2} - 2.\frac{\partial^2 Mxy}{\partial x \partial y} = -p(x,y) \qquad (7.66)$$

The twisting moment is assumed small and negligible (72). Therefore, the equilibrium equation can be partitioned as follows:

$$\frac{\partial^2 Mx}{\partial x^2} = -k.p \quad ; \quad \frac{\partial^2 My}{\partial y^2} = -(1-k).p \qquad (7.67)$$

where, p or p(x,y) is uniformly distributed load.

The load distribution factor, k, for x and y axes are deliberately assumed to be of 1 and 0 in any beam strip. On this basis, The strip moment of a beam strip as shown in Fig.7.39 can be obtained as

$$M(strip) = -\left(\frac{p}{2}\right).x^2 \qquad (7.68)$$

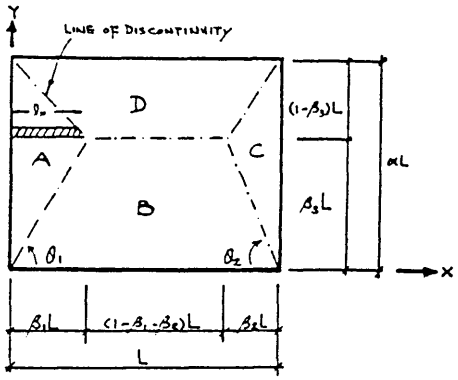

Fig.7.39 Hillerborg's Load Dispersion Diagram

The total moment normal to the support, along the line of discontinuity for a particular region is given with respect to y-axis as

$$\Sigma M = -\int \frac{p}{2} . x^2 . dy \qquad (7.69)$$

and the weighted average moment (29) per unit length is

$$M(ave) = \frac{-p}{2 \cdot Ly} . \int x^2 . dy \qquad (7.70)$$

It is considered that the moment of resistance, Mr, for a region bounded by the lines of discontinuity and support consists of

$$Mr = Mm + Ms$$

where, Mm is moment of resistance in mid-span per unit width;
Ms is moment of resistance at support per unit width.

The principle of this modified strip method is that, at the ultimate limit state, the total moment generated on the slab by the applied load, Mi, based on Hillerborg's load dispersion diagram, is equal to the actual moments of resistance of the slab, Mr. Thus, the moment equation can be developed as

$$Mr(region) = Mi(region)$$
$$\Rightarrow \quad \Sigma Mr(slab) = \Sigma Mi(slab) \qquad (7.71)$$

The total load applied on a region of the slab can be determined as

$$Wr = \frac{2.LyMr}{\int x^2.dy}.Area \tag{7.72}$$

Hence, the total load applied on the slab can be determined as

$$\Sigma W = \int \frac{2.LyMr}{\int x\ .dy}.Area \tag{7.73}$$

The average uniformly distributed load, Wh, can then be obtained as

$$Wh = \frac{\int \frac{2.LyMr}{\int x^2.dy}.Area}{\Sigma Area} \tag{7.74}$$

Considering region A shown in Fig.7.39, the total moment per unit length of the support can be obtained using Eqn.7.69 as

$$Ma = \frac{p}{2.Ly}.\left\{\int_0^{\beta_3.Ly} \left(\frac{\beta_1}{\alpha\beta_3}\right)^2.y^2.dy + \int_0^{(1-\beta_3)Ly} \left[\frac{\beta_1}{\alpha(1-\beta_3)}\right]^2.y^2.dy\right\} \tag{7.75}$$

$$= \frac{p}{6}.(\beta_1.Lx)^2$$

Similarly for region C, the total moment per unit length of the support is

$$Mc = \frac{p}{6}.(\beta_2.Lx)^2 \tag{7.76}$$

For region B, the total moment per unit length of the support is

$$Mb = \frac{p}{2.Lx}\left[\int_0^{\beta_1.Lx}\left(\frac{\alpha\beta_3}{\beta_1}\right)^2.x^2.dx + \int_0^{\beta_2.Lx}\left(\frac{\alpha\beta_3}{\beta_2}\right)^2.x^2.dx + (\beta_3.Ly)^2.(1-\beta_1-\beta_2).Lx\right] \qquad (7.77)$$

$$= \frac{p.\beta_3^{\,2}}{6}.(3-2.\beta_1-2.\beta_2).Ly^2$$

Similarly for region D, the total moment per unit length is

$$Md = \frac{p.(1-\beta_3)^2}{6}.(3-2.\beta_1-2.\beta_2).Ly^2 \qquad (7.78)$$

Hence, the total applied load on the slab can be obtained from Eqn.7.75 and Eqn.7.78 as

$$\Sigma W = \frac{6.Ma}{(\beta_1.Lx)^2}.\frac{\beta_1.Lx.Ly}{2} + \frac{6.Mc}{(\beta_2.Lx)^2}.\frac{\beta_2 Lx.Ly}{2} + \frac{6.Mb}{\beta_3^{\,2}(3-2\beta_1-2\beta_2).Ly^2}.\frac{(2-\beta_1-\beta_2).Lx.\beta_3.Ly}{2} + \frac{6.Md}{(1-\beta_3)^2.(3-2\beta_1-2\beta_2).Ly^2}.\frac{(2-\beta_1-\beta_2).Lx.(1-\beta_3).Ly}{2} \qquad (7.79)$$

The average load capacity is given by dividing the total applied load by the area of the slab i.e. Lx.Ly. Thus,

$$Wh = \frac{3}{Lx^2}\left(\frac{Ma}{\beta_1} + \frac{Mc}{\beta_2}\right) + \frac{3(2-\beta_1-\beta_2)}{(3-2\beta_1-2\beta_2)Ly^2}\left[\frac{Mb}{\beta_3} + \frac{Md}{(1-\beta_3)}\right] \quad (7.80)$$

To minimize the average load carrying capacity of the slab, Eqn.7.80 can be differentiated:

(i) with respect to β_3

$$\frac{\partial Wh}{\partial \beta_3} = \frac{3(2-\beta_1-\beta_2)}{(3-2\beta_1-2\beta_2)Ly^2}\left[\frac{-Mb}{\beta_3^2} + \frac{Md}{(1-\beta_3)^2}\right] \quad (7.81)$$

and using $\partial Wh/\partial \beta_3 = 0$, it gives

$$\beta_3 = \frac{\sqrt{(Mb/Md)}}{1+\sqrt{(Mb/Md)}} \quad (7.82)$$

(ii) with respect to β_2

$$\frac{\partial Wh}{\partial \beta_2} = \frac{-3Mc}{\beta_2^2.Lx^2} + \frac{3}{Ly^2.(3-2\beta_1-2\beta_2)}\left[\frac{Mb}{\beta_3} + \frac{Md}{(1-\beta_3)}\right] \quad (7.83)$$

and giving $\partial Wh/\partial \beta_2 = 0$, it gives

$$\beta_2 = \frac{\alpha.(3-2\beta_1).\sqrt{Mc'}}{1+2\alpha.\sqrt{Mc'}} \quad (7.84)$$

where,

$$Mc' = \frac{Mc}{\frac{Mb}{\beta_3} + \frac{Md}{(1-\beta_3)}}$$

(iii) with respect to β_1

$$\frac{\partial Wh}{\partial \beta_1} = \frac{-3Ma}{\beta_1^2 . Lx^2} + \frac{3}{Ly^2 . (3-2\beta_1-2\beta_2)^2} . \left[\frac{Mb}{\beta_3} + \frac{Md}{(1-\beta_3)}\right] \quad (7.85)$$

and giving $\partial Wh/\partial \beta_1 = 0$, it gives

$$\beta_1 = \frac{\alpha . (3-2\beta_2) . \sqrt{Ma'}}{1+2\alpha . \sqrt{Ma'}} \quad (7.86)$$

where,

$$Ma' = \frac{Ma}{\frac{Mb}{\beta_3} + \frac{Md}{(1-\beta_3)}}$$

Solving Eqn7.84 and Eqn.7.86 simultaneously, it yields

$$\beta_1 \sqrt{Mc'} = \beta_2 \sqrt{Ma'} \quad (7.87)$$

$$\text{Thus, } \beta_1 = \frac{3 . \alpha . \sqrt{Ma'}}{1+2 . \alpha . [\sqrt{Ma'} + \sqrt{Mc'}]} \quad (7.88)$$

$$\text{and } \beta_2 = \frac{3 . \alpha . \sqrt{Mc'}}{1+2 . \alpha . [\sqrt{Ma'} + \sqrt{Mc'}]} \quad (7.89)$$

7.4.3.2 Analysis For R.C. Waffle Slabs Using Modified Strip Method

(i) Analysis For R.C. Waffle Slab B3

The assumed load dispersion diagram for any boundary condition is shown in Fig.7.39. It is assumed that

$$Ma = Mc = My+My' = 2.986+3.336 = 6.322 \text{ kNm/m}$$
$$Mb = Md = Mx+Mx' = 3.346+3.706 = 7.052 \text{ kNm/m}$$
$$\alpha = 0.827$$

From Eqn.7.83, Mb/Md = 1

$$\Rightarrow \quad \beta_3 = \sqrt{1}/(1+\sqrt{1}) = 0.5$$

From Eqn.7.86,

$$Ma' = \frac{6.322}{2.(7.052/0.5)} = 0.224$$

$$\Rightarrow \quad \beta_1 = \beta_2 = \frac{3x0.827x\sqrt{0.224}}{1+ 2x0.827(2\sqrt{0.224})} = 0.458$$

Hence, from Eqn.7.80

$$Wh = \frac{3}{Lx^2}.\left(2.\frac{Ma}{\beta_1}\right) + \frac{3(2-2\beta_1)}{(3-4\beta_1).Ly^2}.(4Mb) \qquad (7.90)$$

$$= 112.806 \text{ kN/m}^2$$

(ii) Analysis For R.C. Waffle Slab E3

The assumed load dispersion diagram for any boundary condition is shown in Fig.7.39. It is assumed that

$$Ma = Mc = My+My' = 3.817+4.408 = 8.225 \text{ kNm/m}$$
$$Mb = Mx = 4.199 \text{ kNm/m}$$
$$Md = Mx+Mx' = 4.199+4.794 = 8.993 \text{ kNm/m}$$
$$\alpha = 0.827$$

From Eqn.7.82,

$$\Rightarrow \quad \beta_3 = \frac{\sqrt{(4.199/8.993)}}{1+\sqrt{(4.199/8.993)}} = 0.406$$

From Eqn.7.84 and Eqn.7.86

$$Ma' = Mc' = \frac{8.225}{\frac{4.199}{0.406} + \frac{8.993}{(1-0.406)}} = 0.323$$

$$\Rightarrow \quad \beta_1 = \beta_2 = \frac{3x0.827x\sqrt{0.323}}{1+ 2x0.827(2\sqrt{0.323})} = 0.490$$

Hence, from Eqn.7.80

$$Wh = 118.942 \text{ kN/m}^2$$

(iii) Analysis For R.C. Waffle Slab F3

The assumed load dispersion diagram for any boundary condition is shown in Fig.7.39. It is assumed that

$$Ma = My+My' = 3.805+4.356 = 8.161 \text{ kNm/m}$$
$$Mc = 0$$
$$Mb = Md = Mx+Mx' = 5.023+5.706 = 10.729 \text{ kNm/m}$$
$$\alpha = 0.827$$

From Eqn.7.83, Mb/Md = 1

$$\Rightarrow \quad \beta_3 = \sqrt{1}/(1+\sqrt{1}) = 0.5$$

From Eqn.7.84,

$$Mc' = 0 \quad \Rightarrow \quad \beta_2 = 0$$

From Eqn.7.86,

$$Ma' = \frac{8.161}{2.(10.729/0.5)} = 0.190$$

$$\Rightarrow \quad \beta_1 = \frac{3x0.827x\sqrt{0.190}}{1+ 2x0.827(2\sqrt{0.190})} = 0.629$$

Hence, from Eqn.7.80

$$Wh = 105.762 \text{ kN/m}^2$$

7.4.3.3 Analytical Results For R.C. Waffle Slabs

Analysis using modified strip method can be applied to any combination of boundary conditions but the application for column supports is not considered here. Slabs with an unsupported edge such as those in Series F, have no reaction at this edge. Thus, there is no moment generated normal to this edge. Applied loads on this region are

therefore considered to be distributed to the adjacent supports. As a result, the span coefficient β_1 in Eqn.7.89 becomes zero. For a simply supported edge such as model slabs in Series E, the support moment, Ms, in this edge does not exist. Thus, the applied loads are assumed to be resisted by the span moment, Mm.

The results for the model slabs of series A, B, C, D, E & F are given in Table 7.20. The modified strip method is not considered for model slabs with either concentrated load or column support conditions. By comparison, the analytical results have an excellent agreement with the loads predicted by Method [1]. It reflects the validity of this method of analysis for R.C. waffle slabs.

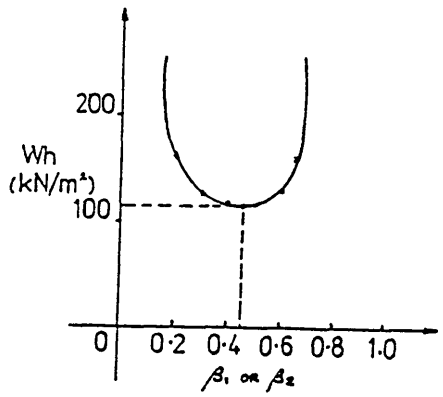

Fig.7.40 Load Capacity Vs Span Coefficient

On the basis of Section 7.4.3.2.1, the span coefficients β_1 and β_2 of the load dispersion diagram are obtained to be 0.458. It has a good correlation to the span coefficient β of 0.438 when using Method [1]. It is therefore evident that both of these methods share a common valid collapse mechanism. However, the load capacity using this method varies with respect to either β_1 or β_2 and the characteristic can be seen in Fig.7.40. It is suggested that this analysis tends to give a minimum load capacity for an R.C. waffle slabs. This is in contrast to the modified yield line method which tends to give an upper bound load capacity of the slab. It can therefore be concluded

that modified strip method can be used to predict the ultimate load capacity of an R.C. waffle slab. This method of analysis tends to give a lower bound and safe load capacity for a valid collapse mechanism of the slab.

Table 7.20: Comparison Of The Experimental And Theoretical Results Using Modified Strip Method

Slab No.	Modified Yield Line Method Method (1) (kN/m²)	Modified Strip Method			
		Span Coefficients β_1	β_2	β_3	Ultimtat Load Capacity (kN/m²)
A1	62.569	0.445	0.445	0.500	62.941
A2	70.670	0.454	0.454	0.500	71.099
A3	80.504	0.454	0.454	0.500	80.982
B1	85.738	0.457	0.457	0.500	86.371
B2	99.179	0.458	0.458	0.500	99.928
B3	111.955	0.458	0.458	0.500	112.806
C1	110.390	0.459	0.459	0.500	111.323
C2	127.057	0.459	0.459	0.500	128.105
C3	143.839	0.459	0.459	0.500	145.072
D1	85.025	0.458	0.458	0.500	85.749
E1	65.960	0.483	0.483	0.411	66.012
E2	92.804	0.487	0.487	0.408	92.789
E3	119.026	0.490	0.490	0.406	118.942
F1	61.867	0.620	0.000	0.500	63.822
F2	85.517	0.626	0.000	0.500	88.510
F3	107.257	0.629	0.000	0.500	111.150

CHAPTER 8

DISCUSSION OF EXPERIMENTAL AND ANALYTICAL RESULTS

The work carried out in this research is to investigate the elastic to plastic behaviour of R.C. waffle slabs. Two 2-dimensional elastic and one 3-dimensional elastic-fracture models are made using finite element approach to predict the characteristic behaviour of the slabs; in addition, three ultimate load methods of analysis (22,23,26,27,43,52) with appropriate modification are also employed to determine the load carrying capacity of the slabs. A qualitative analysis of the results of the tests are presented primarily based on the load-deflection, load-cracking and load-strain characteristics, and then compared to the results of the theoretical analyses.

8.1 Load-deflection Characteristic

The load-deflection behaviour of R.C. waffle slabs with simply supported edges was reported by Marshall (43) in 1983. Similar load-deflection behaviour is also confirmed by the present investigation on a series of model tests with a different combination of boundary and loading conditions. The characteristic of the load-deflection curves on various rib locations of the slabs is similar to that obtained for the control solid model slab D1 which can be seen by comparing Fig.6.21a to Fig.6.21c and Fig.8.1. This characteristic is also found to be similar to the behaviour of the R.C. solid slabs obtained by Park (52) in 1964.

A typical load-deflection relationship has an initial linear portion up to approximately 1/3 of the failure load for the slabs with edges supported and approximately 1/4 of the failure load for the slabs with four corners supported. The occurrence of the cracks significantly affect the deflection characteristic of these slabs. With the appearance of first cracks the deflection curves become non-linear and the load is increased, the rate of change in deflection increases further and eventually establishes a nonlinear behaviour along which the slab undergoes general yielding. At the predicted ultimate load, the main reinforcements yield as indicated in Fig.6.19, Fig.6.27 and Fig.6.30.

The yielding of reinforcement accelerates the rate of increase in deflection. With further increase of load in excess of the predicted ultimate load, slabs behave plastically. Prior to failure, spiral cracks at the corner rib sections are developed and eventually crushing of concrete occurs at the rib supports. The latter effect causes a rapid loss in load carrying capacity of the slab and gives rise to the sudden increase in deflection. This can be seen in Fig.6.21a to Fig.6.21c. The residual strength of these slabs tails off approximately to those theoretical load values predicted by modified yield line method. In fact, Fig.6.21a to Fig.6.21c indicate that the actual load capacity of the slabs is significantly higher than the predicted values. While the crushing of concrete takes place at the rib supports, there is a sudden decrease in load on the slabs and the slab continues to yield at the theoretical ultimate load value. This phenomenon of the reduction of the load capacity occurs when the peak load capacity is reduced. This difference between the peak load and the theoretical ultimate load is considered to be due to the membrane forces induced in the restrained edges.

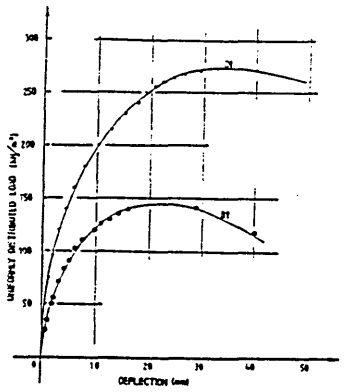

Fig.8.1 Load-Deflection Curves For R.C. Waffle Slab D1

The load-deflection characteristic for model slabs with four corners supported is linear up to approximately 25% of the collapse load until cracks appear, as shown in Fig.6.34. Initially, the deflections in the edge beams in both orthogonal directions are small when compared to those in the slab. Further increase in load causes the slab to behave nonlinearly. Prior to reaching the predicted ultimate load, deflections in the two edge beams along the long span increase rapidly keeping up with the amount of deflection already reached in the

mid-span, and in contrast, deflections in the other edge beams in the short span direction reduce slowly. This indictes that moment redistribution may have occurred which can be seen in Fig.6.34 from the small amount of reversed deflection recorded in the middle of the beams. These slabs eventually fail by excessive yielding with almost the same amount of deflection in the middle of the ribs in long span until collapse, see Fig.8.2. Fig.6.34 shows the characteristic of R.C. waffle slab H2 subjected to uniformly distributed load.

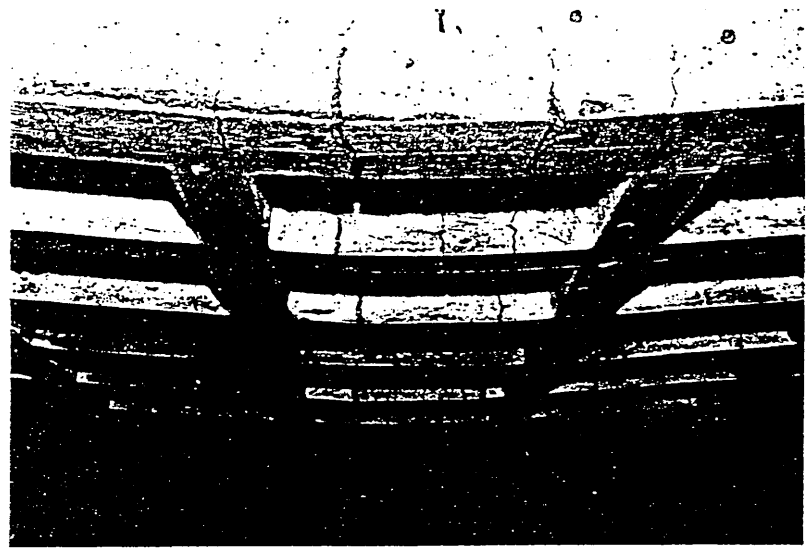

Fig.8.2: View of the Collapse Mechanism for 1/2-scale R.C. Waffle Model Slab J1

This typical load-deflection characteristic is found consistently for all model slabs with either rigid edge supports or four corners supported. Based on these test results, a conclusion can be drawn that the load-deflection characteristic is essentially linear up to approximately 1/3 and 1/4 of the failure loads for R.C. waffle slabs in Series A to F and Series H to J respectively. These loads correspond to the appearance of the first cracks. It is evident that the load carrying capacity of the R.C. waffle slab with restrained supports is enchanced by the membrane action. The amount of this enhancement is dependent on the combination of edges being restrained.

In BS8110, it is recommended that the serviceability limits of deflection and crack width for reinforced concrete structures are that the final deflection of the structure should not exceed span/250 and the maximum acceptable crack width at any point in the structure

should be less than 0.3mm. Only the deflection limit has been investigated for R.C. waffle slabs in the present work. The crack width is ignored due to two reasons: firstly, the critical crack width at support of the slab was impossible to obtain owing to the loading condition; secondly, the scale effect on the crack width of the model is uncertain. Table 8.1 shows the loads of the model slabs at the deflection limit of (1100/250 =) 4.4mm. On this basis, an average factor of safety against the ultimate load capacity of 1.785 is obtained.

Table 8.1: Loads Of R.C. Waffle Slabs At Deflection Limit Of Span/250

(1) Slab No.	(2) Test Load (kN/m^2)	(3) Load at Defn. = Span/250 (4.4 mm)	(4) Load factor (2)/(3)
A1	93.859	48.789	1.923
A2	95.992	52.000	1.846
A3	108.791	69.286	1.570
B1	141.348	83.810	1.686
B2	155.138	101.176	1.533
B3	165.480	94.118	1.758
C1	194.784	116.129	1.677
C2	210.298	127.400	1.650
C3	230.983	127.629	1.808
E1	81.016	34.788	2.329
E2	115.491	61.084	1.891
E3	158.585	90.657	1.749
		Average	1.785
D1	268.905	143.000	1.880

On the basis of the initial portion of the load-deflection curve, the elastic theory using finite element method is used to predict the deflection behaviour of R.C. waffle slabs. Relevant flexural and torsional rigidities of R.C. waffle slabs has been discussed in Section 7.2. Since the elastic analysis in this investigation is

based on bending theory for plate with uniform thickness, the deduced rigidities should therefore be regarded simply as equivalent values. The aim is to establish the appropriate rigidities so that they can be used to predict the behaviour of R.C. waffle slabs with different loading and boundary conditions. Two analytical models using finite element method are carried out ; these are thin plate flexural element model based on the bending plate theory and grillage element model based on the grillage analysis.

8.2 Results Of Elastic Analyses

The load-deflection behaviour of an R.C. waffle slab is discussed in Section 8.1. The results of the twelve model tests up to 1/3 of the test failure load are used to form an upper limit of the elastic behaviour for this type of structure. Fig.7.5 to Fig.7.11 and Fig.7.17 to Fig.7.20 provide a graphical summary of the theoretical results for R.C. waffle model slabs. The deflections at various rib joints or nodes of the ribs obtained from the finite element method (FEM) and grillage analysis (GA) are compared with the experimental results and given in Table 8.2. Theoretical results for R.C. waffle slabs B2 and B3 can also be seen in Fig.8.3 and Fig.8.4 respectively. The correlation is good in that deflections at mid-span nodes are consistently closer to the actual experimental values for slabs in Series A to C. The results for model slab E1, with one long edge simply supported, yield an uncharacteristic result with almost a 50% discrepancy compared to the experimental results. The poor correlation is probably due to loss of end fixity in the restrained edges. However, this apparent shortcoming was rectified for the other slabs in this group and a better agreement between the theoretical and experimental results is obtained for model slabs E2 and E3.

A typical displacement contour for model slab B3 at the initial crack load of 55.160kN/m^2 is shown in Fig.7.5a using FEM is compared with the actual displacement obtained from the tests given in Fig.8.5. The discrepancy between these two sets of contour of displacement can be obtained by comparison of these figures, the overall discrepancy of the theoretical results being within 10% of the test results. This

comparison is made by checking the deflection at the rib joints at A, B, C and D in Fig.8.5 and the discrepancies of -7.3, -10.2, +6.9 and +3.8% of the theoretical values are obtained for these joints respectively.

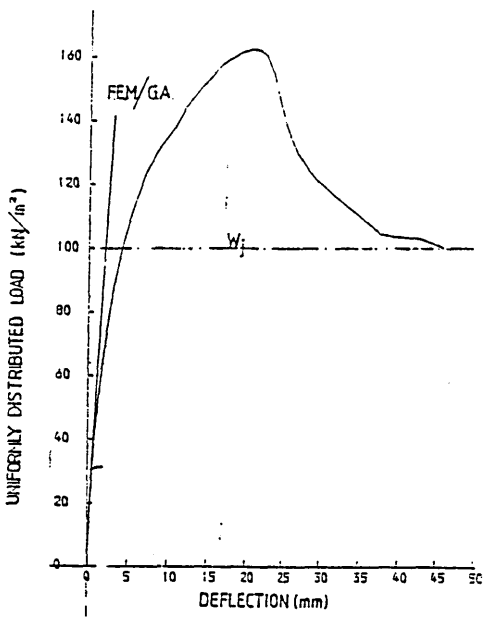

Fig.8.3: Experimental and Theoretical Mid-span Deflections For R.C. Waffle Slab B2

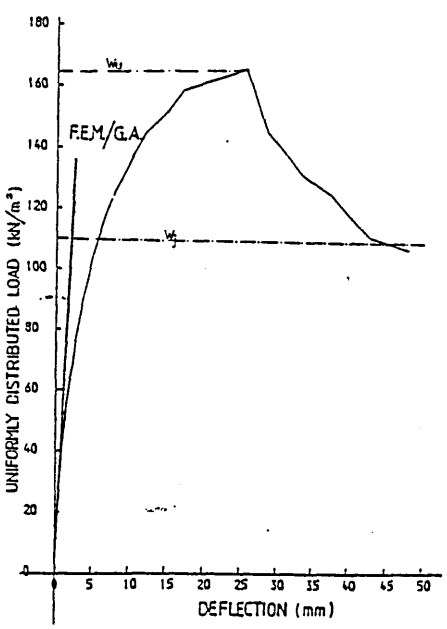

Fig.8.4: Experimental and Theoretical Mid-span Deflections For R.C. Waffle Slab B3

Table 8.2 Deflections of R.C. Waffle Slabs
at the Initial Cracking Load

Slab No.	Node No.	Experimental deflection (mm)	Theoretical deflections FEM (mm)	GA (mm)
A2	1	0.79	0.664	0.688
	2	1.53	1.590	1.662
	Mid	1.73	1.729	1.804
B3	1	0.72	0.596	0.613
	2	1.19	1.416	1.459
	Mid	1.66	1.539	1.583
C1	1	0.56	0.368	0.381
	2	1.02	0.933	0.990
	Mid	1.17	1.022	1.081
E1	1	1.24	0.979	0.922
	2	1.96	1.501	1.465
	Mid	2.20	1.513	1.484
	3	1.89	1.278	1.265
E2	1	0.55	0.543	0.662
	2	0.95	1.082	1.061
	Mid	1.16	1.103	1.074
E3	1	0.42	0.480	0.458
	2	0.63	0.738	0.727
	Mid	0.82	0.743	0.734
	3	0.47	0.621	0.620
	4	0.35	0.241	0.241

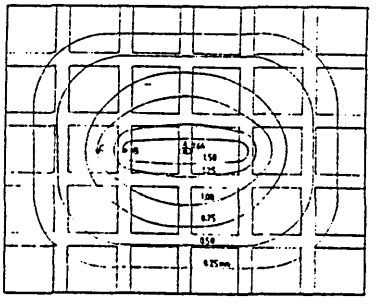

Fig.8.5: Experimental Displacement Contour For R.C. Waffle Slab B3

The deflections determined by the thin plate element and grillage element models bear good comparison with the deflections obtained from the observation of the tests. This can be taken as evidence to indicate that the determination of the flexural and torsional rigidities given in Section 7.2 to be reliable to predict the load-deflection characteristic of R.C. waffle slabs using these elastic analyses. The agreement between these two theoretical models is apparent which is probably because the rigidities of the model slab are derived from the same principle. The comparison of the results between finite element method and grillage analysis suggests that the effect of continuity in the top flange of the idealized T-section is small and can be ignored. The application of these two model analyses in this investiagation has confirmed that the load-deflection characteristic of R.C. waffle slab can be obtained by either finite element method or grillage analysis using the flexural and torsional rigidities determined in Section 7.2.

8.3 Results Of Nonlinear Analysis

The results of the Elastic-Fracture model for slab models A2, A3, B3 and C1 are compared with the experimental results and shown in Fig.7.24 to Fig.7.27 respectively. The analysis gives the entire load-deflection behaviour with the locations of cracks for R.C. waffle slabs subjected to uniformly distributed load. High stress levels at the supports are reached as manifested by the cracks in the models and this phenomenon bears good agreement with the results shown in the load-strain relationship in Fig.6.19. Cracks occur at the outermost top surface at the support of the ribs in both directions. This indicates that stress concentration exists in these ribs. These cracks penetrate into the soffit of the slab and also extend along the edge. The idealized crack pattern for model slab B3 is given in Fig.7.28, which, apart from the absence of the combined cracks, shows a good prediction for the develpoment of cracks when compared to the crack pattern of the test shown in Fig.6.22b.

Fig.7.24 to Fig.7.27 provide the evidence that membrane action siginficantly enhances the load carrying capacity of an R.C. waffle slab with restrained edges. These figures also indicate that the ultimate load methods employed in the present investigation

underestimate the load capacity of an R.C. waffle slab with restrained edges. With this 3-dimensional elastic-fracture model, the load-deflection relationship and the membrane effect on the restrained R.C. waffle slabs can be verified accurately.

The deflections below the elastic limit given by the 3-dimensional analysis are generally lower than those obtained from the tests in Fig.7.24 and Fig.7.27. Two possible causes are thought to affect the theoretical results. Firstly, the short term elastic Young's modulus of 28kN/mm^2 and Poisson's ratio of 0.15 used may be conservative for these model slabs. It is evident that low tensile strength of the concrete is obtained throughout the test series as shown in Table 6.3. This low tensile strength reduces the modulus of elasticity of the concrete in the slab and hence, it may give rise to the premature cracking in the slabs. Secondly, the end fixity given by the test rig is by no means perfect as compared to the restrained edges modelled by the computer. Despite these shortcomings, the theoretical results have a reasonable agreement with the test results for those slabs with high rib depth and these can be seen in Fig.7.26 and Fig.7.27 for model slabs B3 and C1 respectively. The deflections at the yielding stage are also in good correlation with the test results.

Although the theoretical analysis underestimates the delection of the model slabs by almost a 10%, it is felt that a better result can be obtained by increased the number of load increments and also by taking into consideration the effect of aggregate interlock and dowel action in concrete. At the present investigation, an incremental load of 12.5% of the collapse load was used i.e. a total of 8 steps. For each of these steps, it has taken about three and half hours of CPU time to solve the problem. Apart from that, the interpretation of the results and updating the rigidities for cracked or crushed elements are extremely tedious and prohibitively time consuming.

8.4 The Assessment of Elastic Analyses

FEM and GA have used to analyse the elastic behaviour of R.C. waffle slabs using elevant material properties as described in Chapter 7. It is a well known that the behaviour of an R.C. waffle slab is not purely elastic. The linear behaviour, in this investigation, is

regarded simply up to the load at which the initial cracks appear with the aim to establish the basis which may be employed to predict the required moments to satisfy the serviceability limit state and to compare these with the moments provided by the current code BS8110.

In conjunction with the comparison between the moments given by BS8110 and the analyses, the discussion will be focussed on the model slabs with rigid supports i.e. model slabs in series A to E. According to BS8110, the width of middle strip is taken to be three quarters of the width of the slab and the edge strips of the slab in both orthogonal directions should be provided with at least nominal reinforcement. Therefore, in the analysis emphasis will be on the moments in the middle strips in both directions. The moment coefficients obtained using FEM and the coefficients provided by the Code for ribbed slabs with restrained edges are given in Table 7.6. These coefficients are expressed in terms of wLy^2, where w is the design load and Ly is the short span of the slab. The coefficients for these nine slab models are found to be consistent.

From Table 7.6, it can be seen that the Code underestimates the support moments of the waffle slab by 16 and 22% in short and long spans respectively which the span moments are overestimated by 78 and 118% in short and long spans respectively. The sum of the support moments in short span is (0.050+0.018=) $0.068wLy^2$ which is approximately 92% of that provided to be (0.042+0.032=) $0.074wLy^2$ by BS8110; for the long span, the sum of the span moments is $0.052wLy^2$ which is almost 93% of the provided value of $0.056wLy^2$. A comparison of these coefficients indicates that there is a close correlation between the theoretical results and the Code. A conclusion that can be drawn from these results is that the waffle structure attracts higher moments in support and lower moments in span than those given by the Code for R.C. solid slab. The increase in support moments is found almost to be balanced by the reduction in span moments. This finding lends a good agreement with the results obtained by Resis et al (64) and Tebbit et al (71) for ribbed flat slabs. The variation in support and span moments for the short span direction is found to be greater than in the long span.

As a result of keeping the area of steel constant at the supports, it can be seen that the span moments vary with the area of steel and

rib-depth to slab thickness ratios. Significantly, the steel percentage in the waffle slab has a greater effect on the span moment than the rib-depth to top slab thickness ratio. Based on the mean values, the support to span moment ratio of 2.777 for short span and 3.727 for long span are obtained. These figures compared to the support to span moment ratio of 1.333 which is generally adopted by BS8110 indicate that an R.C. waffle slab designed to the Code may be at a substantial risk to exceed the serviceability limit states of deflection and crack.

Coefficients for an R.C. waffle slab with one long span simply supported and three other sides fully fixed are given in Table 7.6. The sum of support moments of $0.0771wLy^2$ and the sum of span moments of $0.0747wLy^2$ found from the table are 78.4 and 114.0% of those recommended by BS8110. The rib depth to top slab thickness ratio and the steel percentage of the slab have small effect, not greater than 6%, on the total moment coefficients. Based on the analytical results, the Code significantly underestimates the moment in the long span by almost one-third of the moment required. The average support to span moment ratios for the fixed edges are found to be 2.338 and 2.717 for short and long spans respectively. It can be seen that moments are distributed fairly evenly in both orthogonal directions and it is surprising to note that support moments obtained in long span are almost equal to those in short span.

The same procedures are carried out to obtain the comparable moment coefficients from the results of the grillage analysis. The values are given in Table 7.7 for waffle slabs with all edges fully fixed, and one long edge simply supported with the other three fully fixed. The sums of the support and span moments are found to be (0.049+0.018=) $0.066wLy^2$ and (0.040+0.008=) $0.048wLy^2$ respectively, and which are equivalent to 89 and 86% of those recommended by the Code for the fully fixed slab. The corresponding values for slabs with one long edge simply supported are $0.0728wLy^2$ for support and $0.0682wLy^2$ for span, and which are equivalent to 74 and 105% of that provided by BS8110. The support to span moment ratios are found to be even greater than the results obtained by the finite element method of 2.722 for short span and 5.0 for long span direction respectively for fully fixed slabs; the corresponding ratios are 2.534 and 3.036 for slabs with one long edge simply supported and three other edges fixed.

Analytical values given in Table 7.6 to Table 7.7 show a good agreement between these two elastic analyses. The comparison between these values indicates that the grillage analysis, in the present investigation, tends to give less span moments than that by the finite element method. The differences in these two methods may possibly reflect the effect of ignoring the continuity in the top slab of the waffle slab in the grillage analysis.

Theoretical analyses using FEM were carried out for R.C. waffle square slabs using the data from model slabs A2, B2 and C2 and the coefficients are given in Table 7.8. Based on these values, it is found that discrepancies of 20% of the support moment and 92% of the span moment are present when these values are compared to the coefficients provided by the Code. It is worthwhile to note that the coefficients of the square waffle slab are comparable to these for the long span direction of the rectangular waffle slab with side ratio of 0.827. In conjunction with the load distribution diagram in Fig.7.39 given for the Modified Strip Method, the weighted average method can be applied to estimate moments in elastic range in terms of the ratio of the lengths of supports. The ratio of the weighted average moment for short to long span can be obtained as

$$Rm = \frac{\beta_3^2(3-2\beta_1-2\beta_2)}{\beta_1^2}.\alpha^2 \qquad (8.1)$$

Based on this ratio, it is seen that the total short span moment will increase with the reduction in side ratio. To verify this, the load distribution diagram with 45^0 is considered for the model slab test with side ratio 0.827. It gives

$$\beta_1 = \beta_2 = \alpha/2$$

and

$$\beta_3 = 1/2$$

Thus, from Eqn.8.1

$$Rm = 1.3459$$

Hence,

$$Mx = 0.051 \times 1.3459 = 0.0686$$

This predicted moment for short span is within 1% of the theoretical values given in Table 7.6. However, the apparent problem is how to distribute the support and span moments appropriately. This may possibly be estimated using the ratio of 3.0 which is approximately equal to that ratio obtained theoretically for the R.C. waffle square slab; this yields a support moment of $0.0514wLy^2$ and a span moment of $0.0172wLy^2$ for the short span. These moments are, in fact, within 5% of the theoretical values given in Table 7.6. The increase in the short span moment using this ratio, Rm, has been checked for R.C. solid slabs with various side ratios. The results are very similar to the values provided by BS8110. It can then be concluded that the sum of the short span moments for a rectangular waffle slab can be estimated accurately by the ratio, Rm, using the moments obtained by the square waffle slab.

8.5 Load-Cracking Characteristic

It has been confirmed that the deflection of R.C. waffle slabs vary linearly with the applied loads until the occurrance of cracks. The observations from the tests have shown that primary cracks occur almost simultaneously in the mid-span of the interior ribs in both orthogonal directions. These cracks with fairly even spacing and normal to the rib axes, suggest that moments distribute uniformly along the interior ribs. These are confirmed by the results shown in Fig.7.5b to Fig.7.5c and Fig.7.6b to Fig.7.6c using finite element method and in Fig.7.17 to Fig.7.19 using grillage analysis. The initial cracks are found consistently at an average value of 31.8% of the failure loads for these nine model slabs in Series A to C given in Table 6.5. The maximum and minimun loads for initial cracks of 40.0 and 20.9% of the failure loads are obtained for model slabs B2 and C3 respectively.

Prior to failure, a series of inclined cracks occur in the sections of the ribs adjacent to the corners. These cracks spiral along the exposed surfaces of the ribs with the angle varying from 40^0 to 50^0 to the rib axis as shown in Fig.6.20a and Fig.6.20b. Based on the results of grillage analysis in Fig.7.17 to Fig.7.19, it is clearly indicated that these portions of rib sections are subjected to combined bending and torsion moments before failure. More cracks

occur in these ribs as the slab undergoes general yielding. These cracks can be described in a pattern radiating from the centre to the corners of the slab. Slabs fail immediately after crushing of concrete at the rib supports.

Nine model slabs in Series A to C with different rib depths and area of steel have been tested to failure. It is found by comparison that these failure crack patterns in Fig.6.22a to Fig.6.22c are very similar to that of the control solid model slab D1 in Fig.6.24 except for the absence of crushing of concrete at the interior rib supports and the development of spiral cracks in the corner ribs prior to the failure in the solid model slab. These may possibly be due to the fact that the recesses of the waffle structure allow high tensile stresses develope in the ribs and reduce torsional rigidity of the slab. As a result, the concentration of the flexural and combined stresses develop in the rib sections.

The crack patterns of the slabs in Series E are similar to those in Series A, B and C, the only difference being that the centre of the radial cracks from each of the slab corners shifts slightly towards the simply supported edge. The initial cracks are found at loads of 25.9, 23.9 and 19.6% of the failure loads as given in Table 6.5 for model slabs E1 to E3 respectively. These give an average value of 23.1% which is almost 28% lower than the average value of 31.8% for model series A to C. More spiral cracks than those seen in previous model slabs develop in the rib-sections at the corners adjoining to the simple supports and diagonal cracks finally develop on the under-side of the top slab radiating from the two corners to the central portion of the slab as given in Fig.6.24. This phenomenon suggests that these ribs are subjected to comparatively higher combined stresses than those ribs adjoining the restrained edges in the slab. As a result, a more severe concrete crushing is recorded at the supports of the ribs adjacent to the simply supported edge beam as shown in Fig.6.24

The crack patterns of the slabs in Series F are similar to those described for the series E but no inclined crack has been found on any of the three short spanning ribs adjacent to the free edge beam in Fig.6.28. Flexural cracks developed on the edge beam widen up more extensively than those observed in the previous tests at collapse.

Concrete crushing is also observed more severely only at the support of the edge beam. The initial cracks are found at the loads of 32.0, 25.1 and 25.3% of the failure loads as given in Table 7.3 for model slabs F1 to F3 respectively which gives an average load percentage of 27.5 which is 11% lower than the average load of 32% for model slabs in series A to C.

The crack patterns for model slabs in Series H to J shown in Fig.6.32a to Fig.6.32c are somewhat different to those of in previous tests. Flexural cracks mainly occur in the middle of the ribs and the edge beams almost simultaneously in both directions. Prior to failure, moment redistribution takes place within the slab. As a result, cracks in the middle of the ribs and edge beam in long span direction widen up extensively. In contrast, cracks close up in both edge beams in the short span direction. Spiral cracks such as those observed in previous tests have not been found in these slabs but diagonal cracks often occur at the rib joints. The initial cracks are found at loads of 28.4% of the failure load for the 1/2 scale model slab J1 which is comparatively higher than the average load of 18.9% for Series H and I. The discrepancy between these load percentages is thought to be mainly due to the scale effect of the models used. It is, therefore, felt that more research is required to investigate the scale-effect of the slab.

The measured crack widths of the slab models are thought to be not very useful due to three reasons:

(1) the critical crack widths at supports could not be measured owing to the loading system;
(2) the readings could only be taken in the selected locations; and
(3) the low tensile strength of concrete obtained by the tests inevitably caused premature cracking.

The first visible cracks are found to occur comparatively earlier than those in the solid slab. However, it is observed that initial cracks occur at a load of about 1/3 of the failure loads as given in Table 8.3 and crack width at these loads are found to be less than 0.12mm for all tests.

Table 8.3: Comparison Between the Failure and Cracking Loads

(1) Slab No.	(2) Slab Thickness (mm)	(3) Cracking Load (kN/m^2)	(4) Failure Load (kN/m^2)	(5) Ratio (3)/(4)
A1	55	34.475	93.859	0.367
A2	55	31.028	95.992	0.323
A3	55	41.369	108.791	0.380
B1	70	48.263	141.348	0.341
B2	70	62.055	155.138	0.400
B3	70	55.160	165.480	0.333
C1	85	51.713	194.784	0.266
C2	85	51.713	210.298	0.246
C3	85	48.265	230.983	0.209
D1	70	44.818	268.901	0.167
E1	55	20.685	81.016	0.255
E2	70	27.580	115.491	0.239
E3	85	30.028	158.585	0.189
F1	55	27.580	64.469	0.428
F2	70	27.580	109.976	0.251
F3	85	34.475	136.521	0.253
H1	85	7.000	41.370	0.169
H2	85	10.343	43.094	0.240
I1	85	5.832*	36.832	0.158
I2	85	5.832*	30.832	0.189
J1	170	25.000*	88.000	0.284

(Total of 4-point loads denoted by *)

The contours of bending moments about X- and Y-axis, and torsion are given in Fig.7.5b to Fig.7.6d. It can be seen from these that the span moments are distributed evenly in the interior rib sections for both orthogonal directions. This is thought to be the reason why the cracks appear almost simultaneously and evenly spaced along these ribs. The diagonal cracks at the interior joints coincide with the direction appropriate for the resultant of the span moments in both orthogonal directions. The maximum torsion moment at first cracking load of $55.160 kN/m^2$ is 0.146kNm/rib which is below the ultimate torsional resistance of the rib of 0.183kNm/rib based on concrete

strength only. No spiral cracks were observed at this load. Superimposing the contour of twisting and bending moments in x- and y-axes, the nature and the location of the cracks in the ribs can be predicted by obtaining the maximum moment values in the ribs as shown in Fig.8.6 which is similar to Fig.7.29.

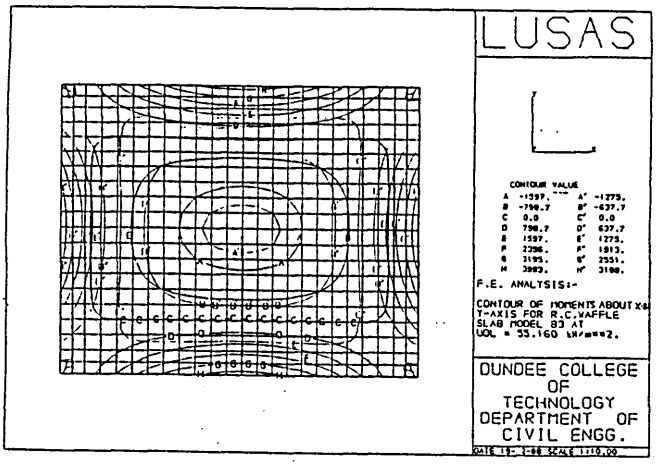

Fig.8.6 Theoretical Result For R.C Waffle Slab B3

The superimposed diagram of bending moment and torsion at the same loading of 55.160kN/m^2 using grillage analysis is also obtained and given in Fig.8.7 which is similar to Fig.7.18. It is clearly possible, using this figure, to locate probable cracks and potential hinges on the ribs and the location of these potential hinges bears good comparison with the predicted crack pattern by FEM. More importantly this predicted crack pattern has excellent correlation with the yield pattern modified from the experimental yield pattern which is shown in Fig.7.36. This indicates that failure mode of a waffle slab can be predicted using either FEM or GA by locating the maximum values of combined bending and torsion moments on the rib sections.

However, based on the load-cracking relationships of these series of tests, several points can be drawn as follows:

(i) The crack patterns of R.C. waffle slabs with fully restrained, simply supported and free edges are similar to those of R.C. solid slabs with similar support conditions at yield load.

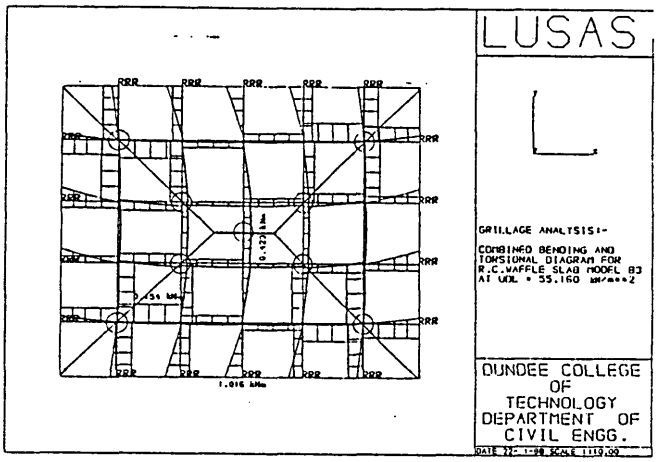

Fig.8.7 Theoretical Result For R.C Waffle Slab B3

(ii) The development of the spiral cracks in the ribs at the restrained corners followed by the crushing of concrete at the interior rib supports characterizes the failure of the slabs. As a result of the recesses in the waffle structure, flexural and combined bending and torsion cracks are concentrated in the rib sections. More spiral cracks occur in the ribs at the corners where the restrained and simple supports meet while only flexural cracks appear in the ribs at the corners where restrained supports intersect with free supports.

(iii) Based on the formation and propagation of the crack pattern, an R.C. waffle slab with four corner supports initially behaves as two-way spanning slab and exhibits an elastic behaviour. After the moment redistribution has taken place, the slab eventually fails with a collapse mode similar to that of a beam mechanism. It is also found that the different loading conditions carried out in these series of tests, have small effect on the failure mode of the slab.

(iv) Initial cracks occur at loads of 30.8, 23.1 and 27.5% of the test failure loads obtained for the waffle model slabs in Series A to C, E and F respectively. The model slabs in Series H to J supported at four corners give the lowest load of 18.9% of the test failure loads of the slabs.

8.6 Ultimate Load Analyses

The load-deflection and-cracking characteristics of R.C. waffle slabs were discussed in Sections 8.1 and 8.5. In all cases substantial vertical displacement occurs when the load increases in excess of the predicted ultimate load. The slab ultimately behaves as a rigid-plastic material. In all model tests, the yield patterns are fully developed before the slabs collapse. Distinct spiral cracks along the rib sections at the supports are observed in test Series A to F only, and these common features appear prior to the failure of the slabs. Spiral cracks with an inclination of approximately 45° to the rib axis characterize the sections at the corner ribs in both orthogonal directions being subjected to combined bending and torsion, see Fig.6.20a and Fig.6.20b. Based on these results, the trend of the failure patterns can be summarised in Fig.8.8.

Attempts have been made based on the load-cracking characteristic to idealize a failure pattern so that the ultimate load capacity of R.C. waffle slabs may be investigated. The failure pattern for these model slabs may be described as either 'anchored circular fans' or 'diagonal yield' as shown in Fig.8.8. In view of the general nature of the crack pattern which is very similar to that for solid slabs, the 'diagonal' yield pattern may be assumed. It is also noted that this pattern can be conventiently used to determine the membrane enhancement of the waffle slabs with fully fixed edges.

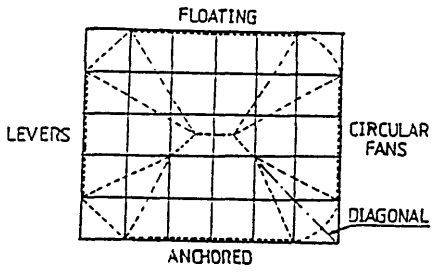

Fig.8.8 Failure Patterns

This failure pattern is very closely related to the simplified diagonal yield pattern idealized by Johansen's (31) yield line theory for R.C. solid slabs shown in Fig.7.29. Therefore, the waffle model slabs are analysed as an equivalent orthotropic uniform slab based on

the 'normal-moment' criterion developed by Johansen, in which the twisting moments along the yield lines are ignored. The load predicted by this modified yield line method is inevitably conservative because of the membrane action due to the restrained edges of the waffle slabs and this can be seen in Table 7.9, and an average load factor of predicted to failure loads of 0.651 is obtained.

The failure pattern of the tests shows that the restrained ribs at the supports are subjected to combined bending and torsional moments causing spiral cracks along the ribs. These spiral cracks together with the crushing of concrete in the ribs form a complete failure mechanism of the slabs. Using the concept of grillage analysis, the actual crack pattern can be modified as plastic hinges to form the collapse mechanism as shown in Fig.7.36 to Fig.7.38. The hinges at the supports and in the mid-span in the interior ribs are subjected to pure flexure based on the nature of cracking. The ultimate strength for each of these hinges due to pure bending is obtained in Section 7.4.1.1 for an idealized Tee-section. As a result of the diagonal yield pattern postulated from the tests as shown in Fig.8.6, the angle of rotation for bending of a combined plastic hinge in the restrained corner rib is equal to the angle of twist. Therefore, the total work done by a combined bending and torsion plastic hinge can be determined in terms of equivalent moment in pure bending by Eqn.7.61. Thus, the total internal work for all the plastic hinges required to form a complete mechanism is equated to the external work done by the applied load. Results for a selection of model slabs, using equivalent grillage analysis, Method [2], are given in Table 7.18 and the predicted ultimate loads compare well with the results from Method [1].

Attempts have been made to estimate the increase in load capacity of a plastic hinge due to bending and torsion interaction in Section 7.4.2.1. This increase in strength can be defined as directly related to the value of $\sec\gamma$, where γ is an angle of interaction which can be determined as the ultimate strength ratio of torsion to bending of the section. However, γ for the model slabs are found to be small as given in Table 7.18 the maximum value being 24.042^{0} which gives a 9.5% increase in the work done of a plastic hinge subjected to combined moments. The overall effect on the increase in ultimate load capacity is found to be negligible. In contrast, there is evidence that this

effect becomes significant for the control solid slab D1 with angle of interaction of 52.85^0 which increases the load capacity by 35%. The close agreement of the results using these two methods reflects that the contribution of combined bending and torsion is small. This fact suggests that the 'normal-moment' criterion of the equivalent yield line anlysis is applicable for R.C. waffle slabs. It is however felt that more investigation will be necessary for a better understanding of this effect on the load capacity of R.C. waffle slabs.

Because of the foregoing argument that the effect of the combined bending and torsion in the ultimate load analysis is small, the modified strip method in Section 7.43 can be applied to R.C. waffle slabs with reasonable accuracy. It is assumed that the load distribution diagram for this method is similar to the assumed yield pattern in Fig.7.39. The weighted average of the moment due to the applied load is obtained for each elastic-plastic region. The average load capacity of the slab can then be minimised with respect to the angles of lines of discontinuity. The proposed modified strip method developed in Section 7.4.3 is applied to model slabs in Series A to F. The results are compared with the experimental results and also the results of Methods [1] and [2] in Table 8.4. It is interesting to note that a close agreement is obtained between these analytical results and this signifies the applicability of this method for analysing waffle slabs. The advantages of using this modified strip method are that it is quicker and simpler to use to obtain the ultimate load of the slab than the equivalent yield line method and open grillage analysis. From the design point of view, it provides the minimum load carrying capacity of a slab at ultimate limit state thus giving a lower bound solution.

From Table 7.19, the lowest angle of discontinuity is found to be 42^0 to the long span for slabs in Series A to E and the highest of 51^0 for slabs in Series F. These angles are comparable to those observed from the tests and also those angles obtained from Method [1] given in Table 7.9. It is therefore concluded that both of these methods share a common valid collapse mechanism. It is seen in Fig.7.40 that Method [3] tends to give the minimum ultimate load, i.e. the lower bound solution, of a slab with an assumed load distribution. On the other hand, Method [1] inevitably provides the maximum failure load, i.e. the upper bound solution, for a similar assumed yield pattern.

Table 8.4:- Experimental and Theoretical Ultimate Load Capacities of R.C. Waffle Slabs

Slab No.	Test Failure Load	Theoretical Load		
		Method[1]	Method[2]	Method[3]
	(kN/m^2)			
A1	93.859	62.569	64.999	62.941
A2	95.992	70.670	72.209	71.099
A3	108.791	80.504	81.912	80.982
B1	141.348	85.738	88.274	86.371
B2	155.138	99.179	101.356	99.928
B3	165.480	111.955	113.663	112.806
C1	194.784	110.390	113.335	111.323
C2	210.298	127.057	129.117	128.105
C3	230.983	143.839	146.281	145.072
D1	268.905	85.035	114.689	85.749
E1	81.016	65.960	60.228	66.012
E2	115.491	92.804	83.931	92.789
E3	158.585	119.026	108.126	118.942
F1	64.469	61.867	61.353	56.281
F2	109.976	85.517	85.483	78.160
F3	136.521	107.257	107.559	105.746

Notes: Method [1]: Modified Yield Line Mothed;
Method [2]: Equivalent Open Grillage Anslysis;
Method [3]: Modified Strip Method.

A close agreement between these analytical results in Table 8.4 may suggest that in accordance with the lower and upper bound theorem, the true failue load of an R.C. waffle slab may lie between the results obtained from these two methods. Table 8.4 also shows a good correlation between the results obtained from these two methods for the slabs with various boundary conditions.

It is appropriate to conclude on the basis of these theoretical results that the three ultimate load methods employed yield a close correlation among each other. Theoretical results show that the

assumed yield patterns in this investigation are applicable to these three methods. From open grillage analysis, it is found that the increase in strength due to combined bending and torsion is negligible but it may become significant for R.C. solid slabs. Modified strip method is found more direct and simpler to apply and it gives a lower bound or safe solution for R.C. waffle slabs. It is believed that the true collapse load of an R.C. waffle slab lies between the loads obtained by modified strip and yield line methods.

The utimate load methods employed in this investigation are found in Table 8.4 to be conservative for waffle slab with restrained edges. It can clearly be seen in Table 7.9 that the ratio of failure to theoretical load varies from 0.567 to 0.740. These factors also depend upon the boundary conditions and d/t ratio, see Fig.7.12, of the waffle slabs. Observation of load-deflection relationship in Section 8.1 and the results of nonlinear finite element analysis from Fig.7.24 to Fig.7.27 clearly indicate that the membrane action has taken place and this significantly enhance the load capacity of R.C. waffle slabs. For the purpose of ultimate load analysis, this effect on restrained waffle slabs cannot be ignored. Otherwise, the factor of safety against the failure of an R.C. waffle slab cannot be evaluated accurately.

As slabs with restrained edges deflect transversely membrane forces are induced along the perimeter of the slab edges. Based on rigid-plastic theory, these forces can be related to a function of the mid-span deflection of the slab. After the load exceeds the predicted flexural load capacity, these membrane forces become more apparent. Both the load-deflection and-cracking characteristics show that while the mid-span deflections reach approximately 1/3 of the slab thickness as shown in Table 6.6, crushing of concrete at the rib supports causes a rapid loss in strength of the slab. Observation of the tests has shown that crushing in concrete sections directly relates to the loss in the membrane forces which reduce the stiffness of the slab quickly. It is also believed that these membrance forces are reduced by the crushing of concrete. The residual strength of the slab is found tailing off at about the predicted ultimate load. After the removal of the membrane forces, the slab undergoes yielding at its ultimate load capacity obtained on the basis of the pure flexural strength of

of the membrane forces, the slab undergoes yielding at its ultimate load capacity obtained on the basis of the pure flexural strength of the slab. These can be seen from the results presented in Fig.8.9 and Fig.8.10 for model slabs in series B and C respcetively.

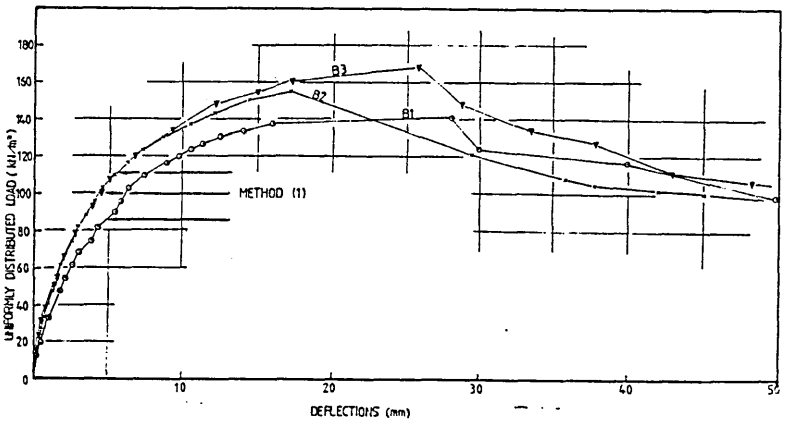

Fig.8.9 Load-Deflection Curves For R.C. Waffle Slabs In Series B

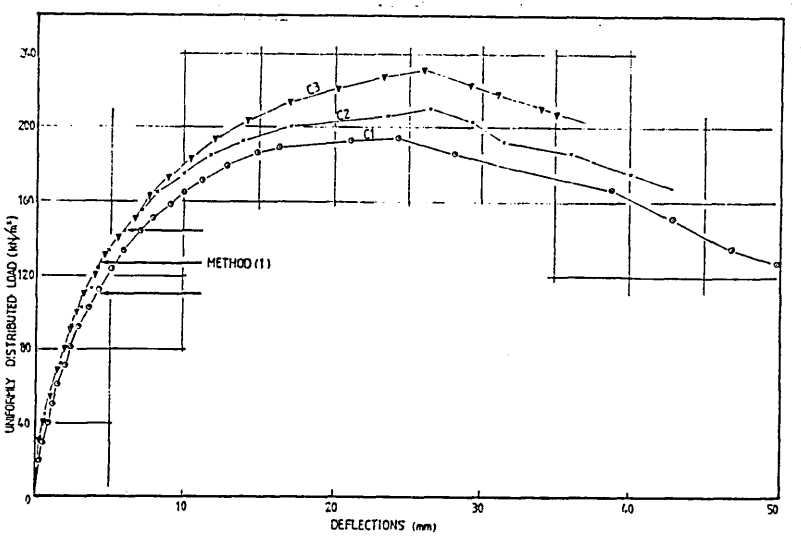

Fig.8.10 Load-Deflection Curves For R.C. Waffle Slabs In Series C

Deflections at collapse of the model slabs in series A, B and C in Table 7.2 are slightly less than 1/3 of the overall slab thickness, and that for the solid model slab D1 is 0.414. These results are rather low when compared with Park's (52) results which showed this to be half of the solid slab thickness. The value of the deflection to the overall slab thickness ratio for model slabs in Series E and F varies with the rib-depth to top slab thickness ratio and averages of

0.524 for series E and 0.523 for seies F are found. It is clear from this that the ratio of deflection at collapse to the slab thickness of an R.C. waffle slab is dependent on the boundary conditions. Test results in Table 6.6 shows that deflection at 1/3 of the slab thickness may provide a good guideline to predict the collapse of the waffle slab with restrained edges. On the other hand the deflection of 1/2 of the slab thickness may be taken for the failure of waffle slabs with either one long edge simply supported or a short edge free, and the other edges fully restrained.

Based on the experimental and analytical results, an idealized load-deflection characteristic curve is established in Fig.8.11 which is in accordance with the conclusion made in Section 5.6 for waffle slabs subjected to uniformly distributed load. In order to provide a basis for comparison and to reflect the order of magnitude of enhanced load capacity, the excess load for each of the tests is deduced from the ultimate load determined by equivalent yield line method in Table 7.9. The trend in the relationship between the enhanced load and the d/t ratio is apparent given in Fig.7.32 that the membrane enhancement increases almost linearly with d/t ratio i.e. rib depth. However, these additional strengths in column 4 of Table 7.9 indicate that the area of steel in the slab has small or negligible contribution to the membrane enhancement.

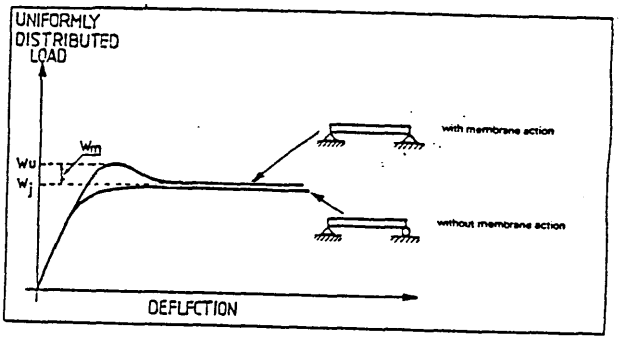

Fig.8.11 Idealized Load-Deflection Characteristic

It is assumed that the diagonal yield line pattern of 45° gives sufficient accuracy (34) for the analysis and the membrane forces are generated within the rectangular rib sections only. The critical deflection of the slabs 1/3 and 1/2 of rib depth are used based on the results of the tests for model slabs in Series A to C and Series E to

F respectively. The corresponding deflections for each of the rib sections along the yield lines can therefore be determined appropriately. Thus, the accumulated work done by the membrane force in each of the yielded rib sections can be evaluated. The external work done should be similar to that used to determine the ultimate load capacity due to flexure in Eqn.7.42.

This approach has been applied to previous slab tests (51,52,57) and it yields an excellent result as shown in Table 7.10 and Table 7.11. Taking into account the predicted membrane enhancement, the predicted load capacities using Eqn.7.32 show a remarkable agreement with the failure load observed from the tests, and which can be seen in Table 8.5. With these results, it can be concluded that the ultimate load of an R.C. waffle slab with restrained edges should take into acount the contribution of the membrane action as well as the flexural strength of the slab.

The following conclusions have been summarised from the above considerations:

(1) The ultimate load methods employed in the present investigation understimate the load carrying capacities of waffle slabs with restrained edges by as much as 75% dependent upon the support conditions, due to the effect of membrane action. The amount of the enhanced load capacity is dependent on the rib depth and support conditions. The effect due to the increase of area of steel is found to be negligible and can conveniently be ignored.

(2) The ratio of mid-span deflection to the rib depth at collapse is found to be 1/3 for the waffle slabs with all edges fully fixed, and this ratio is 1/2 for the waffle slabs with either one long edge simply supported or one short edge free and the other three edges fully restrained.

(3) It is found from the result of the tests that the membrance forces are associated with the geometrical deformation of the slab and these forces are released by the crushing of concrete. Thus, they can be expressed as a function of the vertical mid-span deflection of the slab and this function is primarily dependent on the compressive concrete strength of the rib sections.

(4) It is confirmed in Section 7.4.1.6.4 that the collapse pattern for model slabs in Series H to J is found to be the combined beam and slab mechanism. The ultimate load capacity of the slab is determined by modified yield line method. The failure load of the tests is consistently found to be the minimum load capacity foundfrom the assumed failure patterns.

Table 8.5 :- Comparison between the Theoretical and Experimental Ultimate Loads

SLAB No.	Wj (kN/m^2)	Wm (kN/m^2)	Wj+Wm (kN/m^2)	Wt (kN/m^2)	Wt / Wu
A1	62.569	31.234	93.803	93.859	1.000
A2	70.670	23.954	94.624	95.992	1.009
A3	80.504	30.132	110.636	108.791	0.983
B1	85.738	45.033	130.771	141.348	1.081
B2	99.179	47.544	146.723	155.138	1.057
B3	111.955	46.595	158.550	165.480	1.044
C1	110.390	69.565	179.955	194.784	1.082
C2	127.056	71.968	199.024	210.298	1.056
C3	143.839	83.512	227.351	230.983	1.016
					1.036
E1	65.960	5.262	71.222	81.016	1.138
E2	92.804	17.505	110.309	115.491	1.047
E3	119.026	36.044	155.070	158.585	1.023
					1.069
F1	61.867	6.429	68.296	64.469	0.944
F2	85.517	18.227	103.744	109.976	1.060
F3	107.257	22.849	130.106	136.521	1.049
					1.018

8.7 Load-Strain Relationships

The concrete strain obtained during the tests show characteristics very similar to those of deflections. Strains of concrete respond elastically at the early loading stage. A sudden increase in the rate of strains is recorded at loads of approximately 1/3 of the failure load of the slabs which was due to the effect of the appearance of first cracks. The strain of concrete increases nonlinearly with further applied load until the ultimate load is reached. Typical results of model slabs tested for different loading and boundary conditions are given in Fig.8.4. A small amount of moment redistribution is also observed during the tests from the strain measurement almost at the ultimate load capacity of the slab. No attempt is made to draw quantitative findings from these curves because the readings are taken as average values over a distance of either 100 or 150mm in the rib sections.

Very high strains are obtained for the main reinforcement in the support at cracking load and this has been confirmed by the elastic-fracture model in Section 7.3. All steel in both supports and at mid-span appeared to have reached yield at the predicted ultimate load; however, the results of these load-strain readings are somewhat erratic. It may be due to the slippage of the strain gauges during the tests and this can be seen in Fig.6.27 and Fig.6.30. As a result, the analytical work could not be based on the strain readings althouhg it has been useful to show quatitatively the behaviour of the reinforcements at the predicted ultimate loads so that the work on the membrane enchancement could proceed.

8.8 Effect of Rib-depth to Slab Thickness Ratio and Area of Steel

The characteristic of the ultimate load capacity given in Table 8.6 against area of steel at mid-span is plotted in Fig.8.12 and it is evident that the strength of the slab increases linearly with to the increase in area of steel in mid-span.

The increase in the ultimate load capacity of the slab due to the d/t ratio is more effective than that due to the area of steel. On the basis of the results shown in Fig.8.12, a set of ultimate load

capacities for waffle slabs with the varying area of steel of 1, 2 and 3% is predicted for each different d/t ratios of 3, 4 and 5 in Table 8.7. For a given area of steel at mid-span, the increase in ultimate load capacity of the slab with the increase in d/t ratio is characterized by the curve relationship shown in Fig.8.13. It can therefore be concluded, from the design point of view, that the increase in d/t ratio for R.C. waffle slabs is more effective than the increase in area of steel at mid-span.

Table 8.6: Summary of the Various Parameters and the Failure Load of R.C waffle slabs.

Slab no.	No. of bar	Steel %	d/t ratio	Failure load kN/m^2	Load factor
A1	2	1.117	3	93.859	1.000
B1	2	0.838	4	141.348	1.506
C1	2	0.670	5	194.784	2.075
A2	3	1.676	3	95.992	1.000
B2	3	1.257	4	155.138	1.616
C2	3	1.005	5	210.298	2.191
A3	4	2.234	3	108.791	1.000
B3	4	1.676	4	165.480	1.521
C3	4	1.340	5	230.983	2.123

Table 8.7: Predicted Load Capacities for Various Areas of Steel and d/t Ratios

Steel %	d/t Ratios		
	3	4	5
	kN/m^2		
1.0	90.0	146.0	210.0
1.5	97.5	160.0	238.0
2.0	104.0	175.0	265.0

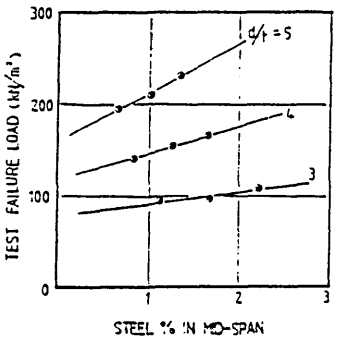

Fig.8.12 Ultimate Load Capacity Vs Area of Steel in Mid-span

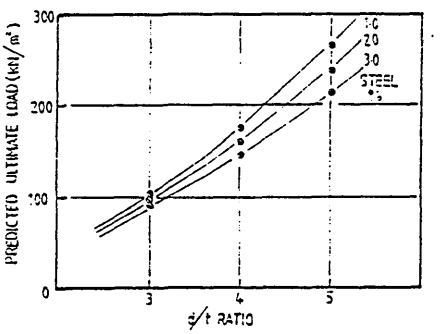

Fig.8.13 Load Vs d/t Ratio

8.9 The Assessment for the Design of R.C. Waffle Slabs

Based on the elastic analysis obtained by the finite element method, the design moments given by BS8110 (5) can be reduced by 8% for both orthogonal directions. The support to span moment ratio of 1.333 used in BS8110 taking into consideration the moment redistribution is somewhat questionable for the application to R.C. waffle slabs when compared to the analytical values, obtained in this study, of 2.777 and 3.727 for short and long spans respectively. The proposed moment coefficients can be found in Table 7.6. The validity of these coefficients for the ultimate load capacity of a waffle slab can be checked by the Modified Strip Method as shown below.

$$Mb = Md = 0.0686w.Ly^2 \qquad \text{where } Lx > Ly$$

$$Ma = Mc = 0.0510w.Ly^2$$

From Eqn.7.82 $\beta_3 = 0.5$

and from Eqn.7.86, $Mc' = \dfrac{0.0510wLy^2}{2(0.0686wLy^2/0.5)} = 0.186$

$$\beta_1 = \beta_2 = \frac{3x0.827x/0.186}{1+2x0.827(2x/0.186)} = 0.441$$

Thus, from Eqn.7.80

$$Ws = 3\left(\frac{0.827}{Ly}\right)^2\left(2x\frac{0.051wLy^2}{0.441}\right) + \frac{3(2-2x0.441)}{(3-4x0.441)Ly^2}x(4x0.0686wLy^2)$$

$$= 1.213w$$

Therefore, the ultimate load capacity is 1.213 times the design load, w. Generally, the design load is taken as 1.6 times the actual live (working) load. Thus, the factor of safety against the working load condition will be (1.213 x 1.6 =) 1.941. This factor of safety is about 92% of tht factor of safety of 2.116 which can be obtained by the M.S. Method but using the coefficients given in BS8110. However, a design using the proposed coefficients obtained in this investigation has a higher expectation to satisfy the serviceability limit states of deflection and hence cracking than that by using BS8110 coefficients. In addition, an R.C. waffle slab with one long side simply supported and the other three sides fully restrained designed in accordance with the proposed coefficients yields a factor of safety of 1.86 at working load condition as compared to a factor of safety of 1.96 obtained in the tests.

CHAPTER 9

CONCLUSIONS

9.1 CONCLUSIONS

The results of this investigation indicate that the deflection characteristics of R.C. waffle slabs comprise an initial elastic behaviour followed by a gradual and then a distinct plastic behaviour of the slab to failure. The initial cracks are found consistently to occur at an average of 31.8% for Series A to C, 23.1% for Series E, 27.5% for Series F, 18.9% for Series H to I and 28.4% for Series J of the test failure loads. Prior to failure, spiral cracks occur along the rib joints near the corners. This indicates that these joints are subjected to combined bending and torsional moments. The trend of the failure patterns can be postulated in Fig.8.6 similar to that of R.C. solid slabs. Typical load-deflection characteristic can be summarized as shown in Fig.8.11. The present investigation, together with Marshall's work (43), provides sufficient data to confirm that an R.C. waffle slab behaves in a very similar way to that of an R.C. solid slab described by Park (52). In addition, several significant findings from the present investigation on the series of R.C. waffle slabs can be reported as follows.

(i) The deflection obtained by the thin plate element and grillage element models bear good correlation to the experimental results up to the occurrence of cracking at load of 1/3 of the test failure load. This can be used as evidence to indicate that elastic flexural and torsional rigidities can be determined with reasonable accuracy as in Section 7.2 to predict the elastic behaviour of R.C. waffle slabs. Results of R.C. waffle slabs on the theoretical basis in Table 7.8 show an excellent correlation to that obtained by Resis et al (64) and Tebbit et al (71). Moment coefficients deduced at the outset of the code are given in Table 7.6 and Table 7.8. Based on the elastic analyses, there is an indication that BS8110 (5) underestimates the support moments by 16 and 22% in short and long spans respectively. In contrast, the BS8110 overestimates the span moments by 78 and 118% in short and long spans respectively. It is found that the voids in R.C. waffle slabs give higher moments at supports and lower moments in span than that given by BS8110 for R.C. solid slabs. It can be seen

from the trend of the values obtained in these slabs that the increase in support moments is found to be balanced by the reduction in span moments. For a waffle slab with fully restrained edges, the ratios of support to span moment of 2.777 and 3.727 are found in the short and long spans respectively; and ratios of 2.338 and 2.716 for slabs with one long side simply supported and the other sides fully fixed. It is therefore concluded that the ratio of support to span moment of 1.333 used by BS8110 is somehow inadequate in terms of deflection and cracking.

(ii) The proposed 3-dimensional elastic-fracture model gives a good prediction of the development of cracking for reinforced concrete waffle slabs when compared to the experimental results. Concentration of stresses are found to develop at the rib sections causing premature tensile cracks at the rib supports. The locations of these cracks can be predicted with reasonable accuracy by this model. A good correlation of the load-deflection characteristic is also obtained between the analytical and experimental results. It is indicated theoretically that the load capacity of R.C. waffle slabs is underestimated by any of the three ultimate load methods employed in the present investigation. It is also concluded that membrane action significantly enhances the load capacity of a restrained waffle slab. However, this theoretical model tends to indicate smaller deflections for R.C. waffle slabs with low d/t ratios.

(iii) The ultimate load methods employed in the present investigation yield a close correlation between each other. It is found that they underestimate the load capacities of R.C. waffle slabs with restrained edges by as much as 75% depending on the support conditions. The modified yield line method and open grillage analysis tend to give the upper-bound load capacity of the slab on the assumed yield pattern, while the modified strip method tends to give the lower-bound load capacity of the slab with the assumed load distribution pattern. The proposed modified strip method is found to be more desirable and easier to use for design purposes.

(iv) Prior to failure, the combined bending and torsion cracks develop on the rib sections at the corners of the restrained edges. The contribution of this combined action is found to have little effect on the load carrying capacity of the slab. The result of analysis

indicates that this factor can be ignored in the ultimate load analysis. However, there is an indiction that this effect may become significant for R.C. solid slab.

(v) It is confirmed theoretically as well as experimentally by the results of the tests that membrane action has a significant effect on the ultimate load capacity of R.C. waffle slabs with restrained edges. The enhanced load capacity is found to be dependent on the strength of concrete and the rib depth of the slab. The effect due to the increase in area of steel is found not to be significant. The maximum membrane action is characterised by the crushing of concrete at the ribs at supports at mid-span deflections of approximately 1/3 of the slab thickness for waffle slabs with all sides fully restrained and approximately 1/2 for waffle slabs either with one longer side simply supported or one short side free and the other sides fully restrained. The predicted ultimate load capacities of the model slabs, taking into account this membrane effect yield a good agreement with the experimental results as shown in Table 7.12. Thus, it can be concluded that the maximum load capacity of an R.C. waffle slab with restrained edges should be determined as the sum of the flexural load capacity and the membrane enhancement as stated in Eqn.7.32.

(vi) The ultimate load carrying capacity of R.C. waffle slabs supported by columns can also be determined using the modified yield line method. An excellent correlation between the experimental and theoretical results indicates that the collapse load of a waffle slab supported by columns can be taken as the least load obtained from all the possible failure modes. The load capacity obtained in this way is contrary to the general procedure conducted by the upper-bound yield line method. The critical mode of failure can be predicted from the criteria proposed in Eqn.7.53a to Eqn.7.54b which is dependent on the strengths of the supporting edge beams and the slab in both orthogonal directions. In the present series, the model slabs tested were 1/4 and 1/2 scale, and from the limited results no significant effect of scale on the behaviour of the slabs has been found.

(vii) The ultimate load carrying capacity of R.C. waffle slabs increases with the increase of rib depth to slab thickness ratio, i.e. d/t ratio, and this increase is characterised by the curve shown in

Fig.8.12 and that the increase in steel area has no significant effect on the ultimate load capacity of the slabs.

9.2 SUGGESTIONS FOR FUTURE RESEARCH

The scope of this investigation has deen necessarily limited and can only be considered as a step forward in the process of establishing general characteristics and criteria for the design of reinforced concrete waffle slabs subjected to various loading and boundary conditions. Future investigations in the similar context are suggested as follows:

(i) fuller experimental and theoretical investigations with various side ratio and other boundary conditions;

(ii) fuller verification of the employed and proposed methods;

(iii) study of the effect of the combined bending and torsion resistance due to the presence of main reinforcements and stirrups in the ribs; and

(iv) fuller investigation into the behaviour of R.C. waffle slabs supported by columns.

REFERENCES:-

1. ACI 318-71
   Building Code requirements for reinforced concrete.
   American Concrete Institute, 1972.

2. Ajdukiewicz A.B. and A.T. Kliszczewicz
   Experimental analysis of limit states in a six-penal waffle flat-plate structure
   ACI Journal, November-December 1986.

3. Bares and Massonnet
   Analysis of beam-grids and orthotropic plates
   Crosby Lockwood & Son LTD.,
   SNTL- Publishers of Technical Literature, Prague, 1968.

4. Brotchie J.F. and Holley M.J.
   Membrane action in slabs
   ACI SP-30, 1970.

5. BS8110:1985
   Code of practice for the structural use of concrete.
   British Standards Institution, Nov. 1972.

6. Chen W.F. and Saleeb A.F.
   Constitutive equations for engineering materials
   Volume 1: Elasticity and Modelling
   A Wiley-Interscience Publication.

7. Christiansen K.P.
   The effect of membrane stresses on the ultimate strength of the interior panel in a reinforced concrete slab.
   The Structural Engineer, No. 8, August 1983.

8. Clark L.A.
   Concrete bridge design to BS 5400.
   Construction Press 1983.

9. Cope R.J. and Clark L.A.
   Concrete slabs- Analysis and Design.
   Elseviver applied science publishers 1984.

10. Cope R.J. and P.Vasudeva Rao
    Nonlinear finite element analysis of concrete slab structures
    Proc. Instn. Engineers, Part 2: 1977, Vol 63, March.

11. Cusens A.R. and Pama R.P.
    Bridge deck analysis
    A Wiley-Intersecience Publican 1975.

12. Cusens A.R. and Zeidan M.A. and Pama R.P.
    Elastic rigidities of ribbed plates
    Building science Vol 7, Pregramon Press 1972.

13. Cowan H.J.
The strength of plain, reinforced and prestressed concrete under the action of combined stresses, with the particular reference to the combined bending and torsion of rectangular sections.
Magzine of concrete research, Vol. 5, No. 14, Dec. 1953.

14. CP110:1972
Code of practice for the structural use of concrete.
British Standards Institution, Nov. 1972.

15. Dean D.L. and Omid'varan C.
Analysis of ribbed plates
Proc. of ASCE Journal of Structural Division, Vol 95, ST3, Mar.,1969.

16. Filonenko-Borodich M
Theory of elasticity
Foreign Languages Publishing House, Moscow.

17. Garas F.K. and Armer G.S.
Reinforced and Prestressed Microconcrete.
The Construction Press.

18. Garnham M.
The effect of compressive membrane action on the strength of reinforced concrete slabs.
The Hatfield Polytechnic, B.Sc. project report 1975.

19. Hambly E.C.
Bridge deck behaviour
Chapman & Hall 1976.

20. Hand F.R., Pecknold D.A. and Schnobrich W.C.
Nonlinear layered analysis of R.C. plates and shells
ASCE, Vol 99, ST7, July 1973.

21. Helal J.C.
Ribbed slabs spanning in two directions
Constructional and Engineering, April,1950.

22. Heyman J.
The limit design of a transversely loaded square grid.
Jour. Applied Mechanics, Vol. 19, 1952.

23. Heymen J.
The plastic design of grillages.
Engineering, Dec. 1953.

24. Heyman J.
Plastic design of frames Vol.2
Cambridge University Press, 1971

25. Ho S.L.
Ultimate strength of rectangular reinforcement concrete slabs with uniform and banded reinforcements by yield line analysis.
Dundee College of Technology, B.Sc.(Hons.) project report 1984.

26. Holmes M.
Plastic collapse loads for beam grillages.
Civil Engineering and P.W. Review, Vol. 56, May 1961.

27. Holmes M.
Plastic Collapse of beam grillages with end restraint.
Civil Engineering and P.W. Review, Vol. 56, Oct. 1961.

28. Holmes M. and Ray-Chaudhuri P.
The ultimate load of beam grillages.
International Journal of Mechnical Sciences, Vol. 7, 1965.

29. Hillerborg A.
Strip method of design
A Viewpoint Publication, 1974.

29'. Jacobson A.
Membrane Flexural failure modes of restained slabs
Proc. ASCE, Structural Division Vol 93, Oct.,1967.

30. Jofriet J.C. and McNiece G.M.
Finite element analysis of reinforced concrete slabs
ASCE, Structural Division, Vol 97, ST3, March 1971.

31. Johansen K.W.
Yield line formulae for slabs.
Cement and Concrete Association, London 1972.

32. Jones L.L.
Ultimate load analysis of reinforced and prestressed concrete structures
Chatto and Windus, London 1962.

33. Jones L.L. and Wood R.H.
Yield line analysis of slabs
Thames and Hudson, Chatto and Windus 1967.

34. Kemp E.L. and Sozen M.A. and Siess C.P.
Torsion in reinforced concrete.
University of Illinoise, Civil Engineering Studies,
Structural Research Series, No. 226, Sept. 1961.

35. Kirk D.W.
Concrete Tee-beams subjected to torsion and combined bending and torsion.
Ph.D. Thesis, Queen's University at Kingston Ontario,
March 1969.

36. Kirk D.W. and Lash S.D.
T-beams subjected to combined bending and torsion.
ACI Journal, Proc. Vol. 68, No. 2, Feb. 1971.

37. Kirk D.W. and Loveland N.C.
Unsymmetrically reinforced T-beams subjected to combined bending and torsion.
ACI Journal, Proc. Vol. 69, No. 8, Aug. 1972.

38. Lessig N.N.
Determination of load-bearing capacity of reinforced concrete elements with retangular cross-section subjected to flexural and torsion.
Concrete and Reinforced Concrete Institute, Moscow.
Proc. No. 5, 1959
Translated as Foreign Literature Study No. 371 by Portland Cement Association, Research and Development Laboratories, Skokie, Illinois.

39. Lin C.S. and Scordelis A.C.
Nonlinear analysis of R.C. shells of general form
ASCE, Structural Division, Vol 101, ST3, March 1975.

40. Livesley R.K.
Analysis of grid frames by an electron digital computer
Engineering 176, London 1958.

41. Livesley R.K.
Matrix methods of structural analysis
Pergamon 1964.

42. Magura D.D. and Gorley W.G.
Test to destructuction of a multipanel waffle slab structure-1964-1965 New York World's Fair
ACI Journal Sept.,1971.

43. Marshall C.M.C.
An investigation into the behaviour at ultimate load of reinforced concrete multipanel slab/beam systems.
M.Phil. Thesis, Hatfield Polytechnic, 1983.

44. McBean R.P.
Analysis of stiffened plates by the finite element method.
Stanford University Ph.D. Thesis 1968.

45. Makin M.
The effect of membrane action on the ultimate strength of reinforced concrete slabs.
The Hatfield Polytechnic, B.Sc. project report 1976.

46. Morice P.B. and Reynolds G.C.
The strength of simply supported slab bridges subjected to concentrated load.
Proc. of Symposium on the strength of concrete structures, London, May 1956.

47. Nadai A.
Theory of flow and fracture of solids.
2nd Eition, McGraw-Hill Book Co., Inc., New York, 1950.

48. Nagaraja R.
The ultimate strength of reinforced concrete two and four beam highway bridges.
Ph.D. Thesis, Queen's University, Kingston, Ontario, 1969.

49. Nagaraja R. and Lash S.D.
Ultimate load capacity of reinforced concrete beam and slab highway bridges.
Proceedings ACI Journal, Vol. 67, Dec, 1970.

50. Neville A.
Properties of concrete
Pitman International, Third edition

51. Ockleston A.J.
Load tests on reinforced concrete slabs spanning in two directions.
Paper No.6, Portland and Cement Institute, Richmond, Johannesburg, Oct. 1958.

52. Park R.
Ultimate strength of rectangular concrete slabs under short-term uniform loading with edges restrained against lateral movement.
Proc. ICE Vol. 28, June 1964.

53. Park R.
The ultimate strength and long-term behaviour of uniformly loaded two-way concrete slabs with partial lateral restraint at all edges.
Magzine of Concrete Research, Vol. 16, No. 48, Sept. 1964.

54. Park R.
The lateral stifness and strength required to ensure membrane action at the ultimate load of a reinforced concrete slab-and-beam floor.
Magazine of concrete research, Vol. 17, No. 50, March 1965.

55. Park R.
Further test on a reinforced concrete floor designed by limit procedures.
ACI Publication SP-30 1970.

56. Parkman S.F.
The effect of compressive membrane action on reinforced concrete slabs.
The Hatfield Polytechnic, B.Sc. project report 1974.

57. Powell D.S.
Ultimate strength of concrete panels subjected to uniformly distributed loads.
Cambridge University Thesis 1956.

58. Powell G.H. and Ogden D.W.
Analysis of orthotropic steel plate bridge decks.
Proc. A.S.C.E., Vol. 95, May 1969.

59. Ramakrishnan V. and Vijayarangan B.
The influence of combined bending and torsion on rectanglur beams without web reinforcement.
The Indian Concrete Journal, Vol. 37, No. 11, Nov. 1963.

60. Ray-Chaudhuri P.
The ultimate load of beam grillages.
Ph.D. Thesis, University of Leeds, 1964.

61. Reddy V.M. and Hendry A.M.
Ultimate load behaviour of composite steel-concrete bridge deck structures.
Indian Concrete Journal, May 1969.

62. Reynolds G.C.
The strength of prestressed concrete slab bridges with edge beams.
Technical report, TRA/237, Cement and Concrete Association, London, Dec. 1956.

63. Reynolds G.C.
The strength of prestressed concrete grillage bridges.
Technical Report, TRA/268, C & C Association, London, June 1957.

64. Reiss M. and Sokal J.
Design of ribbed flat slabs.
The Structural Engineer, Vol. 50, No. 8, 1972.

65. Robinson J.
Integrated theory of finite element methods
A Wiley-International Publication 1973.

66. Sawko F. and Saha G.P.
Ultimate load analysis of bridge decks.
Building Science, Vol.2, 1967

67. State-of-the-Art Report
Finite element analysis of reinforced concrete
ASCE, New York.

68. Tatsa Z.Z. and Levy M.
Two-way skewed ribbed slabs
Proc.Instn.Civil Engineers, Part 2, Vol 59, Dec.,1975.

69. Tasuji M.E., Nilson A.H. and Slate F.O.
Biaxial stress-strain relationship for concrete
MCR, Vol 31, No. 109, Dec.,1979.

70. Tebbett I.E.
Analysis and design of rib-stiffened plates and slabs.
Ph.D. Thesis, University of Leeds, 1976.

71. Tebbett I.E. and Harrop J.
Analytical design of ribbed flat slabs.
The Structural Engineer, Vol. 57A, No. 7, 1979.

72. Thakkar M.C. and Sridhar Ras J.K.
Design of two way reinforced concrete rectangular slabs by modified Hillerborg's strip method
Indian Concrete Journal, Vol 44: No. 4, Apr.,1970.

73. Timoshenko S. and Goodier J.H.
Theory of elasticity
McGraw-Hill, New York 1951.

74. Timoshenko S.P. and Woinowoky-Krieger S.
Theory of plates and shells.
McGraw-Hill Book Co., Second edition 1970.

75. Tong P.Y. and Batchelor B dev.
Compressive membrane enhancement in two-way bridge slabs.
ACI Publication SP-30 1970.

76. Tottenham H. and Brebbia C.
Finite element techniques in structural mechanics
Southampton University press 1970.

77. Tresca H.
Memoire sur I'econlement des corps solides.
Mem. Pres. par div., sav 18, 1868.

78. Ugural A.C.
Stress in plates and shells.
McGraw-Hill Book Company.

79. Victor D.J. and Ferguson P.M.
Reinforced COncrete T-beams without stirrups under combined bending and torsion.
ACI Journal, Proc. Vol. 65, No. 1, Jan. 1968.

80. Victor D.J. and Aravindan P.K.
Prestressed and reinforced concrete T-beams under combined bending and torsion.
ICE Proc. Vol. 47, Nov. 1970.

81. Walsh P.F. and Collins M.P. and Archer F.E. and Hall A.S.
Experiments of the strength of concrete beams in combined flexural and torsion.
UNICIV Report No. R-15, Feb. 1966.
University of New South Wales, Kensington, Australia.

82. Wood R.H. and Armer G.S.T.
The theory of the strip method for design of slabs.
Proc. ICE, Vol 41, Oct. 1968.

83. Woodhead H.R. and McMullen A.E. and De Paiva H.A.R.
Combined bending and torsion in longitudinally reinforced T-beams.
ICE Proc. Vol. 47, Nov. 1970.

84. Zienkiewicz O.C.
The finite element method
McGraw Hill 1970.

APPENDIX A

R.C. Waffle Slab A3

Uniformly Distributed Load Vs Deflections

U.D.L.	Dial Guage No.								
	(1)	(2)	(3)	(4)	(5)	(6)	(7)	(8)	(9)
[kN/m²]	[mm]								
6.895	0.27	0.05	0.12	0.12	0.14	0.20	0.32	0.02	0.03
13.790	0.47	0.09	0.19	0.24	0.21	0.35	0.49	0.02	0.03
20.684	0.71	0.15	0.29	0.33	0.35	0.62	0.75	0.02	0.05
27.579	0.99	0.21	0.41	0.48	0.46	0.80	1.01	0.02	0.00
34.474	1.37	0.30	0.62	0.67	0.65	1.17	1.37	0.06	0.01
41.369	1.81	0.42	0.81	0.94	0.85	1.58	1.85	0.07	0.03
48.263	2.25	0.56	1.05	1.18	1.06	1.97	2.31	0.05	0.06
55.158	2.80	0.71	1.33	1.43	1.33	2.48	2.92	0.06	0.04
62.053	3.44	0.88	1.65	1.80	1.62	3.01	3.64	0.20	0.03
68.946	4.14	1.05	1.97	2.19	1.96	3.58	4.33	0.20	0.07
75.842	5.03	1.33	2.45	2.67	2.36	4.42	5.30	0.24	0.11
82.737	6.18	1.62	2.96	3.28	2.85	5.41	6.41	0.32	0.13
89.632	7.70	2.02	3.65	4.07	3.56	6.72	7.97	0.45	0.20
96.527	9.96	2.53	4.61	5.13	4.48	8.54	10.10	0.65	0.26
103.421	14.92	3.61	6.47	7.41	6.37	12.32	14.75	0.90	0.59
98.250	17.32	4.03	7.48	8.65	7.18	14.13	17.26	1.07	0.91
89.632	23.82	5.37	10.10	11.96	9.78	19.28	24.07	1.53	----
82.737	27.91	6.65	12.11	14.02	12.23	23.10	28.39	1.89	----
79.290	27.92	6.70	12.12	14.04	12.33	23.13	28.40	1.92	----
73.085	33.25	10.06	16.02	17.43	18.54	30.77	35.41	2.80	----

R.C. Waffle Slab A3

Uniformly Distributed Load Vs Concrete Strains

U.D.L.	Demec Gauge No.								
	MID-RIB	(1)	(2)	(3)	(4)	(5)	(6)	(7)	(8)
[kN/m²]	[10^{-3}]								
6.895	0.128	0.021	0.043	0.021	0.011	0.054	0.054	0.086	0.064
13.790	0.246	0.021	0.043	0.054	0.011	0.086	0.064	0.182	0.086
20.684	0.342	0.021	0.054	0.064	0.021	0.128	0.118	0.385	0.26
27.579	0.514	0.021	0.054	0.107	0.032	0.161	0.161	0.417	0.360
34.474	0.770	0.043	0.064	0.128	0.043	0.203	0.246	0.621	0.514
41.369	1.049	0.054	0.075	0.150	0.064	0.289	0.332	0.877	0.696
47.263	1.220	0.054	0.086	0.182	0.096	0.385	0.471	1.102	0.856
55.158	1.616	0.043	0.096	0.203	0.139	0.460	0.717	1.348	1.070
62.053	2.002	0.043	0.118	0.257	0.193	0.556	0.931	1.637	1.241
68.946	2.515	0.043	0.086	0.332	0.257	0.653	1.091	1.947	1.552
75.842	3.296	0.054	0.086	0.439	0.321	0.770	1.305	2.365	1.830
82.737	4.441	0.075	0.086	0.556	0.428	0.910	1.552	2.878	2.215
89.632	6.142	0.139	0.075	0.653	0.567	1.049	1.851	3.520	2.731
96.527	8.935	0.193	0.096	0.824	0.706	1.263	2.226	4.580	3.530
103.421	-----	0.396	0.161	0.830	0.728	1.873	3.039	7.511	5.350

R.C. Waffle Slab A3

Uniformly Distributed Load Vs Steel Strains

U.D.L.	Strain Gauge No.				Edge
	Short Spanning		Long Spanning		Rotation
	Mid-span	Support	Mid-span	Support	
[kN/m^2]	[10^{-3}]		[10^{-3}]		[10^{-3}]
6.895	0.122	0.054	0.112	0.037	0.100
13.790	0.189	0.090	0.159	0.072	0.200
20.684	0.380	0.135	0.227	0.105	0.340
27.579	0.616	0.217	0.301	0.146	0.487
34.474	0.765	0.387	0.374	0.214	0.547
41.369	0.938	0.524	0.450	0.278	0.707
48.263	1.123	0.639	0.532	0.338	0.900
55.158	1.364	0.814	0.632	0.412	1.107
62.053	1.712	0.977	0.769	0.510	1.340
68.946	2.170	1.206	0.939	0.619	1.567
75.842	2.888	1.401	1.184	0.722	1.813
82.737	3.922	1.786	1.542	0.900	2.200
89.632	5.255	2.313	2.034	1.218	2.567
96.527	7.268	3.062	2.818	1.765	3.093
103.421	12.401	8.115	4.350	1.613	3.933
98.250	-----	8.908	4.932	1.300	4.227
89.632	-----	-----	6.956	2.002	4.373
82.737	-----	-----	7.572	3.477	4.413
79.290	-----	-----	-----	3.522	4.353
73.085	-----	-----	-----	5.896	4.133

R.C. Waffle Slab B3

Uniformly Distributed Load Vs Deflections

U.D.L.	Dial Gauge No.					
	(S1)	(S2)	(S3)	(1)	(2)	(3)
[kN/m^2]	[mm]					
6.895	0.02	0.04	0.06	0.00	0.00	0.00
13.790	0.08	0.19	0.20	0.01	0.03	0.06
20.684	0.14	0.32	0.33	0.02	0.15	0.14
27.579	0.24	0.52	0.54	0.07	0.20	0.22
34.474	0.34	0.73	0.75	0.11	0.29	0.33
41.369	0.46	0.97	1.00	0.14	0.36	0.43
48.263	0.63	1.29	1.31	0.23	0.46	0.55
55.158	0.77	1.64	1.66	0.30	0.61	0.72
62.053	1.02	2.02	2.02	0.40	0.78	0.94
68.946	1.21	2.38	2.36	0.45	0.94	1.07
68.946*	1.30	2.57	2.55	0.50	1.01	1.17
75.842	1.47	2.87	2.85	0.55	1.11	1.33
82.737	1.73	3.35	3.31	0.69	1.35	1.57
89.632	1.99	3.85	3.80	0.79	1.56	1.78
96.527	2.36	4.54	4.47	0.95	1.85	2.13
103.421	2.66	5.12	5.06	1.12	2.12	2.42
110.320	3.12	5.99	5.94	1.32	2.48	2.82
117.215	3.57	6.86	6.80	1.60	2.84	3.29
124.110	4.11	7.92	7.85	1.82	3.26	3.78
131.005	4.86	9.30	9.29	2.19	3.85	4.50
137.900	5.46	10.55	10.64	2.47	4.32	5.10
144.795	6.21	12.00	12.19	2.88	4.98	5.92
151.690	7.76	14.85	15.19	3.56	6.22	7.34
158.585	8.81	16.85	17.29	4.03	7.01	8.35
158.585*	10.26	19.70	20.49	4.74	8.36	10.05
165.480	13.06	24.85	25.80	6.05	10.90	12.94
144.795	14.37	27.78	28.79	6.72	12.14	14.52
131.005	16.76	32.45	33.65	7.74	14.27	17.15
124.110	18.76	36.55	37.70	8.67	16.10	19.48
110.320	21.40	41.52	42.92	----	----	----
106.183	25.01	45.65	48.15	----	----	----

R.C. Waffle Slab B3

Uniformly Distributed Load Vs Deflections

U.D.L.	Dial Gauge No.				
	(4)	(5)	(6)	(7)	(8)
[kN/m^2]			[mm]		
6.895	0.00	0.00	0.00	0.00	0.00
13.790	0.01	0.04	0.04	0.00	0.00
20.684	0.06	0.14	0.11	0.00	0.00
27.579	0.13	0.26	0.31	0.00	0.00
34.474	0.18	0.33	0.44	0.00	0.00
41.369	0.23	0.56	0.67	0.00	0.00
48.263	0.35	0.78	0.92	0.00	0.00
55.158	0.44	1.00	1.19	0.00	0.00
62.053	0.57	1.24	1.54	0.00	0.00
68.946	0.69	1.46	1.76	0.00	0.00
68.946*	0.75	1.61	1.92	0.00	0.00
75.842	0.85	1.83	2.23	0.01	0.00
82.737	1.04	2.15	2.57	0.06	0.00
89.632	1.21	2.48	3.01	0.10	0.00
96.527	1.43	2.96	3.62	0.20	0.00
103.421	1.65	3.41	4.21	0.24	0.00
110.320	1.94	4.11	4.96	0.26	0.00
117.215	2.25	4.65	5.79	0.39	0.00
124.110	2.58	5.38	6.75	0.36	0.00
131.005	3.09	6.48	8.09	0.52	0.00
137.900	3.53	7.42	9.26	0.61	0.00
144.795	4.10	8.58	10.76	0.72	0.00
151.690	5.26	10.86	13.66	0.92	0.00
158.585	6.01	12.32	15.49	1.13	0.00
158.585*	7.22	14.81	18.52	1.40	0.18
165.480	9.86	19.71	24.23	1.99	2.21
144.795	11.17	22.29	27.36	2.51	3.14
131.005	13.46	26.57	32.35	3.56	4.84
124.110	15.39	30.25	36.88	5.60	6.21
110.320	----	----	----	----	----
106.183	----	----	----	----	----

R.C. Waffle Slab B3

Uniformly Distributed Load Vs Concrete Strains

U.D.L.	Demec Gauge No.								
	(1)	(2)	(3)	(4)	(5)	(6)	(7)	(8)	(9)
[kN/m^2]					[10^{-3}]				
6.895	0.086	0.000	0.000	0.011	0.064	0.000	0.011	0.011	0.021
13.790	0.161	0.000	0.011	0.075	0.118	0.000	0.011	0.086	0.107
20.684	0.182	0.000	0.021	0.086	0.182	0.000	0.011	0.128	0.203
27.579	0.300	0.043	0.054	0.161	0.278	0.000	0.021	0.171	0.321
34.474	0.449	0.032	0.064	0.246	0.364	0.000	0.032	0.225	0.417
41.369	0.567	0.032	0.075	0.289	0.439	0.000	0.043	0.251	0.556
48.263	0.770	0.054	0.118	0.364	0.610	0.011	0.064	0.300	0.717
55.158	0.984	0.043	0.118	0.449	0.771	0.011	0.075	0.396	0.910
62.053	1.091	0.054	0.139	0.546	0.899	0.011	0.075	0.578	1.124
68.946	1.156	0.054	0.171	0.663	1.070	0.011	0.086	0.610	1.305
75.842	1.605	0.064	0.193	0.824	1.273	0.011	0.107	0.760	1.552
82.737	1.840	0.064	0.235	0.974	1.445	0.011	0.118	0.899	1.776
89.632	2.284	0.075	0.246	1.134	1.605	0.011	0.161	1.051	2.022
96.527	2.729	0.096	0.342	1.327	1.798	0.021	0.203	1.252	2.429
103.421	3.392	0.128	0.385	1.466	1.980	0.075	0.246	1.402	2.825
110.320	4.398	0.193	0.471	1.669	2.183	0.139	0.310	1.616	3.478
117.215	5.532	0.257	0.546	1.873	2.386	0.182	0.417	1.808	4.109
124.110	6.827	0.321	0.653	2.054	2.622	0.235	0.492	1.980	4.858
131.005	8.860	0.428	0.770	2.322	2.921	0.300	0.599	2.194	5.939
137.900	10.893	0.546	0.867	2.547	3.210	0.353	0.685	2.333	6.880
144.795	13.546	0.621	0.974	2.814	3.563	0.417	0.770	2.546	8.111
151.690	18.094	0.792	1.145	3.253	4.194	0.524	0.899	2.868	10.304
158.585	---	0.888	1.252	3.606	4.708	0.599	0.963	3.103	11.866

R.C. Waffle Slab B3

Uniformly Distributed Load Vs Steel Strains

U.D.L.	Strain Gauge No.			
	Short Spanning		Long Spanning	
	Mid-span	Support	Mid-span	Support
[kN/m^2]	[10^{-3}]		[10^{-3}]	
6.895	0.018	0.008	0.014	0.007
13.790	0.065	0.033	0.151	0.066
20.684	0.098	0.055	0.238	0.085
27.579	0.152	0.093	0.297	0.097
34.474	0.279	0.216	0.377	0.110
41.369	0.382	0.262	0.444	0.174
48.263	0.399	0.340	0.490	0.233
55.158	0.243	0.395	0.525	0.450
62.053	0.251	0.443	0.587	0.687
68.946	0.280	0.515	SLIP	0.728
68.946*	0.389	0.519	-----	0.749
75.842	0.463	0.569	-----	0.693
82.737	0.417	0.545	-----	SLIP
89.632	SLIP	0.526	-----	-----
96.527	-----	0.576	-----	-----
103.421	-----	0.631	-----	-----
110.320	-----	0.690	-----	0.704
117.215	-----	0.740	-----	2.292
124.110	-----	0.775	0.631	3.579
131.005	-----	0.866	0.886	5.583
137.99	-----	0.963	-----	7.259
144.795	-----	1.136	-----	9.359
151.690	-----	1.648	-----	10.349
158.585	-----	3.749	-----	10.829

R.C. Waffle Slab C3

Uniformly Distributed Load Vs Deflections

U.D.L.	Dial Gauge No.					
	(1)	(2)	(3)	(4)	(5)	(6)
[kN/m^2]	[mm]					
10.343	0.06	0.09	0.12	0.00	0.07	0.03
20.684	0.11	0.18	0.29	0.02	0.10	0.10
31.028	0.16	0.29	0.44	0.05	0.18	0.17
41.369	0.24	0.43	0.65	0.10	0.24	0.27
48.265	0.30	0.53	0.80	0.10	0.27	0.32
55.160	0.41	0.68	1.03	0.18	0.41	0.49
62.055	0.49	0.86	1.25	0.22	0.51	0.57
68.950	0.60	1.02	1.54	0.26	0.59	0.75
79.293	0.73	1.25	1.89	0.37	0.76	0.88
89.635	0.89	1.51	2.31	0.43	0.94	1.07
99.976	1.08	1.81	2.76	0.51	1.13	1.25
110.320	1.29	2.13	3.21	0.67	1.37	1.52
120.663	1.57	2.57	3.93	0.82	1.62	1.83
131.005	1.84	3.00	4.60	0.94	1.86	2.13
141.348	2.14	3.47	5.30	1.07	2.11	2.41
151.690	2.79	4.41	6.70	1.39	2.65	3.05
162.033	3.17	5.01	7.62	1.56	2.92	3.41
172.375	3.70	5.80	8.85	1.81	3.32	3.85
182.718	4.37	6.80	10.43	2.09	3.82	4.45
193.060	5.08	7.82	12.05	2.42	4.35	5.08
203.403	6.03	9.18	14.20	2.77	5.04	5.92
213.745	7.18	10.85	16.90	3.13	5.68	6.67
220.640	8.57	12.78	19.95	3.75	6.78	8.08
227.535	10.05	14.87	23.15	4.43	7.79	9.48
230.983	11.35	16.65	25.70	4.79	8.57	10.51
222.364	13.20	19.43	29.10	5.27	9.66	11.85
217.193	14.34	21.17	31.02	5.58	10.32	12.73
210.298	16.35	24.14	34.03	6.01	11.17	14.02
206.850	17.02	25.12	35.00	6.15	11.48	14.48

R.C. Waffle Slab C3

Uniformly Distributed Load Vs Deflections

U.D.L.	Dial Gauge No.				
	(7)	(8)	(9)	(10)	(11)
[kN/m^2]	[mm]				
10.343	0.02	0.07	0.09	0.06	0.07
20.684	0.06	0.14	0.20	0.09	0.15
31.028	0.13	0.24	0.35	0.19	0.27
41.369	0.20	0.42	0.54	0.21	0.46
48.265	0.25	0.46	0.65	0.32	0.52
55.160	0.33	0.64	0.89	0.43	0.72
62.055	0.39	0.77	1.08	0.42	0.82
68.950	0.48	1.00	1.32	0.57	1.02
79.293	0.64	1.26	1.64	0.71	1.35
89.635	0.77	1.50	1.97	0.91	1.62
99.976	0.93	1.81	2.28	0.94	1.88
110.320	1.09	2.14	2.75	1.17	2.28
120.663	1.29	2.55	3.22	1.42	2.73
131.005	1.50	2.91	3.77	1.61	3.20
141.348	1.72	3.29	4.26	1.84	3.61
151.690	2.21	4.27	5.45	2.30	4.62
162.033	2.51	4.71	6.08	2.57	5.15
172.375	2.83	5.38	6.88	3.00	5.90
182.718	3.28	6.25	7.95	3.41	6.88
193.060	3.75	7.20	9.15	4.00	7.94
203.403	4.44	8.43	10.67	4.58	9.31
213.745	5.04	9.61	12.16	5.28	10.53
220.640	6.01	11.48	14.52	6.23	12.69
227.535	7.04	13.44	16.90	7.28	14.77
230.983	7.76	14.89	18.88	8.12	16.39
222.364	8.73	16.74	21.24	9.13	18.29
217.193	9.28	17.94	22.82	9.77	19.56
210.298	10.06	19.50	25.10	10.62	21.24
206.850	10.34	20.05	25.97	10.96	21.89

R.C. Waffle Slab C3
Uniformly Distributed Load Vs Concrete Strains

U.D.L. [kN/m²]	Demec Gauge No. [10⁻³] (1)	(2)	(3)	(4)	(5)	(6)
10.343	0.021	0.000	0.011	-0.021	0.011	0.000
20.684	-0.032	0.011	0.021	0.021	0.032	0.021
31.028	-0.011	0.032	0.000	0.054	0.054	0.032
41.369	-0.011	0.075	0.000	0.086	0.075	0.032
48.265	-0.032	0.075	-0.011	0.107	0.086	0.043
55.160	-0.032	0.075	-0.011	0.145	0.107	0.043
62.055	-0.011	0.075	0.000	0.193	0.150	0.064
68.950	0.032	0.118	0.011	0.268	0.193	0.086
79.293	0.021	0.118	-0.021	0.342	0.225	0.107
89.635	-0.021	0.139	-0.011	0.407	0.321	0.128
99.976	0.011	0.150	-0.021	0.492	0.375	0.161
110.320	0.096	0.193	-0.032	0.567	0.439	0.182
120.633	0.161	0.289	-0.021	0.674	0.535	0.225
131.005	0.203	0.375	-0.011	0.813	0.631	0.268
141.348	0.246	0.471	-0.021	0.867	0.728	0.300
151.690	0.417	0.706	-0.021	1.081	0.910	0.396
162.033	0.503	0.813	-0.021	1.198	1.027	0.449
172.375	0.567	1.078	-0.032	1.295	1.166	0.514
182.718	0.706	1.145	-0.054	1.423	1.305	0.599
193.060	0.835	1.295	-0.096	1.541	1.455	0.642
203.403	0.931	1.477	-0.150	1.701	1.659	0.674
213.745	1.081	1.637	-0.182	1.937	1.873	0.738
220.640	1.273	1.851	-0.203	2.194	2.140	0.792
227.535	1.487	2.044	-0.203	2.386	2.354	0.803

U.D.L. [kN/m²]	Demec Gauge No. [10⁻³] (7)	(8)	(9)	(10)	(11)	(12)
10.343	0.043	0.032	0.011	0.032	0.064	0.107
20.684	0.086	0.075	0.021	0.043	0.118	0.268
31.028	0.107	0.150	0.032	0.053	0.150	0.428
41.369	0.161	0.246	0.043	0.043	0.193	0.621
48.265	0.203	0.321	0.053	0.021	0.235	0.706
55.160	0.300	0.417	0.064	0.000	0.300	0.845
62.055	0.353	0.599	0.096	0.032	0.364	1.006
68.950	0.417	0.728	0.118	0.032	0.449	1.166
79.293	0.482	0.888	0.150	0.043	0.524	1.423
89.635	0.567	1.070	0.171	0.053	0.631	1.712
99.976	0.663	1.252	0.289	0.096	0.760	1.990
110.320	0.813	1.477	0.353	0.086	0.889	2.301
120.663	1.006	1.755	0.439	0.086	1.059	2.643
131.005	1.156	2.001	0.514	0.107	1.220	2.996
141.348	1.295	2.247	0.599	0.096	1.380	3.306
151.690	1.573	2.729	0.813	0.107	1.744	4.013
162.033	1.733	3.071	1.006	0.096	1.980	4.537
172.375	1.958	3.456	1.188	0.086	2.279	5.179
182.718	2.247	3.959	1.412	0.043	2.664	5.949
193.060	2.568	4.483	1.669	-0.011	3.060	6.709
203.403	3.007	5.254	2.001	-0.107	3.612	7.907
213.745	3.552	5.981	2.311	-0.225	4.505	9.673
220.640	4.291	7.148	2.868	-0.289	5.789	12.690
227.535	5.147	8.271	3.392	-0.385	6.773	13.236

R.C.Waffle Slab C3

Uniformly Distributed Load Vs Concrete Strains

U.D.L. [kN/m^2]	Demec Gauge No. (13)	(14)	(15)	[10^{-3}] (16)	(17)
10.343	0.064	0.011	0.021	0.011	0.011
20.684	0.171	0.021	0.054	0.021	0.054
31.028	0.225	0.032	0.054	0.043	0.064
41.369	0.492	0.043	0.075	0.054	0.096
48.265	0.631	0.064	0.086	0.096	0.128
55.160	0.792	0.064	0.118	0.118	0.161
62.055	0.920	0.054	0.150	0.150	0.182
68.950	1.102	0.075	0.225	0.214	0.268
79.293	1.327	0.118	0.321	0.246	0.342
89.635	1.530	0.161	0.417	0.321	0.439
99.976	1.915	0.182	0.482	0.396	0.514
110.320	2.386	0.225	0.579	0.449	0.685
120.663	3.039	0.278	0.696	0.535	0.792
131.005	3.756	0.321	0.803	0.621	0.910
141.348	4.590	0.364	0.899	0.717	1.006
151.690	6.367	0.460	1.070	0.910	1.252
162.033	7.576	0.524	1.198	1.027	1.380
172.375	9.298	0.642	1.359	1.188	1.541
182.718	11.513	0.781	1.519	1.391	1.712
193.060	14.027	0.910	1.669	1.605	1.862
203.403	17.505	1.027	1.851	1.915	2.054
213.745	18.522	1.220	2.097	2.268	2.258
220.640	---	1.380	2.386	2.664	2.472
227.535	---	1.541	2.600	3.060	2.675

R.C.Waffle Slab C3

Uniformly Distributed Load Vs Steel Strains

U.D.L. [kN/m^2]	Demec Gauge No. [10^{-3}] (1)	(2)	(3)	(4)	(5)	(6)	(7)	(8)
10.343	0.110	0.051	0.025	0.023	0.088	0.018	0.010	0.008
20.684	0.165	0.122	0.043	0.042	0.214	0.040	0.020	0.014
31.028	0.340	0.229	0.065	0.064	0.343	0.070	0.031	0.023
41.369	0.615	0.368	0.086	0.085	0.494	0.082	0.044	0.031
48.265	0.714	0.452	0.101	0.099	0.578	0.156	0.056	0.039
55.160	0.870	0.587	0.124	0.113	0.661	0.284	0.073	0.051
62.055	0.975	0.701	0.310	0.274	0.714	0.390	0.094	0.071
68.950	1.132	0.848	0.470	0.340	0.000	0.539	0.216	0.140
79.293	1.377	1.016	0.616	0.462	0.000	0.731	0.489	0.258
89.635	1.707	1.222	0.632	0.596	0.000	0.804	0.646	0.266
99.976	2.119	1.482	1.098	0.668	0.000	0.957	0.740	0.306
110.320	3.800	1.990	2.422	0.745	0.000	1.149	0.863	0.717
120.663	7.041	2.680	6.879	0.825	0.000	1.348	1.056	2.109
131.005	9.169	3.443	11.129	0.802	0.000	1.577	1.459	3.247
141.348	0.000	3.995	13.967	0.903	0.000	1.778	1.442	4.369
151.690	0.000	2.028	0.000	1.001	0.000	2.070	1.549	8.749
162.033	0.000	2.343	0.000	1.132	0.000	2.234	1.728	10.785
172.375	0.000	2.669	0.000	1.269	0.000	2.252	2.045	12.437
182.718	0.000	3.021	0.000	1.444	0.000	2.242	3.533	14.786
193.060	0.000	3.360	0.000	1.613	0.000	0.000	9.068	0.000
203.403	0.000	3.337	0.000	1.920	0.000	0.000	0.000	0.000
213.745	0.000	6.878	0.000	2.452	0.000	0.000	0.000	0.000
220.640	0.000	0.000	0.000	2.970	0.000	0.000	0.000	0.000
227.535	0.000	0.000	0.000	3.935	0.000	0.000	0.000	0.000
230.983	0.000	0.000	0.000	5.047	0.000	0.000	0.000	0.000
222.364	0.000	0.000	0.000	7.019	0.000	0.000	0.000	0.000
217.193	0.000	0.000	0.000	8.212	0.000	0.000	0.000	0.000
210.298	0.000	0.000	0.000	10.998	0.000	0.000	0.000	0.000
206.850	0.000	0.000	0.000	11.808	0.000	0.000	0.000	0.000

R.C. WAFFLE SLAB D1

Uniformly Distributed Load Vs. Deflections

U.D.L. [kN/m²]	Dial Gauge No. (S3)	(S2)	(S1)	(1)	(2)	(3)
			[mm]			
6.895	0.01	0.05	0.02	0.00	0.03	0.00
13.790	0.03	0.09	0.04	0.00	0.07	0.01
24.133	0.11	0.16	0.07	0.00	0.07	0.05
34.475	0.28	0.29	0.12	0.03	0.07	0.07
44.818	0.46	0.43	0.18	0.06	0.15	0.15
55.160	0.65	0.59	0.25	0.06	0.17	0.18
65.503	0.83	0.74	0.32	0.06	0.18	0.20
75.845	1.09	0.96	0.42	0.15	0.29	0.30
86.188	1.34	1.19	0.54	0.21	0.38	0.42
96.530	1.71	1.52	0.70	0.29	0.55	0.59
106.873	2.27	2.00	0.95	0.45	0.69	0.81
117.215	2.87	2.47	1.20	0.60	0.94	1.07
127.558	3.34	2.84	1.39	0.70	1.12	1.22
127.558	3.63	3.05	1.49	0.80	1.22	1.34
137.900	4.04	3.36	1.65	0.90	1.37	1.49
148.243	4.77	3.94	1.96	1.08	1.57	1.74
158.585	5.55	4.55	2.28	1.30	1.88	2.01
168.928	6.39	5.21	2.64	1.52	2.12	2.30
179.270	7.43	6.02	3.05	1.78	2.46	2.62
189.613	8.58	6.87	3.50	2.09	2.87	3.03
199.955	10.88	7.86	4.02	2.43	3.30	3.49
206.850	11.82	8.45	4.40	2.68	3.59	3.81
213.745	12.66	9.18	4.47	2.85	3.85	4.09
220.640	14.99	10.17	5.25	3.18	4.33	4.57
227.535	15.08	10.96	5.68	3.49	4.66	4.93
234.430	16.35	11.90	6.17	3.79	5.06	5.36
241.325	17.38	12.64	6.56	4.07	5.43	5.75
248.220	18.62	13.54	7.03	4.38	5.82	6.15
255.115	20.50	14.87	7.78	4.90	6.48	6.78
258.563	22.45	16.27	9.50	5.40	7.03	7.43
262.010	23.80	17.95	10.42	5.99	7.77	8.16
268.905	26.00	19.50	10.25	6.61	8.60	9.05
275.800	29.00	21.60	12.40	7.31	9.57	10.07

R.C. WAFFLE SLAB D1

Uniformly Distributed Load Vs. Deflections

U.D.L. [kN/m²]	Dial Gauge No. (4)	(5)	(6) [mm]	(7)	(8)
6.895	0.01	0.02	0.00	0.01	0.01
13.790	0.05	0.07	0.04	0.02	0.04
24.133	0.06	0.11	0.09	0.04	0.11
34.475	0.08	0.20	0.22	0.04	0.19
44.818	0.15	0.34	0.37	0.05	0.36
55.160	0.17	0.40	0.44	0.10	0.48
65.503	0.24	0.53	0.54	0.08	0.51
75.845	0.29	0.70	0.72	0.17	0.73
86.188	0.36	0.87	0.91	0.29	0.88
96.530	0.50	1.08	1.23	0.36	1.11
106.873	0.66	1.47	1.61	0.50	1.50
117.215	0.84	1.85	2.06	0.75	1.85
127.558	0.99	2.15	2.41	0.91	2.18
127.558	1.08	2.28	2.64	0.97	2.35
137.900	1.21	2.52	2.93	1.03	2.64
148.243	1.37	2.91	3.38	1.13	3.02
158.585	1.57	3.43	3.85	1.36	3.40
168.928	1.77	3.80	4.43	1.52	3.88
179.270	2.03	4.37	5.09	1.61	4.45
189.613	2.29	4.99	5.85	1.89	5.05
199.955	2.67	5.77	6.68	2.34	5.78
206.850	2.94	6.30	7.28	2.54	6.34
213.745	3.14	6.79	7.80	3.04	6.82
220.640	3.50	7.54	8.67	2.94	7.53
227.535	3.79	8.18	9.38	2.92	8.17
234.430	4.15	8.84	10.15	3.14	8.83
241.325	4.40	9.51	10.87	3.84	9.42
248.220	4.75	10.20	11.61	3.59	10.12
255.115	5.22	11.29	12.80	4.34	11.18
258.563	5.72	12.33	13.97	4.73	12.23
262.010	6.30	13.58	15.31	5.13	13.45
268.905	7.01	14.98	16.83	5.80	14.81
275.800	7.84	16.60	18.70	6.00	16.48

R.C. WAFFLE SLAB D1

Uniformly Distributed Load Vs. Concrete Strains

U.D.L. [kN/m^2]	Demec Gauge No. (1)	(2)	(3)	(4)	(5)	(6)
			[10^{-3}]			
6.895	0.011	0.000	0.011	0.021	0.000	0.021
13.790	0.011	0.021	0.011	0.118	0.000	0.021
24.133	0.021	-0.011	0.000	0.086	0.000	0.000
34.475	0.011	-0.011	0.000	0.096	0.032	0.000
44.818	0.021	0.000	0.000	0.096	0.043	-0.011
55.160	0.054	0.118	-0.021	0.107	0.054	-0.021
65.503	0.182	0.193	-0.032	0.096	0.064	-0.032
75.845	0.300	0.353	-0.064	0.086	0.043	-0.054
86.188	0.407	0.471	-0.086	0.096	0.054	-0.064
96.530	0.599	0.642	-0.107	0.107	0.054	-0.086
106.873	0.824	0.899	-0.118	0.107	0.064	-0.086
117.215	1.017	1.145	-0.128	0.161	0.032	-0.086
127.558	1.166	1.316	-0.128	0.203	-0.021	-0.064
127.558	1.134	1.370	-0.139	0.246	-0.021	-0.086
137.900	1.188	1.455	-0.161	0.278	-0.021	-0.086
148.243	1.273	1.616	-0.161	0.417	-0.021	-0.107
158.585	1.423	1.830	-0.171	0.524	-0.011	-0.128
168.928	1.594	2.087	-0.171	0.631	-0.021	-0.139
179.270	1.830	2.418	-0.193	0.749	-0.011	-0.150
189.613	2.119	2.836	-0.193	0.888	0.011	-0.193
199.955	2.461	3.403	-0.214	0.931	0.024	-0.203
206.850	2.664	3.766	-0.214	0.984	0.075	-0.182
213.745	2.814	4.087	-0.235	1.049	0.118	-0.161
220.640	3.060	4.569	-0.235	1.156	0.203	-0.118
227.535	3.285	4.965	-0.256	1.241	0.235	-0.086
234.430	3.692	5.832	-0.278	1.434	0.353	-0.043
241.325	3.938	6.302	-0.278	1.530	0.396	-0.021
248.220	4.291	7.030	-0.289	1.669	0.471	0.021
255.115	4.590	7.747	-0.300	1.830	0.535	0.054
258.563	4.997	8.507	-0.300	2.001	0.653	0.118

R.C. WAFFLE SLAB D1

Uniformly Distributed Load Vs. Concrete Strains

U.D.L. [kN/m^2]	Demec Gauge No. (7)	(8)	(9)	(10)	(11)	(12)
			[10^{-3}]			
6.895	0.021	0.011	0.000	0.021	0.000	0.021
13.790	0.031	0.054	0.000	0.042	0.032	0.043
24.133	0.031	0.075	0.000	0.021	0.021	0.054
34.475	0.043	0.075	0.000	0.021	0.032	0.064
44.818	0.064	0.096	0.021	0.000	0.064	0.043
55.160	0.075	0.278	0.021	0.000	0.064	0.054
65.503	0.128	0.471	0.032	-0.021	0.086	0.075
75.845	0.128	0.503	0.032	-0.021	0.086	0.064
86.188	0.139	0.696	0.043	-0.032	0.086	0.075
96.530	0.150	0.931	0.054	-0.043	0.107	0.096
106.873	0.150	1.263	0.086	-0.043	0.128	0.171
117.215	0.161	1.562	0.086	-0.032	0.235	0.364
127.558	0.182	1.787	0.086	-0.032	0.289	0.546
127.558	0.182	1.894	0.096	-0.043	0.332	0.696
137.900	0.193	2.001	0.107	-0.054	0.375	0.899
148.243	0.193	2.258	0.118	-0.032	0.439	1.263
158.585	0.203	2.579	0.128	-0.043	0.492	1.616
168.928	0.225	2.932	0.139	-0.054	0.556	1.937
179.270	0.225	3.392	0.150	-0.043	0.642	2.365
189.613	0.278	3.820	0.182	-0.065	0.706	2.985
199.955	0.321	3.938	0.193	-0.075	0.760	3.863
206.850	0.353	3.970	0.235	-0.086	0.835	4.451
213.745	0.460	4.291	0.257	-0.086	0.899	4.954
220.640	0.503	4.537	0.278	-0.107	0.984	5.746
227.535	0.567	4.717	0.300	-0.107	1.091	6.420
234.430	0.631	5.147	0.385	-0.128	1.316	7.758
241.325	0.663	5.382	0.407	-0.128	1.455	8.485
248.220	0.728	5.714	0.460	-0.139	1.669	9.544
255.115	0.781	6.056	0.503	-0.128	1.873	10.636
258.563	0.835	6.452	0.546	-0.171	2.108	12.904

R.C. WAFFLE SLAB E3

Uniformly Distributed Load Vs Deflections

U.D.L.	Dial Gauge No.					
	(1)	(2)	(3)	(4)	(5)	(M)
[kN/m²]	[mm]					
10.324	0.050	0.070	0.100	0.040	0.080	0.220
20.685	0.120	0.140	0.180	0.080	0.240	0.490
31.028	0.170	0.290	0.350	0.190	0.450	0.820
41.370	0.310	0.510	0.570	0.310	0.720	1.350
51.713	0.400	0.630	0.810	0.450	1.000	1.820
62.055	0.560	0.870	1.070	0.540	1.290	2.500
72.398	0.710	1.130	1.350	0.710	1.620	3.070
82.740	0.870	1.280	1.570	0.830	1.940	3.780
93.083	1.020	1.610	1.880	1.050	2.290	4.590
103.425	1.290	2.020	2.370	1.430	2.930	5.840
113.768	1.590	2.520	2.900	1.850	3.730	6.170
124.110	2.000	3.170	3.600	2.450	4.830	9.030
134.453	2.570	4.010	4.540	3.130	6.140	11.170
144.795	3.260	5.180	5.870	4.160	8.080	14.110
151.690	4.730	7.520	8.400	6.010	11.740	19.180
158.585	6.440	10.480	11.530	8.410	16.330	26.000
144.795	8.270	13.860	12.850	11.330	22.000	34.000
141.348	10.300	---	---	14.700	28.550	44.000
137.900	---	---	---	---	---	46.000

U.D.L.	Dial Gauge No.						
	(6)	(7)	(8)	(9)	(10)	(11)	(12)
[kN/m²]	[mm]						
10.324	0.007	0.050	0.010	0.050	0.060	0.110	0.130
20.685	0.230	0.050	0.070	0.350	0.130	0.230	0.270
31.028	0.470	0.030	0.200	0.630	0.200	0.350	0.420
41.370	0.810	0.130	0.350	1.120	0.320	0.560	0.660
51.713	1.070	0.170	0.520	1.520	0.430	0.770	0.900
62.055	1.410	0.150	0.630	2.120	0.590	1.050	1.220
72.398	1.860	0.190	0.860	2.530	0.711	1.270	1.480
82.740	2.110	0.320	1.040	3.170	0.880	1.550	1.800
93.083	2.520	0.360	1.340	3.800	1.070	1.820	2.160
103.425	3.240	0.640	1.870	4.750	1.380	2.370	2.690
113.768	4.150	0.950	2.570	5.740	1.680	2.840	3.220
124.110	5.490	1.250	3.460	7.160	2.100	3.480	3.930
134.453	7.100	1.770	4.580	8.690	2.560	4.200	4.710
144.795	9.470	2.500	6.060	10.850	3.180	5.170	5.800
151.690	13.910	3.950	9.110	14.600	4.260	6.820	7.630
158.585	19.690	5.940	13.020	19.900	5.610	8.970	10.130
144.795	27.530	8.550	17.930	26.200	7.000	11.350	13.270
141.348	36.830	11.890	---	34.500	8.900	14.500	17.200
137.900	---	---	---	35.950	9.250	15.100	17.750

R.C. Waffle Slab E3

Uniformly Distributed Load Vs Concrete Strains

U.D.L.	Demec Gauge No.							
	(1)	(2)	(3)	(4)	(5)	(6)	(7)	(8)
[kN/m^2]				[10^{-3}]				
10.324	0.008	0.016	0.040	0.008	0.056	0.008	0.008	0.064
20.685	0.024	0.032	0.080	0.016	0.112	0.000	0.000	0.112
31.028	0.032	0.048	0.128	0.016	0.128	-0.016	-0.008	0.128
41.370	0.032	0.064	0.184	0.008	0.192	-0.024	-0.024	0.176
51.713	0.024	0.072	0.264	0.024	0.288	-0.048	-0.040	0.216
62.055	0.016	0.096	0.304	0.040	0.352	-0.032	-0.048	0.360
72.398	-0.008	0.120	0.344	0.064	0.488	-0.008	-0.048	0.440
82.740	-0.024	0.136	0.400	0.104	0.608	0.008	-0.064	0.504
93.083	-0.048	0.184	0.488	0.232	0.720	0.000	-0.064	0.632
103.425	-0.024	0.296	0.624	0.304	0.848	0.024	-0.040	0.832
113.768	-0.024	0.424	0.760	0.384	1.040	0.000	0.040	0.952
124.110	0.000	0.568	0.928	0.488	1.248	-0.080	0.088	1.272
134.453	0.016	0.728	1.104	0.544	1.520	-0.224	0.120	1.552
144.795	0.096	0.928	1.304	0.600	1.952	-0.392	0.120	1.872
151.690	0.320	1.152	1.672	0.648	2.792	-0.592	0.104	2.608
158.585	0.512	1.264	2.024	0.568	3.808	-0.784	0.096	3.768

U.D.L.	Demec Gauge No.							
	(9)	(10)	(11)	(12)	(13)	(14)	(15)	(16)
[kN/m^2]				[10^{-3}]				
10.324	0.048	0.072	0.088	0.088	0.032	0.024	0.040	0.064
20.685	0.104	0.152	0.224	0.176	0.064	0.104	0.120	0.176
31.028	0.168	0.248	0.416	0.240	0.072	0.176	0.232	0.272
41.370	0.256	0.424	0.632	0.384	0.080	0.224	0.360	0.432
51.713	0.360	0.640	0.816	0.600	0.080	0.288	0.456	0.608
62.055	0.560	0.944	1.024	0.816	0.072	0.344	0.600	0.888
72.398	0.744	1.176	1.200	0.952	0.080	0.432	0.704	1.088
82.740	0.928	1.448	1.448	1.120	0.072	0.520	0.808	1.312
93.083	1.048	1.728	1.728	1.232	0.072	0.632	0.952	1.504
103.425	1.392	2.032	2.144	1.320	0.056	0.768	1.104	1.712
113.768	1.600	2.352	2.640	1.320	0.064	0.952	1.264	1.896
124.110	1.760	2.728	3.392	1.288	0.048	1.168	1.448	2.160
134.453	1.920	3.232	4.400	1.240	0.080	1.408	1.600	2.416
144.795	2.064	3.792	5.888	0.880	0.112	1.760	1.824	2.816
151.690	2.344	4.688	8.504	0.936	0.152	2.384	2.200	3.448
158.585	2.984	5.808	11.608	0.680	0.192	3.024	2.840	3.768

R.C. Waffle Slab E3

Uniformly Distributed Load Vs Concrete Strains

U.D.L.	Demec Gauge No.							
	(9)	(10)	(11)	(12)	(13)	(14)	(15)	(16)
[kN/m^2]				[10^{-3}]				
10.324	0.048	0.048	0.000	0.064	0.080	0.080	0.080	0.216
20.685	0.088	0.160	-0.016	0.104	0.200	0.272	0.208	0.360
31.028	0.192	0.288	-0.008	0.144	0.288	0.496	0.344	0.496
41.370	0.328	0.440	-0.016	0.200	0.408	0.808	0.664	0.776
51.713	0.376	0.624	-0.040	0.296	0.480	1.080	0.848	1.024
62.055	0.536	0.912	-0.032	0.400	0.592	1.408	1.056	1.320
72.398	0.640	1.160	-0.040	0.520	0.680	1.656	1.216	1.584
82.740	0.944	1.400	-0.056	0.696	0.784	2.080	1.456	1.920
93.083	1.128	1.776	-0.056	0.864	0.920	1.712	1.760	2.304
103.425	1.440	2.016	-0.088	1.088	1.048	3.320	2.312	3.040
113.768	1.728	2.120	-0.112	1.328	1.160	4.288	3.080	3.952
124.110	2.104	2.120	-0.160	1.672	1.256	5.616	4.472	5.344
134.453	2.648	2.088	-0.232	2.080	1.320	7.192	6.232	7.032
144.795	3.448	1.880	-0.312	2.680	1.216	9.552	8.872	9.880
151.690	4.832	1.496	-0.632	3.712	1.000	14.256	13.512	14.960
158.585	6.080	0.760	-0.632	5.080	1.000	17.256	17.352	17.360

R.C. Waffle Slab E3

Uniformly Distributed Load Vs Steel Strains

U.D.L.	Strain Gauge No. [10^{-3}]				
[kN/m^2]	(1)	(2)	(3)	(4)	(5)
10.324	0.360	0.530	1.989	5.600	0.360
20.685	0.860	2.261	5.778	4.691	0.800
31.028	1.510	6.946	6.151	6.130	1.270
41.370	1.825	0.773	9.524	---	1.810
51.713	---	---	13.715	---	2.080
62.055	---	---	20.175	---	5.970
72.398	---	---	23.890	---	7.490
82.740	---	---	28.000	---	8.782
93.083	---	---	32.490	---	10.205
103.425	---	---	---	---	11.930
113.768	---	---	---	---	13.700
124.110	---	---	---	---	16.430
134.453	---	---	---	---	20.240
144.795	---	---	---	---	25.910
151.690	---	---	---	---	32.630
158.585	---	---	---	---	38.950

R.C. Waffle Slab F3
Uniformly Distributed Load Vs Deflections

U.D.L.	Dial Gauge No. [mm]							
[kN/m²]	(1)	(2)	(3)	(4)	(5)	(6)	(7)	(8)
6.895	0.050	0.000	0.000	0.040	-0.010	0.080	0.010	0.030
13.790	0.050	0.000	0.020	0.080	0.010	0.120	0.130	0.090
20.685	0.050	0.000	0.050	0.130	0.020	0.210	0.170	0.180
27.580	0.120	0.040	0.070	0.180	0.100	0.270	0.320	0.280
34.475	0.120	0.050	0.160	0.280	0.160	0.360	0.320	0.430
41.370	0.120	0.100	0.220	0.390	0.230	0.550	0.320	0.620
48.265	0.210	0.180	0.290	0.520	0.390	0.740	0.280	0.840
55.160	0.260	0.280	0.420	0.700	0.520	1.010	0.710	1.180
55.160	0.280	0.280	0.440	0.780	0.590	1.090	0.710	1.260
62.055	0.330	0.350	0.560	0.950	0.770	1.400	0.960	1.570
68.950	0.400	0.450	0.710	1.130	0.920	1.660	1.090	1.910
75.845	0.510	0.550	0.880	1.430	1.150	2.100	1.360	2.440
82.740	0.640	0.720	1.150	1.790	1.460	2.660	1.790	3.240
89.635	0.850	0.960	1.450	2.360	1.940	3.460	2.300	4.320
96.530	1.060	1.120	1.770	2.860	2.420	4.270	2.840	5.350
103.425	1.300	1.460	2.210	3.650	2.940	5.440	3.600	6.840
110.320	1.690	1.900	2.820	4.740	3.800	7.070	4.610	9.020
113.768	2.000	2.280	3.370	5.640	4.580	8.400	5.560	10.760
117.215	2.290	2.730	3.960	6.690	5.400	9.970	6.580	12.900
120.663	2.620	3.150	4.500	7.720	6.200	11.440	7.720	14.920
124.110	3.600	4.640	6.400	11.310	9.280	16.660	11.910	22.960
118.939	3.720	4.950	6.740	11.940	9.790	17.710	12.650	24.430
115.491	3.870	5.210	7.050	12.540	10.370	18.710	13.470	25.890

U.D.L.	Dial Gauge No. [mm]							
[kN/m²]	(9)	(10)	(11)	(12)	(13)	(14)	(15)	(16)
6.895	0.130	0.130	0.110	0.080	0.050	0.110	0.100	0.150
13.790	0.240	0.250	0.230	0.160	0.120	0.200	0.180	0.110
20.685	0.360	0.390	0.370	0.240	0.150	0.310	0.240	0.180
27.589	0.490	0.550	0.530	0.350	0.210	0.480	0.440	0.270
34.475	0.710	0.810	0.810	0.510	0.300	0.770	0.690	0.420
41.370	0.970	1.120	1.130	0.700	0.410	1.050	0.960	0.570
48.265	1.280	1.500	1.530	0.930	0.550	1.410	1.220	0.770
55.160	1.650	1.950	1.970	1.220	0.740	1.830	1.720	1.010
55.160	1.780	2.100	2.120	1.300	0.790	1.940	1.830	1.070
62.055	2.190	2.590	2.640	1.580	0.970	2.400	2.230	1.350
68.950	2.590	3.100	3.150	1.860	1.160	2.870	2.720	1.620
75.845	3.290	3.970	4.070	2.370	1.480	3.740	3.500	2.060
82.740	4.230	5.210	6.410	3.080	1.930	4.990	4.610	2.700
89.635	5.550	6.900	7.290	4.080	2.570	6.770	6.120	3.540
96.530	6.780	8.490	9.040	5.030	3.150	8.440	7.540	4.300
103.425	8.540	10.780	11.630	6.480	4.060	10.940	9.700	5.500
110.320	10.990	14.100	15.300	8.580	5.320	14.470	12.830	7.200
113.768	12.820	16.500	19.100	10.240	6.350	17.200	15.270	8.560
117.215	15.100	19.500	21.500	12.280	7.630	20.650	18.350	10.240
120.663	17.100	22.400	24.750	14.280	8.900	24.050	21.500	11.900
124.110	24.420	32.850	37.350	22.850	14.400	38.380	34.750	18.750
118.939	25.510	34.500	39.320	24.280	15.320	40.700	36.900	19.800
115.491	26.600	36.100	41.350	25.730	16.320	43.100	39.100	20.950

R.C. Waffle Slab F3

Uniformly Distributed Load Vs Concrete Strains

U.D.L.	Dial Gauge No.						
	(1)	(2)	(3)	(4)	(5)	(6)	(7)
[kN/m²]	[mm]						
6.895	0.004	0.003	0.001	0.002	-0.002	-0.006	0.003
13.790	0.004	0.005	0.002	0.002	0.001	-0.007	0.010
20.685	0.005	0.007	-0.001	0.003	0.000	-0.008	0.013
27.580	0.007	0.008	-0.001	0.005	0.000	-0.005	0.021
34.475	0.009	0.011	-0.002	0.006	0.000	0.000	0.029
41.370	0.014	0.013	-0.002	0.009	-0.002	0.008	0.040
48.265	0.018	0.020	-0.003	0.010	-0.002	0.015	0.055
55.160	0.026	0.025	-0.004	0.012	-0.002	0.031	0.068
62.055	0.031	0.031	-0.008	0.014	-0.004	0.034	0.084
68.950	0.038	0.036	-0.008	0.017	-0.004	0.063	0.096
75.845	0.051	0.043	-0.010	0.019	-0.004	0.088	0.119
82.740	0.066	0.054	-0.012	0.025	-0.004	0.109	0.145
89.635	0.089	0.070	-0.018	0.032	-0.002	0.170	0.176
96.530	0.112	0.088	-0.021	0.039	0.000	0.235	0.196
103.425	0.141	0.114	-0.027	0.044	0.003	0.338	0.227
110.320	0.192	0.151	-0.032	0.050	0.009	0.475	0.270
113.768	0.239	0.178	-0.037	0.057	0.015	0.575	0.296

U.D.L.	Dial Gauge No.						
	(8)	(9)	(10)	(11)	(12)	(13)	(14)
[kN/m²]	[mm]						
6.895	0.001	0.002	0.003	-0.001	0.007	0.002	0.002
13.790	0.002	0.006	0.004	0.021	0.019	0.005	0.006
20.685	0.004	0.006	0.004	0.007	0.020	0.007	0.005
27.580	0.007	0.008	0.004	0.024	0.029	0.010	0.005
34.475	0.007	0.011	0.005	0.039	0.038	0.013	0.008
41.370	0.010	0.013	0.007	0.059	0.054	0.014	0.008
48.265	0.012	0.015	0.011	0.072	0.074	0.015	0.012
55.160	0.014	0.018	0.014	0.076	0.089	0.024	0.015
62.055	0.018	0.022	0.018	0.099	0.109	0.029	0.019
68.950	0.019	0.027	0.017	0.131	0.128	0.034	0.021
75.845	0.020	0.034	0.022	0.169	0.154	0.037	0.025
82.740	0.021	0.049	0.025	0.279	0.181	0.043	0.031
89.635	0.024	0.064	0.030	0.410	0.206	0.052	0.036
96.530	0.027	0.079	0.038	0.551	0.218	0.057	0.036
103.425	0.032	0.088	0.046	0.812	0.251	0.066	0.038
110.320	0.041	0.098	0.056	1.116	0.290	0.079	0.036
113.768	0.046	0.106	0.067	1.354	0.329	0.086	0.033

R.C. Waffle Slab F3

Uniformly Distributed Load Vs Concrete Strains

U.D.L.	Dial Gauge No.						
	(15)	(16)	(17)	(18)	(19)	(20)	(21)
[kN/m²]	[mm]						
6.895	-0.001	0.014	0.005	0.002	0.001	0.003	0.004
13.790	0.000	0.018	0.011	0.004	0.004	0.006	0.010
20.685	0.005	0.025	0.018	0.005	0.003	0.006	0.015
27.580	0.007	0.034	0.024	0.008	0.006	0.007	0.026
34.475	0.005	0.051	0.035	0.013	0.007	0.008	0.049
41.370	0.004	0.072	0.053	0.015	0.011	0.010	0.069
48.265	0.012	0.094	0.068	0.019	0.018	0.009	0.093
55.160	0.013	0.115	0.082	0.022	0.016	0.015	0.114
62.055	0.019	0.141	0.104	0.028	0.019	0.017	0.146
68.950	0.022	0.183	0.119	0.035	0.025	0.021	0.177
75.845	0.029	0.263	0.142	0.049	0.025	0.057	0.248
82.740	0.033	0.400	0.169	0.068	0.026	0.033	0.397
89.635	0.040	0.601	0.191	0.083	0.029	0.043	0.647
96.530	0.046	0.807	0.209	0.102	0.026	0.048	0.919
103.425	0.056	1.144	0.233	0.122	0.026	0.060	1.345
110.320	0.068	1.611	0.264	0.157	0.023	0.071	1.842
113.768	0.079	1.871	0.291	0.177	0.018	0.085	2.052

U.D.L.	Demec Gauge No.						
	(22)	(23)	(24)	(25)	(26)	(27)	(28)
[kN/m²]	[mm]						
6.895	0.008	0.002	0.008	0.001	0.002	0.006	0.002
13.790	0.013	0.005	0.024	0.003	0.007	0.010	0.003
20.685	0.021	0.004	0.029	0.004	0.012	0.017	0.005
27.580	0.025	0.006	0.031	0.006	0.020	0.026	0.005
34.475	0.041	0.009	0.034	0.008	0.051	0.033	0.006
41.370	0.059	0.010	0.037	0.009	0.072	0.045	0.009
48.265	0.091	0.013	0.039	0.009	0.097	0.065	0.012
55.160	0.121	0.015	0.042	0.011	0.113	0.104	0.011
62.055	0.158	0.017	0.043	0.012	0.142	0.151	0.008
68.950	0.191	0.017	0.046	0.013	0.174	0.189	0.006
75.845	0.240	0.022	0.053	0.016	0.244	0.255	0.009
82.740	0.285	0.032	0.043	0.021	0.402	0.311	0.004
89.635	0.313	0.043	0.019	0.025	0.670	0.329	0.002
96.530	0.321	0.045	0.039	0.058	1.012	0.312	-0.002
103.425	0.331	0.058	0.039	0.035	1.367	0.301	-0.002
110.320	0.341	0.069	0.075	0.043	1.852	0.319	-0.002
113.768	0.341	0.076	0.044	0.051	2.062	0.334	-0.001

R.C. Waffle Slab F3

Uniformly Distributed Load Vs Steel Strains

U.D.L.	Strain Gauge No.					
	(1)	(2)	(3)	(4)	(5)	(6)
[kN/m^2]			[10^{-3}]			
6.895	-0.037	0.019	0.040	0.055	0.045	0.033
13.790	-0.012	0.035	0.078	0.091	0.113	0.063
20.685	0.005	0.045	0.105	0.171	0.335	0.105
27.580	0.090	0.059	0.147	0.259	0.858	0.124
34.475	0.090	0.085	0.302	0.453	1.754	-1.132
41.370	0.117	0.121	0.313	0.936	2.163	-1.170
48.265	0.278	0.531	0.318	2.057	2.527	-1.038
55.160	1.141	1.232	0.318	3.087	2.951	-0.931
62.055	1.375	1.276	0.308	3.049	2.735	-0.782
68.950	1.775	1.591	0.210	2.087	3.455	-0.778
75.845	1.987	1.730	0.273	1.812	4.538	-0.753
82.740	2.251	1.811	0.210	1.429	8.114	-0.711
89.635	2.329	1.378	0.110	1.333	10.783	-0.632
96.530	2.921	1.199	0.066	1.227	10.578	-0.538
103.425	3.172	1.244	0.111	1.072	10.494	-0.501
110.320	3.072	1.518	0.172	1.024	10.582	-0.476
113.768	1.321	1.886	0.091	0.963	10.575	-0.433
117.215	1.204	1.568	0.190	0.896	10.440	-0.405
120.663	1.258	1.464	0.073	0.774	10.388	-0.392
124.110	1.326	1.185	0.065	0.694	10.724	-0.380

U.D.L.	Strain Gauge No.			
	(7)	(8)	(9)	(10)
[kN/m^2]			[10^{-3}]	
6.895	0.012	0.001	0.025	0.021
13.790	0.025	0.003	0.069	0.038
20.685	0.024	0.003	0.084	0.042
27.580	0.046	0.005	0.099	0.051
34.475	0.063	0.006	0.129	0.073
41.370	0.092	0.007	0.138	0.090
48.265	0.145	0.015	0.190	0.097
55.160	0.259	0.020	0.239	0.051
55.160	0.319	0.035	0.227	0.023
62.055	0.499	0.049	0.328	-0.002
68.950	0.805	0.310	0.336	-0.032
75.845	1.309	0.982	0.159	-0.065
82.740	1.413	2.368	-0.125	-0.141
89.635	1.421	2.265	-0.372	-0.199
96.530	1.280	3.246	-0.577	-0.195
103.425	1.526	4.241	-0.558	-0.178
110.320	2.033	5.267	-0.549	-0.018
113.768	2.387	3.707	-0.528	0.084
117.215	2.622	3.209	-0.469	0.159
120.663	2.641	3.497	-0.444	0.204

R.C. Waffle Slab I2

Uniformly Distributed Load Vs. Deflections

U.D.L. [kN/m²]	Dial Gauge No. (1)	(2)	(3)	(4)	(5)	(6)	(7)
				[mm]			
2.5	1.55	0.40	1.11	1.05	0.64	0.23	1.41
5.0	2.36	1.14	1.69	1.62	1.50	0.58	2.10
7.5	3.12	2.82	2.23	2.13	3.32	1.00	2.84
10.0	4.08	3.65	2.85	2.67	4.34	1.53	3.57
12.5	5.16	4.54	3.44	3.24	5.40	2.20	4.33
15.0	6.16	5.38	4.03	3.80	6.57	2.79	5.22
17.5	7.50	6.60	4.90	4.63	8.06	3.53	6.35
20.0	9.43	8.33	6.19	5.86	10.05	4.69	7.92
22.5	12.68	11.43	8.78	8.30	13.30	7.14	10.75
25.0	21.55	20.57	16.90	15 80	22.60	15.89	19.00
27.0	39.18	38.20	33.50	31.00	38.50	35.45	31.42
28.0	53.13	54.45	49.40	46.00	60.00	60.00	47.42

U.D.L. [kN/m²]	(8)	(9)	(10)	(11)	(12)	(13)	(14)
				[mm]			
2.5	0.48	0.78	0.92	0.94	-0.05	0.04	0.02
5.0	0.77	1.16	1.41	1.47	-0.04	0.09	0.09
7.5	1.06	1.54	1.89	2.00	-0.04	0.13	0.17
10.0	1.32	1.95	2.48	2.53	-0.00	0.28	0.33
12.5	1.63	2.41	3.11	3.16	0.03	0.43	0.47
15.0	1.94	2.93	3.76	3.80	0.01	0.51	0.59
17.5	2.39	3.58	4.48	4.60	0.05	0.62	0.68
20.0	3.03	4.46	5.49	5.62	0.00	0.70	0.76
22.5	4.22	5.93	7.15	7.22	-0.07	0.70	0.80
25.0	7.64	10.93	11.51	11.50	-0.60	0.37	0.46
27.0	17.53	17.69	19.32	19.06	-1.95	-0.84	-0.72
28.0	24.72	25.34	26.79	26.23	-3.34	-2.33	-2.20

Uniformly Distributed Load Vs. Concrete Strains

U.D.L. [kN/m²]	Strain Gauge No. (1)	(2)	(3)	(4)	(5)	(6)	(7)	(8)	(9)
				[10^{-3}]					
2.5	0.345	0.364	0.139	0.246	0.161	0.388	0.567	0.712	0.357
5.0	0.546	0.770	0.214	0.396	0.268	0.718	0.848	1.042	0.790
7.5	0.781	1.049	0.407	0.621	0.417	1.049	1.128	1.371	1.223
10.0	1.038	1.295	0.589	0.728	0.653	1.218	1.595	1.760	1.179
12.5	1.241	1.573	0.706	0.877	0.845	0.564	2.138	2.183	1.184
15.0	1.477	1.873	0.803	0.974	0.984	0.496	2.765	2.631	1.214
17.5	1.776	2.333	0.920	1.102	1.145	0.462	3.629	3.163	1.255
20.0	2.172	3.039	1.017	1.241	1.359	0.435	13.054	13.159	1.304
22.5	3.242	4.601	1.091	1.445	1.605	0.410	---	---	1.364
25.0	7.843	9.309	1.124	1.744	2.001	0.382	---	---	1.432
27.0	---	15.772	1.091	1.980	2.258	0.355	---	---	1.439
28.0	---	---	---	---	---	0.323	---	---	1.449

R.C. Waffle Slab H2

Uniformly Distributed Load Vs. Deflections

U.D.L. [kN/m²]	Dial Gauge No. (1)	(2)	(3)	(4) [mm]	(5)	(6)	(7)
3.448	0.73	0.58	0.34	0.74	0.66	0.55	0.48
6.895	1.11	0.85	0.47	1.11	0.98	0.80	0.71
10.343	2.07	1.54	0.78	2.12	1.90	1.59	1.46
13.790	3.63	2.94	1.04	2.92	2.63	2.21	2.08
17.238	4.54	3.40	1.61	4.63	4.12	3.38	3.15
20.685	5.50	4.10	1.92	5.50	4.88	3.95	3.67
24.133	6.61	4.95	2.33	6.72	5.89	4.85	4.53
27.580	8.00	5.92	2.73	8.10	7.30	5.89	5.49
31.028	10.82	7.15	3.17	10.10	9.06	7.40	6.95
34.475	14.31	9.74	3.71	15.60	14.30	12.05	11.12
37.923	23.80	14.40	3.95	27.40	25.80	22.50	20.21
39.646	28.00	18.45	4.15	37.40	35.90	31.60	28.24
41.370	38.60	22.00	4.78	45.30	43.50	38.10	33.79
43.094	43.60	24.85	5.50	50.30	48.40	43.10	---

U.D.L. [kN/m²]	Dial Gauge No. (8)	(9)	(10)	(11) [mm]	(12)	(13)	(14)
3.448	0.29	0.64	0.47	0.19	0.71	0.49	0.22
6.895	0.44	0.92	0.69	0.24	1.08	0.81	0.38
10.343	0.84	1.78	1.28	0.36	2.09	1.52	0.63
13.790	1.18	2.49	1.71	0.47	2.86	2.00	0.80
17.238	1.84	3.93	2.69	0.76	4.47	3.29	1.38
20.685	2.16	4.73	3.22	0.97	5.42	4.02	1.65
24.133	2.65	5.68	3.98	1.09	6.56	4.83	1.99
27.580	3.19	6.85	4.79	1.33	7.87	5.80	2.33
31.028	4.01	8.50	5.78	1.49	9.73	6.87	2.73
34.475	6.12	13.11	8.26	1.72	14.29	9.59	3.22
37.923	10.39	22.47	12.73	1.74	23.42	14.17	3.36
39.646	14.21	30.74	16.74	1.88	31.66	18.22	3.51
41.370	16.97	36.70	19.76	2.25	38.03	21.52	4.12
43.094	---	---	---	---	---	---	---

R.C. Waffle Slab H2

Uniformly Distributed Load Vs Concrete Strains

U.D.L. [kN/m²]	Demec Gauge No. [10⁻³] (1)	(2)	(3)	(4)	(5)	(6)	(7)	(8)
3.448	0.161	0.203	0.139	0.150	0.000	0.139	2.932	0.107
6.895	0.268	0.342	0.342	0.246	-0.011	0.203	2.932	0.139
10.343	0.535	0.824	0.877	0.578	0.021	0.482	3.007	0.332
13.790	0.728	1.145	1.145	0.835	0.043	0.749	3.050	0.492
17.238	1.134	1.776	1.680	1.241	0.054	1.156	3.135	0.674
20.685	1.359	2.161	2.033	1.541	0.054	1.552	3.199	0.792
24.133	1.605	2.686	2.450	1.862	0.086	1.594	3.285	0.888
27.580	1.990	3.531	3.264	2.418	0.096	1.808	3.381	1.027
31.028	2.686	5.018	4.601	3.285	0.096	2.054	3.467	1.134
34.475	5.703	10.293	7.651	5.735	0.139	2.311	3.563	1.049
37.923	18.329	32.549	18.351	11.117	0.182	2.675	3.692	1.166

U.D.L. [kN/m²]	Demec Gauge No. [10⁻³] (9)	(10)	(11)	(12)	(13)	(14)	(15)	(16)
3.448	0.096	0.096	0.064	0.011	0.075	0.054	0.054	0.096
6.895	0.171	0.096	0.086	-0.011	0.118	0.075	0.086	0.128
10.343	0.375	0.257	0.171	0.011	0.182	0.118	0.161	0.257
13.790	0.482	0.375	0.235	0.000	0.235	0.128	0.203	0.385
17.238	0.738	0.781	0.460	0.032	0.449	0.225	0.375	0.663
20.685	0.877	0.877	0.663	0.032	0.674	0.225	0.471	0.835
24.133	1.081	1.081	0.824	0.043	0.845	0.375	0.514	0.942
27.580	1.284	1.327	1.038	0.032	1.049	0.524	0.567	1.091
31.028	1.498	1.519	1.231	0.043	1.263	0.621	0.653	1.241
34.475	1.776	1.819	1.370	0.064	1.445	0.813	0.706	1.412
37.923	2.172	2.247	1.402	0.075	1.209	0.910	0.460	1.669

U.D.L. [kN/m²]	Demec Gauge No. [10⁻³] (17)	(18)	(19)	(20)	(21)	(22)
3.448	0.139	0.011	0.043	-0.011	0.096	0.096
6.895	0.182	0.054	0.054	0.032	0.150	0.150
10.343	0.342	0.075	0.096	0.043	0.300	0.310
13.790	0.524	0.011	0.128	0.064	0.460	0.503
17.238	0.910	0.064	0.203	0.064	0.717	0.770
20.685	1.113	0.096	0.289	0.075	0.845	0.984
24.133	1.284	0.107	0.375	0.118	0.952	1.145
27.580	1.498	0.107	0.578	0.171	1.081	1.380
31.028	1.776	0.107	0.706	0.203	1.252	1.616
34.475	2.258	0.096	0.984	0.225	1.455	1.980
37.923	2.921	0.021	2.215	0.086	1.626	3.413

R.C. Waffle Slab J1

4-point Load Vs Deflections

LOAD [kN]	COMP.	Dial Gauge No. (1)	(2)	(3) [mm]	(4)	(5)	(6)
0.0	0.00	0.00	0.00	0.00	0.00	0.00	0.00
0.5	0.00	0.03	0.03	0.00	0.01	0.02	0.03
5.0	0.19	0.53	0.53	0.19	0.91	-0.28	0.54
10.0	0.50	1.05	0.72	0.27	1.16	-0.04	0.65
15.0	0.90	1.38	0.93	0.30	1.47	0.25	0.94
20.0	1.26	1.74	1.14	0.42	1.84	0.56	1.19
25.0	1.90	1.98	1.48	0.55	2.40	1.03	1.46
30.0	2.50	3.01	1.90	0.67	3.18	2.06	1.89
30.0	3.15	3.36	2.15	0.77	3.51	1.96	2.23
35.0	3.57	3.76	2.41	0.86	3.94	2.29	2.58
40.0	4.47	4.61	2.94	1.02	4.82	3.05	3.21
45.0	5.55	5.64	3.58	1.24	5.85	3.94	3.91
50.0	6.50	6.61	4.21	1.50	6.87	4.77	4.54
55.0	7.56	7.76	4.78	1.87	8.02	5.70	5.21
60.0	8.66	8.86	5.73	2.15	9.01	6.52	5.78
65.0	9.86	10.06	6.58	2.52	10.25	7.52	6.51
70.0	11.15	11.41	7.42	2.85	11.57	8.62	7.32
75.0	12.81	12.21	8.49	3.21	13.37	10.05	8.38
80.0	15.55	15.91	10.08	3.74	17.17	12.29	9.99
85.0	23.42	28.96	14.39	4.22	25.32	20.67	17.36
88.0	---	---	31.63	4.00	---	---	---

LOAD [kN]	Transducer No. (1)	(2)	(3)	(4) [mm]	(5)	(6)	(7)	(8)
0.84	0.00	0.00	0.01	0.00	0.05	0.02	-0.10	0.06
5.0	0.14	0.17	0.32	0.48	0.58	0.52	0.59	0.88
10.0	0.18	0.27	0.44	0.63	0.80	0.65	0.85	1.16
15.0	0.21	0.31	0.53	0.78	0.94	0.86	0.85	1.46
20.0	0.26	0.39	0.66	0.97	1.18	1.13	1.40	1.83
25.0	0.28	0.46	0.82	1.26	1.47	1.39	1.84	2.31
30.0	0.36	0.56	1.08	1.56	1.88	1.84	2.43	2.98
30.0	0.41	0.63	1.17	1.74	2.08	2.01	2.66	3.28
35.0	0.44	0.70	1.33	1.94	2.34	2.35	3.05	3.69
40.0	0.52	0.83	1.61	2.36	2.81	2.87	3.72	4.51
45.0	0.64	1.04	1.93	2.87	3.38	3.50	4.54	5.48
50.0	0.74	1.29	2.23	3.42	3.97	3.74	5.33	6.40
55.0	0.88	1.55	2.55	4.00	4.72	4.73	6.21	7.43
60.0	1.03	1.79	2.84	4.49	5.29	5.21	6.94	8.34
65.0	1.20	2.15	3.21	5.14	6.13	5.91	7.94	9.53
70.0	1.37	2.40	3.62	5.73	6.90	6.60	8.93	10.72
75.0	1.55	2.76	4.19	6.63	7.88	7.65	10.29	12.47
80.0	1.80	3.23	4.99	7.89	9.39	9.05	12.37	14.90
85.0	1.80	3.44	7.94	11.79	13.47	15.33	19.65	22.88
88.0	-5.35	-4.88	24.90	29.33	---	36.61	39.83	40.35

R.C. Waffle Slab J1

4-point Load Vs Steel Strains

LOAD [kN]	Strain Gauge No. (1)	(2)	(3)	(4)	(5)	(6)	(7)	(8)
				[10^{-3}]				
0.84	0.002	-0.003	0.004	0.004	0.005	0.000	0.002	0.003
5.0	0.027	0.035	0.055	0.048	0.056	0.016	0.029	0.048
10.0	0.033	0.046	0.073	0.059	0.069	0.020	0.036	0.061
15.0	0.040	0.056	0.094	0.067	0.077	0.023	0.042	0.073
20.0	0.047	0.065	0.118	0.077	0.088	0.024	0.047	0.085
25.0	0.058	0.079	0.152	0.097	0.098	0.027	0.053	0.102
30.0	0.104	0.128	0.231	0.152	0.134	0.058	0.089	0.161
30.0	0.094	0.120	0.229	0.154	0.115	0.046	0.072	0.149
35.0	0.100	0.131	0.252	0.168	0.127	0.046	0.076	0.163
40.0	0.100	0.150	0.372	0.198	0.139	0.049	0.082	0.185
45.0	0.119	0.181	0.504	0.225	0.164	0.051	0.088	0.219
50.0	0.128	0.234	0.599	0.139	0.230	0.052	0.093	0.291
55.0	0.140	0.290	0.774	-1.177	0.307	0.058	0.101	0.571
60.0	0.149	0.332	0.835	-1.820	0.405	0.062	0.109	0.705
65.0	0.159	0.454	0.921	-2.540	0.531	0.063	0.113	0.888
70.0	0.169	0.870	0.999	-2.986	0.629	0.067	0.124	1.015
75.0	0.178	1.564	1.069	-3.327	0.734	0.071	0.139	1.134
80.0	0.199	2.123	1.149	-3.693	0.861	0.080	0.177	1.329
85.0	0.338	2.667	1.294	-4.152	1.029	0.084	0.230	1.600
88.0	0.379	---	0.970	-4.023	1.008	0.060	0.150	1.233

LOAD [kN]	Strain Gauge No. (9)	(10)	(11)	(12)	(13)	(14)	(15)	(16)
				[10^{-3}]				
0.84	0.004	0.004	0.003	0.002	0.003	-0.003	0.002	0.001
5.0	0.080	0.064	0.023	0.031	0.065	0.026	0.072	0.030
10.0	0.094	0.085	0.023	0.041	0.081	0.042	0.091	0.042
15.0	0.115	0.116	0.030	0.046	0.094	0.060	0.103	0.048
20.0	0.144	0.129	0.031	0.051	0.106	0.082	0.114	0.051
25.0	0.199	0.159	0.031	0.053	0.121	0.113	0.125	0.068
30.0	0.286	0.246	0.059	0.088	0.173	0.114	0.174	0.118
30.0	0.296	0.236	0.038	0.069	0.159	0.065	0.152	0.086
35.0	0.324	0.280	0.040	0.073	0.170	0.054	0.161	0.090
40.0	0.380	0.441	0.034	0.075	0.184	0.699	0.204	0.096
45.0	0.518	0.536	0.035	0.079	0.213	0.372	0.302	0.101
50.0	0.650	0.640	0.037	0.083	0.290	0.371	0.444	0.105
55.0	0.792	0.785	0.034	0.089	0.628	0.575	0.626	0.113
60.0	0.914	0.900	0.040	0.093	0.856	0.972	0.796	0.121
65.0	1.053	1.029	0.044	0.095	1.086	2.447	0.995	0.125
70.0	1.180	1.142	0.055	0.098	1.235	1.478	1.177	0.132
75.0	1.311	1.269	0.066	0.093	1.409	2.193	1.358	0.138
80.0	1.525	1.466	0.081	0.071	1.519	0.828	1.478	0.169
85.0	1.808	1.790	0.061	0.060	1.519	0.782	1.481	0.221
88.0	1.321	1.322	0.032	0.006	0.903	1.367	1.089	0.381

R.C. Waffle Slab J1

4-point Load Vs Steel Strains

LOAD [kN]	Strain Gauge No. (17)	(18)	(19)	(20)	(21)	(22)	(23)	(24)
				[10^{-3}]				
0.84	0.002	0.001	0.004	0.001	0.004	0.006	0.002	0.003
5.0	0.056	0.062	-0.006	0.057	0.015	0.064	0.080	0.096
10.0	0.074	0.081	-0.375	0.072	0.021	0.085	0.103	0.125
15.0	0.095	0.096	-0.700	0.085	0.021	0.107	0.098	0.153
20.0	0.112	0.114	-0.992	0.102	0.021	0.140	0.025	0.185
25.0	0.141	0.146	-1.429	0.134	0.023	0.167	0.014	0.249
30.0	0.251	0.263	-2.108	0.211	0.038	0.201	0.066	0.401
30.0	0.259	0.319	-2.503	0.259	0.025	0.201	0.122	0.452
35.0	0.301	0.364	-3.045	0.339	0.028	0.215	0.157	0.504
40.0	0.365	0.427	-3.673	0.533	0.030	0.263	0.236	0.622
45.0	0.472	0.464	-3.817	0.641	0.031	0.300	0.402	0.751
50.0	0.592	0.573	-3.831	0.730	0.033	0.337	0.524	0.873
55.0	0.668	0.675	-3.873	0.841	0.037	0.417	0.662	1.008
60.0	0.741	0.777	-3.929	0.935	0.037	0.489	0.787	1.118
65.0	0.837	0.875	-4.097	1.027	0.044	0.630	0.920	1.258
70.0	0.932	0.977	-4.241	1.355	0.049	0.754	1.043	1.394
75.0	1.023	1.162	-4.335	1.499	0.050	0.883	1.173	1.474
80.0	1.181	1.514	-4.246	1.543	0.058	0.991	1.331	1.488
85.0	1.301	1.749	-3.141	1.721	0.058	1.049	1.469	1.679
88.0	1.335	3.380	2.422	0.555	0.053	0.799	0.942	0.837

LOAD [kN]	Strain Gauge No. (25)	(26)	(27)	(28)	(29)	(30)
				[10^{-3}]		
0.84	0.008	0.001	0.002	0.004	0.002	0.004
5.0	0.097	0.019	0.041	0.184	0.075	0.092
10.0	0.174	0.023	0.058	0.248	0.099	0.120
15.0	0.326	0.024	0.066	0.322	0.126	0.162
20.0	0.450	0.021	0.070	0.375	0.176	0.251
25.0	0.523	0.022	0.079	0.500	0.383	0.336
30.0	0.698	0.036	0.100	0.641	0.605	0.527
30.0	0.731	0.026	0.087	0.649	0.647	0.524
35.0	0.797	0.026	0.099	0.709	0.702	0.600
40.0	0.916	0.027	0.155	0.790	0.707	0.761
45.0	1.032	0.030	0.228	0.907	0.553	0.949
50.0	1.130	0.030	0.342	1.013	0.320	1.112
55.0	1.239	0.035	0.470	1.154	-0.026	1.293
60.0	1.340	0.038	1.096	1.270	-0.250	1.451
65.0	1.460	0.039	3.381	1.404	-0.698	1.605
70.0	1.595	0.041	4.143	1.509	-0.913	1.690
75.0	1.921	0.041	4.070	1.553	-1.091	1.730
80.0	1.930	0.035	3.858	1.204	-1.059	1.781
85.0	4.216	0.030	3.715	1.218	-1.105	1.682
88.0	---	0.007	1.805	---	1.414	0.539

R.C. Waffle Slab J1

4-point Load Vs. Concrete Strains

Load [kN]	Demec Gauge No. (1)	(2)	(3)	(4)	(5)	(6)	(7)	(8)	(9)
					[10^{-3}]				
5	-0.048	-0.040	-0.016	-0.008	0.016	0.040	0.056	0.064	0.000
10	-0.064	-0.048	-0.016	-0.008	0.024	0.056	0.064	0.040	0.048
15	-0.088	-0.056	-0.024	-0.000	0.032	0.072	0.096	0.120	0.096
20	-0.104	-0.080	-0.032	-0.000	0.048	0.096	0.128	0.144	0.088
25	-0.128	-0.104	-0.040	-0.008	0.064	0.128	0.152	0.160	0.152
30	-0.168	-0.120	-0.040	-0.024	0.096	0.168	0.208	0.232	0.208
35	-0.192	-0.136	-0.040	-0.040	0.136	0.216	0.264	0.304	0.256
40	-0.224	-0.176	-0.040	-0.080	0.192	0.208	0.360	0.440	0.464
45	-0.264	-0.192	-0.040	-0.128	0.224	0.328	0.408	0.512	0.512
50	-0.280	-0.220	-0.024	-0.128	0.264	0.352	0.464	0.568	0.576
55	-0.304	-0.240	-0.024	-0.152	0.280	0.408	0.536	0.664	0.696
60	-0.336	-0.248	-0.024	-0.160	0.312	0.464	0.600	0.736	0.784
65	-0.376	-0.272	-0.016	-0.184	0.376	0.560	0.712	0.896	0.952
70	-0.416	-0.288	-0.024	-0.232	0.408	0.624	0.808	1.056	1.072
75	-0.472	-0.336	-0.024	-0.240	0.480	0.712	0.928	1.160	1.232
80	-0.552	-0.400	-0.032	-0.296	0.560	0.840	1.096	1.392	1.344
85	-0.608	-0.456	-0.048	-0.312	0.624	0.936	1.224	1.536	1.680
88	-0.184	-0.880	2.464	6.080	8.056	11.696	13.616	15.720	16.504

Load [kN]	Demec Gauge No. (10)	(11)	(12)	(13)	(14)	(15)	(16)	(17)	(18)
					[10^{-3}]				
5	0.120	0.072	0.032	0.016	-0.008	-0.008	-0.008	-0.008	0.024
10	0.168	0.088	0.056	0.000	-0.008	-0.008	-0.016	0.016	0.016
15	0.224	0.088	0.048	0.016	-0.016	-0.024	-0.008	0.032	0.032
20	0.272	0.104	0.072	0.016	-0.016	-0.016	-0.016	0.032	0.040
25	0.328	0.024	0.080	0.032	-0.024	-0.024	-0.016	0.032	0.048
30	0.440	0.248	0.104	0.056	-0.032	-0.024	-0.016	0.048	0.064
35	0.568	0.248	0.208	0.064	-0.048	-0.032	-0.016	0.040	0.080
40	0.752	0.264	0.160	0.040	-0.064	-0.040	-0.016	0.040	0.104
45	1.016	0.320	0.208	0.040	-0.080	-0.056	-0.016	0.032	0.128
50	1.200	0.480	0.248	0.056	-0.112	-0.088	-0.024	0.048	0.160
55	1.336	0.480	0.304	0.040	-0.144	-0.104	-0.016	0.056	0.240
60	1.496	0.584	0.392	0.048	-0.160	-0.104	-0.008	0.080	0.288
65	1.672	0.704	0.512	0.088	-0.192	-0.112	0.000	0.104	0.352
70	1.864	0.832	0.512	0.072	-0.200	-0.136	0.008	0.144	0.400
75	2.144	1.048	0.904	0.096	-0.208	-0.144	0.008	0.168	0.448
80	2.552	1.216	1.104	0.096	-0.232	-0.152	0.016	0.216	0.528
85	5.864	1.464	1.312	0.088	-0.296	-0.184	0.024	0.280	0.672
88	15.784	2.048	2.032	0.096	-0.224	-0.160	-0.008	0.200	0.520

R.C. Waffle Slab J1
4-point Load Vs Steel Strains

Load [kN]	Demec Guage No. (19)	(20)	(21)	(22)	(23)	(24)	(25)	(26)
				[10^{-3}]				
5	0.024	0.032	0.056	0.064	0.072	0.048	0.040	0.072
10	0.032	0.040	0.072	0.080	0.080	0.064	0.032	0.008
15	0.040	0.048	0.088	0.128	0.112	0.104	0.048	-0.080
20	0.056	0.064	0.104	0.130	0.120	0.096	0.048	0.096
25	0.064	0.088	0.136	0.152	0.152	0.112	0.056	0.016
30	0.096	0.112	0.184	0.208	0.184	0.176	0.056	0.032
35	0.112	0.152	0.232	0.233	0.224	0.200	0.088	0.032
40	0.152	0.184	0.280	0.264	0.296	0.208	0.128	0.072
45	0.176	0.248	0.360	0.344	0.408	0.280	0.144	0.048
50	0.264	0.240	0.544	0.448	0.480	0.400	0.168	0.040
55	0.368	0.280	0.680	0.568	0.552	0.488	0.200	0.088
60	0.424	0.328	0.796	0.696	0.648	0.576	0.232	0.056
65	0.512	0.392	0.928	0.824	0.760	0.688	0.248	0.088
70	0.576	0.432	1.048	0.936	0.808	0.808	0.320	0.024
75	0.648	0.448	1.152	1.016	0.888	0.960	0.400	0.064
80	0.760	0.584	1.328	1.216	0.984	1.216	0.536	0.080
85	0.976	0.768	1.680	1.560	1.128	1.496	0.768	0.056
88	0.768	0.592	1.288	1.240	0.832	1.128	0.632	0.000

R.C. Waffle Slab J1
4-point Load Vs. Concrete Strains

Load [kN]	Concrete Strain Gauge No. (1)	(2)	(3)	(4)	(5)	(6)	(7)	(8)
				[10^{-3}]				
0.84	0.001	0.002	0.000	0.002	0.003	0.001	0.001	0.002
5	0.014	0.063	0.037	0.093	0.308	0.020	0.017	0.053
10	0.018	0.082	0.046	0.113	0.417	0.028	0.021	0.067
15	0.018	0.096	0.049	0.137	0.535	0.030	0.022	0.077
20	0.016	0.110	0.048	0.224	0.656	0.028	0.023	0.085
25	0.018	0.137	0.052	0.352	0.813	0.037	0.028	0.101
30	0.054	0.249	0.088	0.560	1.045	0.112	0.069	0.190
30	0.023	0.203	0.055	0.545	1.154	0.055	0.041	0.149
35	0.020	0.226	0.057	0.617	1.364	0.055	0.041	0.158
40	0.019	0.028	0.059	0.763	1.724	0.056	0.045	0.169
45	0.018	0.263	0.057	0.889	2.033	0.058	0.048	0.178
50	0.018	0.288	0.053	0.996	2.292	0.058	0.050	0.171
55	0.022	0.293	0.051	1.207	2.466	0.062	0.054	0.165
60	0.022	0.307	0.045	1.429	2.671	0.067	0.057	0.156
65	0.023	0.301	0.035	1.750	2.963	0.067	0.063	0.152
70	0.023	0.275	0.019	1.408	3.254	0.070	0.068	0.171
75	0.021	0.265	-0.003	1.408	3.613	0.071	0.077	0.270
80	0.021	0.391	-0.020	1.409	3.689	0.075	0.089	0.364
85	0.016	1.184	-0.030	1.409	3.674	0.075	0.095	0.558
88	0.038	---	-0.046	1.409	2.326	0.062	0.073	0.449

R.C. Waffle Slab J1

4-point Load Vs. Concrete Strains

Load [kN]	Concrete Strain Gauge No. (9)	(10)	(11)	(12)	(13)	(14)	(15)	(16)
					[10^{-3}]			
0.84	0.002	0.001	0.008	0.002	0.002	0.001	0.001	0.003
5	0.048	0.056	0.370	0.008	0.049	0.024	0.018	0.005
10	0.061	0.083	0.752	0.017	0.053	0.033	0.026	-0.002
15	0.068	0.115	1.302	0.020	0.053	0.037	0.028	-0.013
20	0.074	0.198	1.826	0.026	0.052	0.037	0.028	-0.026
25	0.088	0.284	2.821	0.046	0.053	0.044	0.034	-0.026
30	0.165	0.429	2.006	0.138	0.114	0.109	0.098	-0.014
30	0.110	0.432	---	0.107	0.059	0.062	0.050	-0.046
35	0.117	0.493	---	0.121	0.064	0.063	0.063	-0.050
40	0.131	0.857	---	0.147	0.061	0.065	0.050	-1.066
45	0.158	1.318	---	0.199	0.056	0.067	0.050	-0.081
50	0.196	1.608	---	0.240	0.055	0.068	0.051	-0.089
55	0.284	1.882	---	0.295	0.057	0.073	0.054	-0.091
60	0.366	2.108	---	0.332	0.098	0.075	0.057	-0.096
65	0.485	2.326	---	0.366	0.815	0.074	0.057	-0.103
70	0.576	2.499	---	0.396	0.301	0.075	0.058	-0.110
75	0.659	2.822	---	0.430	1.657	0.074	0.057	-0.117
80	0.842	1.657	---	0.475	1.960	0.074	0.061	-0.112
85	0.972	1.658	---	0.421	2.039	0.074	0.062	-0.121
88	0.709	2.136	---	0.224	1.550	0.050	0.067	-0.098

Load [kN]	Concrete Strain Gauge No. (17)	(18)	(19)	(20)
		[10^{-3}]		
0.84	0.012	0.003	0.001	0.001
5	0.028	0.061	0.017	0.015
10	0.028	0.077	0.026	0.020
15	0.032	0.084	0.029	0.022
20	0.043	0.071	0.031	0.021
25	0.088	0.073	0.031	0.022
30	0.276	0.129	0.095	0.051
30	0.657	0.073	0.046	0.037
35	0.739	0.072	0.042	0.037
40	0.895	0.073	0.040	0.036
45	1.081	0.079	0.057	0.036
50	1.260	0.086	0.063	0.037
55	1.514	0.089	0.067	0.040
60	2.081	0.089	0.063	0.042
65	2.547	0.098	0.057	0.042
70	3.344	0.191	0.052	0.043
75	---	0.220	0.043	0.038
80	---	0.306	0.032	0.038
85	---	0.318	0.010	0.026
88	---	0.155	-0.003	0.010

APPENDIX B

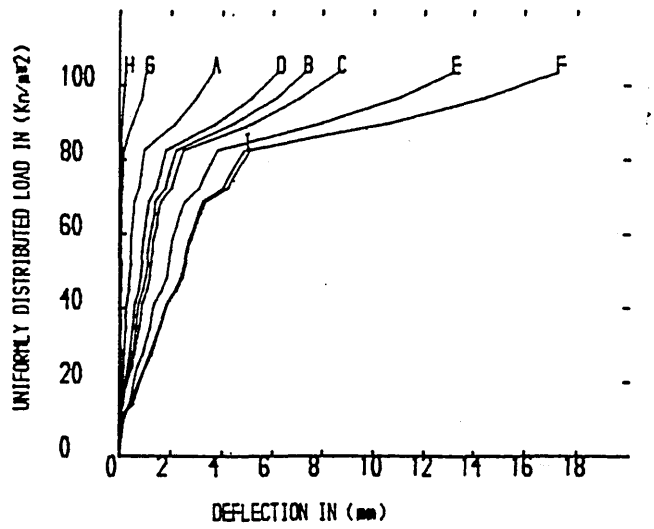

Load-Deflection Curves of R.C.Waffle Model Slab A1

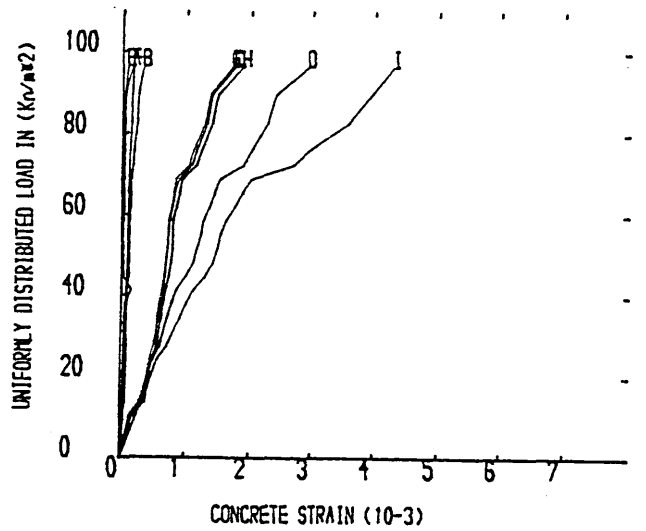

Load-Concrete Strain Curves of R.C.Waffle Model Slab A1

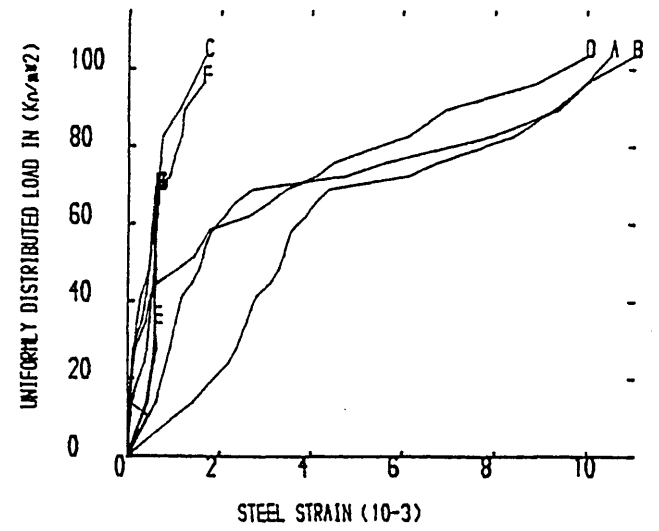

Load-Steel Strain Curves of R.C.Waffle Model Slab A1

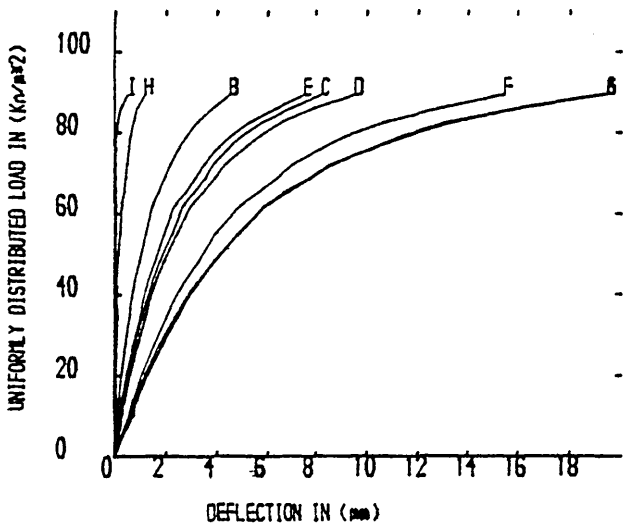

Load-Deflection Curves of R.C.Waffle Model Slab A2

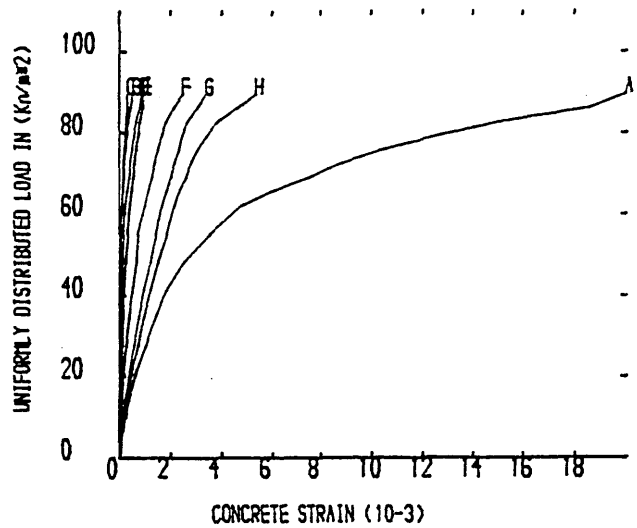

Load-Concrete Strain Curves of R.C.Waffle Model Slab A2

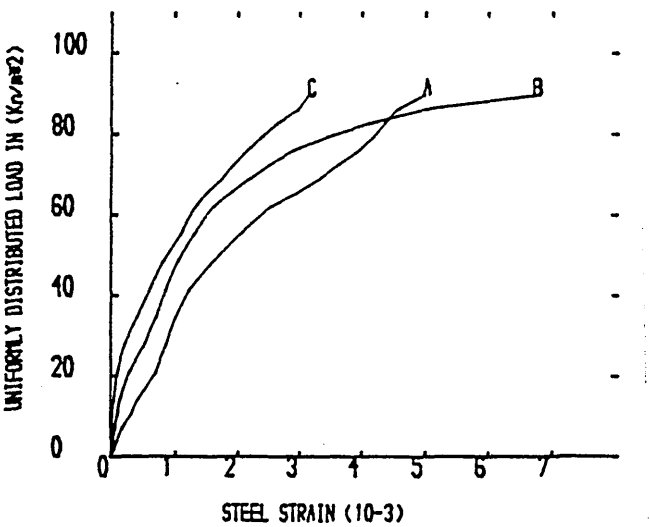

Load-Steel Strain Curves of R.C.Waffle Model Slab A2

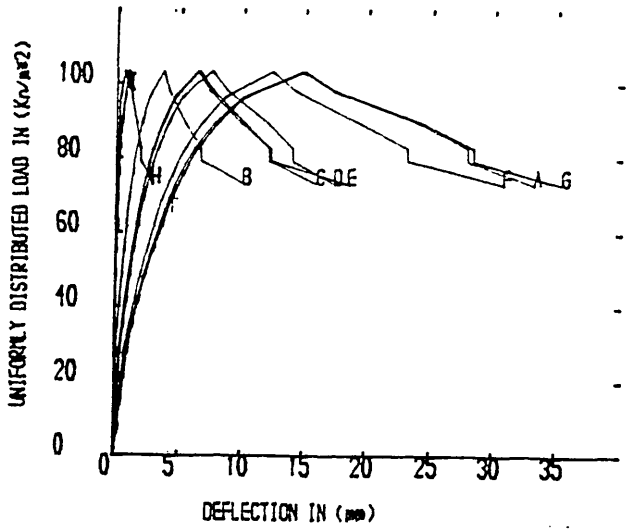

Load-Deflection Curves of R.C.Waffle Model Slab A3

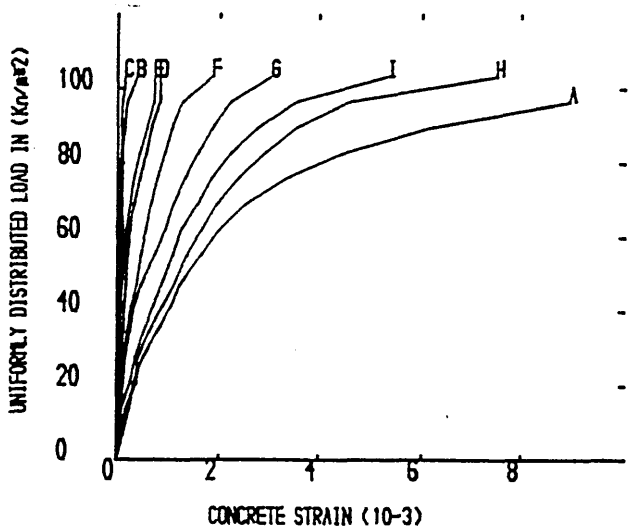

Load-Concrete Strain Curves of R.C.Waffle Model Slab A3

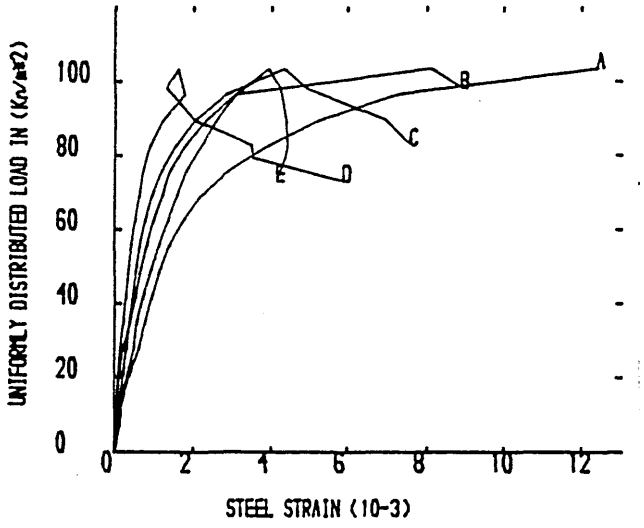

Load-Steel Strain Curves of R.C.Waffle Model Slab A3

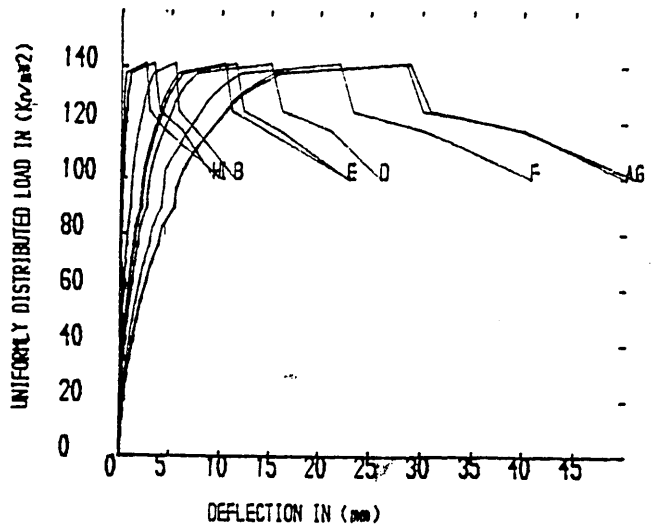

Load-Deflection Curves of R.C.Waffle Model Slab B1

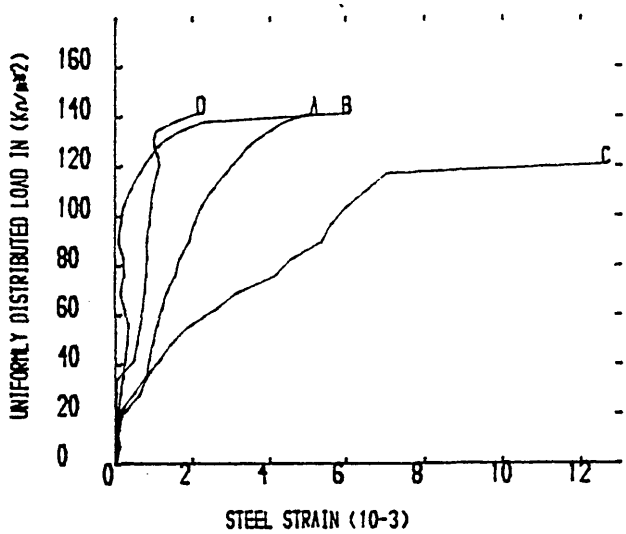

Load-Steel Strain Curves of R.C.Waffle Model Slab B1

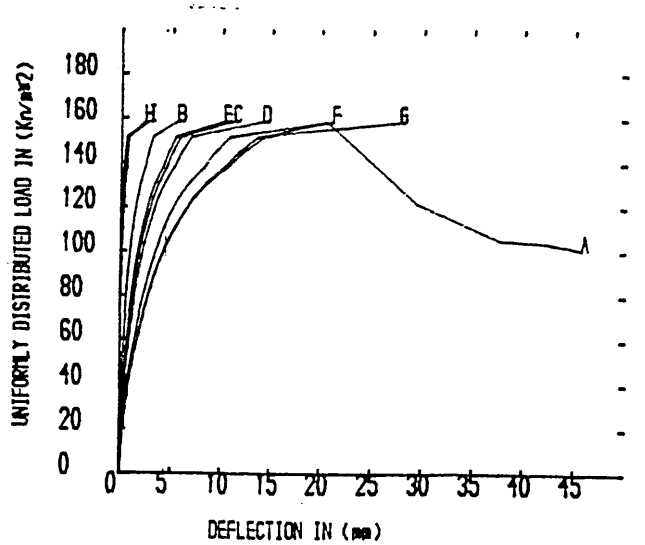

Load-Deflection Curves of R.C.Waffle Model Slab B2

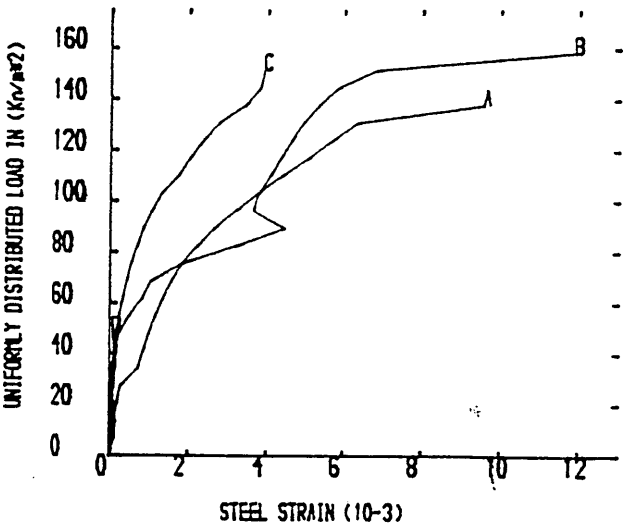

Load-Steel Strain Curves of R.C.Waffle Model Slab B2

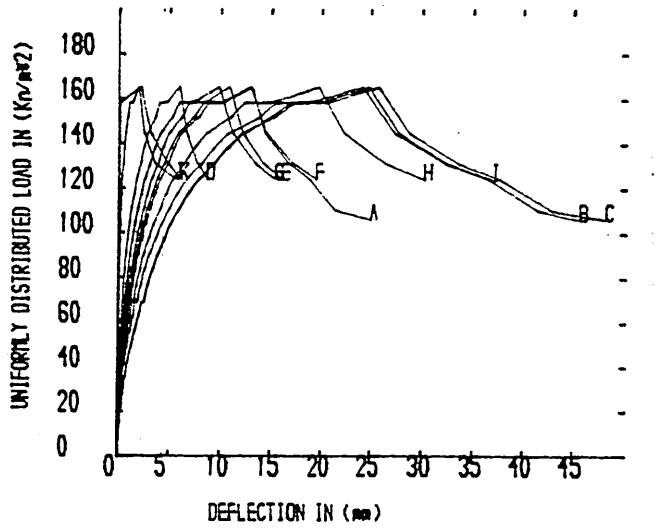

Load-Deflection Curves of R.C.Waffle Model Slab B3

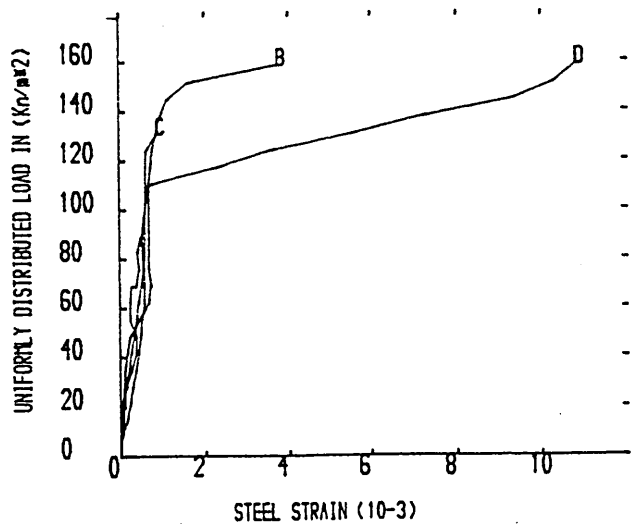

Load-Steel Strain Curves of R.C.Waffle Model Slab B3

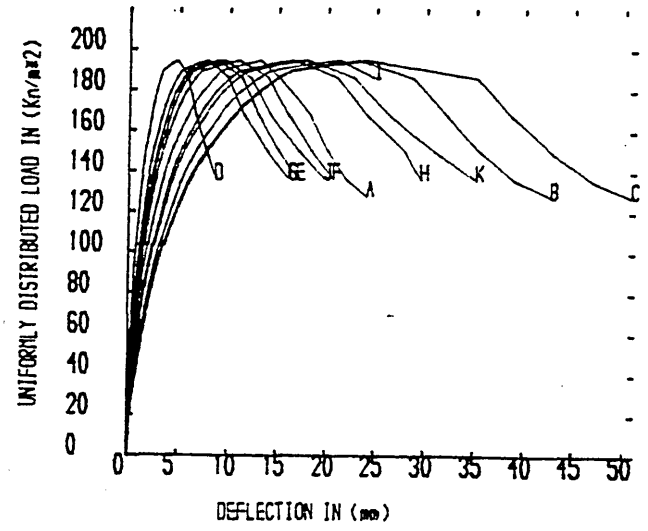

Load-Deflection Curves of R.C.Waffle Model Slab C1

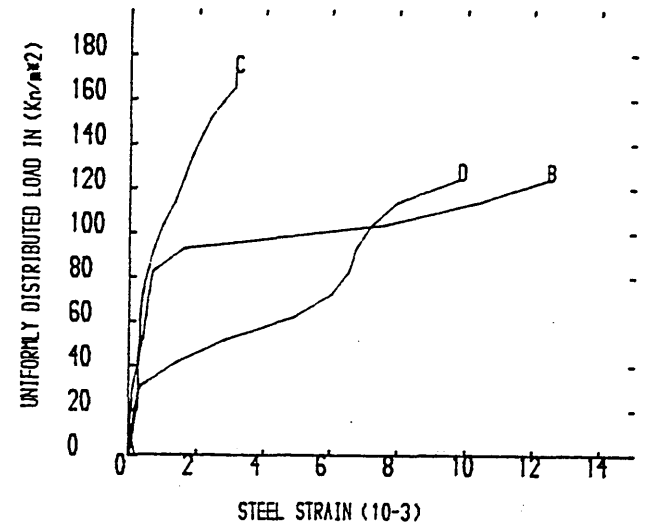

Load-Steel Strain Curves of R.C.Waffle Model Slab C1

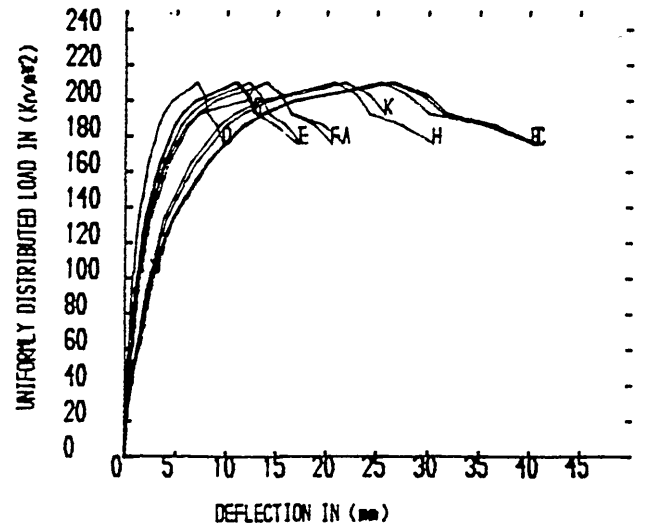

Load-Deflection Curves of R.C.Waffle Model Slab C2

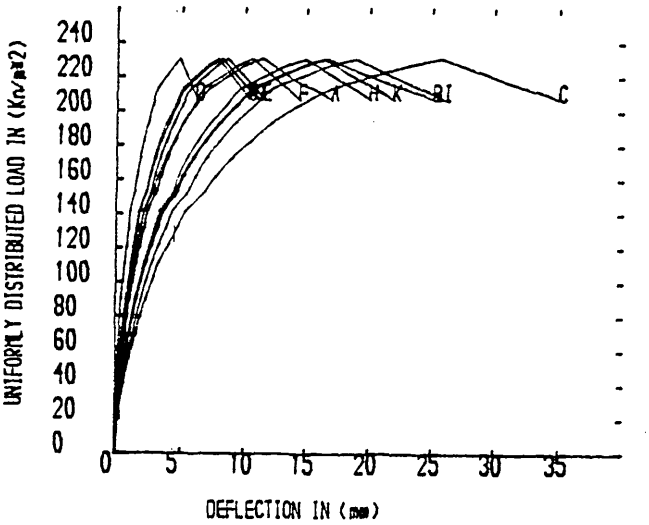

Load-Deflection Curves of R.C.Waffle Model Slab C3

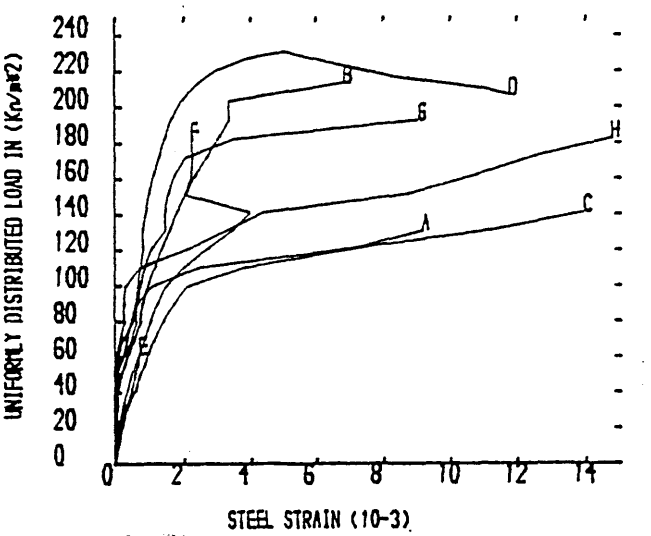

Load-Steel Strain Curves of R.C.Waffle Model Slab C3

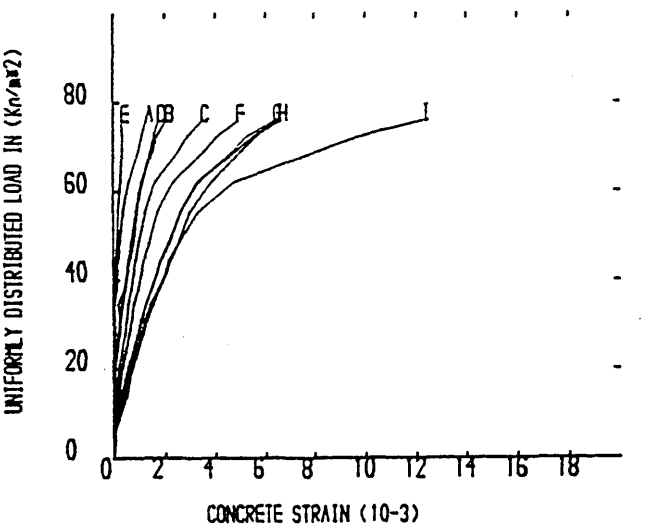

Load-Concrete Strain Curves (1) of R.C.Waffle Model Slab E1

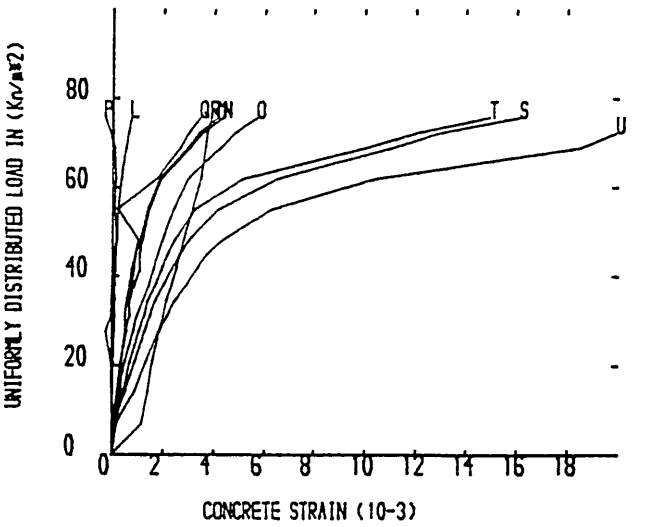

Load-Concrete Strain Curves (2) of R.C.Waffle Model Slab E1

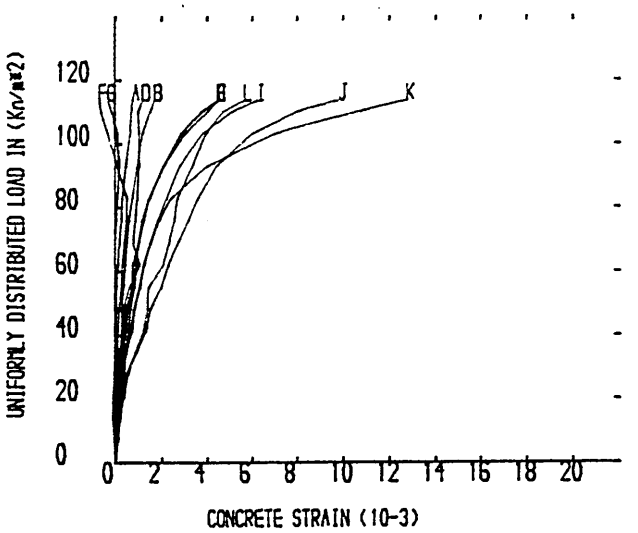

Load-Concrete Strain Curves (1) of R.C.Waffle Model Slab E2

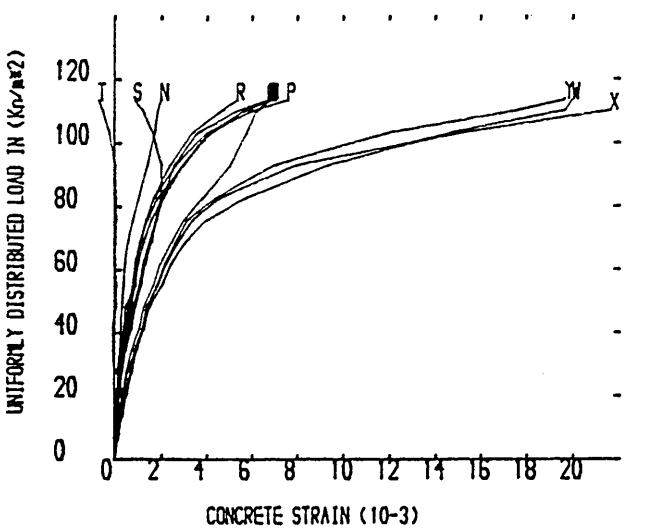

Load-Concrete Strain Curves (2) of R.C.Waffle Model Slab E2

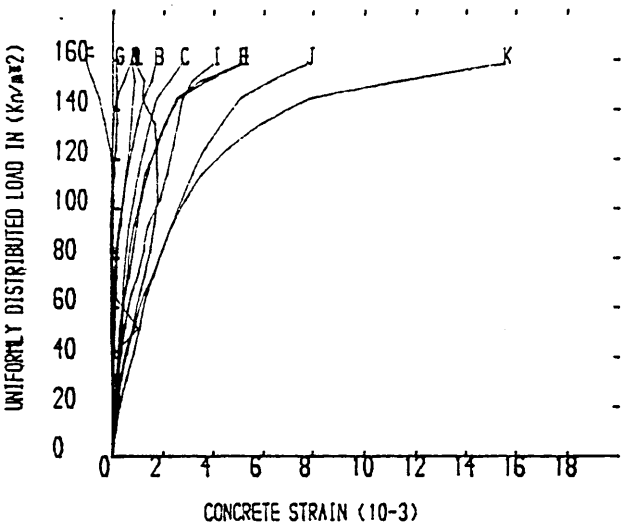

Load-Concrete Strain Curves (1) of R.C.Waffle Model Slab E3

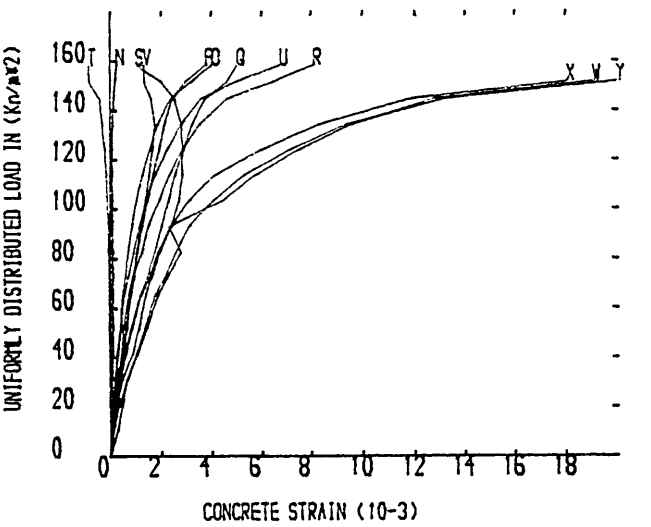

Load-Concrete Strain Curves (2) of R.C.Waffle Model Slab E3

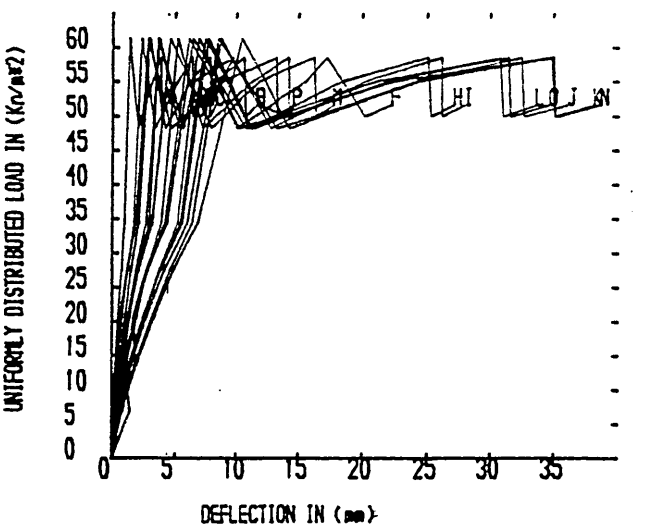

Load-Deflection Curves of R.C.Waffle Model Slab F1

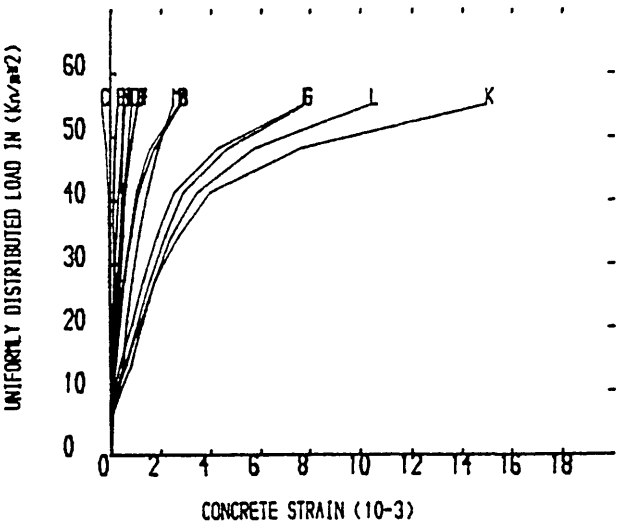

Load-Concrete Strain Curves (1) of R.C.Waffle Model Slab F1

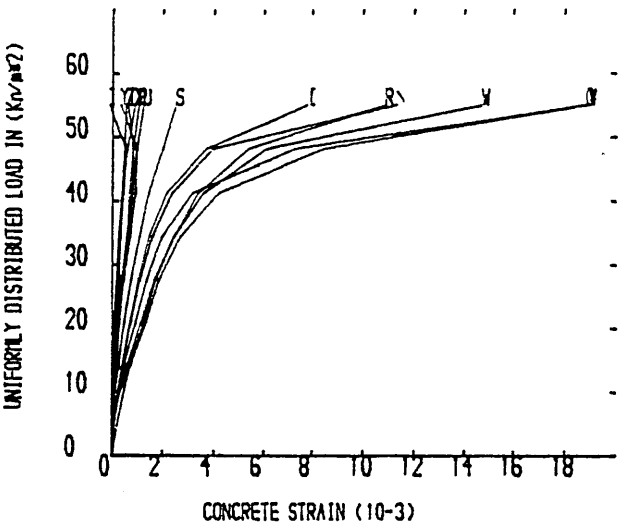

Load-Concrete Strain Curves (2) of R.C.Waffle Model Slab F1

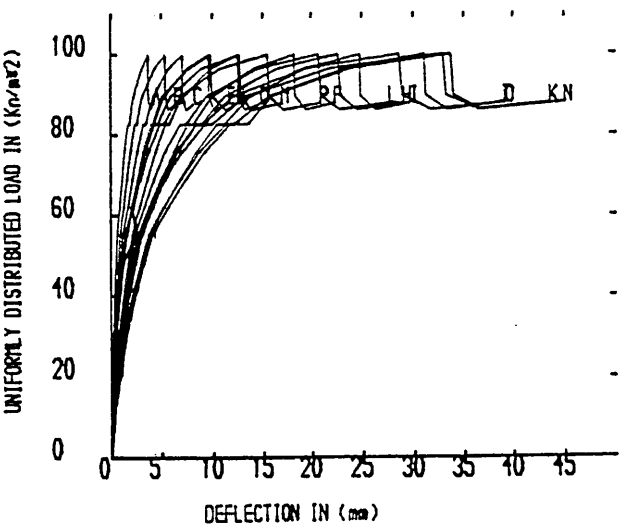

Load-Deflection Curves of R.C.Waffle Model Slab F2

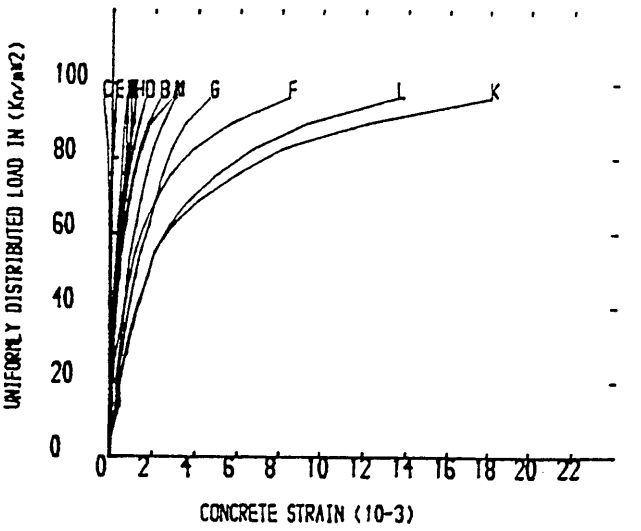

Load-Concrete Strain Curves (1) of R.C.Waffle Model Slab F2

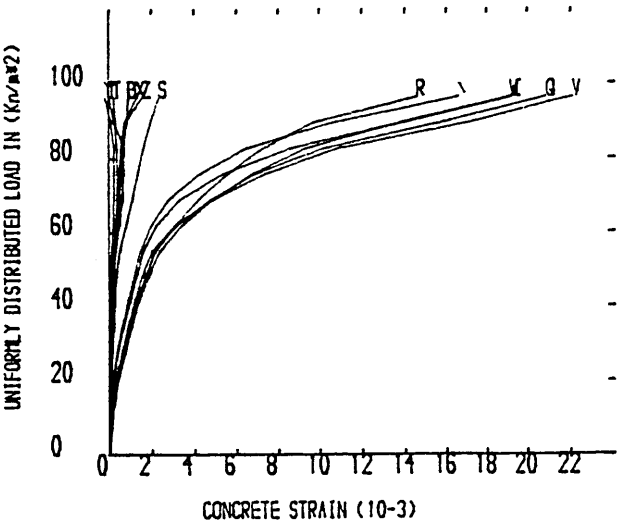

Load-Concrete Strain Curves (2) of R.C.Waffle Model Slab F2

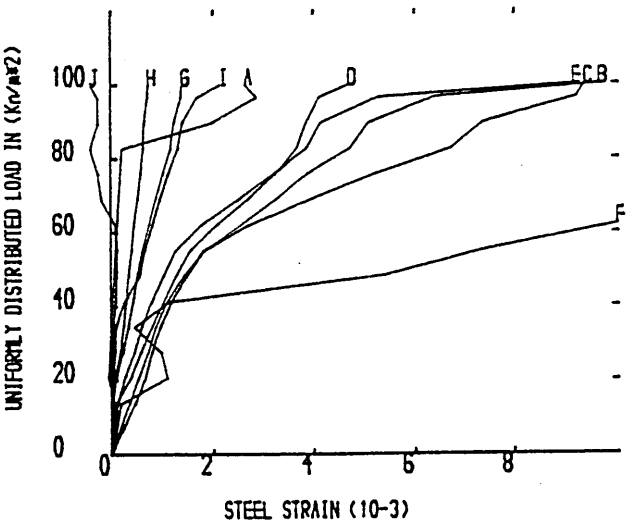

Load-Steel Strain Curves of R.C.Waffle Model Slab F2

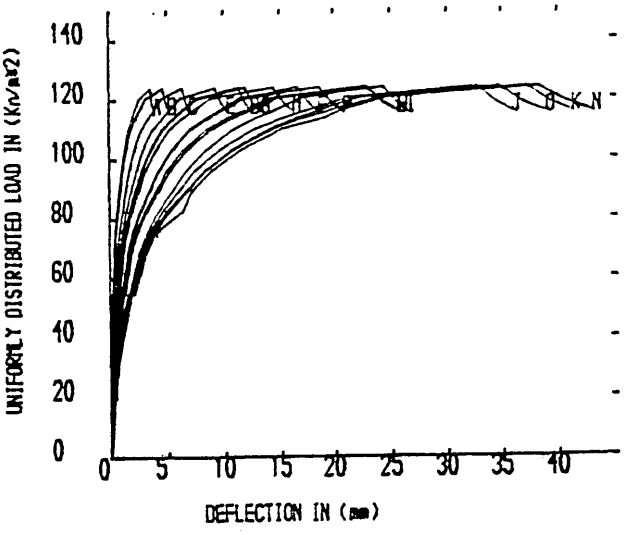

Load-Deflection Curves of R.C.Waffle Model Slab F3

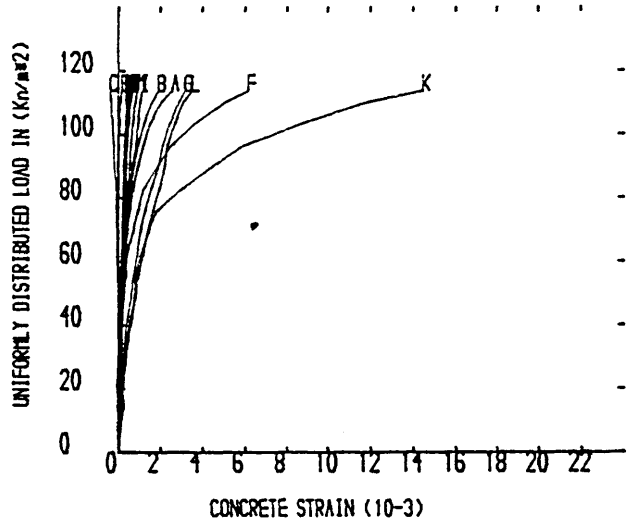

Load-Concrete Strain Curves (1) of R.C.Waffle Model Slab F3

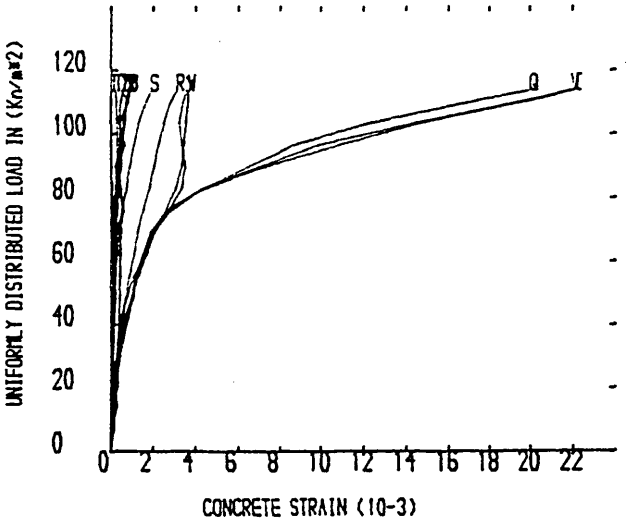

Load-Concrete Strain Curves (2) of R.C.Waffle Model Slab F3

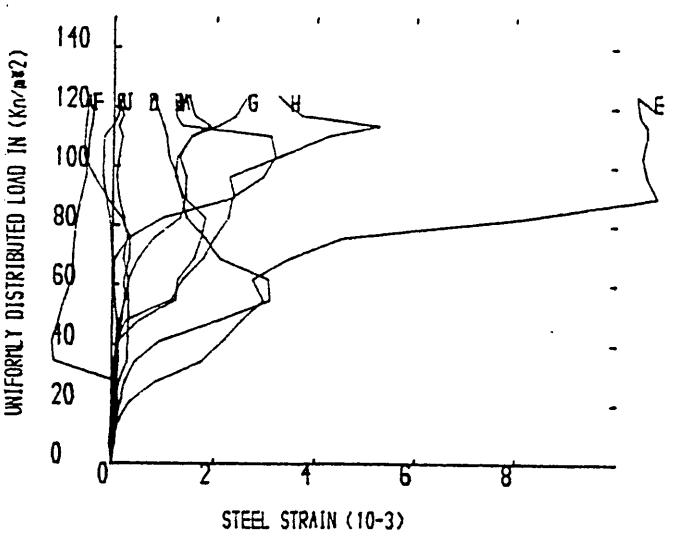

Load-Steel Strain Curves of R.C.Waffle Model Slab F3

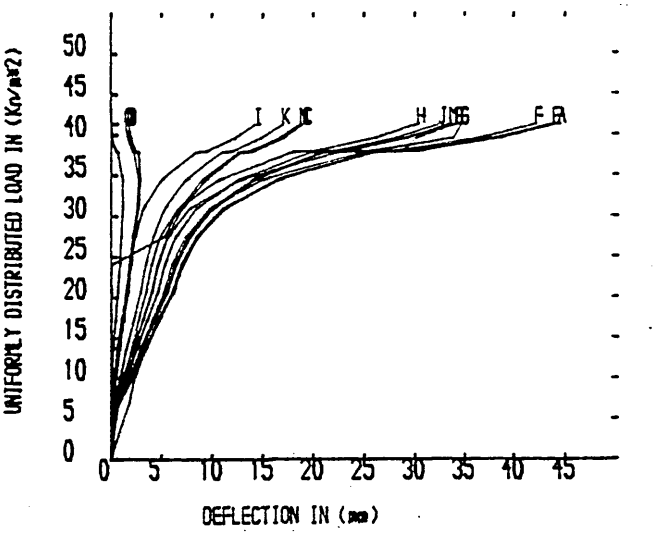

Load-Deflection Curves of R.C.Waffle Model Slab H1

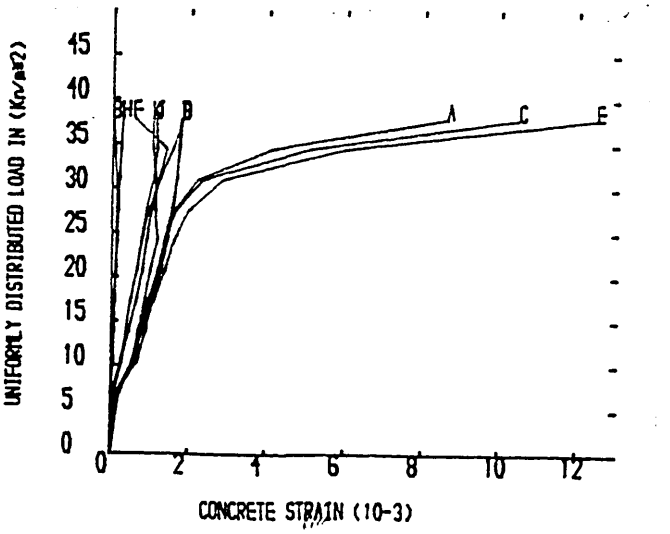

Load-Concrete Strain Curves (1) of R.C.Waffle Model Slab H1

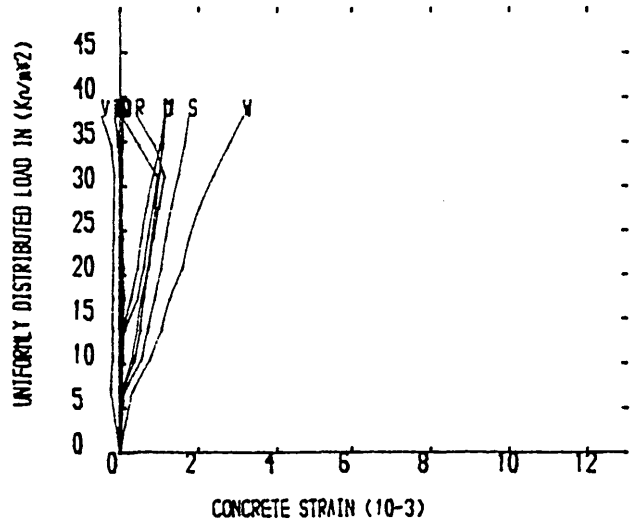

Load-Concrete Strain Curves (2) of R.C.Waffle Model Slab H1

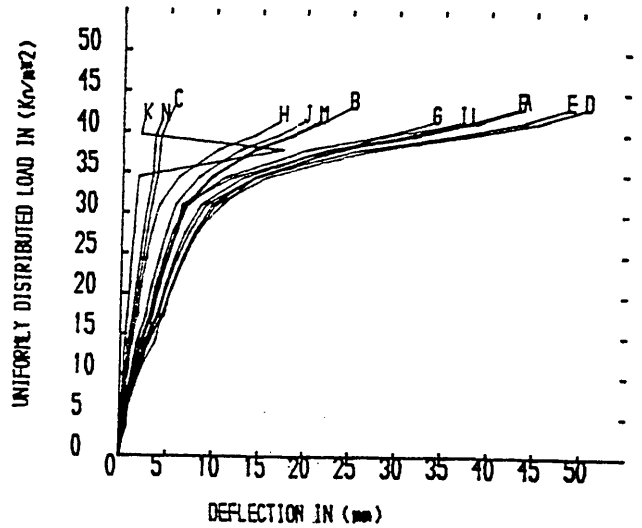

Load-Deflection Curves of R.C.Waffle Model Slab H2

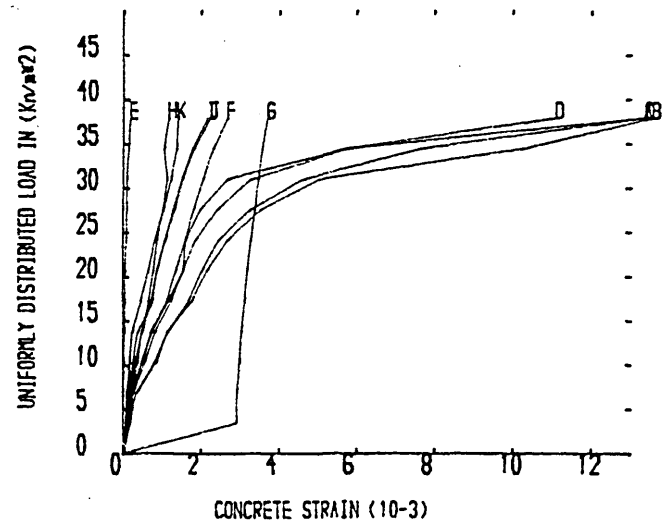

Load-Concrete Strain Curves (1) of R.C.Waffle Model Slab H2

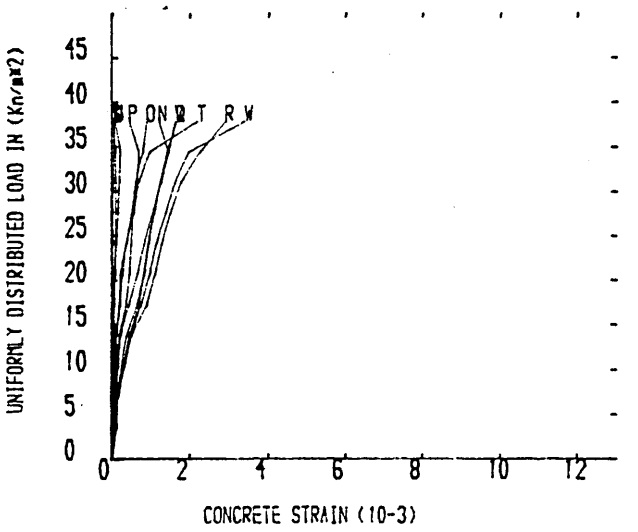

Load-Concrete Strain Curves (2) of R.C.Waffle Model Slab H2

APPENDIX C

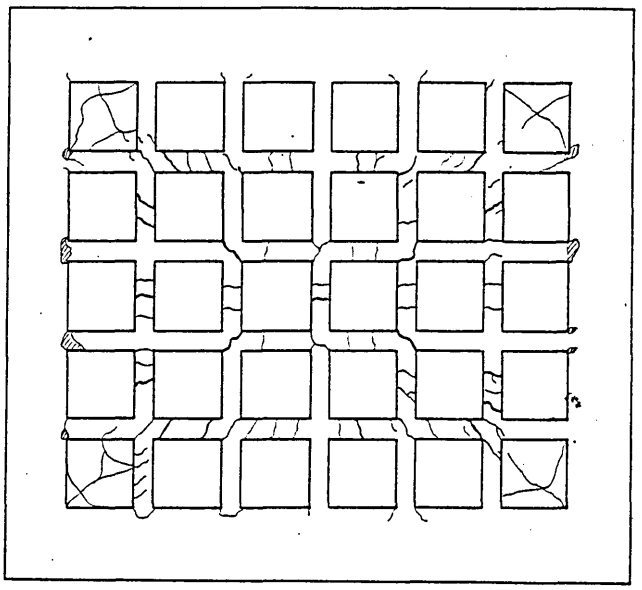

Failure Crack Pattern of R.C. Waffle model Slab A1

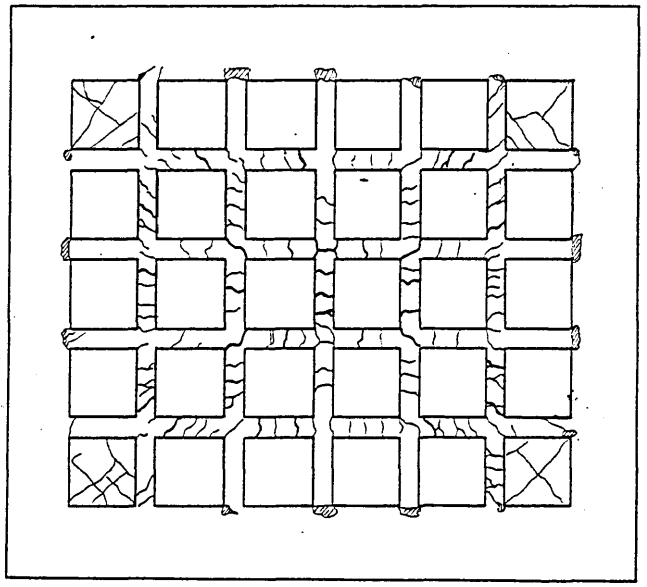

Failure Crack Pattern of R.C. Waffle model Slab A2

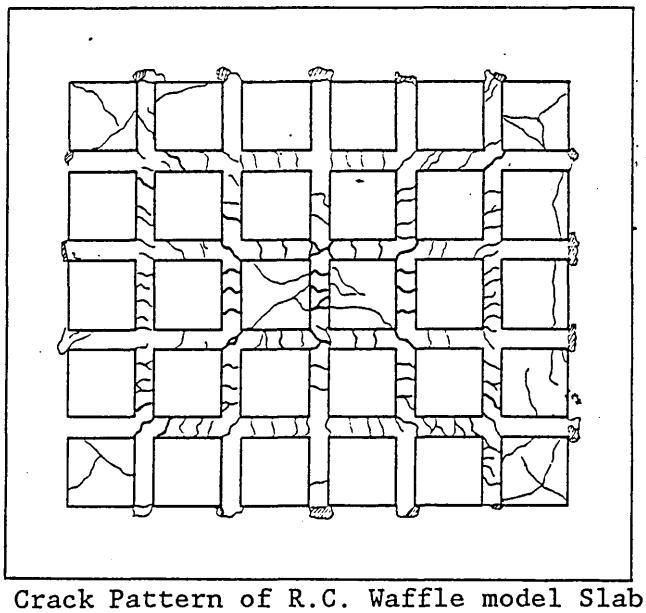

Failure Crack Pattern of R.C. Waffle model Slab A3

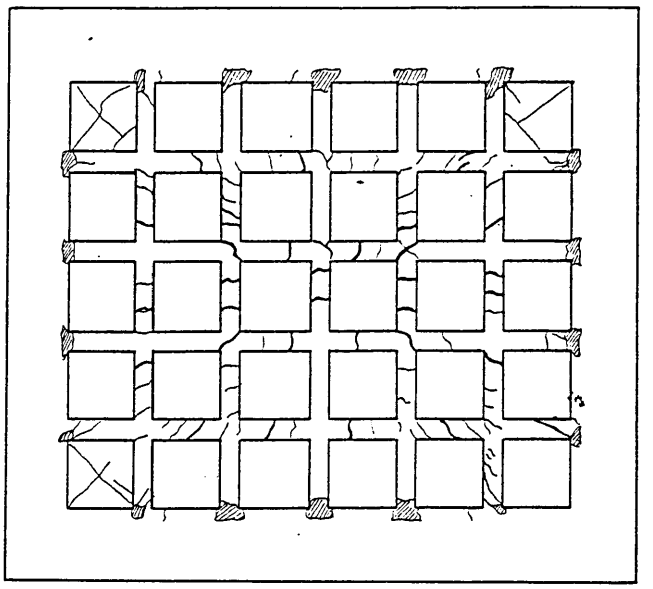

Failure Crack Pattern of R.C. Waffle model Slab B1

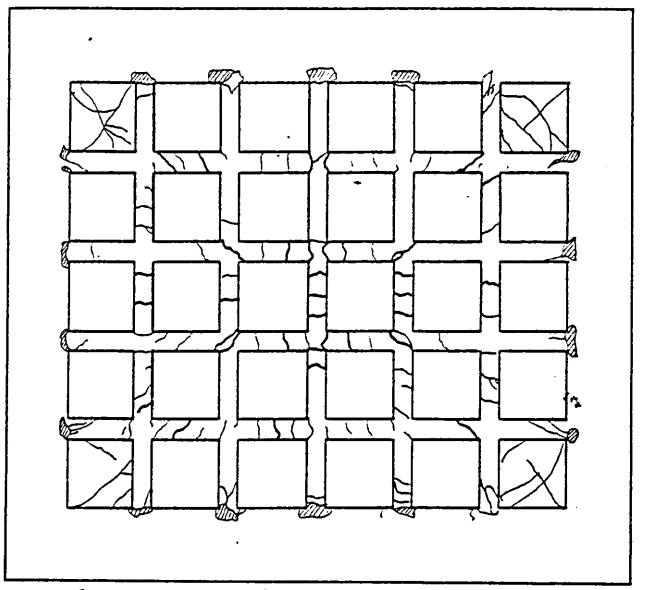

Failure Crack Pattern of R.C. Waffle model Slab B2

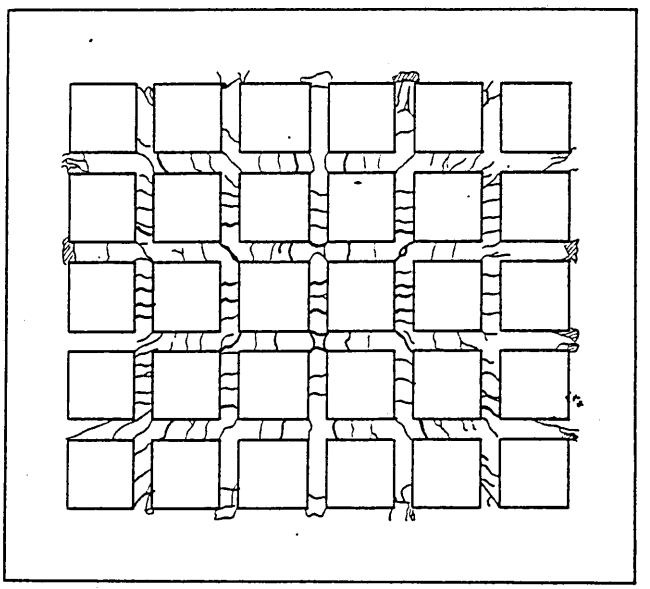

Failure Crack Pattern of R.C. Waffle model Slab B3

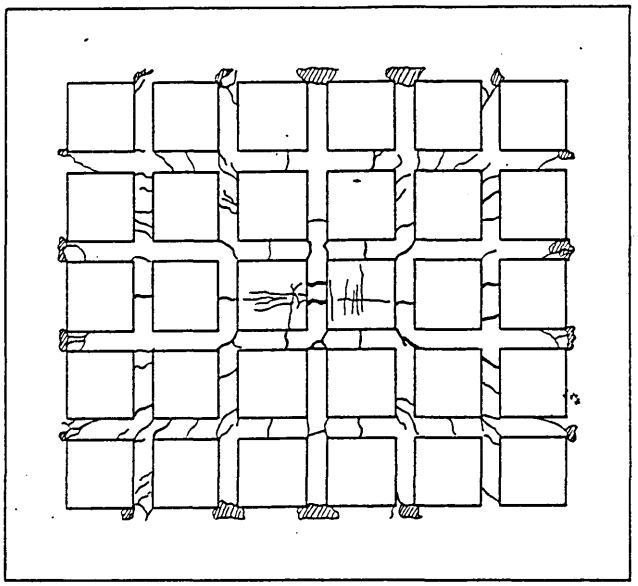

Failure Crack Pattern of R.C. Waffle model Slab C1

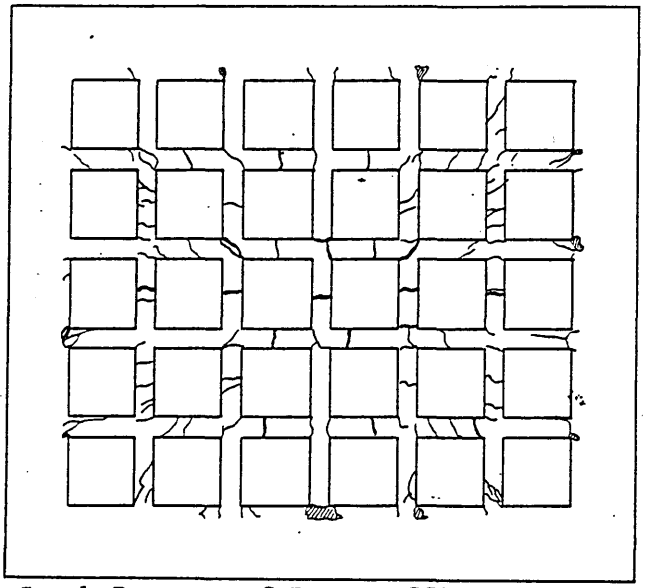

Failure Crack Pattern of R.C. Waffle model Slab C2

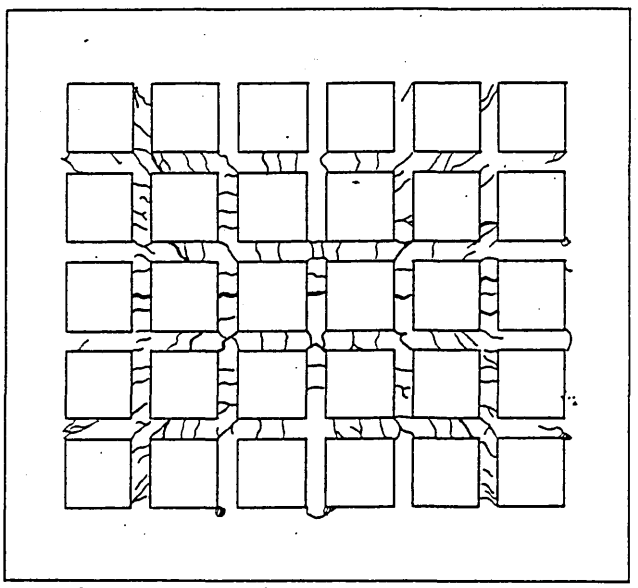

Failure Crack Pattern of R.C. Waffle model Slab C3

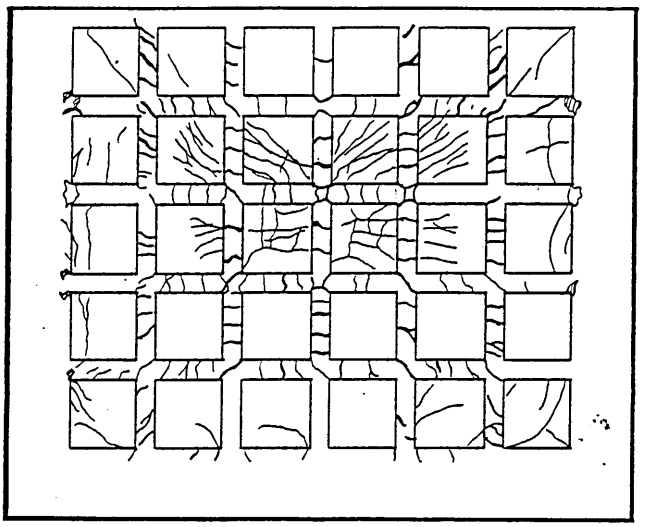

Failure Crack Pattern of R.C. Waffle model Slab E1

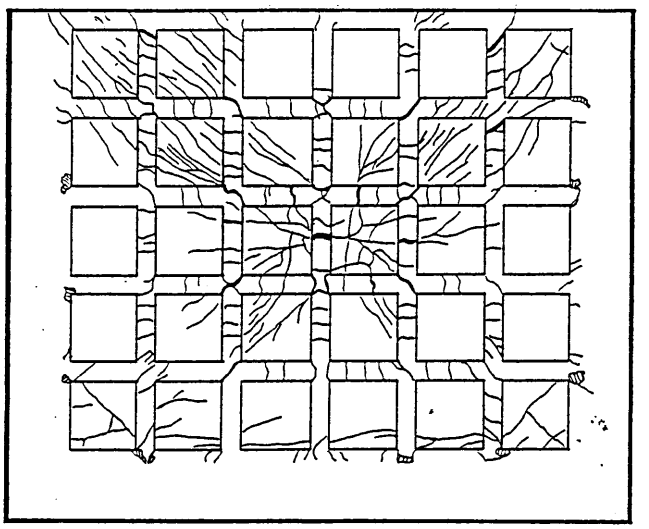

Failure Crack Pattern of R.C. Waffle model Slab E2

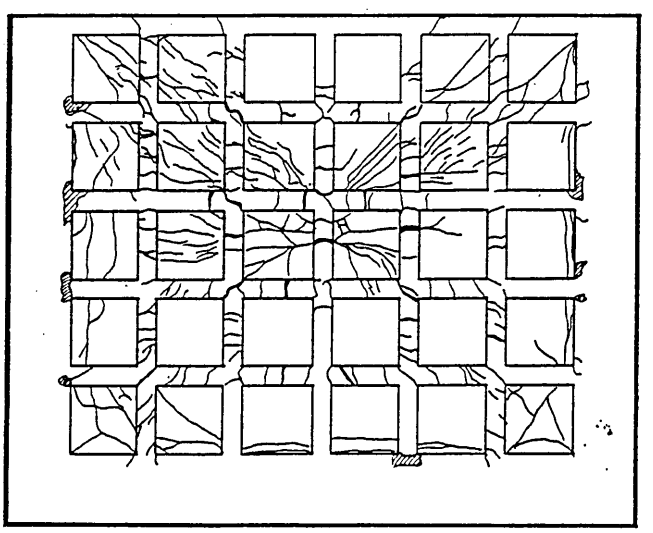

Failure Crack Pattern of R.C. Waffle model Slab E3

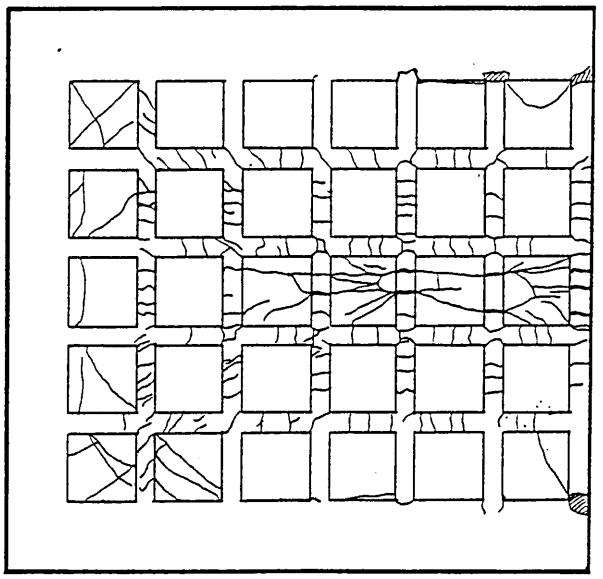

Failure Crack Pattern of R.C. Waffle model Slab F1

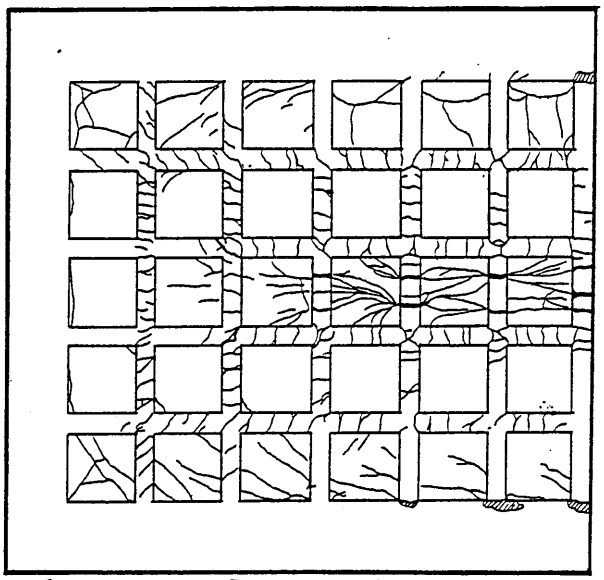

Failure Crack Pattern of R.C. Waffle model Slab F2

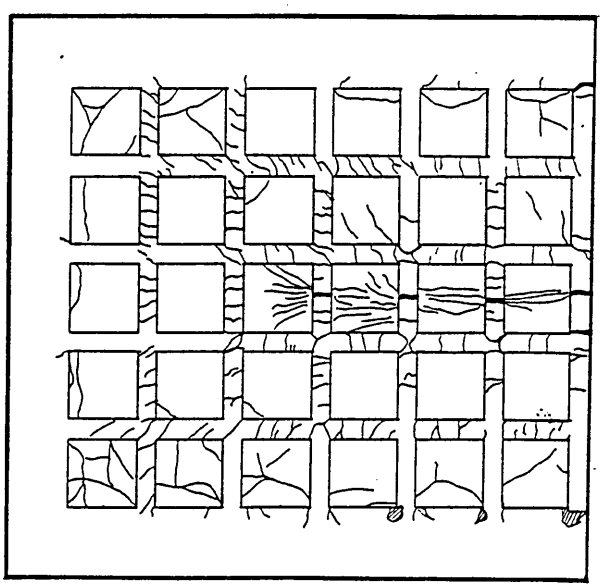

Failure Crack Pattern of R.C. Waffle model Slab F3

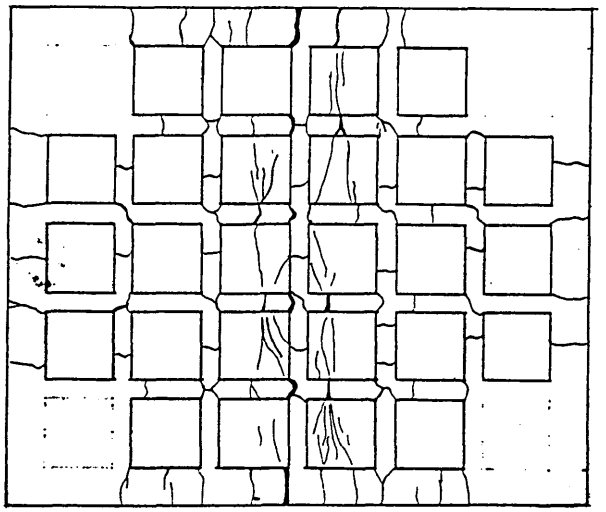

Failure Crack Pattern of R.C. Waffle model Slab H1

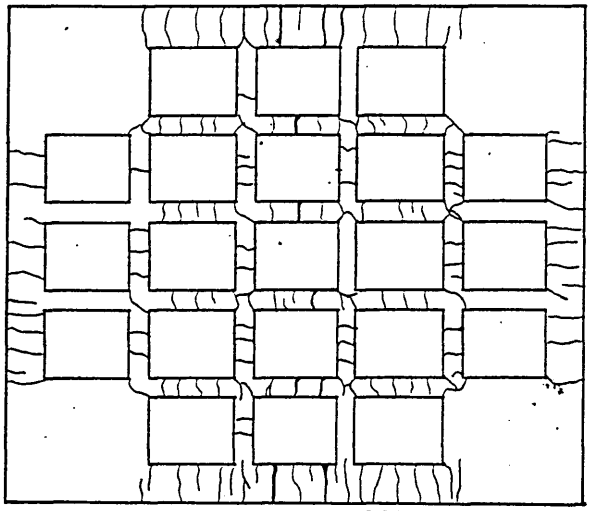

Failure Crack Pattern of R.C. Waffle model Slab H2

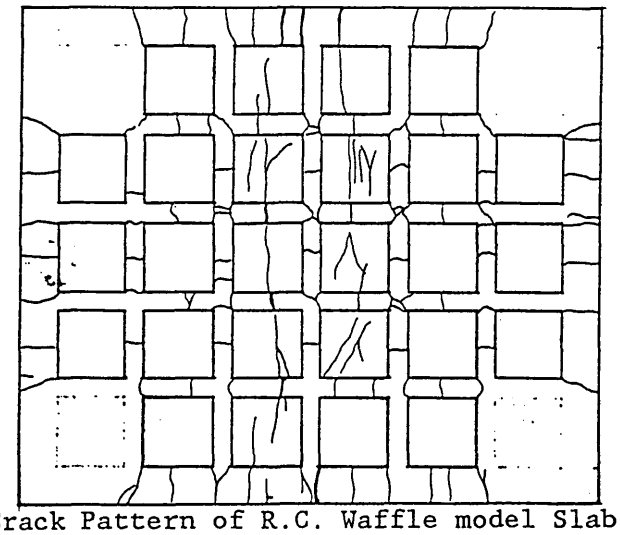

Failure Crack Pattern of R.C. Waffle model Slab I1

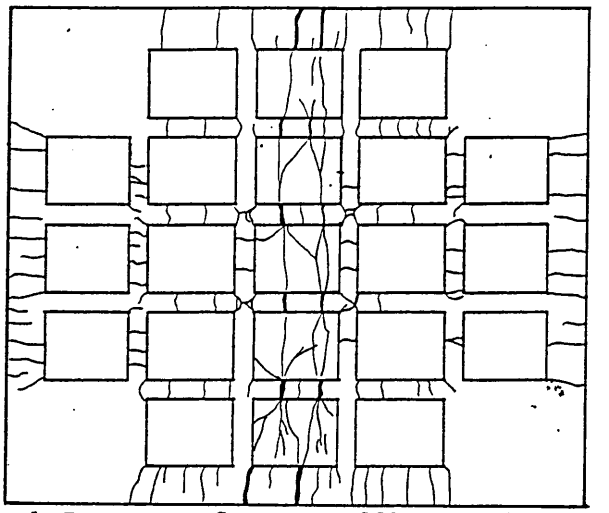

Failure Crack Pattern of R.C. Waffle model Slab I2

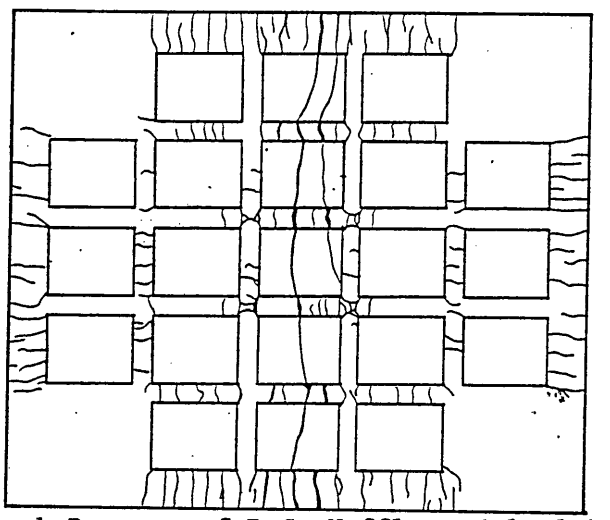

Failure Crack Pattern of R.C. Waffle model Slab J1

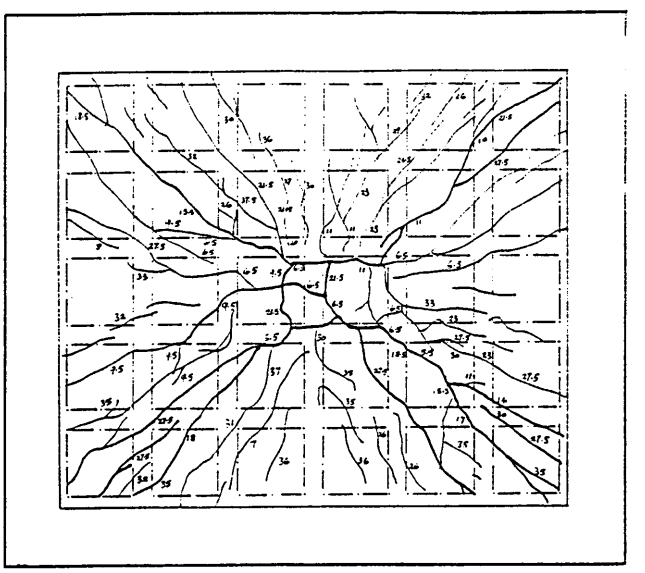

Failure Crack Pattern of R.C. Waffle model Slab D1